

UNIVERSITÁ DEGLI STUDI DI MILANO

Facoltà di Scienze e Tecnologie

Dipartimento di Chimica

Doctorate Course in Chemical Sciences – XXVIII Cycle



Design of New Chiral Brønsted Acid Catalysts and
Rationalization of H-Bond Mediated Reactions

Tutor: Prof. Franco Cozzi

Co-tutor: Prof. Michele Ceotto

Candidato: Manuel Orlandi

Matricola: R10037

2012 – 2015

*A mia moglie Federica
e ai miei genitori*

Table of Contents

Summary	iv
1. Literature Background	1
1.1. Introduction	1
1.2. Catalysts' Synthesis	2
1.3. Chiral Brønsted Acid Catalysis: Reactions and Applications	4
1.3.1 Activation of Imines	4
1.3.2. Activation of Other Electrophilic Substrates	7
1.4. Chiral Brønsted Acid Catalysis: a Chemico-Physical Perspective	14
2. Brønsted Acid Catalysis: Chemico-Physical Studies	21
2.1. Introduction	21
2.2. pK_a Scale of Common Brønsted Acids as Determined by $^1\text{H-NMR}$	21
2.3. Low Temperature NMR experiments	23
2.4. The Acidity:Activity Dualism: Kinetic Experiments	27
2.5. Conclusions	34
3. Development of New Chiral Brønsted Acid Catalysts	35
3.1. Introduction	35
3.2. Synthesis of <i>trans</i> -Diaminocyclohexane-Derived Brønsted Acids	35
3.4. Synthesis of Tartaric Acid-Derived Brønsted Acids	41
3.5. Conclusions	42
4. Theoretical Modelling of the Proline-Catalyzed Aldol Reaction	44
4.1. Introduction	44
4.2. Reversibility of the Proline-catalyzed Aldol Reaction	44
4.3. The Multi Transition States Approach	47
4.4. Conclusions	54
5. HSiCl_3-mediated Reduction of Nitrogroups	55
5.1. Introduction	55
5.2. Metal-free Reduction of Nitrogroups: Literature Background	55
5.3. HSiCl_3 -mediated Reduction of Nitrogroups: Reaction Scope	58
5.4. HSiCl_3 -mediated Reduction of Nitrogroups: Mechanistic Studies	60
5.4.1. HSiCl_3 : Interaction with Lewis and Brønsted Bases	60

5.4.2. SiCl_3^- vs. SiCl_2 , Which is the Active Reducing Species?	62
5.5. Definitive Mechanism Hypothesis	67
5.6. Conclusions.....	69
6. Experimental Section	71
6.1. General Information	71
6.2. Information on Chapter 2	71
6.2.1. Synthesis of Imines 43, 47 and 48	71
6.2.2. Synthesis of Brønsted Acids 44b, 45	72
6.2.3. Synthesis of Brønsted Acid 46	73
6.2.4. Synthesis of Imine 51	73
6.2.5. Acidity Scales: Determination of the Salts' Chemical Shifts	74
6.2.6. Kinetic Experiments: Friedel-Craft Alkylation of Indole with <i>N</i> -4-Methoxyphenyl Imine 43	78
6.2.7. Kinetic Experiments: Friedel-Craft Alkylation of Indole with <i>N</i> -4-Methoxyphenyl Imine 47	79
6.2.8. Kinetic Experiments: Friedel-Craft Alkylation of Indole with <i>N</i> -4-Methoxyphenyl Imine 48	81
6.2.9. Kinetic Experiments: Friedel-Craft Alkylation of Indole with <i>N</i> -Tosyl Imine 51	81
6.2.10. Kinetic Experiments: Friedel-Craft Alkylation of <i>N</i> -Benzyl Indole with <i>N</i> -Tosyl Imine 51.....	83
6.3. Information on Chapter 3	85
6.3.1. Synthesis of Aldehyde 58a.....	85
6.3.2. Synthesis of Aldehyde 58b.....	86
6.3.3. Synthesis of Aldehyde 58c-f.....	87
6.3.4. Synthesis of the (<i>R,R</i>)-DACH-based Diamines.....	89
6.3.5. Synthesis of the (<i>R,R</i>)-DACH-based Diols.....	91
6.3.6. Synthesis of the (<i>R,R</i>)-DACH-based Catalysts 59a-g	92
6.3.7. Stereoselective Friedel-Craft Alkylation	93
6.3.8. Stereoselective Transfer Hydrogenation with Hantzsch Esters	94
6.3.9. Synthesis of Phosphoric Acid 78.....	95
6.4. Information on Chapter 4	97
6.4.1. General Procedure for the Proline-Catalyzed Aldol Reaction.....	97
6.4.2. Proline-Catalyzed Retro-Aldol Reaction.....	98
6.4.3. Geometries of Reaction the Involving Propionaldehyde	98
6.4.4. Geometries of the Proline-Catalyzed Addition of Cyclohexanone to Aldehydes 85a-c.....	103
6.5. Information on Chapter 5	121

6.5.1. General Procedure for the HSiCl ₃ -Mediated Reduction of NO ₂ -groups.....	121
6.5.2. Characterization of the Anilines 97a-v	122
6.5.3. Use of the HSAB Theory	125
6.5.4. Generation of SiCl ₂ from other sources.....	127
6.5.5. ¹ H- and ²⁹ Si-NMR experiments	127
6.5.6. Determination of the Reaction Rate Determining Step	130
6.5.7. Geometries of TSs A, B, C and D	130
7. References and Notes	133

Summary

The present thesis work is mainly focused on the study of the influence of the Brønsted acid-base interaction on different chemical systems. In the first chapter an overview of chiral Brønsted catalysis is provided. Due to the recent publication of exhaustive reviews,¹⁻³ this introductory chapter assumes a conceptual role, avoiding the listing of the numerous published papers on the topic. Indeed, after an overview on the synthesis of the most common acidic catalysts, only the most significant examples of their application are reported, which represent the most known modes of activation involved in this kind of catalysis. In particular, few examples of mono, dual and bifunctional activation of imines by chiral phosphoric acids are presented. The reasons for the development of other acidic functional groups are then illustrated, and an overview on the activation of other electrophiles is reported. As last part of this first chapter, the few published chemico-physical works on the topic are summarized, introducing the reader to the state of the art about: (i) the establishment of pK_a scales of acidic catalysts in organic solvents; (ii) the study of the acid-base interaction through NMR techniques; (iii) the study of the nature of the interactions responsible for the stereoselectivity in chiral Brønsted acid catalysis.

In chapter 2, several chemico-physical studies performed in our laboratories are presented. The exploration of the use of the NMR as an easily available and suitable tool for the assessment of pK_a scales of Brønsted acids is presented. Low temperature NMR studies on acid-base pairs are then reported, which allowed to provide new insight in the understanding of the mechanism involved in the Brønsted acid activation of imines (typical substrates for chiral Brønsted acid catalysis). In the second part of chapter 2, investigations about the Brønsted catalysis law *via* kinetic experiments are reported. Specifically, the importance of the influence of steric effects on the catalytic activity of Brønsted acids is proved by taking into account the Friedel-Craft alkylation of *N*-tosylimines, a classical reaction where we have found a counterintuitive violation of the Brønsted catalysis law.

Chapter 3 is centered on the synthesis of new chiral phosphoric acids. Since the development of chiral Brønsted acid catalysis, the most existing catalysts rely on the BINOL or SPINOL scaffolds. Despite their huge use and high efficiency, these catalysts are expensive and, sometimes, difficult to synthesize. On the basis of a geometry analysis, new compounds supposed to be similarly hindered to BINOL and SPINOL catalysts have been designed, and seven derivatives of a new (*R,R*)-diaminocyclohexane-based class of compounds have been synthesized. The obtained catalysts have been tested in two typical reactions providing promising results. On the basis of the reaction outcome, a structural analysis of the tested compounds was performed.

In chapters 4 and 5 two projects that lie outside the field of Brønsted acid catalysis are presented. In the first a computational study of the proline-catalyzed aldol reaction is reported. Since the computational rationalization of this important reaction has not provided yet any good prediction of the experimentally obtained results, we introduced a new theoretical approach which allowed us to take into account not only the kinetic of the process, but also the thermodynamic properties of the catalytic system. This is particularly important in the light of several experiments that we have performed, which highlighted the thermodynamic nature of this reaction especially when electronrich ketols are formed. Indeed, this kind of compounds have

shown to easily give retro-aldol reaction in the presence of proline. Thus, the inclusion of such effects in the computational model allowed us to predict, for the first time, realistic conversions and stereoselectivity.

In the second side project that we have included in this thesis (chapter 5), new mechanistic studies performed on the trichlorosilane-mediated reduction of nitro groups are reported. This reaction, that we have recently published, represents the first example of metal-free reduction of nitrocompounds performed under mild conditions, and was found to be highly efficient and selective. On the basis of several experiments, we hypothesized that the evanescent species SiCl_2 , known to be generated under our reaction conditions, may be the actual reducing agent (especially when stabilized by a tertiary amine). Some competition experiments highlighted the nucleophilic nature of the reductant, and computational studies confirmed that the most probable reduction pathway involves the $\text{R}_3\text{N-SiCl}_2$ species.

Finally, in chapter 6, the experimental details regarding all the studies reported from chapters 2 to 5 are provided.

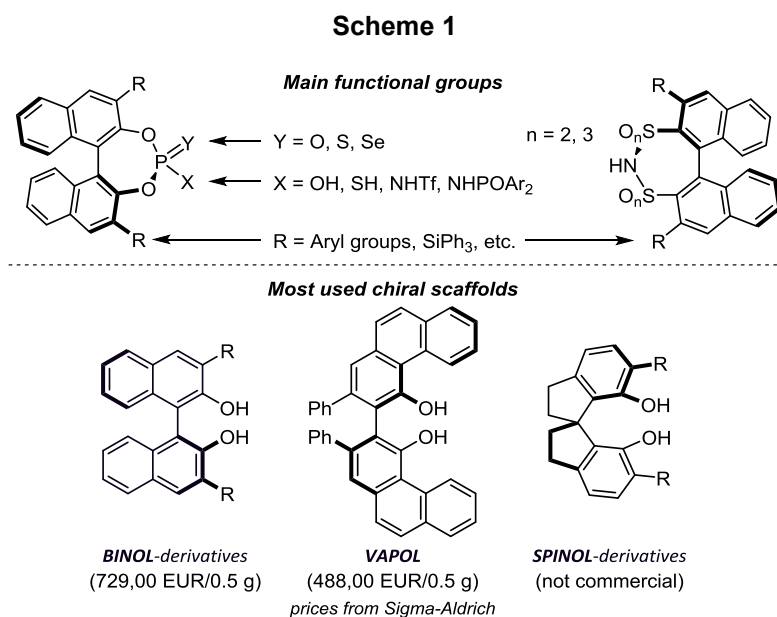
1. Literature Background

1.1. Introduction

During the last decades, organocatalysis has emerged as a powerful, efficient and sustainable methodology for the promotion of complex stereoselective transformations. One of the main approaches in organic catalysis is Brønsted acid catalysis, which aims the promotion of stereoselective reactions by means of chiral organic Brønsted acids. This thesis is focused on the study and development of the so called “stronger Brønsted acids”.¹

Brønsted acid catalysis is known from a long time as a powerful tool for the promotion of chemical transformations. In particular, acidic compounds have been employed primarily as catalysts for the formation and cleavage of C–O and C–N bonds, as in hydrolysis and formation of esters, acetals, imines, and other simple functional groups. However, during the first years 2000, Brønsted acids emerged as efficient catalysts for a range of more valuable transformations involving the formation of C–C bonds.² Indeed, today Brønsted acids are known to activate carbonyls, imines, alkenes, alkynes, and hydroxyl groups towards the attack of nucleophilic species.¹ Due to these important developments, and since the activation of a substrate by a chiral catalyst is now regarded as one of the most powerful synthetic strategies, an increasing attention has been devoted to the development of new Chiral Brønsted Acids (CBA). So far, dozens of new chiral acidic compounds able to promote the formation of C–C, C–N and C–O bonds in a stereoselective fashion have been developed, and hundreds of new CBA catalyzed reactions have been reported.^{1,3}

The main functional groups and chiral scaffolds, which characterize the commonly known and used CBAs, are summarized in Scheme 1. In the same scheme the price of the most common diols precursors of the relative phosphoric acids are reported. Despite their high cost (due to their non-natural origins) these scaffolds have been seeing a progressively increasing number of applications in different fields of chemistry because of their quite general efficiency.^{3a} However, the chemists' community is still constantly looking for new cheaper and easy-to-synthesize alternative scaffolds.

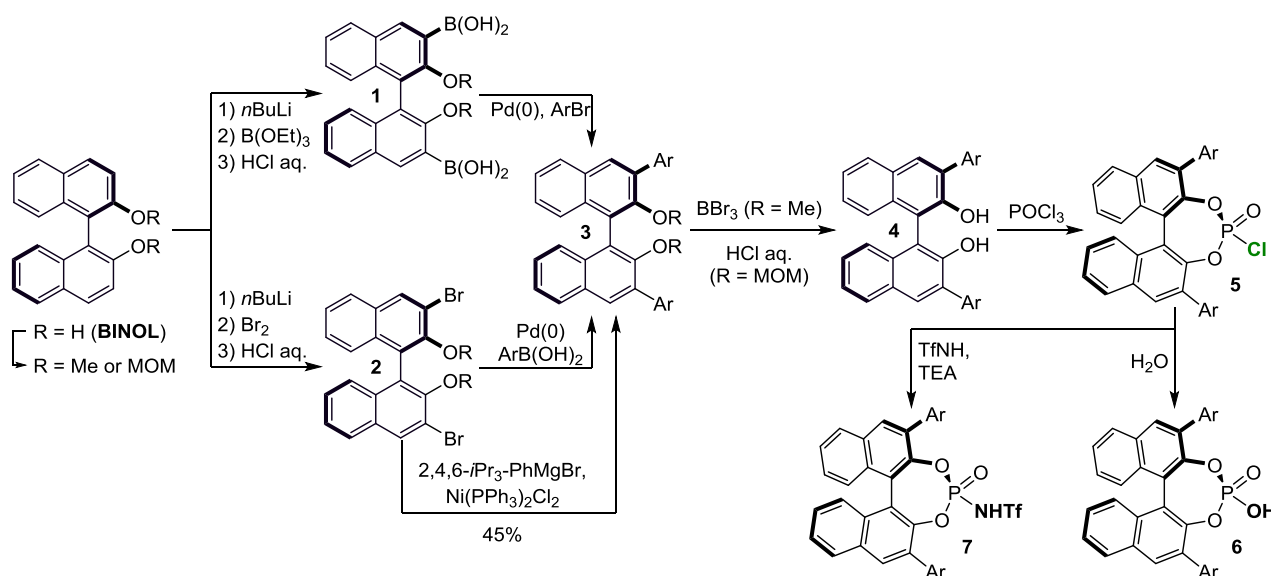


1.2. Catalysts' Synthesis

As just mentioned, most CBAs derive from the BINOL and SPINOL chiral scaffolds (Scheme 1). Since part of the present thesis work aims to the development of Brønsted acids based on new chiral scaffolds, in the present section we give an outlook of the synthesis of the existing catalysts in order to facilitate a comparison of our work with that of the literature.³

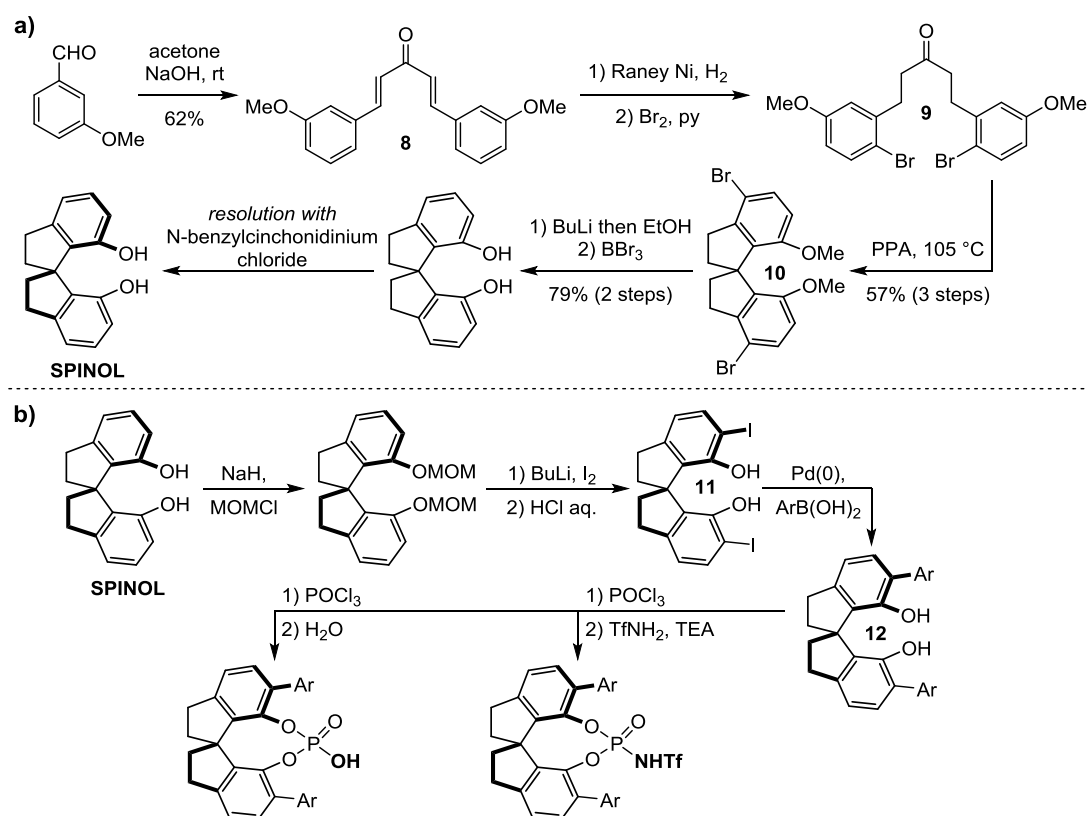
The most common scaffold on which CBAs are based is the 3,3'-disubstituted BINOL. Despite its non-natural origin, BINOL can be considered relatively inexpensive (ca. 36€/g from Sigma-Aldrich). The synthesis of such derivatives is reported in Scheme 2. The first step is the protection of the two hydroxyl group as either methyl ether or methoxymethyl acetal (MOM). Then, the double *ortho*-lithiation followed by either a borylation or a bromination leads to compounds **1** and **2** respectively. The following step is a Pd-catalyzed Suzuki cross-coupling to give the 3,3'-diarylated derivative **3**. Compound **1** could be considered a convenient precursor to **3**, since many more aryl halides than aryl boronic acids are commercially available. However, the use of **1** requires the functionalization of the two 3,3' positions by Suzuki coupling, thus precluding the synthesis of bulkier CBAs which usually need more active cross-coupling partners such as Grignard reagents or organolithium compounds (Kumada reaction). For example, the introduction of 2,6- or 2,4,6-poly-alkyl arenes requires the use of the corresponding Grignard reagent in order to be accomplished even in low yields (Scheme 2). The deprotection of the two OH groups in **3** can be performed by either BBr₃ or concentrated HCl depending on the protecting group to give diol **4**. This is the immediate precursor of BINOL derived CBAs. Indeed, starting from **4**, the desired acidic functional group can be introduced in a one pot procedure. In Scheme 2 only the two most commonly used functional groups are reported: phosphoric acids and N-triflyl phosphoramides (NTPs). The introduction of the former one is accomplished by reacting **4** with POCl₃ to give **5** and then by quenching the reaction mixture with water. On the other hand, if a mixture of trifluoromethane sulfonamide and triethylamine in dry propionitrile is added to **5** rather than water, NTP **7** can be obtained. In summary, starting from BINOL, a typical CBA can be obtained in five synthetic steps generally in good yields.

Scheme 2



SPINOL is another widely used chiral scaffold. Since it is not commercially available, its use is more limited than that of the more widely employed BINOL derivatives. Moreover, its synthesis is reported to be more tedious due to the higher number of steps: seven for the synthesis of the optically pure scaffold plus five more steps for the 6,6'-functionalization procedure (Scheme 3). The synthesis of SPINOL starts from 3-methoxybenzaldehyde. The aldol reaction with acetone in the presence of NaOH give dienone **8** which by hydrogenation with Raney Nickel and subsequent bromination gives ketone **9**. The polyphosphoric acid catalyzed intramolecular double Friedel-Craft alkylation allows the formation of the stereogenic center in compound **10**. The removal of the bromine atoms by lithiation and subsequent quenching with ethanol, followed by the cleavage of the methyl ester moieties by BBr₃ finally lead to racemic SPINOL. The resolution has been proved to be feasible by inclusion crystallization with *N*-benzylcinchonidinium chloride (even on a multi-kilogram scale) or by formation of diastereomeric carbonates of menthol (Scheme 3a). The 6,6'-functionalization of SPINOL can be performed in a way similar to that of BINOL. Protection of the two OH groups as acetals followed by *ortho*-lithiation, iodination and treatment with concentrated hydrochloric acid give compound **11**. By means of a cross-coupling reaction, iodine atoms can be substituted with a desired aryl ring to furnish diol **12**, which, as for BINOL derivatives **4**, can be functionalized with different acidic groups (for example through reaction with POCl₃ and subsequent quench with H₂O or TfNH₂) (Scheme 3b).

Scheme 3



Only few other catalysts have been synthesized which do not rely on the BINOL or SPINOL scaffolds. Specifically TADDOPs⁴ (the TADDOLs phosphoric acid derivatives) and Marinetti's ferrocene derivatives⁵ were found to be effective catalysts in some few reactions. However, the scarce general activity of TADDOPs and the difficult synthetic route to ferrocene based acids, have limited further developments and uses of such catalysts.

Hence, due to the scarce presence in the literature of other chiral scaffolds on which new CBAs can be developed, and to the high cost of the existing catalysts, new chiral scaffolds are still strongly needed.

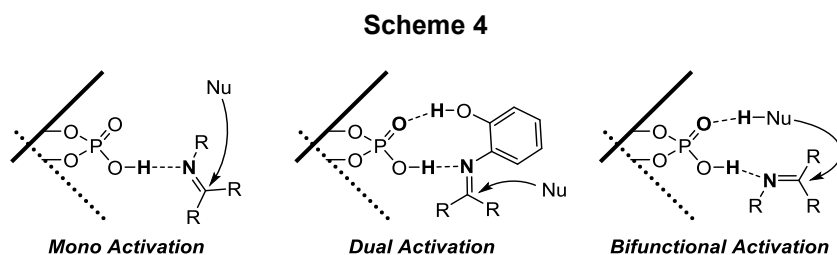
1.3. Chiral Brønsted Acid Catalysis: Reactions and Applications

So far, hundreds of CBAs' catalyzed reactions have been reported. Reviewing all these papers is not the aim of this thesis work, as comprehensive and recent reviews have been published on the topic.^{1,3} However, in the present section, selected examples of the most representing modes of activation by a CBA of a wide range of different functional groups are summarized.

1.3.1 Activation of Imines

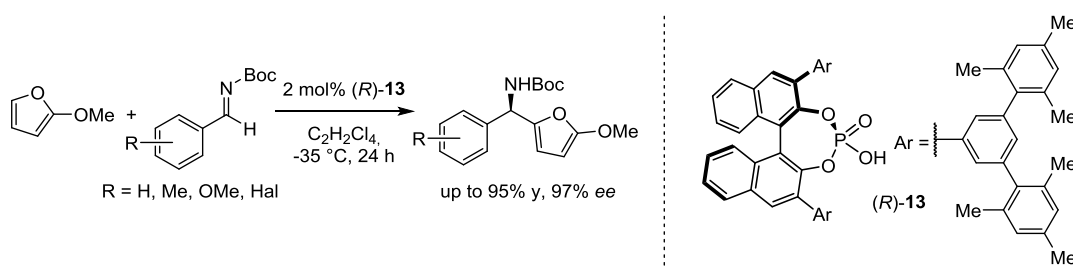
Typical substrates susceptible of a strong activation by acidic catalysis are imines, which may derive either from aldehydes or ketones. Imines have been largely used as substrates towards the attack of different nucleophiles such as: 1,3-diketones (Mannich reaction),⁶ silyl ketene acetals, silyl enol ethers (Mukaiyama-Mannich reaction),⁷ indoles, furans, pyrroles, electron-rich arenes (Friedel-Craft reaction),⁸ diazo compounds (aza-Darzens reaction),⁹ cyanides (Strecker reaction),¹⁰ hydride ion as released from Hantzsch esters (transfer hydrogenation reaction),¹¹ vinyl ethers (Povarov reaction),¹² and many others.^{2,3}

It must be highlighted that, in Brønsted acid catalysis, substrates (and in particular imines) can be activated by three different modes of activation: mono, dual and bifunctional activation (Scheme 4). In the first case, the acidic catalyst simply acts as a proton donor, coordinating the substrate by a single H-bond, so the nucleophile attacks the activated imine without being previously coordinated. In the second case, the electrophilic substrate is coordinated by more than one H-bond, and the nucleophile still behaves as an independent species. Finally, in the third mode of activation, the catalyst acts both as an acid (through the P-OH moiety) and as a base (through the P=O basic site), thus activating both the electrophile and the nucleophile by coordination (Scheme 4).



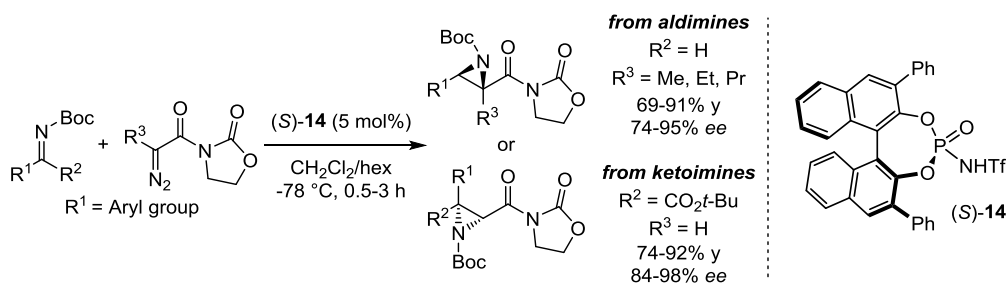
We report here, as representative works, only few examples for each mode of activation of imines. A typical reaction working with mono activation of imines is the addition of 2-methoxyfurans to *N*-Boc imines reported by Terada.^{8a} Here the nucleophile does not have acidic protons susceptible of coordination; hence, it behaves as a non-coordinated nucleophile. The reaction can be efficiently run in different solvents, but the one of choice resulted to be C₂H₄Cl₂, in which the reaction occurs at -35°C in good yields (85 to 95%) and excellent ee (up to 97%). Notably, despite the reaction is generally performed with a catalyst loading of only 2 mol%, the reaction can be performed even with 0.5 mol% of catalyst (*R*)-**13** (Scheme 5) without dramatic losses in the catalytic efficiency. The authors explored the reaction scope by locating some substituents on the imines' aryl ring, including Me, OMe, Br, Cl and F in different position; all the reported substrates have been found to give the Friedel-Craft reaction in good yields and stereoselectivities.

Scheme 5



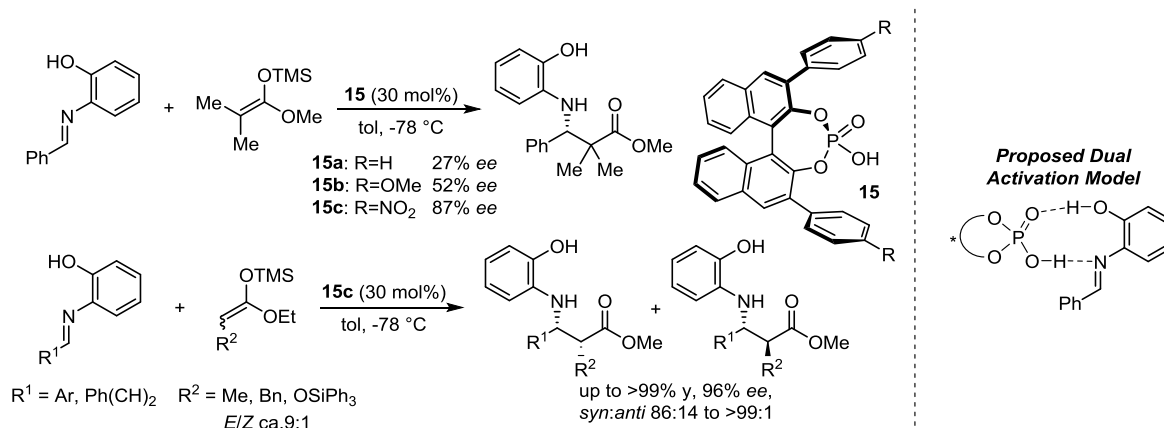
Also the Darzens aziridination is supposed to proceed by a mono activation mechanism. Despite the first examples of CBA catalyzed aziridination were reported by Akiyama and Zhong in 2009 to give disubstituted aziridines,^{9a-b} in Scheme 6 the latest example by Maruoka is reported, since synthesis of more complex trisubstituted aziridines have been accomplished.^{9c} In this paper it was shown how phosphoric acids are unable to promote this reaction (contrary to the cases of disubstituted aziridines by Akiyama and Zhong), hence, the use of more acidic *N*-triflyl phosphoramidate (S)-14 is necessary to activate the reagents. Also α -ketimino esters were found to be suitable substrate towards the *in situ* generated carbene analogue, allowing the introduction of a carboxylic moiety on the final cyclic amine. Good to excellent stereoselectivities and yields have been reached (69-92% yield and 74-98% ee for the single *trans* isomer), it was found that variation on the 3,3' substituents of the BINOL scaffold do not lead to significant improvements of the reaction outcome.

Scheme 6



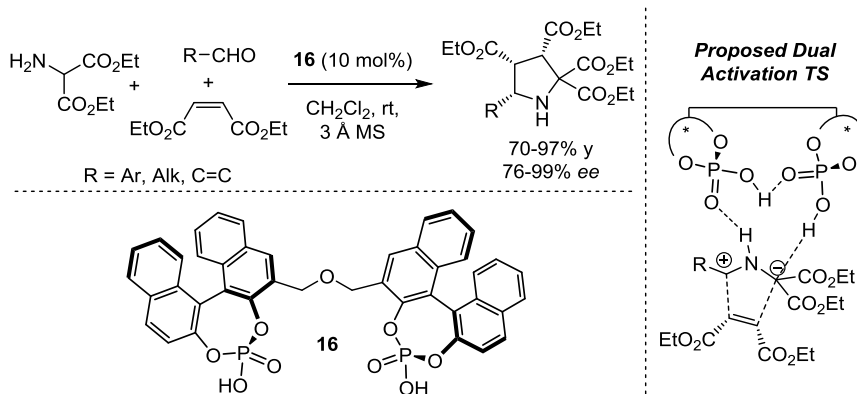
The first example of dual activation is due to Akiyama, who in 2004 reported the chiral phosphoric acid catalyzed Mukaiyama-Mannich reaction.^{7a} The optimal substrates for this reaction are *N*-2-hydroxyphenyl imines. The presence of the hydroxyl group was found to be crucial for securing high levels of stereoselection, thus suggesting the involvement of a dual interaction between the PO_2H group and the imine. The nucleophilic partners for this reaction are silyl ketene acetals. The reaction has shown a strong dependence of the stereoselectivity on the catalyst's aryl substituent, the catalyst of choice resulted to be the 4-nitrophenyl substituted BINOL-derivative **15c** (Scheme 7). Interestingly, when mono-substituted silyl ketene acetals are used as mixture of isomers (*E/Z* > 87:13), high diastereoselections are achieved (86:14 to >99:1 *syn:anti* ratios), still maintaining high levels of enantioselectivity (81-96%) (Scheme 7).

Scheme 7



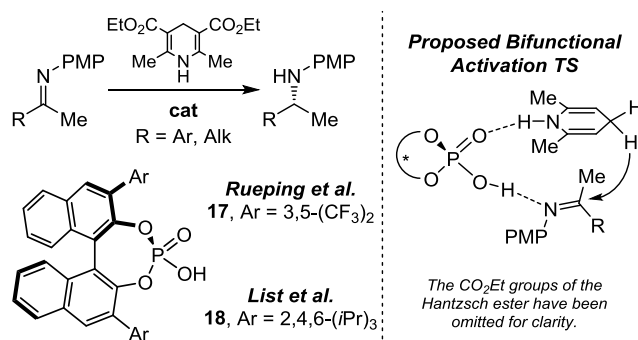
Another significant example of dual activation is due to Gong et al.,¹³ who developed the CBA catalyzed three-component 1,3-dipolar cycloaddition of alkenes to azomethine ylides. The authors have found that catalyst **16** is able to achieve higher stereoselections with respect to typical BINOL-based phosphoric acid. Here the imine is generated *in situ* by an aldehyde and the amine, and can exist in three main forms of resonance, one of which present a 1,3-dipolar pattern as depicted in Scheme 8 (red structure of the proposed dual activation TS). The coordination of such a dipole by the catalyst allows the obtainment of a polysubstituted pyrrolidine as a single diastereoisomer in high yields and excellent enantioselectivity (70-97% y and 76-99% ee) (Scheme 8).

Scheme 8



The most representative example of bifunctional activation in CBA catalysis is probably the Hantzsch ester mediated transfer hydrogenation of ketoimines. Rueping and List have almost simultaneously reported the first stereoselective example of this paradigmatic reaction.^{11a-c} Calculations by Goodman¹⁴ and Himo,¹⁵ have also proved that the P=O group of the catalysts is accepting a H-bond from the N-H moiety of the Hantzsch ester. This coordination guarantees a rigid TS responsible for the high stereoselectivity obtained (Scheme 9). Moreover calculations seem to suggest a *Z* configuration of the C=N double bond at the TS level. The optimum reaction conditions were found to involve the use of aromatic solvents at temperatures between 35 and 60°C. In Scheme 9, the results obtained by List and Rueping, who have used different catalysts (**17** and **18**), are compared. After the works published by Rueping and List, MacMillan developed the one pot reductive amination where ee up to 96% were achieved.^{11c}

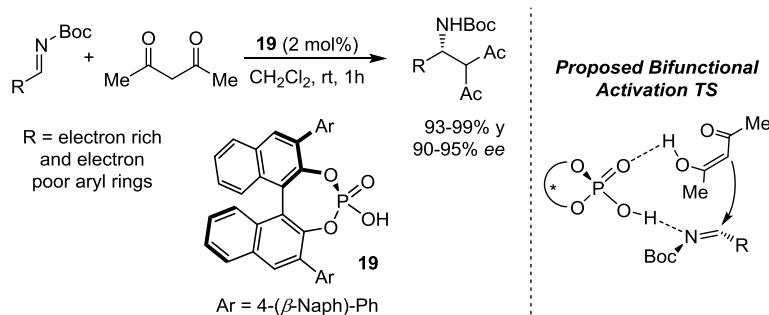
Scheme 9



cat (mol%)	R	solvent	T (°C)	y (%)	ee (%)
17 (20)	Ph	PhH	60	76	74
17 (20)	Napht	PhH	60	82	70
17 (20)	2-F-Ph	PhH	60	82	84
18 (1)	Ph	tol	35	96	88
18 (1)	Napht	tol	35	85	84
18 (1)	2-F-Ph	tol	35	95	85

Terada reported in the 2004 the stereoselective direct Mannich reaction catalyzed by chiral phosphoric acids.⁶ Here the nucleophile is acetylacetone, which existing in two tautomeric forms, allows the proceeding of the reaction through a bifunctional activation (Scheme 10). The reaction proceeds in only 1 h at room temperature with a 2 mol% loading of catalyst **19**. All the substrates tested have shown excellent activity, leading to the products in high yields (93-99% y) and enantioselectivities (90-98% ee) (Scheme 10).

Scheme 10

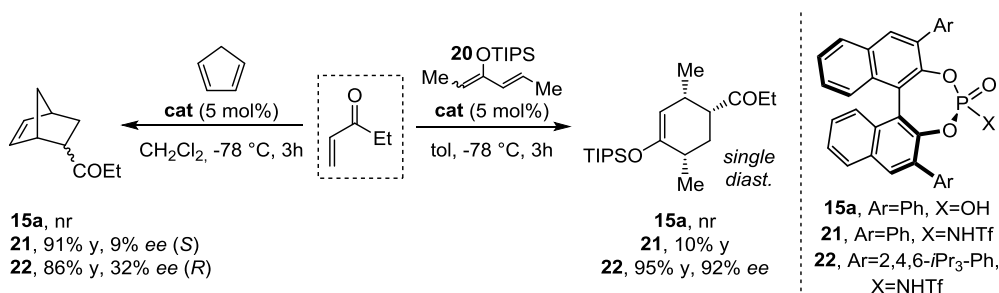


1.3.2. Activation of Other Electrophilic Substrates

The BINOL structure of CBAs has been widely developed, in the last decade, in order to make possible the access to a huge number of substrates. However, until the development by Yamamoto of *N*-triflyl phosphoramidate derivatives (NTP),¹⁶ the activation scope of the Brønsted acid catalysis was mainly limited to imines, which indeed are ideal substrates for phosphoric acid catalysts. However, since the works of Yamamoto, a great number of papers aiming to the development of new acidic functional groups appeared. We hereby report only some examples of Brønsted acid catalyzed reactions where substrates different from imines have been used. Among these substrates there are carbonyls, alcohols, epoxides, aziridines, sulfides and, more remarkably, alkenes.³

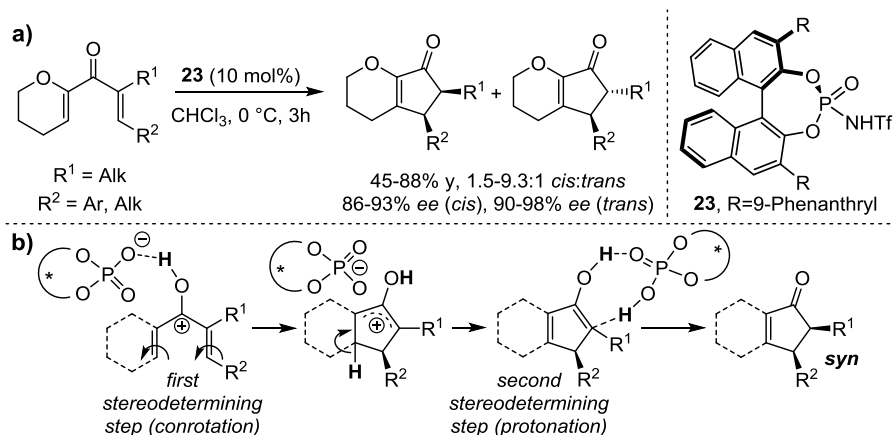
The first work aiming to the activation of ketones was reported in 2006. Yamamoto and coworkers performed a Diels-Alder reaction between ethyl vinyl ketone and cyclopentadiene or diene **20**. While phosphoric acid **15a** was ineffective, replacement of the OH group with the more acidic moiety NHTf in the catalyst (thus passing from catalyst **15a** to catalysts **21** and **22**), allowed the promotion of the reaction in good yields (Scheme 11). Furthermore, the scope of the addition of several dienes similar to **20** to vinyl ketones was explored, showing a quite general good activity and the achievement of enantioselections between 82 and 92% with catalyst **22**.

Scheme 11



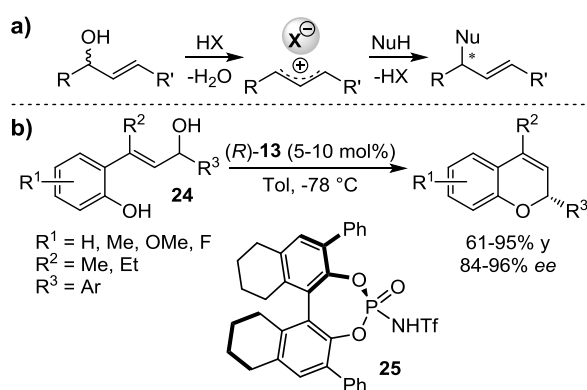
A second example of ketone activation was reported by Rueping et al.¹⁷ Here, the Nazarov cycloaddition of divinyl ketones has been accomplished in moderate to good yields (61-92%) and high stereoselectivities (86-98% ee). While the use of phosphoric acids required higher temperatures (60°C) in order to promote the reaction, catalyst **23** was found to be able to promote the cycloaddition in only few minutes at 0°C (Scheme 12a). The solvent was found to have a dramatic effect on the stereochemical outcome of the reaction; in particular, chloroform provided the best results both in terms of chemical and stereochemical activity. Interestingly, the reaction exhibits a diastereoselectivity in favor of the *syn* isomer, which is the kinetic isomer, thus suggesting also the occurrence a stereoselective protonation step. Hence, in this reaction, the catalyst is responsible for a double stereoselective process, determining both the enantio- as well as the diastereo-selection; the former is determined by influencing the conrotatory direction of the electrocyclic reaction, the latter by protonation of the resulting enol (Scheme 12b). By treatment of the major *syn* isomer with alumina, the authors found an almost total epimerization toward the most stable *anti* diastereoisomer, the thermodynamic product.

Scheme 12



Also the first Brønsted acid catalyzed activation of alcohols is due to Rueping et al.¹⁸ When an allylic alcohol is in the presence of a strong acid, such as NTP, the stabilized carbocation generated by dehydration leads to the formation of the relative ion pair (Scheme 13a). The allylic cation is a reactive electrophilic species, hence, if the counteranion is chiral, one could hypothesize that a nucleophile may be able to attack such a cation in a stereoselective fashion. Rueping and coworkers realized this hypothesis by promoting the first metal-free catalytic asymmetric allylic substitution on substrates with general structure **24**. After the generation of the carbocation, the intramolecular attack of the phenolic hydroxyl moiety can occur leading to the formation of 2H-1-benzopyran derivatives in good to high yields (61-95%) and high enantioselectivities (84-96%). It was also shown how phosphoric acid **15a** is an ineffective catalyst unable to promote the reaction. On the other hand, by changing the acidic group from a phosphoric acid to a *N*-triflyl phosphoramidate (catalyst **25**), a good chemical activity was achieved. The best aryl substituent for the scaffold was found to be the Ph group. Moreover, some improvements were obtained by changing the chiral scaffold from BINOL to the saturated [H₈]-BINOL (**25** in Scheme 13b). After this report by Rueping, other intermolecular versions of the Brønsted acid catalyzed allylic substitution have been reported by other authors.¹⁹

Scheme 13

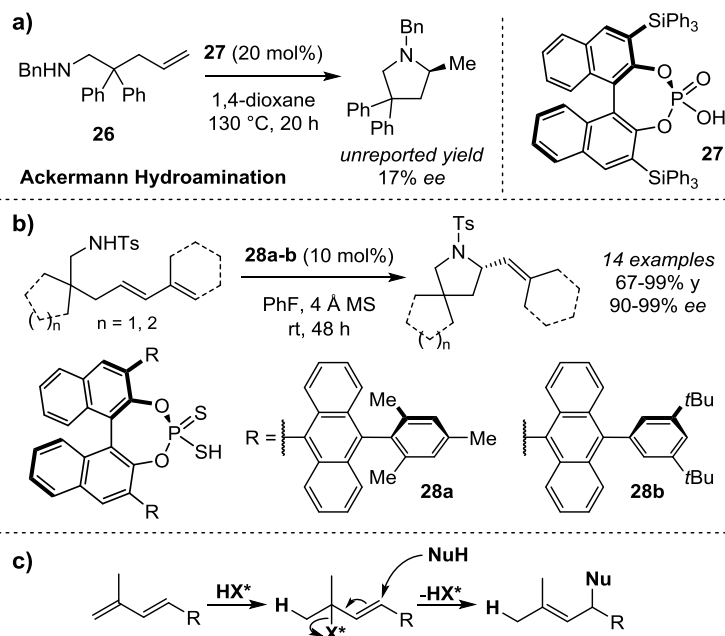


Until few years ago, it was generally accepted that stereoselective activation of olefins would have been possible only through transition metal catalysis. However, in 2008, Ackermann showed a remarkable example of hydroamination of an unsaturated amine. Treating **26** with 20 mol % of **27** at 130 °C overnight gave the relative pyrrolidine derivative in an unreported yield and 17% ee (Scheme 14a).²⁰ Only in 2011, Toste and coworkers developed the first efficient and selective asymmetric intramolecular amination of dienes (Scheme 14b).²¹ Dithiophosphoric acids and thio-*N*-triflyl phosphoramidates were found to be effective catalysts, while phosphoric acids and *N*-triflyl phosphoramidates were found to be incapable to catalyze the reaction. Hence, the sulfur atom seems to play a fundamental role in this reaction. On the basis of this observation, the authors hypothesize a S_N2' mechanism (Scheme 14c). By introducing extremely bulky groups in the 3 and 3' positions of the BINOL scaffold (catalysts **28a-b**), high ee can be reached (up to 99%) still maintaining a high chemical activity (67-99% yield) (Scheme 14b).

It is important to point out that this reaction lies at the limit of acidic catalysis definition. Indeed, in H-bond catalysis, Brønsted acid catalysis, and in counterion catalysis, the only present interactions are either electrostatic or hydrogen bonds; so, to some extent, only relatively weak interactions are involved. However, in this case, a covalent bond between the S atom of the catalyst and the substrate is formed (Scheme 14c).

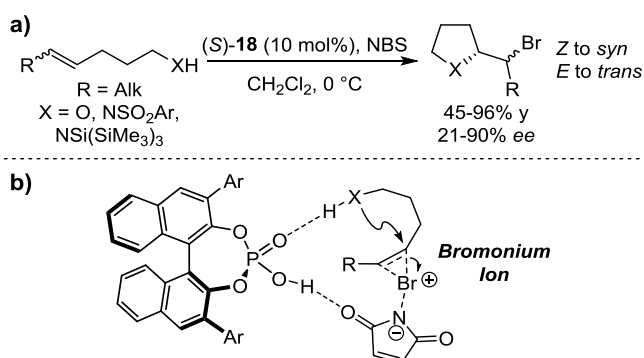
Thus, we could regard this interesting example as a combination between Brønsted acid catalysis (because of the initial activation of the C=C double bond) and Lewis base catalysis (because the dithiophosphate anion acts as a nucleophile by forming a covalent C-S bond).

Scheme 14



C=C bonds have also been activated in Brønsted acid catalysis through the formation of halonium ions. Shi et al. reported in 2011 the bromocyclization of alkenes where the Br^+ source is *N*-Bromo succinimide (NBS). The generation of the bromonium cation in a chiral environment, guaranteed by the coordination of phosphoric acid (*S*)-**18**, allows the tri-membered cycle opening reaction to occur in stereoselective fashion (see the mechanism in Scheme 15b). Hence, the intramolecular attack by either an hydroxyl or a nitrogen nucleophilic moiety allows the formation of brominated tetrahydrofurans and pyrrolidines in good yields (45-96%) and modest to high stereoselectivities (21-90% ee). Notably, only one diastereoisomer is obtained, with the relative configuration dictated by the starting configuration of the alkene (Scheme 15a). It must also be noted that *Z*-alkenes provide higher ee than *E*-olefins.

Scheme 15



An intermolecular analogous reaction was reported by Masson et al., who studied the addition of NBS to enamides.²² Interestingly, Masson and coworkers found that by the use of phosphoric acid **18** rather than its

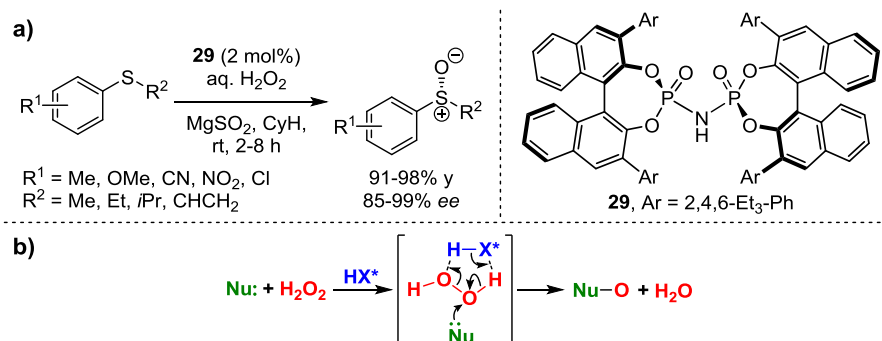
calcium phosphate salt, opposite configurations for the products are obtained. In both cases high ee are obtained (81-98%) even using only 1 mol% of catalyst loading.

Also the activity of phosphate salt of catalyst **15a** was proved with good results in the α -amination of enamides by Masson and Zhu.²³

Several oxidation reactions catalyzed by phosphoric acids have been reported in the literature. In particular, reactions such as 2-hydroxylation of 1,3-diketones,²⁴ α -hydroxylation of enecarbamates,²⁵ stereoselective bromination of biaryls,²⁶ and sulfoxidation²⁷ are paradigmatic examples.

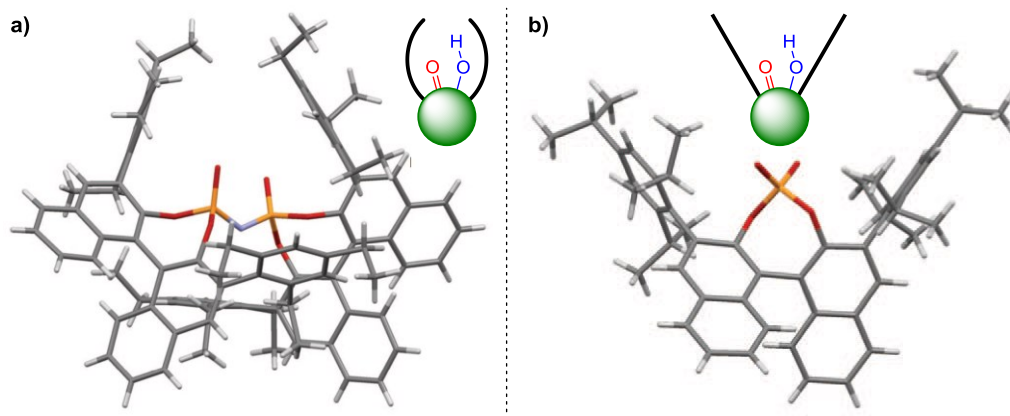
Sulfoxidation was firstly reported by Wang and Tao in 2012. The authors show how phosphoric acids are capable to activate H_2O_2 towards sulfides obtaining the chiral sulfoxides in good yields and with stereoselections between 66 and 82% ee. In the same year, List at al. reported the same reaction to be catalyzed by bisphosphorylimide **29** in excellent yields (91-98%) and ee (85-99%) even at low catalyst loading (2 mol%) (Scheme 16).

Scheme 16



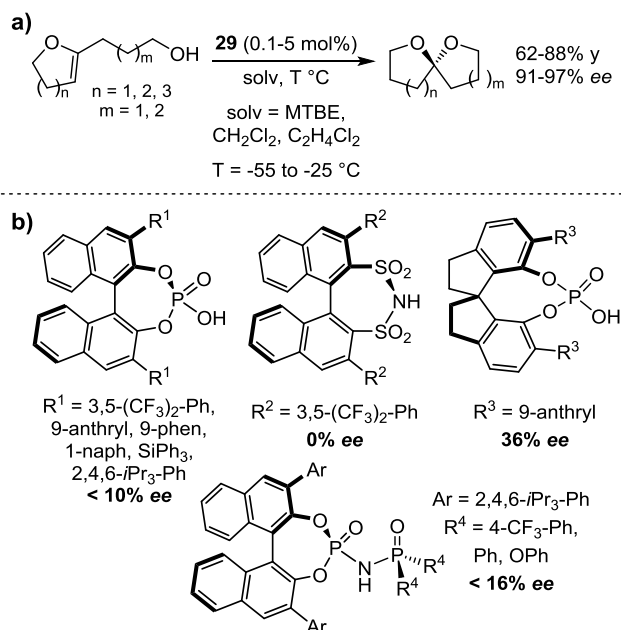
The efficiency of bisphosphorylimides in comparison with typical phosphoric acids is ascribed to the pocket featuring their scaffold. In Figure 1 the X-ray structure of **29** and **18** are compared. It can be easily observed the shape difference between the two catalysts: while phosphoric acid **18** (Figure 1b) is characterized by an opened pocket with an easily accessible acidic group, imidodiphosphoric acid **29** presents a closer shape with an hindered active site (Figure 1a).

Figure 1



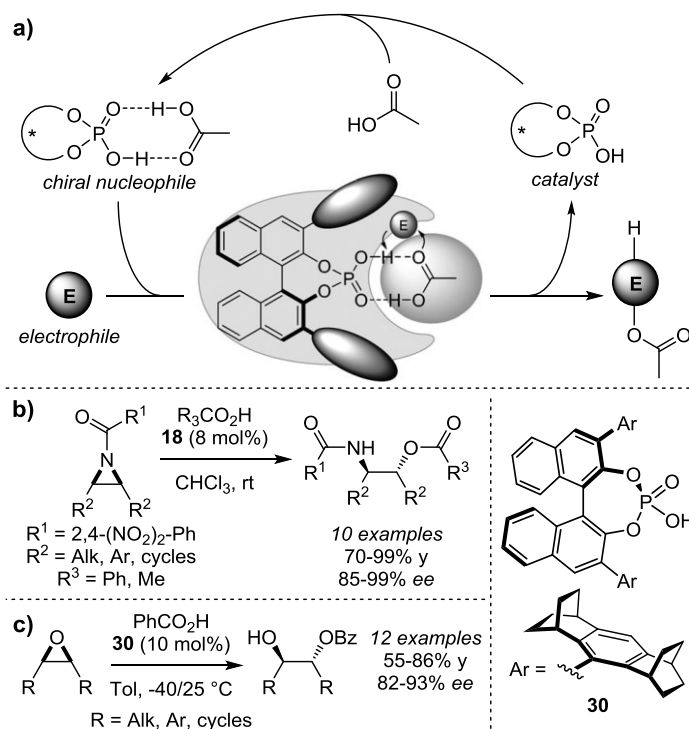
This peculiar structure allows catalyst **29** to achieve high levels of stereoselectivity even in those reaction that result to be more arduous for typical phosphoric acids. A further proof of this ability was presented by List, who, in 2012, reported the asymmetric spiroacetalization catalyzed by Brønsted acids.²⁸ Firstly an extended catalysts' screening has been performed; fourteen different Brønsted acids have been tested allowing the achievement of a maximum ee of 41% (Scheme 17b). However, the employment of catalyst **29** directly lead to the obtainment of excellent enantioselections (91-97% ee) and good yields (62-88%) with low loadings (Scheme 17a).

Scheme 17



Recently, List and coworkers also discovered that CPAs strongly interact with carboxylic acids.²⁹ On the basis of NMR experiments, the authors hypothesized the somewhat counterintuitive possibility that heterodimerization between the two functional groups leads to a synergistic activation: the enhancement of both the nucleophilicity of the carboxylic acid and the acidity of the catalyst (Scheme 18a). This dual activation leads to the suitability of such a reactive system for the stereoselective ring opening reaction of epoxides and aziridines to give 1,2-diols or 1,2-aminoalcohols. Indeed, in the same paper, List et al. have reported both the stereoselective ring opening of *meso*-aziridines and *meso*-epoxides as well as the kinetic resolution of the racemic *trans*-isomer of the same compounds. While for the reaction with aziridines catalyst **18** was found to be able to achieve high yields (70-99%) and stereoselectivities (85-99% ee) (Scheme 18b), the reaction with epoxides required the development of a specific catalyst (**30**). Indeed, **18** is capable to achieve enantiomeric excesses lower than 57%. On the other hand, **30** featured a bulkier pocket which allows the obtainment of the diol derivatives with higher selectivities (82-93%) (Scheme 18c).

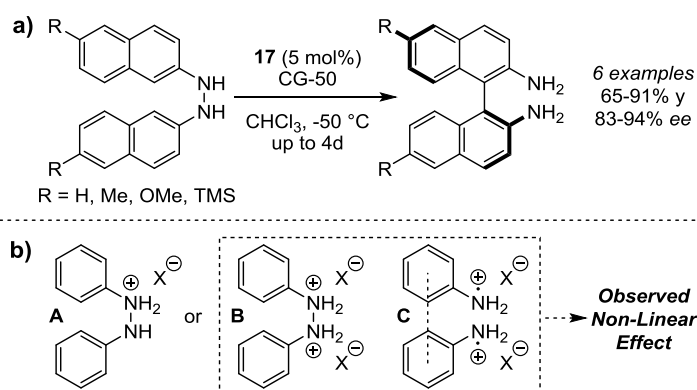
Scheme 18



Another interesting example of the CBAs activity was reported by List. The author described the first example of chiral Brønsted acid catalyzed reaction stereoselectively forming a stereogenic axis. By performing the acid catalyzed benzidine rearrangement of N,N'-dinaphthyl hydrazine derivatives **31** with catalyst **17**, enantioenriched binaphthylidiamines are obtained. Despite the addition of an acidic resin (CG-50) accelerates the reaction, reaction times up to 4 days are needed; however, the product is usually isolated in good yields (65-91%) and stereoselectivities (83-94% ee) (Scheme 19a).

Until today, no generally accepted mechanism of the benzidine rearrangement has been established. There is considerable debate concerning the question whether the reaction proceeds through a monocationic pathway (involving a structure such as **A**) or through a dicationic, potentially radical-cation-involving pathway (via structures **B** or **C**) (Scheme 19b). In this context, the authors have observed a sensible non-linear effect in the stereoselectivity of the reaction, thus supporting the hypothesis of a dicationic TS where two catalyst molecules are involved.

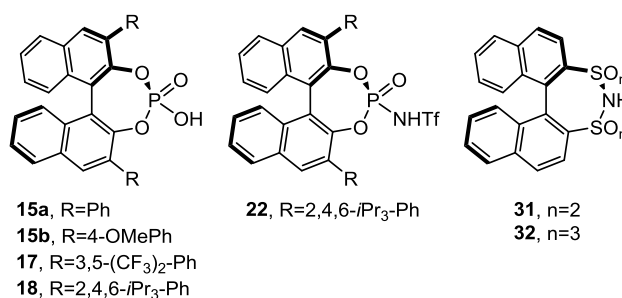
Scheme 19



1.4. Chiral Bronsted Acid Catalysis: a Chemico-Physical Perspective

Despite the great development of this branch of organocatalysis in an applicative direction, only few papers dealt with the comprehension and to the rationalization of the observed stereochemical outcomes. In particular, most of the works aim to the determination of the pK_a values of the most common acidic catalysts. A first general determination of pK_a in DMSO was firstly published by O'Donoghue and Berkessel in 2011.³⁰ By using UV-Vis methods and several indicators such as 4-nitrophenol, 2,4-dinitrophenol, 4-chloro-2,6-dinitrophenol and 2,4-dinitronaphthol, a pK_a scale has been established. Some selected data are reported in Table 1.

Table 1



cat	pK_a^{DMSO}	cat	pK_a^{DMSO}
15a	3.9	31	1.8
15b	3.5	32	1.7-2.0
17	2.4-2.6	HCl	1.8
18	4.2	HBr	0.9
22	3.3	MsOH	1.6

From the presented results the following considerations may be drawn: (i) the pK_a^{DMSO} value of **22** is lower than the relative pK_a^{DMSO} value of phosphoric acid **18** (3.3 vs. 4.2). Hence, one can conclude that PONHTf is more acidic than PO₂H. (ii) The 3,3' substituent on the BINOL scaffold influences dramatically the pK_a^{DMSO} value. Indeed, catalyst **17** presents a lower pK_a^{DMSO} value than **22** (2.4-2.6 vs. 3.3). In other words, the R substituents seems to determine the catalyst's acidity more than the functional group does. Notably, there is not a relationship between the EWG/EDG character of the R group and the measured pK_a^{DMSO} values (compare **15a-b**, **17** and **18**). (iii) Bis-sulfonylimide **31** and bis-sulfurylimide **32** present similar acidity. In addition these compounds were found to be more acidic than other catalysts and are characterized by pK_a^{DMSO} values similar to methanesulfonic acid and hydrochloric acid.

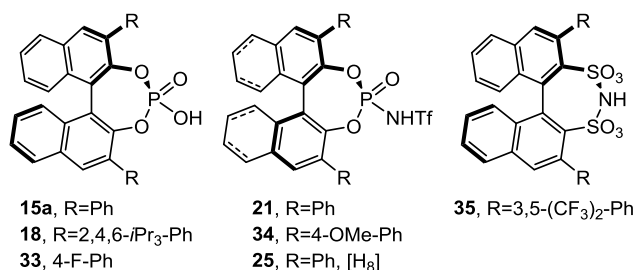
In the early 2000, Leito and coworkers measured pK_a values of a huge number of acidic compounds through UV-Vis methods in non-protic solvents such as dichloroethane and acetonitrile.³¹ In 2013, Rueping and Leito applied this knowledge to establish an acidity scale for the commonly used chiral Brønsted acid catalysts in acetonitrile.³²

In Table 2, the results obtained by Rueping and Leito are reported. It can be observed that the acidity of the three reported main classes of catalysts (phosphoric acids, *N*-triflyl phosphoramides and bis-sulfurylimides) has been determined and compared with a list of commonly available Brønsted acids (among of which is also present the bis-sulfonylimide Tos₂NH). While phosphoric acids (CPAs), which compose the most

common class of catalysts, present pK_a^{MeCN} values between 12 and 14, N-triflyl phosphoramides (NTPs) were found to be much stronger acids, with pK_a^{MeCN} values of about 6.3-6.9. Hence, contrary to what found by Berkessel in DMSO, the main feature directly influencing pK_a^{MeCN} values is the acidic functional group. On passing from PO_2H to PONHTf , the catalyst's acidity increases of about 6 pK_a^{MeCN} units, that is an increase in acidity of about 1,000,000 times. On the other hand, the modification of the electronic properties of the 3,3'-substituents lead to little a pK_a^{MeCN} change of up to 2 unit for CPAs and up to 0.6 unit for NTPs.

Interestingly, Rueping and Leito have found the bis-sulfonylimide Tos_2NH to be only slightly more acidic than phosphoric acids (12.0 vs. 12.5-14 pK_a^{MeCN} unit). This is in contrast with the observation of Berkessel and O'Donoghue, who found bis-sulfonylimide **31** to be more acidic even than NTP **22** in DMSO. Another main difference between the two works is about the acidity of bis-sulfonylimides; while Berkessel and O'Donoghue found this functional group to be roughly as acidic as bis-sulfonylimides (**31** vs. **32** in Table 1), Rueping and Leito have found **35** to be the most acidic compound among the studied CBAs. In particular, it was found to be even more acidic than HBr.

Table 2

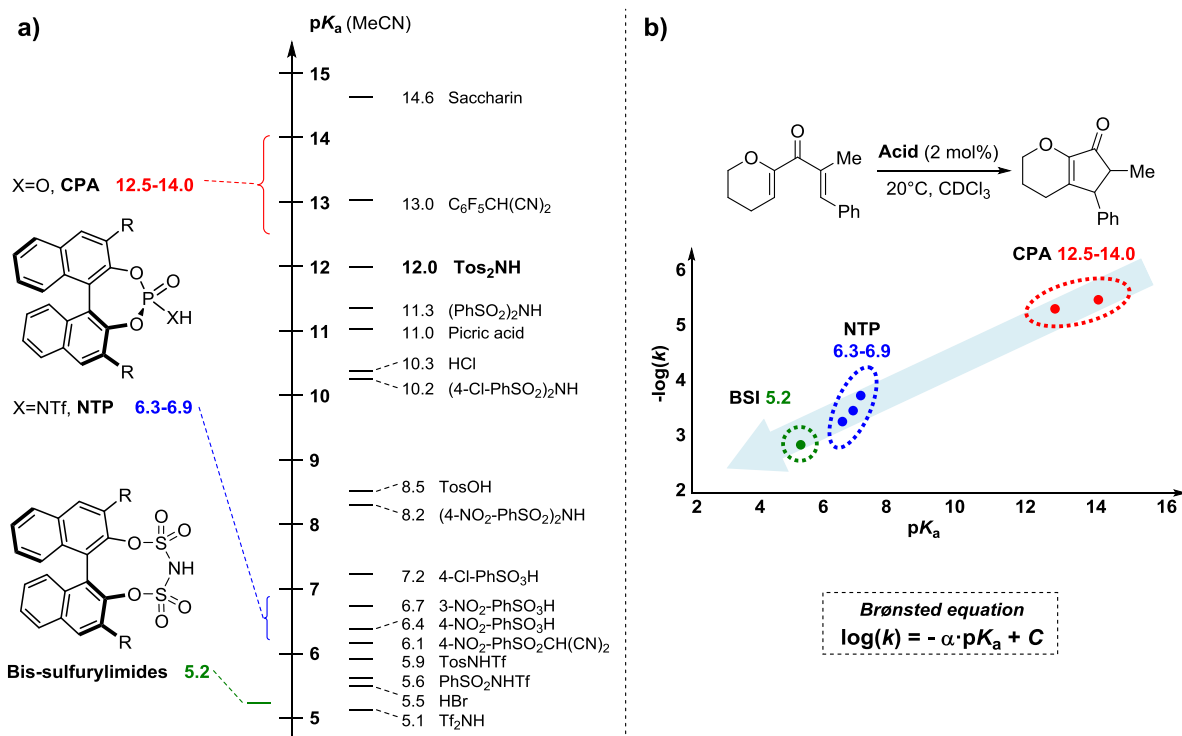


cat	pK_a^{MeCN}	cat	pK_a^{MeCN}
15	12.7	25	6.7
18	13.6	35	5.2
33	12.5	Tos₂NH	12.0
21	6.4	HCl	10.3
34	6.4	HBr	5.5

The results hereby summarized explain the NTPs ability to activate also less reactive substrates with respect to CPAs. Despite bis-sulfonyl imides present an even higher acidity, this functional group has not already found a useful application in catalysis. On the other hand, since bis-sulfonylimides have recently emerged as a powerful functional group for the activation of several substrates inaccessible to CPAs,³³ it is noteworthy the reported pK_a^{MeCN} value of bis-tosylimide (Tos_2NH) of 12.

In Scheme 20a, a direct comparison of the measured pK_a^{MeCN} values by Rueping and Leito with other commonly available acidic compounds is provided. After the assessment of a pK_a scale in acetonitrile, the authors have also proved the linear relationship between the measured pK_a values and the measured rate constants (expressed as $-\log(k)$) of a Nazarov cyclization under catalytic conditions in chloroform.^{17,32} As expected and shown in Scheme 20b, the lower the pK_a , the faster the catalyzed reaction, in agreement with the Brønsted catalysis equation.³⁴

Scheme 20



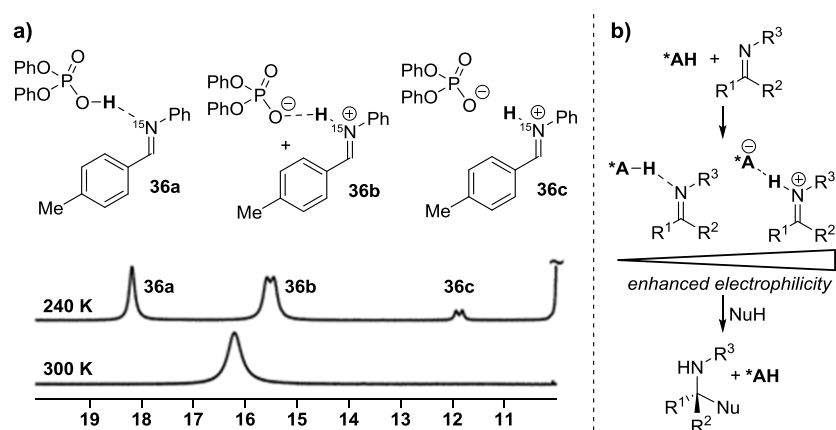
Because of the rapid development of computational chemistry, the pK_a values of organic acids in solution can currently be calculated with similar accuracy than those determined experimentally.³⁵⁻³⁶ In 2013, a theoretical work appeared where Cheng and Li calculated the pK_a values of a huge number of BINOL-derived phosphoric acids in DMSO.³⁷ It must be noted that the authors chose to use the data reported by Berkessel as reference values, obtaining calculated pK_a values for other 36 compounds. In particular pK_a values were found to range between 1.5 and 5.1 unit for CPAs, -3.1 and 1.9 for thiophosphoric acids (PSOH), and between -3.0 and -4.2 for dithiophosphoric acids (PS₂H). Despite in this first publication by Cheng and Li no information about NTPs, bis-sulfonylimides or bis-sulfurylimides was provided, in a second paper published in 2014 by the same authors, new data completed the computational study.³⁸ Here the pK_a values for many additional acidic compounds are provided; in particular NTPs, bis-sulfonylimides and bis-sulfurylimides were calculated to have pK_a of -3.9 to -2.2, 0.1 to 1.9 and -3.7 and -2.3 respectively. Hence, despite the calculated values do not fit with those experimentally determined by Berkessel, the calculations present a trend that is in quite good agreement with the experimental data provided by Rueping and Leito in acetonitrile (i.e. bis-sulfurylimides \leq NTPs < bis-sulfonylimides < CPAs).

In conclusion, on the basis of the work by Leito and coworkers about the determination of the pK_a of "superacidic" compounds,³¹ and due to the better agreement with the chemical activity data reported in the literature and with calculations by Cheng and Li,³⁷⁻³⁸ the results obtained by Rueping seem to be more reliable. Hence, further discussion regarding the acidity of CBAs in the present thesis work will refer to the report by Rueping and Leito.³²

While few papers have been published about the determination of the pK_a value of CBAs in organic solvents, even way less studies have been performed in order to understand the chemico-physical basis of Brønsted acid catalysis. An important work regarding the characterization of the main species involved in acidic

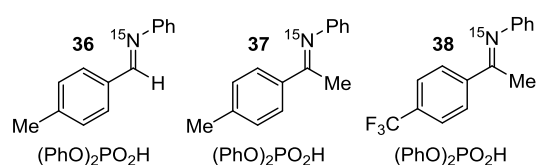
catalysis is due to Gschwind and Rueping.³⁹ Elucidating the exact mechanisms involved in chiral phosphoric acid catalyzed systems is not an easy task due to the large number of possible interactions that could occur between the catalyst and the large variety of substrates used in the reactions. By performing NMR characterization of the ¹⁵N-labeled adduct **36** (in toluene-d₈ as a solvent), the authors have found three different species in solution: the H-bonded complex **36a**, the ion-pair complex **36b**, and the dissociated ion pair **36c** (Scheme 21a). While at 300 K only one broad ¹H-NMR signal was detectable at ca. 16.2 ppm, by lowering the temperature this signal split in three broad signals. These signals become sharper as the temperature was further decreased to 240 K, at which temperature a singlet at δ=18.16 ppm and two doublets at δ=15.50 and 11.87 ppm with ¹J_{H,N} coupling constants of 86.01 and 69.5 Hz were observed. On the basis of further characterization (1D ³¹P, ¹H INEPT, 2D ¹H, ¹⁵N HMQC and ¹H DOSY), these signals were assigned respectively to **36a**, **36b** and **36c** (Scheme 21a).

Scheme 21



As expected, the authors found that reducing the nitrogen basicity by changing the imine's substituents, the **a:b** ratio decreases. The tested substrates are reported in Table 3 together with both the **a:b:c** relative amount of each species for each salt.

Table 3



salt	a	b	c
36	0.38	0.62	0.08
37	0.42	0.58	0.18
38	0.51	0.49	0.11

From Table 3 it can be observed how the ratio between the H-bond complex (**a**) and the ion pair complex (**b**) changes towards **b** quite accordingly with the imines' basicity (where the basicity order of the imine is **37** ≈ **36** > **38**). On the other hand, the relative amount of **c** with respect to **a** and **b** can be hardly rationalized. On the basis of the measured chemical shifts, the authors have also qualitatively evaluated the strength of the

involved H-bond accordingly with the studies performed by Limbach on an enzymatic system,⁴⁰ confirming that it increases as the amine basicity improves.

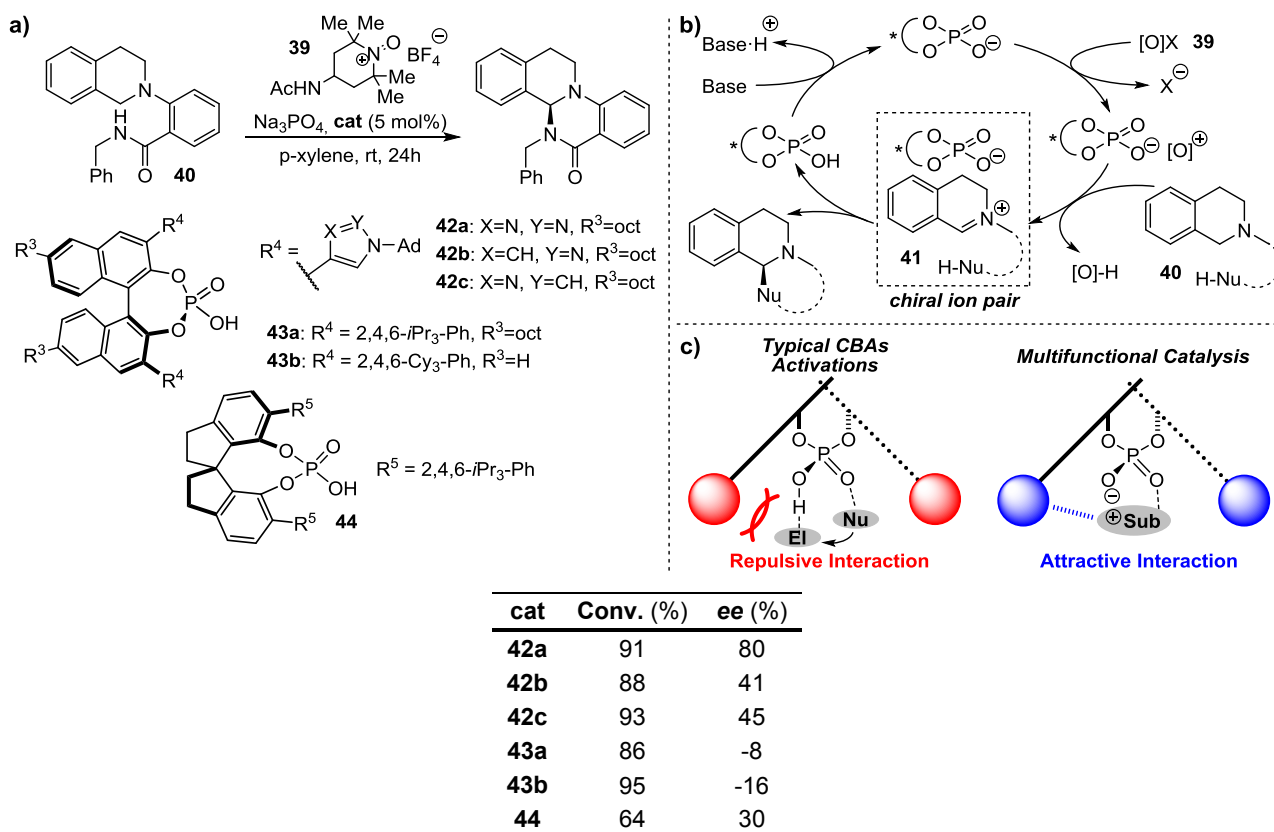
In this context, it is extremely important to be able to evaluate the ability of a catalyst to protonate, coordinate or activate a substrate. Since an iminium ion is more reactive than the relative imine, it can be pointed out that the greater is the **a:b** ratio, the more efficient is the activation of the substrate by the catalyst (Scheme 21b). At the same time, a tight ion pair is necessary to achieve higher stereoselectivities. Hence, the optimum conditions for the development of an efficient catalysis (both in terms of chemical and stereochemical activity) are related to the relative amount of the tight ion pair with respect to the H-bond complex and to the dissociated ion pair.

All the hereby presented works, in which either the acidity or the binding ability of the CBAs have been determined, give an excellent perspective on the chemical activity of Brønsted acids. On the other hand, our understanding of the factors responsible of the stereochemical outcome of stereoselective Brønsted acid catalyzed reactions is still very limited. Furthermore, the outputs of many Brønsted acid catalyzed reactions are often hard to rationalize. In this context, despite many computational investigations, especially by Goodman and Houk,⁴¹ have provided some insight on the rationalization of several reactions' mechanisms, only one experimental work published by Sigman and Toste has provided a valid experimental explanation of the strong dependence of the enantioselectivity on the catalytic system structure.⁴² Indeed, for the case study, a very small change either in the catalyst or in the substrate structure leads to a great variation of the stereoselectivity in a non-obvious way.

The original report on the studied reaction is by Toste et al.,⁴³ who in 2013 developed the asymmetric cross-dehydrogenative coupling depicted in Scheme 22a. The reaction mechanism involves oxoammonium salt **39** as an oxidant that, by the formal abstraction of an hydride from the substrate (**40**), allows the formation of intermediate **41** (Scheme 22b). Under the influence of a chiral Brønsted acid catalyst, this can undergo a stereoselective cyclization delivering the final product in an enantioenriched form (Scheme 22b). By screening a variety of catalysts, typical phosphoric acids (few examples are reported in Scheme 22a: **43** and **44**) have demonstrated to be chemically active even though inefficient from a stereochemical point of view. Hence, the authors have developed a new class of BINOL-derived compounds, where the bulky groups in the BINOL's 3,3' positions are spaced by a triazole moiety (catalysts **42a** is an example). By using this new class of catalysts, the authors were able to achieve high level of stereoselection (up to 94% *ee* for the opposite enantiomer with respect to catalysts **43**) while still maintaining a good chemical activity (38-93% yield depending on the substrate).

Toste and coworkers hypothesized that this improvement could be due not only to the different steric hindrance, but also to a cooperative coordination of the substrate by the triazole N atoms to give a "multifunctional catalysis" (Scheme 22c). To check this hypothesis a pyrazole and an imidazole substituted derivatives have been synthesized and tested (catalysts **42b-c**). These two catalysts have shown a lowered stereochemical activity, promoting the formation of the product with low *ee*. Indeed, in the table of Scheme 22 it is evident how the simple variation from a CH moiety to a N atom in catalysts **42a-c** produces the increase of the *ee* from 41 to 80%.

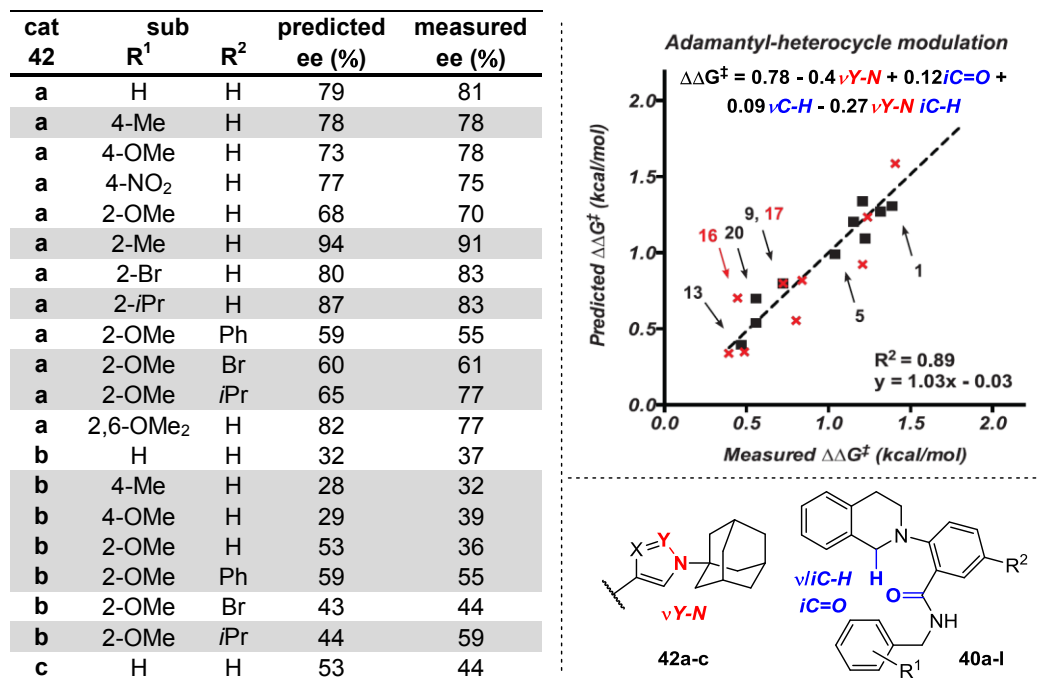
Scheme 22



In order to provide a plausible explanation for this phenomenon, Sigman and Toste envisioned a strategy for mechanistic studies involving the application of modern data analysis techniques.⁴² This approach relies on the generation of mathematical correlations between quantifiable properties describing the interacting reaction partners' molecular structures (molecular descriptors) and a measurable outcome of the reaction (for example, enantioselectivity). Indeed, the combination of appropriate experimental design, data organization, and trend analysis techniques provides the basis to distinguish causal relations, producing testable hypotheses regarding the structural origin of the reaction outcome. The use, in the case study, of this mathematical analysis previously developed in Sigman's laboratories,⁴⁴ have led to the formulation of an equation containing the parameters that mainly affect the stereoselection of the process. Within a larger study involving the determination of such parameters from a library of 9 catalysts and 12 substrates, a smaller study has addressed the influence of the spacer ring (triazole, pyrazole or imidazole) on the stereoselectivity. Here, catalysts **42a-c** were combined with 12 different substrates **40a-l** (Scheme 23) for a total 36 possible reaction combinations, ten of which were performed as a "training set" in order to obtain the desired equation. Another set of ten reactions was used as an external validation. At the beginning a plethora of calculated vibrational modes are introduced in the starting equation as parameters in order to explore a greatest as possible chemical space. However, by fitting the equation on the observed results of the training set by a linear regression algorithm, only the included parameters that are actually supposed to participate in the stereoselective process remain. The obtained equation is reported in Scheme 23 together with the observed results. In the table the training set is highlighted in grey and in the graph with black squares. The validation set is reported as red crosses in the graph. Interestingly, the parameters that mainly induce a discrimination between the three catalysts are the stretching frequencies and intensities of the N-H

and C=O bonds of the substrate and of the Y-N bond of the spacer ring of the catalyst (Scheme 23). Remarkably, the obtained model fits the real catalytic system with $R^2=0.89$, a slope of 1.03 and an intercept of -0.03, highlighting a high degree of precision and accuracy (Scheme 23).

Scheme 23



From the obtained equation, it seems that it is essential that the vibrational motions of catalyst and substrate are coupled in order to obtain the best accommodation of the substrate into the catalyst's pocket. This secures the achievement of higher stereoselection. Additional studies in the same paper extend the applied methodology to a set of 12 differently substituted catalysts, highlighting also the importance of the torsional angle between the triazole moiety and the aryl ring in a series of catalysts where the adamantyl group is substituted by different arenes.

These studies performed by Toste and Sigman shed light on the delicate balance of the interactions governing the stereoselection in CBAs catalyzed reaction, where it is of crucial importance to achieve the optimum vibrational coupling between the reaction partners and the catalyst. Certainly, further studies are needed in this field as such as in the determination of the Brønsted acid chemical activation of different electrophiles in order to achieve a good comprehension of the forces involved in this very important field of organocatalysis. This aim has guided the thesis work hereby reported.

2. Brønsted Acid Catalysis: Chemico-Physical Studies

2.1. Introduction

In the introduction of the present thesis, an overview on the concepts relative to Brønsted acid catalysis has been provided. The few works published on the topic from a chemico-physical perspective make evident the lack of information and knowledge regarding this paradigmatic mode of activation that nevertheless has found an incredibly wide application. Such studies aimed to: (i) the establishment of a pK_a scale, which can find obvious application by virtue of the Brønsted catalysis law, (ii) the characterization of the species actually involved in the catalytic process, and (iii) the determination of the factors that influence the stereochemical outcome.

The determination of the acidity of CBAs as developed by Rueping and Leito is performed with sophisticated experiments. Indeed, the use of a UV-Vis spectrophotometer within a glove-box under inert atmosphere where both H_2O and O_2 concentrations are kept below 1ppm is needed in order to reproduce the experiments as described by Leito and coworkers.³¹ Hence, in the next paragraph of this chapter a study voted to the development of a new, simpler method for the determination of the pK_a of organic Brønsted acids is presented.

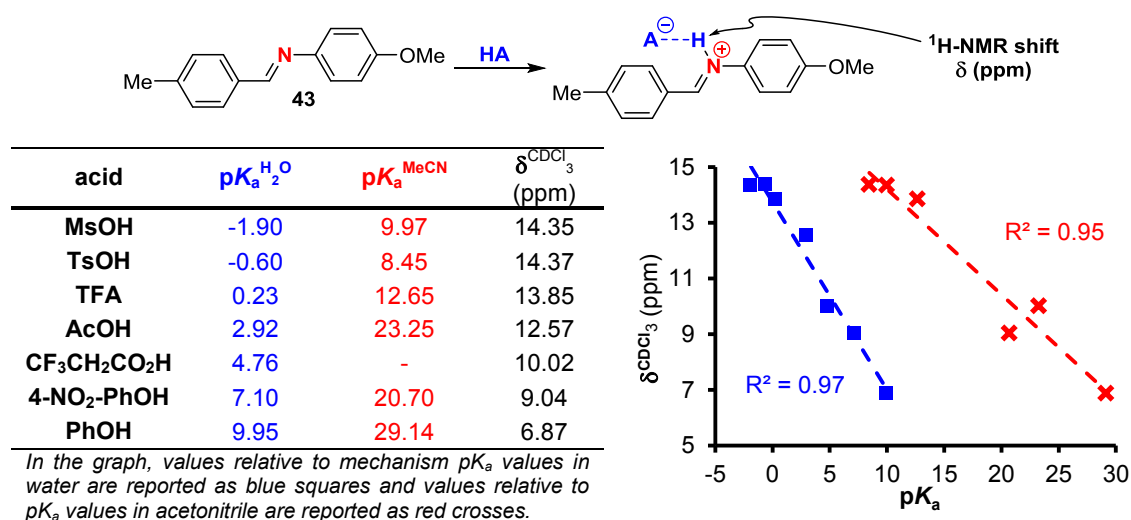
2.2. pK_a Scale of Common Brønsted Acids as Determined by 1H -NMR

NMR spectroscopy is probably the most diffuse analytical technique in organic chemistry. It allows the obtainment of a huge number of information about a chemical system and it is accessible to almost all research groups worldwide. Thus, it would be an instrument of choice for the development of new simple methods for the measurement of pK_a values. In this context, in the '70s Gutmann reported the establishment of a Lewis acidity/basicity scale by measurement of the ^{31}P -NMR shifts of the complexes between several Lewis acids and a standard Lewis base (tributylphosphine oxide).⁴⁵

Similarly, we thought that it may be possible to achieve a Brønsted acidity/basicity scale using a Brønsted pair instead of a Lewis pair. Furthermore, it would be even more attracting the possibility to use a common substrate for Brønsted acid catalysis, such as imines, as a reference base on which assess such a scale. Starting from these considerations, we found that a linear correlation is present between the strength of the acid and the chemical shift of the mobile proton of its salt with an organic base at room temperature. More specifically, the 1H -NMR chemical shifts of the acidic proton of several Brønsted acids in the presence of imine **43** have been recorded. The chosen acids are representative of three functional groups: phenols, carboxylic acids and sulfonic acids; indeed, these acids span a quite huge range of $pK_a^{H_2O}$ values, that is from 9.95 for phenol up to -1.90 for methanesulfonic acid in water.

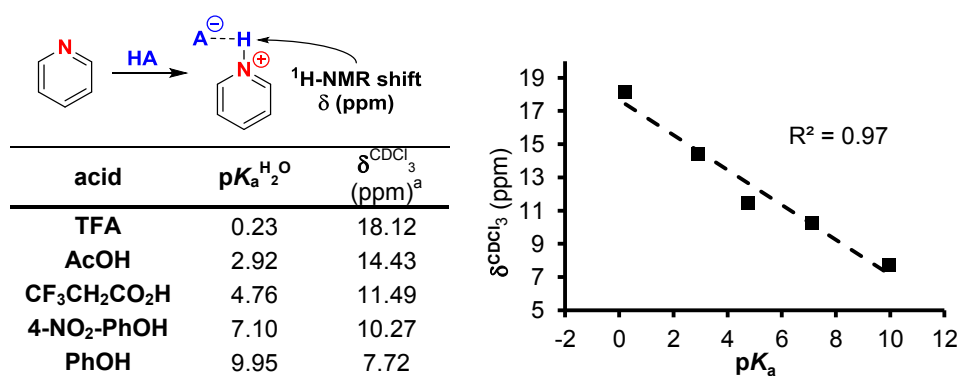
The measurements have been made in chloroform-*d* on a 0.3 M 1:1 mixture of the two Brønsted partners. The observed chemical shifts are reported in Scheme 24. They exhibit a good linear correlation with the pK_a values reported in the literature both in water and in acetonitrile, with R^2 values of 0.97 and 0.95 respectively (Scheme 24).

Scheme 24



As a validation experiment we also used pyridine, a stable base, with a pK_b value similar to that of imines. Unfortunately the pyridinium salts of sulfonic acids exhibit poor solubility in $CDCl_3$, thus preventing the reliable determination of chemical shifts. In Scheme 25 the data obtained by determination of the chemical shift of five different pyridinium salts are reported. Even in this case a good correlation with the pK_a values in water is obtained ($R^2=0.97$).

Scheme 25

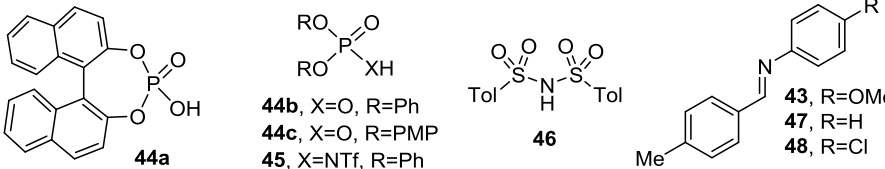


As shown in the first chapter of this thesis, the acidic functional groups mainly used in catalysis are phosphoric acids (PAs), N-triflyl phosphoramides (NTPs) and bis-sulfonylimides (BSIs). Thus, we turned our attention to the study of such compounds. We have applied our methodology to PAs **44a-c**, NTP **45** and BSI **46**. The measurements have been taken using three different solvents: chloroform-*d*, acetonitrile-*d*₃ and benzene-*d*₆, which are representative of the most used solvents in Brønsted acid catalysis. However, due to the poor solubility of the generated salts in benzene, we report in Table 4 only results relative to the first two solvents, that is $CDCl_3$ and CD_3CN .

In order to extend the scope of the methodology we tested three imines bearing differently *N*-aryl groups, which are characterized by an increasing *N*-basicity. Imine **43**, bearing a 4-OMe-Ph group should feature higher basicity than imine **47** and **48** respectively, which present a Ph or a 4-Cl-Ph group (Table 4). It is important to specify that the pK_a values of acids **44a-c** and **45** have never been determined, hence, as

reference values, we take the pK_a^{MeCN} ranges provided by Rueping and Leito: 12.5-14.0 for PAs and 6.3-6.9 for NTPs.³¹

Table 4



44a, **44b**, **44c**, **45**, **46**, **43**, **47**, **48**

acid	imine	pK_a^{MeCN}	δ^{CDCl_3} (ppm)	δ^{MeCN} (ppm)
44a	43	12.5-14.0	15.4	- ^a
44b	43	12.5-14.0	15.8	13.2
44c	43	12.5-14.0	15.3	13.5
45	43	6.3-6.9	12.9	14.1
46	43	12	12.4	10.4
44b	47	12.5-14.0	14.3	14.5
45	47	6.3-6.9	13.4	12.9
46	47	12	13.5	11.0
44b	48	12.5-14.0	13.6	11.8
45	48	6.3-6.9	14.4	12.3
46	48	12	- ^a	- ^a

a) An insoluble salt precipitated.

Some interesting considerations may be done about the observed values of chemical shifts. Despite **45** and **46** exhibit a higher acidity with respect to **44a-c**, the expected trend for the chemical shifts is reversed. Indeed, according to the correlation between pK_a and δ found in Scheme 24, we would expect salts **45•43** and **46•43** to present a δ value greater than 15.8 in chloroform. Interestingly, the trend is partially respected only in acetonitrile, where the *N*-triflyl phosphoric amide's salt **45•43** gives a δ value higher than 13.5 found for **44c•43**. However, the **46•43** salt's chemical shift still remain much lower than for **44c•43** even in acetonitrile. (ii) By lowering the basicity of the imine on passing from **43** to **47**, the $\Delta\delta$ value between salts **45•47**, **46•47** and **44b•47** is lowered. Moreover, further changing the base from **47** to **48**, the expected trend between **44b** and **45** seems to be restored in both the solvents (unfortunately salt **46•48** is insoluble in all the used solvents, so only few data are available for imine **48**).

By comparing the chemical shift of **44a-c•43** with data reported in Scheme 24, one finds that the values observed for PAs are higher than expected. Hence, while common Brønsted acids in Scheme 24 and 25 exhibit a defined and rational behavior, other acidic compounds such as **44a-c**, **45** and **46** give totally unexpected results which can be hardly rationalized without further studies. Thus, we moved towards additional experiments which are presented in the next paragraph.

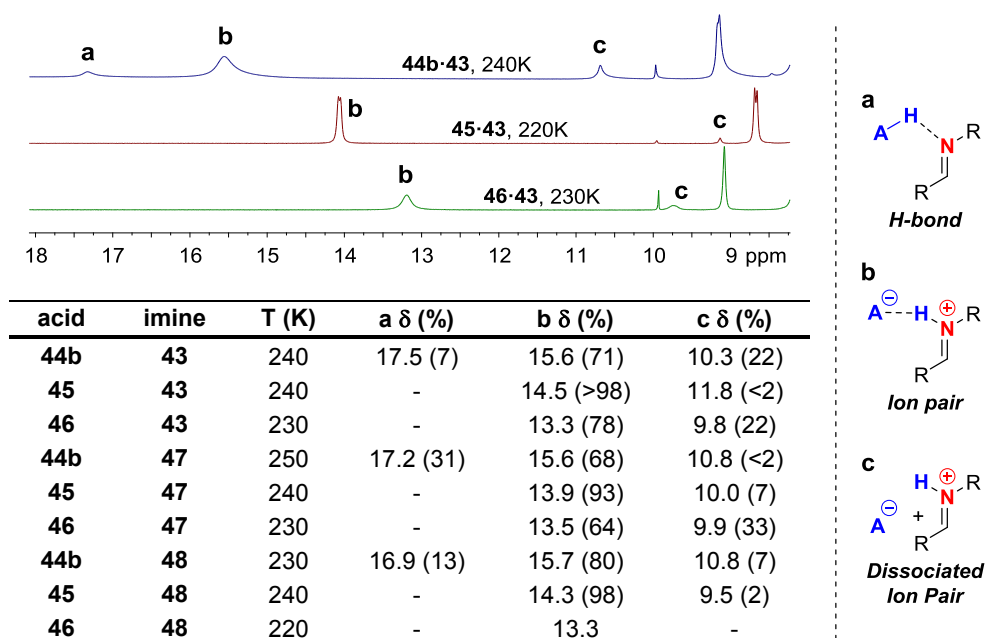
2.3. Low Temperature NMR experiments

An explanation for the unexpected reversal of the chemical shifts of **44a-c** with **45** and **46** may be found by exploring the nature of the observed NMR signal (the signal of the salts' mobile proton). In agreement with the low temperature NMR experiments previously reported by Rueping and Gschwind,³⁹ the measured chemical shift at room temperature is the averaged contribute of the three species reported in Scheme 21 (Chapter 1). Hence, we hypothesized that a greater counteranion's ability to be solvated could lead to a

greater contribution of the dissociated ion pair species, leading to an up-field shifting of the signal at room temperature. Indeed, NTPs and BSIs present a functional group composed by many more electronegative heteroatoms with respect to PAs. This leads to a higher delocalization of the negative charge of the counteranion that could make their salts more solvable in non-polar solvents. In order to verify this hypothesis, we performed low temperature $^1\text{H-NMR}$ experiments to evaluate the dissociation constants for the salts obtained by mixing acids **44b**, **45** and **46** with imines **43**, **47** and **48**.

Low temperature $^1\text{H-NMR}$ experiments show a picture very similar to the one reported by Rueping and Gshwind, in which the peak of the acidic proton splits in other signals due to the three contributing species: **a**, **b** and **c** (Scheme 26). In Scheme 26 the spectra of complexes deriving from **43** with the three acids in CDCl_3 (0.21 M) are reported. In the same scheme, a table shows the values obtained also with imines **47** and **48**. Only data recorded at the temperature giving the best peaks width are reported (T between 230 and 250 K).

Scheme 26



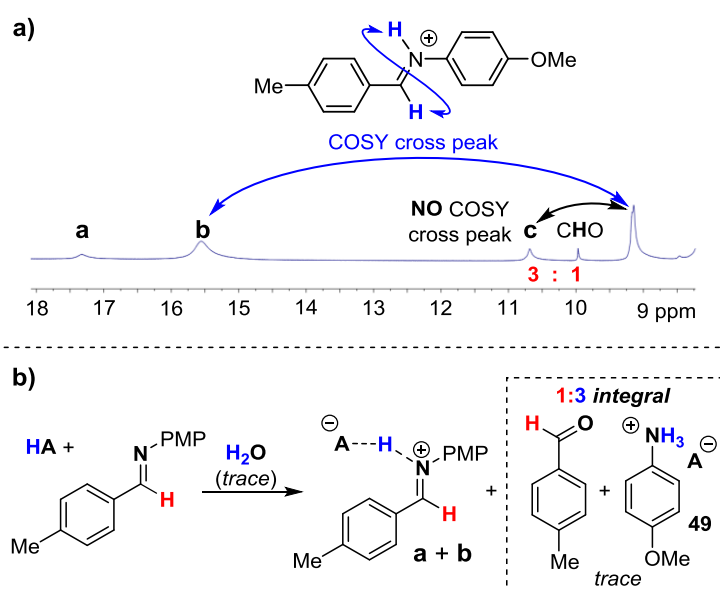
*In the table the chemical shift δ is reported for species **a**, **b** and **c** for all the salts. The integral of each signal is reported in parenthesis expressed as percentage.*

The analysis of the reported data raises several issues: (i) since for **45** and **46** no signals relative to the H-bonded species **a** are detectable for any imines, all the base present in solution should be protonated to give **b** and **c**. On the other hand, **44b** always give a mixture of the three different adducts; this data is consistent with the fact that PAs are less acidic than NTPs and BSIs. (ii) For all the reported salts, **b** is the dominating species, and the chemical shifts of **b** of the different acids still do not respect the expected acidity trend. Indeed, **45-43-b** and **46-43-b** exhibit lower δ than **44b-43-b** (14.5 and 13.3 ppm vs 15.6 ppm). Hence, the deviating behavior of these species is not due to the contribution of the different species **a**, **b** and **c** at room temperature, but is an intrinsic property of the studied salts. (iii) A confirmation of the structure of **b** can be obtained observing that the peak due to **45-43-b** presents a doublet due to the coupling with the $\text{N}=\text{C}-\text{H}$ hydrogen of the imine, thus confirming that the acidic proton resides, for most of the time, on the imine's N atom.

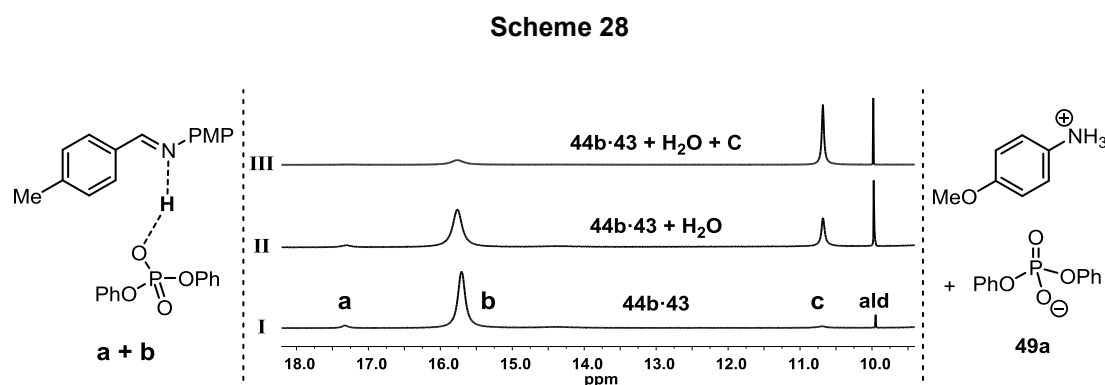
This last observation led us to perform COSY experiments to establish the presence of such spin-coupling even in other salts. The experiments showed the expected cross peak in species **b** for all the complexes; however, no signal related to the same coupling in species **c** was detected (Scheme 27a). Moreover, we noticed that small amounts of 4-Me-benzaldehyde (O=C-H signal at 9.9 ppm) were present in all the performed experiments due to partial hydrolysis of imine **43**. As a consequence, the same small amount of 4-substituted aniline must be present in solution leading to the formation of the relative anilinium salt **49** (Scheme 27b). Since integrals of species **c** for all the salts resulted to be in ca. 3:1 ratio with the CHO aldehyde peak, we hypothesized that such a species, until now supposed to be due to the dissociated iminium ion, may be actually due to the C-NH₃⁺ anilinium salt **49** resulting from the hydrolysis of the substrate.

This hypothesis is also consistent with the reported NMR analysis provided by Rueping and Gschwind. Indeed, the attribution of the up-field peak was attributed to **c** on the basis of the following observations: (i) salts **44b**•**43-c** and **HBF₄**•**43** (which is supposed to exist almost totally in a dissociated form) have similar chemical shifts (11.87 vs 11.39 respectively). (ii) **c** has a higher diffusion coefficient than **a** and **b** (calculated through DOSY experiments). However, the great variability of the chemical shift of the peak under exam by changing the counteranion that we have observed (compare **44b**•**43-c**, **45**•**43-c** and **46**•**43-c**, that present δ ranging from 9.8 to 11.8 ppm) is not consistent with the first scenario proposed by the authors; moreover, also the anilinium salts' chemical shifts can lie around such values (9-11 ppm). Furthermore, since anilinium salt **49** is smaller than adducts **a** and **b** due to the loss of a 4-Me-benzaldehyde molecule, it should present lower diffusion coefficient consistently with the observations by Rueping and Gschwind. Finally, we have also observed different relative amount of **c** depending on the batches of the synthesized acid **44b** with a same imine. This is inconsistent with the fact that the **a**:**b**:**c** ratio is a thermodynamic property of the system which depend uniquely on the relative stability of the three species. On the other hand, batches with different residual water content would explain this behavior.

Scheme 27



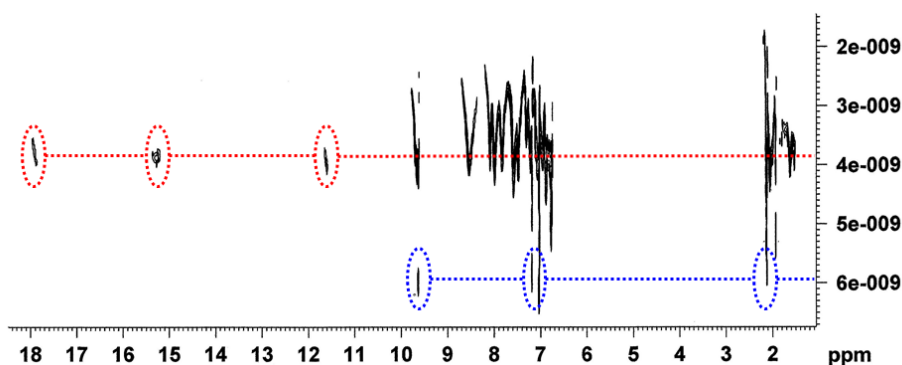
To further verify our hypothesis, we acquired the low temperature $^1\text{H-NMR}$ spectrum of salt **44b**·**43** in dry conditions. From the spectrum the presence of only small amounts of aldehyde (**ald**) and **c** are detectable (Scheme 28, spectrum I). However, the addition of a small amount of non-dry solvent resulted in the increase of the integral of such species with a **ald**:**c** ratio 1:3 (Scheme 28, spectrum II); notably, the integral of the newly formed species **c** is not redistributed in **a** and **b**, thus proving that **c** is not in thermal equilibrium with **a** and **b**. Moreover, the further addition of a solution of preformed 4-anisidinium phosphate **49a** to the mixture resulted in an increase of the high field peak **c**, thus confirming our hypothesis (Scheme 28, spectrum III).



As a last additional point supporting our hypothesis, we specify that DOSY experiments performed by Rueping and Gschwind have been done at different temperature by observing the diffusion of the methyl groups signal of the tolyl moiety (as the peaks of the mobile proton were unsuitable for this purpose) of species **a**, **b** and **c** of salt **44b**·**47** (see supporting information of ref. 31). Interestingly, they claim that at 300 K (a temperature at which **a**, **b** and **c** all coalesce in one peak) two methyl moieties are detectable; one was attributed to **a**+**b** (with diffusion coefficient $D_{a+b}^{300K}=2.69\cdot 10^{-10}$ m²/s), whereas the second to **c** (with diffusion coefficient $D_c^{300K}=3.92\cdot 10^{-10}$ m²/s). By lowering the temperature down to 240 K a similar picture was found. However, at 220 K the authors found a peak separation good enough to perform the experiment on the different methyl groups. Thus, they report the following diffusion coefficients: $D_a^{220K}=2.22\cdot 10^{-10}$ m²/s, $D_b^{220K}=2.15\cdot 10^{-10}$ m²/s and $D_c^{220K}=3.82\cdot 10^{-10}$ m²/s. Hence, as expected, similar diffusion coefficients were obtained for **a** and **b**.

In order to get additional information, we performed the same DOSY experiments that Rueping and Gschwind did (by using the same solvent and concentration: 0.1 M **44b**·**47** in toluene-*d*₈). We found that at 300 K two methyl peaks were detectable: one due to the coalesced Brønsted adducts and the second due to 4-Me-benzaldehyde. By lowering the temperature to 220 K, diffusion coefficients of the same order of magnitude reported by Rueping and Gschwind were recorded. However, while species **a**, **b** and **c** were found to diffuse with roughly the same rate (that is reasonable as the three species are in equilibrium), 4-Me-benzaldehyde was the only compound present in solution which showed higher D^{220K} (see the 2D spectra in Scheme 29). Unfortunately, due to a non-optimal peaks' separation, a quantitative determination of D^{220K} was impossible; however, from the reported 2D spectrum, values of $D_{a+b}^{220K}=4\cdot 10^{-9}$ m²/s and $D_{\text{CHO}}^{220K}=6\cdot 10^{-9}$ m²/s can roughly be extrapolated.

Scheme 29



Hence, in our opinion, the experimental observations by Rueping and Gschwind and by our research group, suggest that the actual species arising from the Brønsted acid activation of imines (a typical substrate in Brønsted acid catalysis) are only the H-bond complex **a** and the ion pair **b**. The dissociated ion pair **c** is not detectable, being disfavored in non-polar solvents, and others previously reported conclusions by other authors might have raised from a misleading interpretation of the experiments due to the intrinsic complexity of the system.

These conclusions are not trivial and bear some strong consequences on the interpretation of Brønsted acid catalysis activation. As long as the peak of the anilinium salt is attributed to the dissociated iminium salt **c**, one may dissert about the influence of such dissociation on the stereoselectivity of the catalytic process. Thus, one could be involved in the useless search of a catalyst which minimizes the contribute of the species **c** with respect to **a** and **b**. Instead, one should just focus his research towards the finding of catalysts able to give the lowest possible **a:b** ratio, which indicates a better chemical activation of the system. In fact, in our opinion, no information regarding the stereochemical induction of an acidic chiral catalyst can be done by performing the low temperature NMR experiments here presented.

The conclusions reported in this paragraph also give some useful insight for a better interpretation of the results obtained in the attempt to assess a NMR based pK_a scale. Indeed, the observed chemical shifts may depend on several, concomitant factors: the different inductive effect of the O atom with respect to the N atom, the different steric hindrance and the different Lewis basicity of the resulting anion, the relative hardness/softness of the ion pairs, etc. Thus, we cannot consider reliable a NMR pK_a scale that comprehends all acids with a same base as a reference totally neglecting the different nature of the tested acids. It would be otherwise more reasonable to assess different scales based on acids of the same class (with similar functional groups).

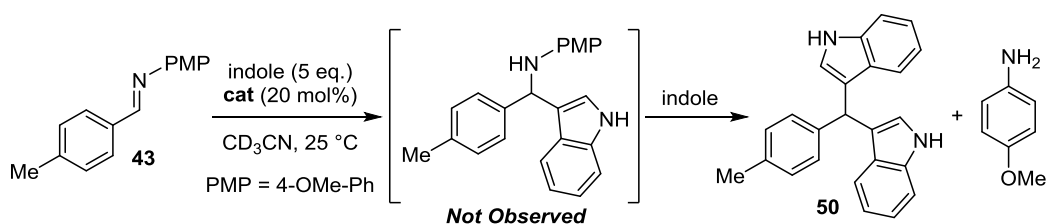
2.4. The Acidity:Activity Dualism: Kinetic Experiments

The proportionality between the acidity of a catalyst and its ability to activate chemical reactions is a well-established topic which has also been mathematized with the Brønsted catalysis law.³⁴ In the context of chiral Brønsted acid catalysis, Rueping has shown the validity of this law by finding a linear correlation between the measured pK_a of several CBAs and the reaction rate of a catalyzed Nazarov cyclization (see Chapter 1).³²

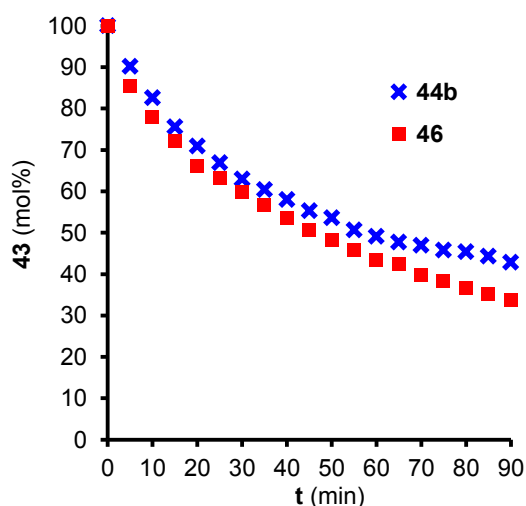
In order to find a similar correlation for the acid activation of imines, we have performed some kinetic experiments. It must be pointed out that this reaction may be affected by product-inhibition, indeed, the addition of a nucleophile to an imine generates an amine which may be involved in an acid-base reaction with the acidic catalyst thus quenching the reaction. In order to take into account this undesired drawback, we performed the reaction both with *N*-aryl imines and with *N*-tosyl imines,⁴⁶ which present a reduced basicity at the product's nitrogen (a sulfonamide). The chosen model reaction is the indole alkylation in Scheme 30. Indole was used in large excess (5:1 ratio, where the electrophile is the limiting reagent). The catalyst loading was fixed at 20 mol%.

The reaction profiles have been obtained by monitoring the reaction by ¹H-NMR and acquiring a spectrum every 5 minutes. The reactions have been performed in CDCl₃, CD₃CN and C₆D₆ at a concentration of 0.1 M. As similar results have been found for the different solvents, we here report only the profiles obtained in acetonitrile. In Scheme 30 the profiles of the reaction involving imine **43** catalyzed by acids **44b** and **46** are reported; no graph is reported for the reaction catalyzed by **46** as it was completed in less than 5 minutes. The only observed species during the reaction are the starting material **43** and the product relative to the attack of two indole molecules to the imine **50**, leading to the delivery of one molecule of 4-anisidine (Scheme 30). Thus, of the two reaction steps involved, the first is the rate determining one.

Scheme 30



t (min)	cat 44b 43 (mol%)	cat 46 43 (mol%)
0	100.0	100.0
5	90.2	85.5
10	82.6	78.0
15	75.6	72.1
20	70.9	66.1
25	66.9	63.1
30	63.0	59.8
35	60.4	56.6
40	58.0	53.5
45	55.3	50.6
50	53.6	48.1
55	50.7	45.7
60	49.1	43.5
65	47.7	42.3
70	47.0	39.7
75	45.8	38.4
80	45.4	36.5
85	44.3	35.2
90	42.9	33.7



The rate of the different reactions reflects the acidity of the catalytic species (**45**>**46**~**44b**) showing correspondence with the common acidity-activity dualism typical of to this type of catalysis. In particular, the reactions promoted by **45** proceed in less than 5 minutes, while the reactions promoted by **44b** and **46**

proceed with similar rates, according with the small difference in their pK_a measured by Rueping and Leito (12.5-14.0 and 12 respectively). The reaction has been performed also with imines **47** and **48** (*N*-Ph and *N*-4-Cl-Ph imines of 4-tolualdehyde), which show higher rates but the same qualitative trend (**45** > **46** ≈ **44b**).

As stated before, for the reaction depicted in Scheme 30 a reaction inhibition by products can be hypothesized. In order to experimentally confirm such a reasonable hypothesis, we have derived the kinetic equation of the present system assuming no catalyst's interactions with reagents and products, hence, the reaction can be simplified as follow:



Since the intermediate product is non-detectable by NMR spectroscopy (that is $k' \gg k$), by using the stationary intermediate approximation, the system of differential equations is:

$$\begin{cases} -\frac{d[43]}{dt} = [43][\text{Ind}]k \\ -\frac{d[\text{Ind}]}{dt} = [43][\text{Ind}]k + [\text{Int}][\text{Ind}]k' \\ -\frac{d[\text{Int}]}{dt} = [\text{Int}][\text{Ind}]k' - [43][\text{Ind}]k \cong 0 \\ \frac{d[50]}{dt} = [\text{Int}][\text{Ind}]k' \cong [43][\text{Ind}]k = -\frac{d[43]}{dt} \end{cases}$$

By considering that because of the stoichiometry of the reaction in each moment $[\text{Ind}] = [\text{Ind}]_0 + 2([\text{43}] - [\text{43}]_0)$, where $[\text{Ind}]_0$ and $[\text{43}]_0$ are the concentration of indole and imine **43** at the beginning of the reaction (that is at $t=0$), one gets the equation:

$$-\frac{d[43]}{dt} = [43]([\text{Ind}]_0 - 2[\text{43}]_0 + 2[43])k$$

Which can be analytically integrated by partial fraction as follow:

$$\int \frac{d[43]}{[43]([\text{Ind}]_0 - 2[\text{43}]_0 + 2[43])} = - \int k dt$$

$$\frac{1}{[\text{Ind}]_0 - 2[\text{43}]_0} \left[\ln \left(\frac{[43]}{2[43] + [\text{Ind}]_0 - 2[\text{43}]_0} \right) - \ln \left(\frac{[\text{43}]_0}{[\text{Ind}]_0} \right) \right] = -kt$$

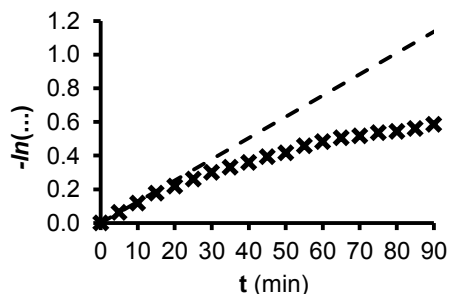
After rearranging the equation one gets the final expression:

$$-\ln \left(\frac{[43][\text{Ind}]_0}{(2[43] + [\text{Ind}]_0 - 2[\text{43}]_0)[\text{43}]_0} \right) = ([\text{Ind}]_0 - 2[\text{43}]_0)kt$$

By inserting the experimentally obtained concentrations of **43** during time in the left member of the equation we obtained the values that we denote as $-\ln(\dots)$. By plotting such values against the time we extrapolated Graph 1. Accordingly with the equation, the plot should result in a straight line with angular coefficient $([\text{Ind}]_0 - 2[\text{43}]_0)k$ and intercept equal to zero. However, we rather obtain a curve which underestimates the mathematical prevision, consistently with the fact that the kinetic constant, which can be expressed as $k = k_0 + k_{\text{cat}}[\text{cat}]$, decreases during time due to catalysis inactivation by product formation (Graph 1). In the following graph a line is reported which is obtained by prediction of the line interpolating the first two point of

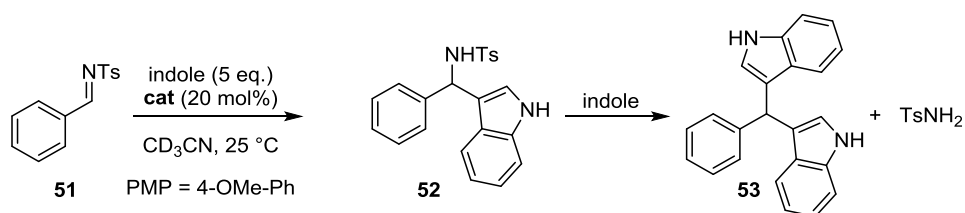
the curve, where the catalysis inactivation is less significant because of the low amount of product generated; such a line predicts which profile the function $-\ln(\dots)$ would have had if the reaction had not been affected by catalyst's quenching.

Graph 1

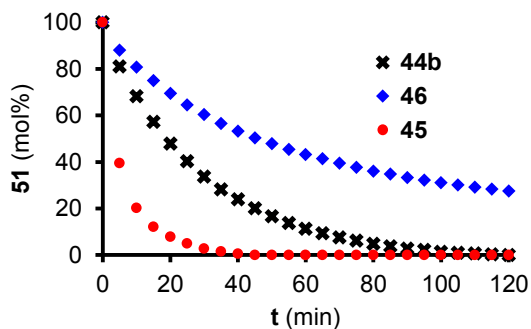
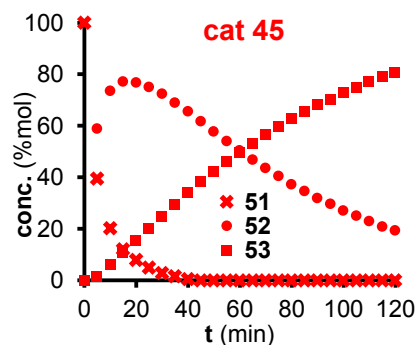
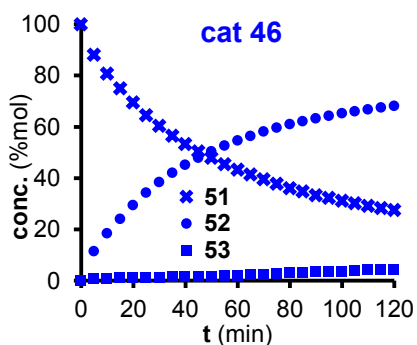
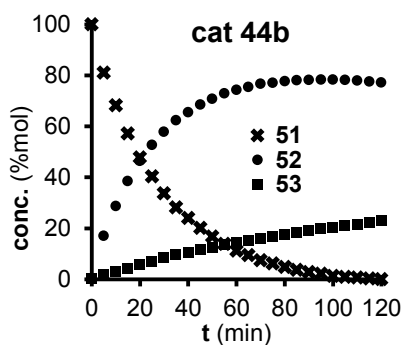


We have also performed kinetic experiments with a *N*-tosylimine instead of *N*-arylimines. Interestingly, a deviation from the expected reactivity is found when **51** is used. While NTP **45** still provides the fastest reaction, **44b** and **46** exhibit a substantially different reactivity where the PA gives an higher rate with respect to the BSI by a factor ca. 2.7 (compare imine half-life time: ca. 20 min for **44b** vs ca. 55 min for **46**). In Scheme 31 the reaction profiles are reported for each acid, showing the disappearance of imine **51** and the appearance of products **52** and **50**. In the same scheme, a graph comparing the disappearance of the imine for the three reactions is reported.

Scheme 31



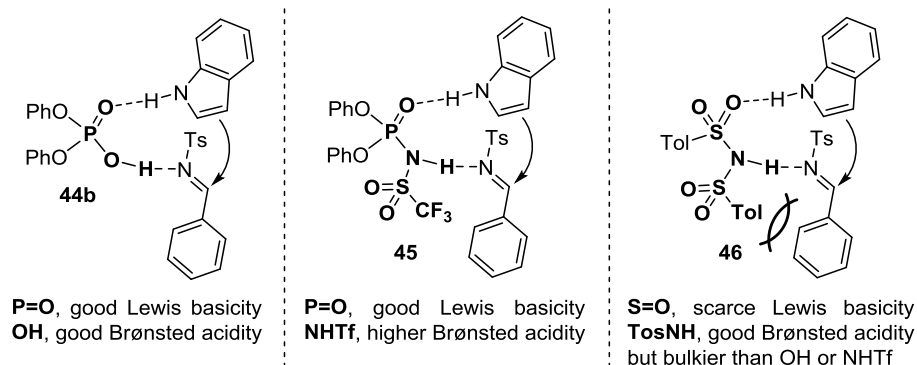
t (min)	Cat 44b			cat 46			cat 45		
	51 (%)	52 (%)	53 (%)	51 (%)	52 (%)	53 (%)	51 (%)	52 (%)	53 (%)
0	100.0	0.0	0.0	100.0	0.0	0.0	100.0	0.0	0.0
5	81.0	17.0	2.0	88.1	11.4	0.6	39.5	1.6	58.9
10	68.3	28.7	3.0	80.8	18.5	0.8	20.2	6.2	73.6
15	57.2	38.4	4.3	74.9	24.1	1.0	12.0	10.9	77.1
20	47.8	46.3	5.8	69.5	29.4	1.1	7.9	15.4	76.7
25	40.3	52.7	7.0	64.5	34.3	1.2	5.0	20.0	75.0
30	33.6	57.8	8.5	60.3	38.4	1.3	2.8	24.9	72.4
35	28.2	62.3	9.5	56.5	42.1	1.5	1.6	29.5	69.0
40	24.0	65.5	10.5	53.3	45.2	1.5	0.5	34.0	65.5
45	20.1	68.4	11.5	50.4	47.9	1.7	0.0	38.3	61.7
50	16.7	70.8	12.5	47.9	50.3	1.7	0.0	42.3	57.7
55	13.8	72.9	13.3	45.4	52.6	2.0	0.0	46.0	54.0
60	11.3	74.3	14.5	43.2	54.7	2.1	0.0	49.6	50.4
65	9.4	75.4	15.2	41.3	56.4	2.3	0.0	53.2	46.8
70	7.5	76.6	15.9	39.5	58.1	2.4	0.0	56.4	43.6
75	6.1	77.0	16.8	37.7	59.6	2.6	0.0	59.6	40.4
80	4.8	77.7	17.5	36.0	61.0	3.0	0.0	62.7	37.3
85	3.7	78.0	18.2	34.8	62.1	3.1	0.0	65.3	34.7
90	2.8	78.2	19.0	33.3	63.3	3.4	0.0	68.1	31.9
95	2.1	78.2	19.6	32.2	64.3	3.5	0.0	70.3	29.7
100	1.3	78.3	20.4	31.1	65.2	3.6	0.0	72.9	27.1
105	1.0	78.1	20.9	30.1	66.0	3.9	0.0	74.9	25.1
110	0.6	77.9	21.5	29.2	66.7	4.1	0.0	77.1	22.9
115	0.3	77.6	22.2	28.3	67.5	4.2	0.0	79.1	20.9
120	0.0	77.1	22.9	27.5	68.1	4.4	0.0	80.7	19.3



As previously stated, the data reported in Scheme 31 contrast with the common knowledge that stronger the acid, the higher its catalytic activity. Hence, it is clear that factors other than acidity seem to affect the reaction. According with the proposed reaction mechanism,⁴⁶ both steric hindrance and the Lewis basicity of the catalyst's coordinating site may be responsible for such unexpected behavior. Indeed, the reaction involves a bifunctional activation of the substrates (as described in Chapter 1 and Scheme 32), and it can be stated that a better coordinating ability of the catalyst towards the N-H moiety of indole may results in a higher catalytic efficiency.

In this context, the three functional groups of catalysts **44b**, **45** and **46** present radically different properties. **45** and **46** are stronger acids than **44b**, but at the same time **44b** and **45** have a good coordinating ability due to the presence of a P=O group, which is a better Lewis base than the S=O moiety of BSI **46**. Additionally, **46** could be considered more sterically hindered than both **44b** and **45**, by virtue of the conformational disposition of the bis-sulfonylimidic moiety (Scheme 32).

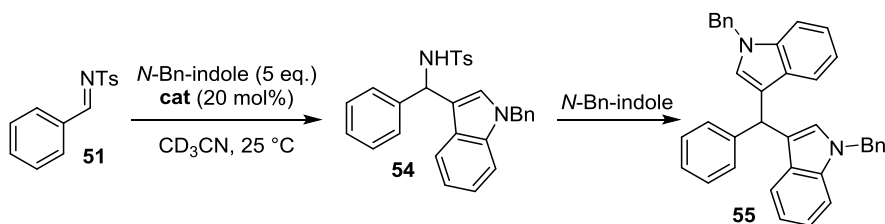
Scheme 32



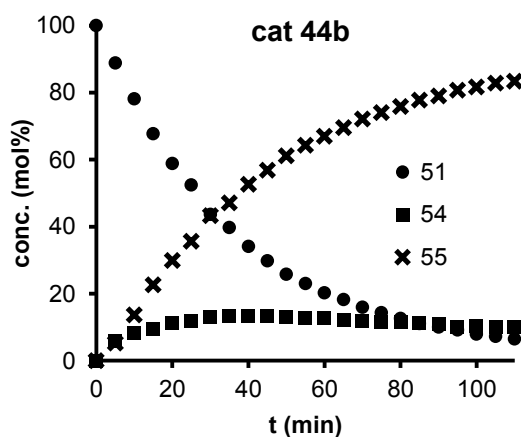
In order to verify whether the Lewis basicity or the steric hindrance are responsible for the observed inverted reactivity, the performed kinetic experiments involving imine **51** were repeated with *N*-benzylindole. The elimination of the H-bond site on the nucleophile, by substitution of the proton with a benzyl group, prevents the coordination to the catalyst, and in addition increases the indole's size emphasizing possible steric effects. In other words, the involved operating mechanism changes from a bifunctional activation to a mono-activation (see Chapter 1).

The results obtained by the reaction between *N*-benzylindole and *N*-tosylimine **51** are reported in Scheme 33 for both catalysts **44b** and **46** (**45** gave reaction times shorter than 5 minutes). Notably, the reaction profile of the reactions involving the two catalysts are even much more differentiated. While the reaction catalyzed by **44b** proceeds in only a slightly slowed rate with respect to the same reaction involving the N-H indole (ca. 25 vs 20 min of imine's half-life time), we find that for catalyst **45** the reaction rate is ca. 72 times greater (25 vs 1800 min of imine's demi-life time) (Scheme 33, note the time scale in tables and graphs).

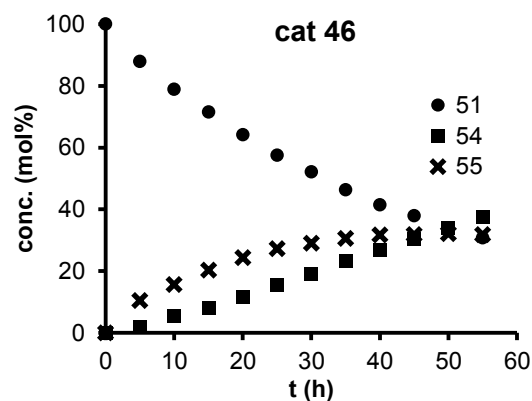
Scheme 33



t (min)	cat 44b		
	51 (mol%)	54 (mol%)	55 (mol%)
0	100	0.0	0.0
5	88.8	5.9	5.2
10	78.1	8.2	13.7
15	67.8	9.6	22.7
20	58.9	11.2	29.9
25	52.5	11.9	35.7
30	43.6	13.1	43.3
35	39.8	13.1	47.1
40	34.1	13.3	52.6
45	29.8	13.4	56.9
50	25.8	13.1	61.1
55	23.0	12.7	64.3
60	20.3	12.8	67.0
65	18.2	12.2	69.5
70	15.9	12.0	72.1
75	14.3	11.7	74.0
80	12.6	11.6	75.8
85	11.1	11.2	77.7
90	10.0	11.0	79.0
95	9.1	10.2	80.7
100	8.0	10.4	81.7
105	7.3	9.9	82.8
110	6.5	10.1	83.4



t (h)	cat 46		
	51 (mol%)	54 (mol%)	55 (mol%)
0	100.0	0.0	0.0
5	87.9	10.4	1.7
10	78.8	15.6	5.6
15	71.6	20.3	8.2
20	64.1	24.4	11.5
25	57.5	27.2	15.3
30	52.1	29.0	18.9
35	46.4	30.6	23.1
40	41.4	31.8	26.8
45	37.9	31.8	30.3
50	34.0	32.1	34.0
55	30.8	31.8	37.4



The removal of a possible coordination site for the nucleophile by substituting an H atom with a benzyl group notably improves the performance of catalyst **44b** with respect to **46**. This observation is in contrast with the fact that the P=O moiety is known to have a better coordinating ability with respect to the S=O group. Indeed, if the reaction proceeded through a relevant energetically advantageous coordination between the catalyst's basic site and the indole N-H portion, we would observe an improvement of **46**'s performance with respect to **44b**. Thus, these experiments seem to suggest that the increased steric hindrance of the nucleophile is the major responsible of the performances' difference between catalysts **44b** and **46**.

2.5. Conclusions

New investigations on chiral Brønsted acid catalysis have been performed and presented in this chapter of the thesis work. First studies have been aimed to assess a NMR pK_a scale by the correlation of the chemical shifts of the complexes generated by different acidic compounds and a standard base (imines and pyridine were used), with the known pK_a of some common acids. Despite promising results were obtained using phenols, carboxylic acids and sulfonic acids, the new developed method have not proved to be useful for the treatment of other functional groups usually present in CBAs (that is PAs, NTPs and BSIs).

Low temperature $^1\text{H-NMR}$ experiments devoted to explaining of the reasons for this deviation from the expected behavior have been performed in line with previous reports by Rueping and Gschwind. These studies have led to the exclusion of the dissociated ion pair among the known species involved in the acidic catalysis, thus highlighting that the actually observed species are the H-bond complex and the ion pair adduct. This observation may have a strong impact on the rationalization of stereochemical outcome.

These experiments have also shown that major deviation from the chemical-shift/ pK_a trend are probably due to an intrinsic property of the system, that is to the nature of the atom directly bearing to the mobile proton. Hence, we stated that the establishment of a NMR pK_a scale may be feasible only for acidic compounds which present similar functional groups. In order to confirm this hypothesis, in our research group, the establishment of a pK_a scale by using N-H acids is in progress.

We then turned our attention towards kinetic experiments that may confirm the acidity/activity dualism as previously done by Rueping and Leito. We have found that Brønsted acid catalysis obeys to the Brønsted catalysis law depending on the substrate. Indeed, steric effects seem to play a key role in the catalytic process depending on the chosen imine; on the other hand, in the studied reactions the catalyst's ability to coordinate the nucleophile was found to be of minor importance. In order to further verify the influence of the hereby supposed steric effects, the synthesis of other less steric demanding BSIs is ongoing in our research group.

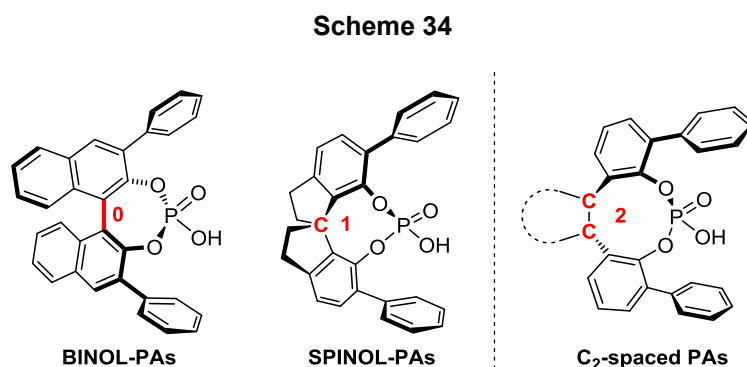
3. Development of New Chiral Brønsted Acid Catalysts

3.1. Introduction

As described in the introductory chapter, CBAs have been widely employed as catalysts able to promote a huge number of reactions in a stereoselective fashion. The existing catalysts of this class are almost uniquely based on either BINOL or SPINOL scaffolds, and both of them are characterized by the presence of stereogenic axis. We decided to develop a new class CBAs based on a simple and possibly less expensive scaffold. In this chapter the results obtained in the synthesis of new derivatives which rely on *trans*-diaminocyclohexane and tartaric acid scaffolds are reported.

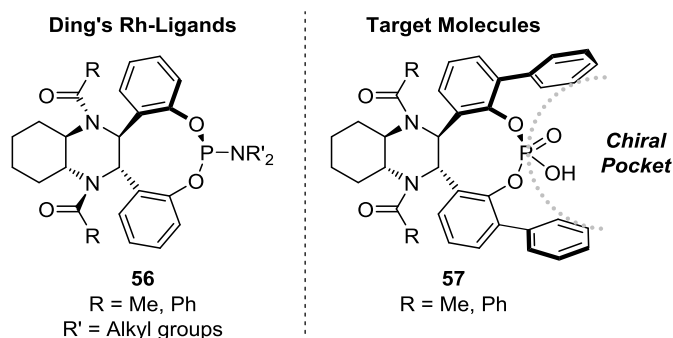
3.2. Synthesis of *trans*-Diaminocyclohexane-Derived Brønsted Acids

An important feature that characterizes efficient CBAs is their C_2 symmetry. Hence, we chose *trans*-diaminocyclohexane as a cheap starting material. By comparing the two most used chiral scaffolds for CBAs (BINOL and SPINOL) it can be noted that while the first has no spacers between the two naphthol moieties, the second presents a carbon atom which separates the two aryl rings that directly bear the acidic functional group. Thus, we wondered if it would be possible to build a scaffold characterized by a two-carbon spacer (Scheme 34).



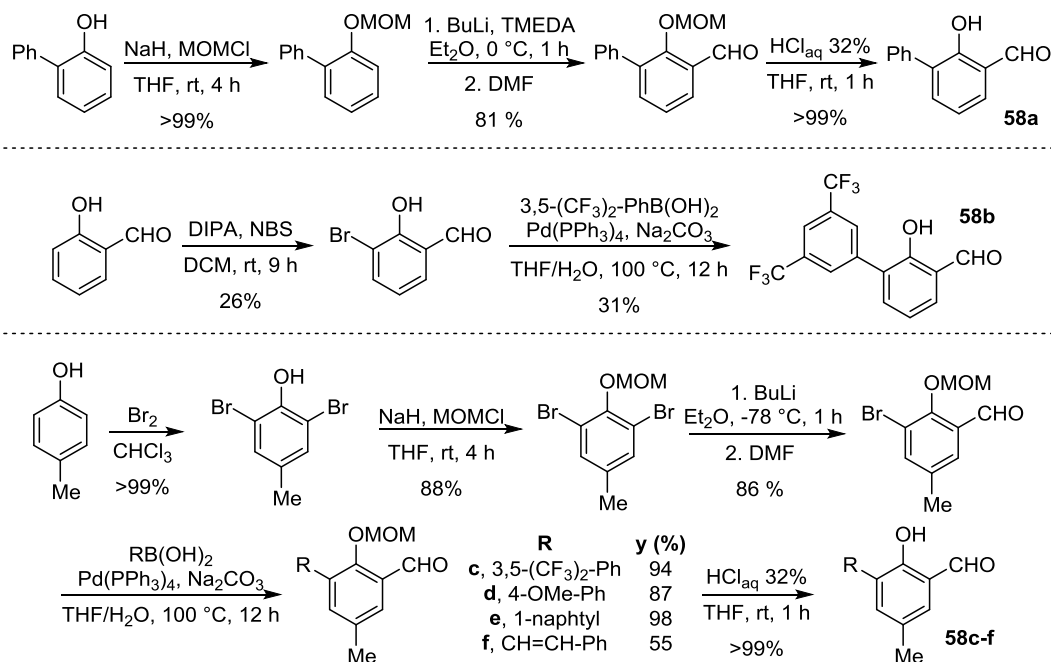
Ding et al. inspired us with their synthesis of new Rhodium monodentate ligands **56** which were efficiently used in the hydrogenation of prochiral enamides.⁴⁷ While such phosphoramidites do not present any bulky groups in the *ortho* position of the aryl ring that bring the active site, we designed the synthesis of catalysts with general formula **57**, which is characterized by an extended chiral pocket similar to that of SPINOL and BINOL PAs derivatives (Scheme 35).

Scheme 35



The synthesis requires the preparation of a properly substituted salicylaldehyde. Since this class of aldehydes are used as building blocks for the synthesis of Jacobsen's SALEN complexes, numerous methodologies exist for their obtainment. In particular, aldehydes **58** have been synthesized through different synthetic pathways as reported in Scheme 36. For example, we managed to synthesize compounds **58c-f** because of their higher synthetic accessibility with respect to aldehyde **58b**. Indeed, the selective *ortho*-bromination of phenols is a difficult issue, and the obtainment of a large amount of 3-bromo salicylaldehyde is prohibitive. On the other hand, starting from 4-cresol, selectivity is not an issue; thus, even if longer, the synthetic route to **58c-f** is much more simpler. The first synthesized aldehyde is **58a**, which was obtained starting from 2-phenyl phenol (70 €/kg from Sigma-Aldrich) on a gram scale.

Scheme 36

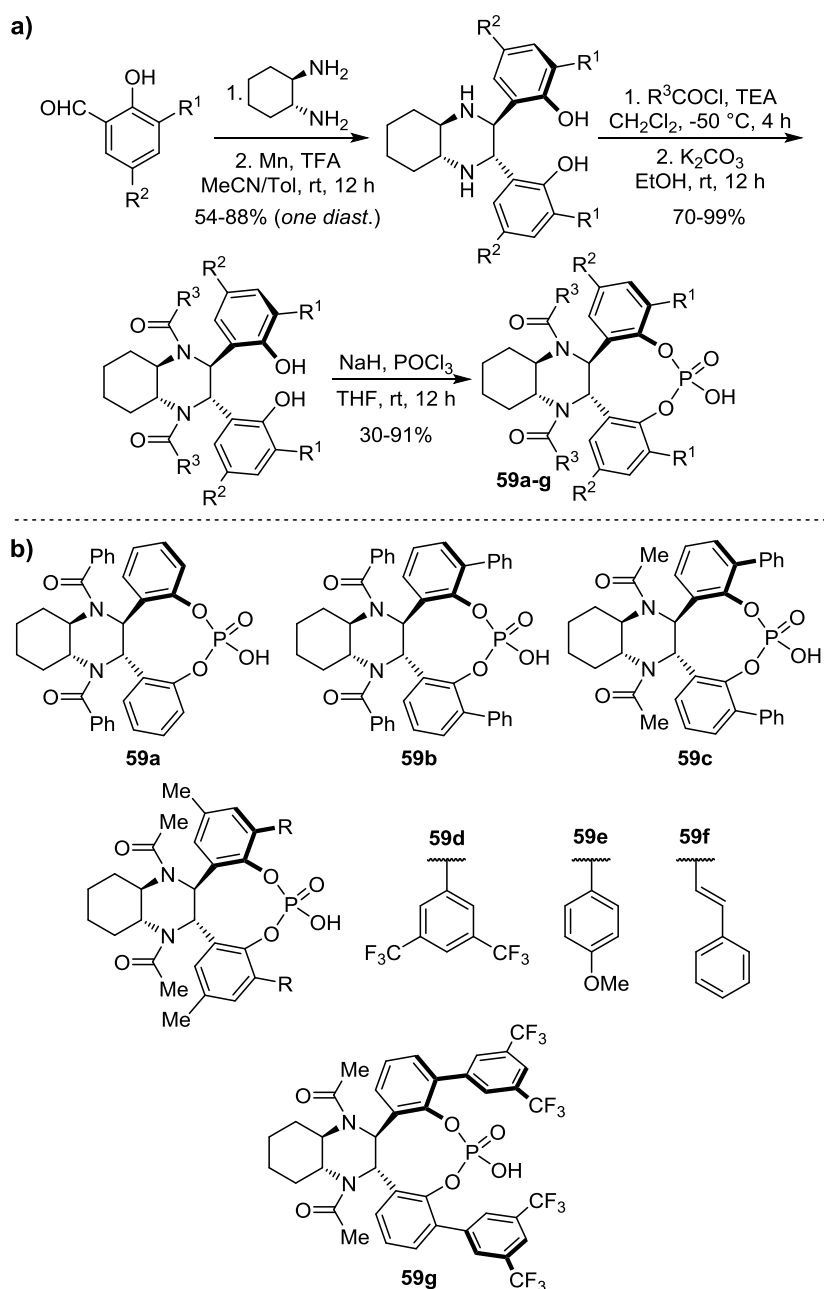


With the desired salicylaldehydes in hand, we performed the condensation with (*R,R*)-diaminocyclohexane thus obtaining the corresponding SALEN ligands, which were then treated with manganese in acidic media in order to induce the pinacol reaction accordingly with the protocol developed by Sigman et al.⁴⁸ The radical nature of this reaction prevented us to perform the reaction starting from halogenated aldehydes, which would have allowed us to obtain a common precursor to all the catalysts with a considerable reduction of the synthetic efforts. On the other hand, this coupling reaction proceeds in moderate to good yields with total

stereocontrol to give only the diastereoisomer depicted in Scheme 37. The obtained chiral diamines were efficiently protected at nitrogens as acetyl or benzoyl amides, and then the nine-membered ring closure was performed by phosphorylation with POCl₃ under basic condition to give the final catalysts **59**. This last step is strongly dependent on the steric hindrance on the phenolic aryl ring as the reactions involving more bulky diols usually proceeded more sluggishly.

The synthesis of these compounds is reported in Scheme 37a, while the final structure of all the obtained catalysts is reported in Scheme 37b.

Scheme 37

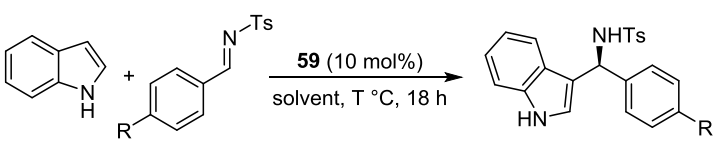


The obtained catalysts have been selected to span the widest possible chemical space. Compounds **59a-c** experience different steric hindrance in the two tunable site of the molecule; **59a** presents a bulky groups at the N atoms and no directing groups on the phenol rings. For **59c** the scenario is inverted, as two small

acetyl moieties protect the N atoms, and two phenyl groups are present on the phenolic rings to form a chiral pocket. A combination between the steric hindrance of **59a** and **59c** gives compound **59b**, which brings bulkier groups both on the N atoms and on the aromatic rings. **59d-e** have been designed to explore the effect of aryl rings with different electronic properties. Indeed, while **59d** presents two electronwithdrawing groups (CF₃), **59e** bears an electron donating group (OMe). A comparison between **59d** and **59g** can be done in order to verify the influence of the methyl in the *para*-position with respect to the phosphate group. Finally, **59f** experiences a more extended chiral pocket, as the ethylene moieties act as a spacer which remove the bulky groups from the catalytic site.

Compounds **59a-g** were tested in two typical CBA catalyzed reactions: the Friedel-Craft alkylation of indole with N-tosyl imines, and the transfer hydrogenation of ketoimines with Hantzsch esters. We first report the results obtained in the stereoselective alkylation of indole,⁴⁶ which are reported in Scheme 38.

Scheme 38



entry	59	R	solvent	T (°C)	y (%)	ee (%)
1	a	H	tol	-50	70	-37
2	b	H	tol	-50	99	60
3	c	H	tol	-50	99	74
4	c	H	tol	-20	95	61
5	c	H	tol	0	95	58
6	c	H	CH ₂ Cl ₂	-50	99	77
7		H	CH ₂ Cl ₂	-78	85	79
8	c	H	MeCN	-50	99	73
9	c	Cl	tol	-50	95	48
10	c	Me	tol	-50	no reaction	
11	c	Me	tol	-20	37	56
12	c	OMe	tol	-50	96	63
13	d	H	tol	-50	20	45
14	d	H	tol	25	92	44
15	e	H	tol	-50	61	53
16	e	H	tol	25	78	33
17	f	H	tol	-50	99	40
18	g	H	tol	-50	99	51

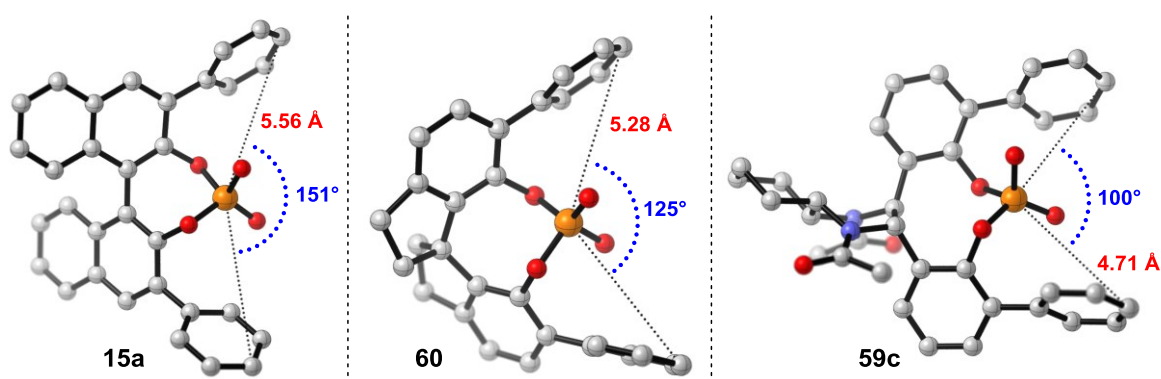
The reported data provide several information about the chiral environment generated by the catalysts. By comparing catalysts **59a-c** it is clear that inclusion of bulky groups either on the N atoms or on the phenol rings has an opposite effect on the stereoselection, indeed, **59a** and **59c** provided opposite enantiomers of the product. Since **59c** provides higher ee than **59a** (up to 79%), it seems that hindrance on the phenol moieties dominates over the one on the N atoms. Further proof of this fact is the performance of **59b**, which gives the (*S*)-product but in lower ee than **59c** by virtue of the mismatching relationship between the two operating bulky moieties (entries 1-3).

Other catalysts **59d-g** furnished lower stereoselections (40-50% ee). Thus, independently of the electronic effects, it seems that the increasing of the steric hindrance on the aryl rings has deleterious effect on the reagents' accommodation in the chiral pocket (entries 12-17), as also lower chemical activity was recorded

(entries 12 and 14); the obtainment of higher yields with catalysts **59d** and **59e** required higher reaction temperatures. Even by changing the substrate from the benzaldehyde- to the 4-tolualdehyde-derived imine, a dramatic decrease of the chemical activity is observed (entries 9-10). In other words, these data suggest that the active site is located in a too hindered portion of space thus preventing the obtainment of good stereochemical results.

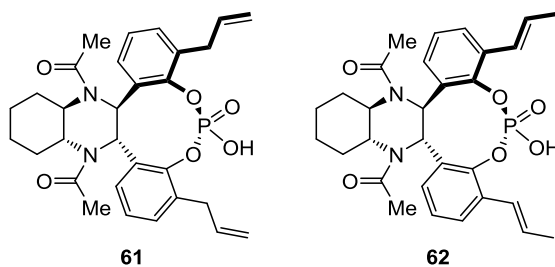
This fact can be confirmed by a comparative analysis of the optimized structures (with semi-empirical method PM6) of BINOL-derived catalyst **15a**, SPINOL derived acid **60**, and **59c** (Figure 1, all the hydrogen atoms have been removed for clarity). All these compounds bear two phenyl groups as stereodirecting elements, and differ only in the chiral scaffold. The calculated geometries indicate that passing from **15a** to **60** and then to **59c**, the chiral pocket became smaller. Indeed, by measuring the distance between the P atom and the more distant phenyl ring's carbon, the values decrease from 5.56 to 5.28 Å passing from **15a** to **60**, and then to 4.71 Å for catalyst **59c**. Analogously, the C-P-C angle (where C refers to the two farthest carbon atoms of the phenyl rings), decreases from 151 to 100°, for **15a** and **59c**, by passing from 125° for **60**. Thus, this computational analysis suggests that **59c** presents a too hindered active site which could be, in principle, responsible for its scarce stereochemical performances.

Figure 2



On the basis of this observation, our research group is now synthesizing less steric demanding catalysts, where other groups than aryl rings are attached to the *ortho*-position with respect to the phosphoric moieties. Due to their synthetic accessibility, compounds **61** and **62** will be the first tested compounds (Scheme 39).

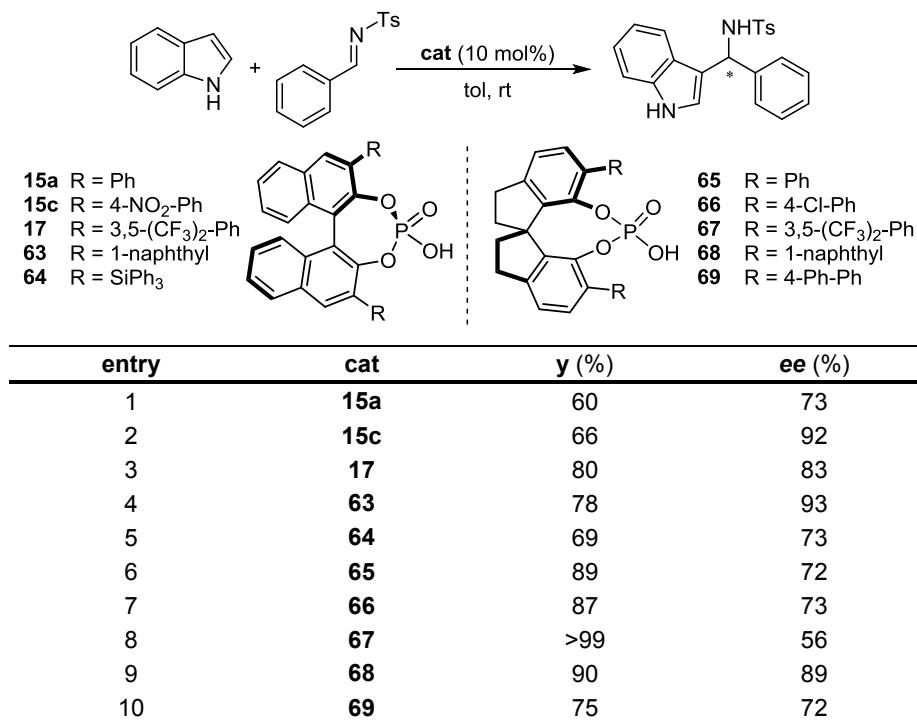
Scheme 39



It must be pointed out that CBAs need strict steric requirements in order to achieve high level of stereoselection; hence, a meticulous tuning of the catalyst's structure is strongly recommended. Indeed, in the literature it can be seen that also BINOL- and SPINOL-derivatives necessitate specific substituents

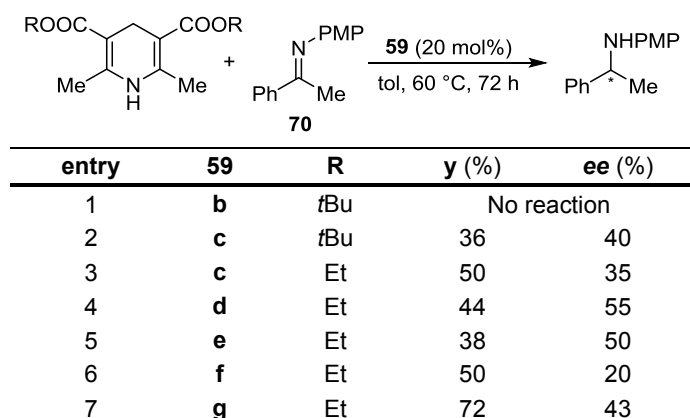
depending on the reaction in which they were used. In particular, in the indole addition to *N*-tosylimines, only catalysts **15c**, **63** and **68** provide high ee, while other structurally related PAs lead to lower stereoselectivities (entries 2, 4 and 9 of Scheme 40).⁴⁶

Scheme 40



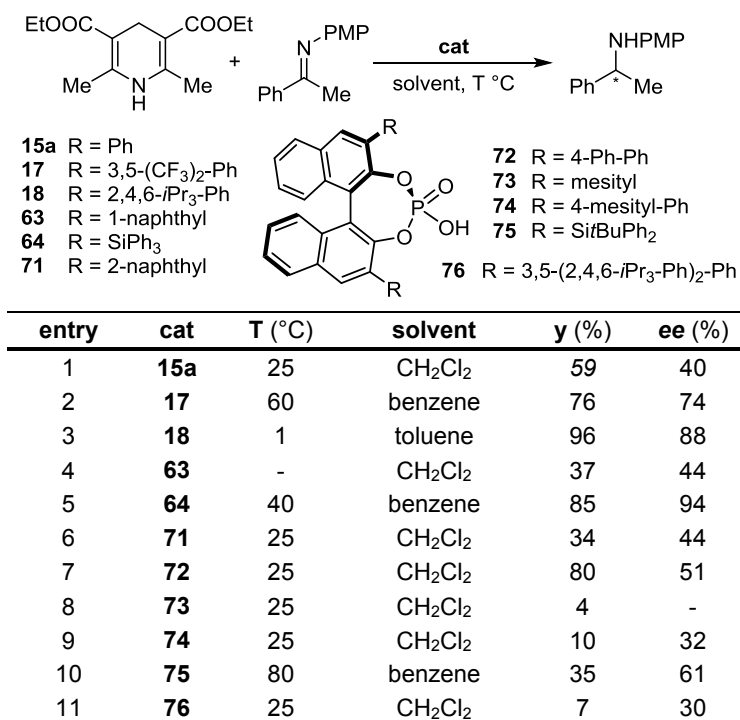
The second reaction in which our catalysts have been tested was the transfer hydrogenation of ketoimines with Hantzsch esters (Scheme 41). The reduction of the benchmark substrate **70** furnished the enantioenriched product in generally moderate yields and scarce stereoselections. Between the two tested Hantzsch esters, the *t*-butyl derivative demonstrated to be less chemically active probably due to steric hindrance, while the ethyl substituted one proved to be suitable to obtain higher yields even if slightly lower stereoselections (entries 1-3). This reaction is known to be efficiently catalyzed by very bulky PAs such as **18** or **64**,^{11b-c} and even in our case, the increase of steric hindrance in the proximity of the catalytic site, furnished an improved ee (entries 3-6). Curiously, the presence of methyl groups in the *para* position with respect to the phosphoric group seem to be beneficial (entries 4 and 7).

Scheme 41



This transfer hydrogenation reaction is known to be challenging for CBA catalysis, as among the huge number of tested catalysts, only **18** and **64** provided ee higher than 74% (Scheme 42 entries 3 and 5). For sake of comparison, we report in Scheme 43 the results reported in the literature by Rueping, List and MacMillan.^{11a-c} It is evident that, with the only exceptions of **17**, **18** and **64**, independently on the nature of the 3,3' substituents, ee usually lower than 60% are obtained.

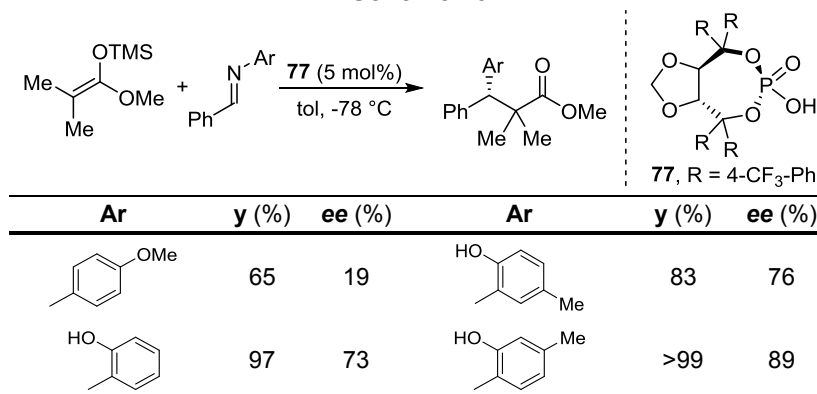
Scheme 42



3.4. Synthesis of Tartaric Acid-Derived Brønsted Acids

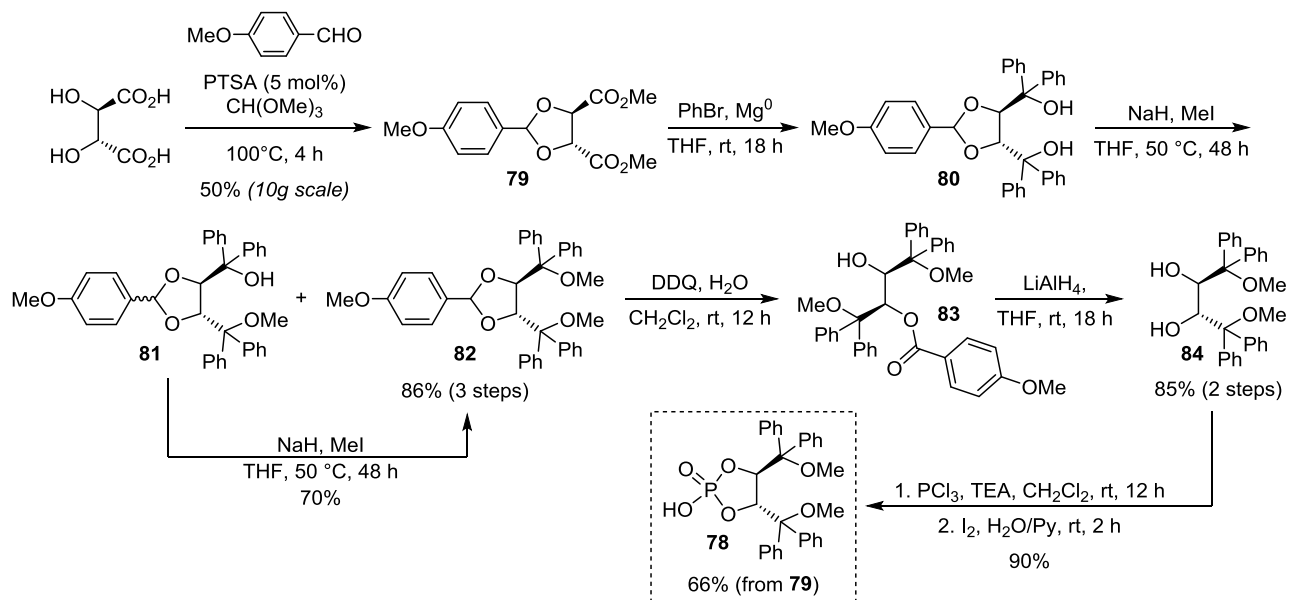
Tartaric acid is another important C₂ symmetric chiral scaffold on which, for its low cost and wide availability, it would be convenient to base the development of new chiral catalysts. As mentioned in Chapter 1, CBAs based on the TADDOL scaffold already exist. Since the use of these catalysts remained underdeveloped due to their poor reactivity we report here the results relative to one of the few papers published on the topic.⁴ In 2005 Akiyama et al. tested TADDOP **77** in a stereoselective Mukayama-Mannich reaction. The imine substrate required a fine tuning in order to achieve good stereoselections, but eventually ee up to 89% were obtained (Scheme 43).

Scheme 43



Differently from TADDOP, our synthetic approach was based on the use of the two hydroxyl groups of the tartrate scaffold as substituents for the phosphorous atom and of the two carboxylic acid moieties to create steric hindrance around the acidic site. Thus, we synthesized catalyst **78** as depicted in Scheme 44; using a synthesis that in part has been previously developed by Pietruszka et al..⁴⁹

Scheme 44



Starting from (*R,R*)-tartaric acid it is possible to synthesize, in a one pot procedure, the benzylidene acetal dimethyl ester **79**. Despite the yield of this first step is moderate, the reagents are cheap, the reaction can be performed on large scale (10 g of product were obtained) and **79** can be easily purified by trituration with *i*Pr₂O. The following addition of phenyl magnesium bromide allows the obtainment of TADDOL **80** which can be used in the following step without any purification. Methylation of **80** gives **82**; despite some mono-methylated compound **81** was isolated, a second treatment of this compound with NaH and CH₃I allows to obtain an additional amount of intermediate **82**. The oxidative cleavage of the benzylidene acetal by DDQ furnished benzoic ester **83**, which upon reduction with LiAlH₄ gives **84** in 85% yield from **82**. **84** is the direct precursor of the target molecule **78**; indeed, its treatment with PCl₃ furnished the corresponding phosphite which after oxidation with I₂ in a H₂O/Py mixture as solvent, gave the final compound **78** in 90% yield. Notably, the acidic catalyst **78** was obtained in 66% yield from the key starting material **79**, which, as previously stated, can be obtained in large amounts from cheap reagents.

Catalyst **78** was tested in typical Brønsted acid catalyzed reactions. Unfortunately, however, only a low catalytic activity was observed. We believe that this is mainly due to the chemical instability of **78** as the literature reports that five-membered cyclic phosphates undergo hydrolysis millions of times faster than their six-membered analogues.⁵⁰ Thus, further developments of this class of CBAs were abandoned.

3.5. Conclusions

In conclusion, two new different classes of CBAs have been obtained. The synthesis of tartaric acid derivative **78** required seven steps, which have been accomplished in good overall yield, but this compound showed to be an unsuitable catalyst because of its intrinsic instability.

On the other hand, diaminocyclohexane-based acids were found to be much more promising catalyst candidates. Their synthesis requires only three steps starting from a proper salicylaldehyde, from which the final desired PA can be obtained in variable yields depending on the nature of the selected substituents.

It is evident, from the comparison with the data reported in the literature, that the performance of a generic CBA catalyst can be strongly improved by small variation in the catalyst's structure. Hence, even if the use of our new catalysts have not provided excellent results, an intensive work devoted to the synthesis of new derivatives is ongoing in our laboratories. Indeed, the catalysts based on the diaminocyclohexane scaffold, were found to give results in line with other BINOL and SPINOL-based PAs, when non-optimal bulky groups are present on the catalyst.

In our laboratories, new efforts are also currently dedicated to the synthesis of new derivatives which rely on different diamine scaffolds, aiming to the development of a new efficient classes of CBAs.

4. Theoretical Modelling of the Proline-Catalyzed Aldol Reaction

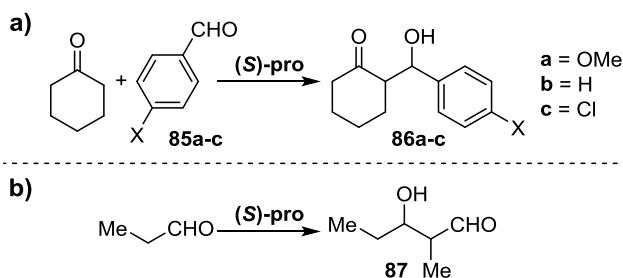
4.1. Introduction

After the pioneering works by List and Barbas,⁵¹ Jacobsen,⁵² and MacMillan,⁵³ organocatalyzed reactions have been studied by experimental techniques and theoretical methods to rationalize the stereochemical behavior of a great number of catalysts.⁵⁴ Among others, Blackmond, List and Houk have extensively investigated the intramolecular and intermolecular proline-catalyzed aldol reactions of ketones and aldehydes.^{55,56} In their contributions the observed stereoselectivity is rationalized also on the basis of the computational analysis of the involved Transition States (TSs), leading to the formulation of the commonly accepted stereoselection model, known as the Houk-List model.⁵⁶ More recently, Rzepa et al. have revisited this work and found partial and qualitative agreements between experimental and computational results by applying the Curtin Hammett Principle (CHP).⁵⁷ Nevertheless, a quantitative prediction and a full computational rationalization of the stereochemical outcome of such reactions is still missing.

In this work, we focus our attention on the reactions of Scheme 45 as prototypes of proline catalyzed reactions. While some previous reports demonstrated the stability of ketol **86b** under the usual proline-catalyzed aldol reaction conditions,⁵⁸ NMR studies have clearly showed that the *syn:anti* ratio of aldol **87** depends on the reaction time.⁵⁹ These NMR experiments definitely proved the existence of an equilibration between products through a proline-catalyzed retro-aldol reaction.

Motivated by the different reported kinetic behaviors of **86b** and **87**, we performed a comparative study of the reactions reported in Scheme 45.

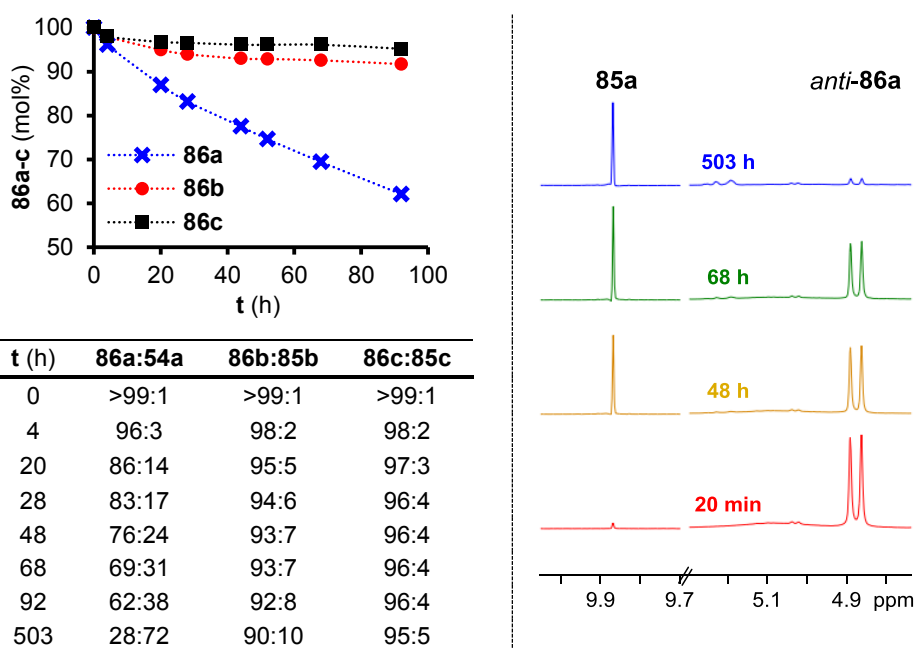
Scheme 45



4.2. Reversibility of the Proline-catalyzed Aldol Reaction

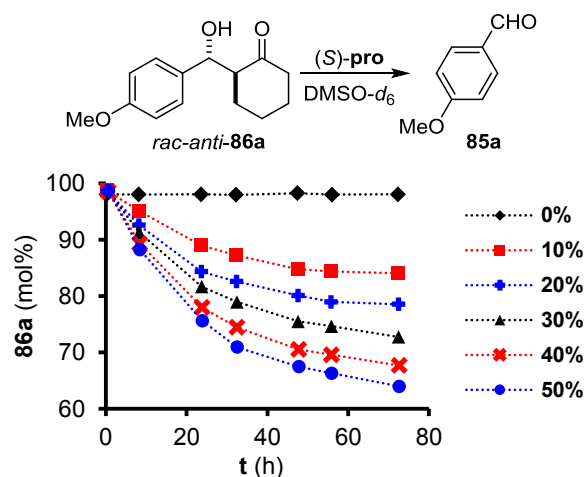
Following Houk, List⁵⁵ⁱ and Gschwind,⁵⁹ we assess the reversibility of this extensively studied catalytic process by performing kinetic experiments. The behavior of racemic, diastereopure ketols **86** in the presence of proline was monitored by ¹H-NMR techniques. Despite ketols **86b-c** exhibited quite good stability (in agreement with literature data),⁵⁸ we find **86a** to deliver back macroscopic amounts of aldehyde **85a** after relatively short reaction times (Scheme 46) and up to 72% of retroaldolization process for long enough reaction times (500 h) (see the spectra in Scheme 46).

Scheme 46



To understand in more details the kinetic of the retro-aldol reaction of **86a**, we reacted *anti*-**86a** with different loadings of (*S*)-proline in DMSO-*d*₆. We found a linear dependency of the reaction rate with respect to the proline's concentration. Scheme 47 shows the typical single exponential decay of a first order process respect to the catalyst's loading.

Scheme 47



0 mol%		10 mol%		20 mol%		30 mol%		40 mol%		50 mol%	
t (h)	86a ^a	t (h)	86a ^a	t (h)	86a ^a	t (h)	86a ^a	t (h)	86a ^a	t (h)	86a ^a
0.2	98.1	0.3	98.7	0.4	98.7	0.5	98.7	0.6	98.5	0.7	98.7
8.1	98.0	8.2	95.1	8.2	92.6	8.3	91.2	8.4	89.3	8.5	88.2
23.6	98.0	23.6	89.0	23.7	84.3	23.8	81.7	23.9	78.0	23.9	75.6
32.2	98.0	32.3	87.2	32.4	82.6	32.4	79.0	32.5	74.5	32.5	70.9
47.4	98.2	47.5	84.8	47.6	80.1	47.6	75.5	47.7	70.5	47.8	67.5
56.0	98.0	55.7	84.4	55.7	79.0	55.8	74.7	55.8	69.6	55.9	66.3
72.3	98.0	72.4	84.0	72.5	78.5	72.5	72.7	72.6	67.7	72.7	64.0

a) Expressed in mol%

By interpolating the obtained reaction profiles with third order polynomials, we obtained the expressions:

$$^{10}[\mathbf{86a}] = -2 \cdot 10^{-5}t^3 + 0.006t^2 - 0.553t + 98.972$$

$$^{20}[\mathbf{86a}] = -7 \cdot 10^{-5}t^3 + 0.013t^2 - 0.883t + 98.951$$

$$^{30}[\mathbf{86a}] = -1 \cdot 10^{-4}t^3 + 0.016t^2 - 1.070t + 99.114$$

$$^{40}[\mathbf{86a}] = -1 \cdot 10^{-4}t^3 + 0.020t^2 - 1.306t + 99.147$$

$$^{50}[\mathbf{86a}] = -1 \cdot 10^{-4}t^3 + 0.024t^2 - 1.519t + 99.583$$

Where $^x[\mathbf{86a}]$ refers to the reaction profile of the retro-aldol reaction catalyzed by X mol% of proline. These equations give an excellent description of the variation of the concentration of **86a** with time (t), as all of them fit the data with a $R^2=0.99$. Hence, their derivatives give us the value of the reaction rate in each point of the selected time range (0-72h). The derivate expressions are:

$$\frac{d^{10}[\mathbf{86a}]}{dt} = -6 \cdot 10^{-5}t^2 + 0.013t - 0.553$$

$$\frac{d^{20}[\mathbf{86a}]}{dt} = -2.1 \cdot 10^{-4}t^2 + 0.027t - 0.883$$

$$\frac{d^{30}[\mathbf{86a}]}{dt} = -3 \cdot 10^{-4}t^2 + 0.033t - 1.070$$

$$\frac{d^{40}[\mathbf{86a}]}{dt} = -3 \cdot 10^{-4}t^2 + 0.040t - 1.306$$

$$\frac{d^{50}[\mathbf{86a}]}{dt} = -3 \cdot 10^{-4}t^2 + 0.048t - 1.519$$

The initial rates associated to the five profiles can be obtained simply by calculating the limit of these polynomials for $t \rightarrow 0$. We obtain:

$$\left(\frac{d^{10}[\mathbf{86a}]}{dt} \right)_{t=0} = -0.553$$

$$\left(\frac{d^{20}[\mathbf{86a}]}{dt} \right)_{t=0} = -0.883$$

$$\left(\frac{d^{30}[\mathbf{86a}]}{dt} \right)_{t=0} = -1.070$$

$$\left(\frac{d^{40}[\mathbf{86a}]}{dt} \right)_{t=0} = -1.306$$

$$\left(\frac{d^{50}[\mathbf{86a}]}{dt} \right)_{t=0} = -1.519$$

These initial rates are expressed as mol%/h, and give us the percentage variation of **86a** at the very beginning of the reaction. Proline is a catalyst and the only reagent is **86a**, thus we can hypothesize the first order kinetics:

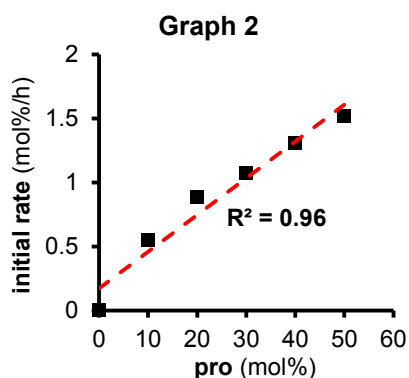
$$\frac{d[\mathbf{86a}]}{dt} = -[\mathbf{86a}]k'$$

Where $k'=k[\mathbf{pro}]$, and for $t=0$:

$$\left(\frac{d[\mathbf{86a}]}{dt} \right)_{t=0} = -[\mathbf{86a}]_0[\mathbf{pro}]k$$

Since $[\mathbf{86a}]_0$ and k are common to each reaction profile, we will obtain the relative initial reaction rates to be directly proportional to the relative amount of catalyst. Hence, by plotting the proline loading against the calculated initial rates we should obtain a linear relationship (Graph 2). The experimental data clearly show a linear dependence of the retro-aldol reaction by the proline concentration with good correlation ($R^2=0.96$), thus confirming the hypothesized first order kinetic and the involvement of a single proline molecule in the

process (in the graph the point 0,0 was added, since in Scheme 47 it is evident that the retro-aldol reaction do not proceed in absence of catalyst). This kinetic experimental results are consistent with the reaction model proposed by Houk and List where only one proline molecule promotes the aldol reaction.⁵⁵ⁱ



Moreover, when pure *anti*-**86a** was mixed with (*S*)-proline (30 mol%) and cyclohexanone (4 eq), the appearance of *syn*-**86a** was detected. More notably, the CSP-HPLC analysis of the crude mixture after 72 h revealed a 1:3 *syn:anti* ratio and 53% *ee* for the *RS* enantiomer of *anti*-**86a**, evidencing a kinetic resolution of the racemic starting material. Thus, the involvement of proline in the retro-aldol reaction of ketol **86a** is clearly demonstrated by different experiments.

As a consequence of this equilibration, we observed that by performing the aldol reactions of Scheme 45a, for long reaction times the *ee* decreases. We observed also that this behavior is not shared by the electron poor aldehydes **85c**, which, as reported before, gives the most stable ketol **86c** (Table 5).

Table 5

product	t (h)	conv. (%)	<i>syn:anti</i>	<i>ee</i> _{<i>syn</i>} (%)	<i>ee</i> _{<i>anti</i>} (%)
86a	22	19	59:41	63	70
	140	64	63:37	56	60
86b	22	94	55:45	81	83
	14	98	55:45	76	75
86c	22	>99	54:46	87	84
	170	>99	54:46	87	84

Given this reversible and dynamic nature of the proline-catalyzed aldol reaction (which depends on the electronic nature of the aldehyde), simple Transition State approaches such as the Curtin-Hammet principle (CHP), can no longer be applied.

4.3. The Multi Transition States Approach

Even if the CHP⁶⁰ is extensively employed in the determination of stereoselectivity of organic reactions, this approximation is correct only if (i) rapidly interconverting reagents, such as conformers, are involved and (ii) the considered processes lead irreversibly to the products.⁶¹ Despite its popularity, the CHP application should be limited only to irreversible processes affording non-interconverting products.

Unfortunately, it is not possible to know a priori when these conditions are satisfied, and the CHP is often applied indiscriminately. Here, we propose an alternative, simple and versatile new method for the treatment of equilibrating reactions, which involves parallel multiple transition states and takes into account relative

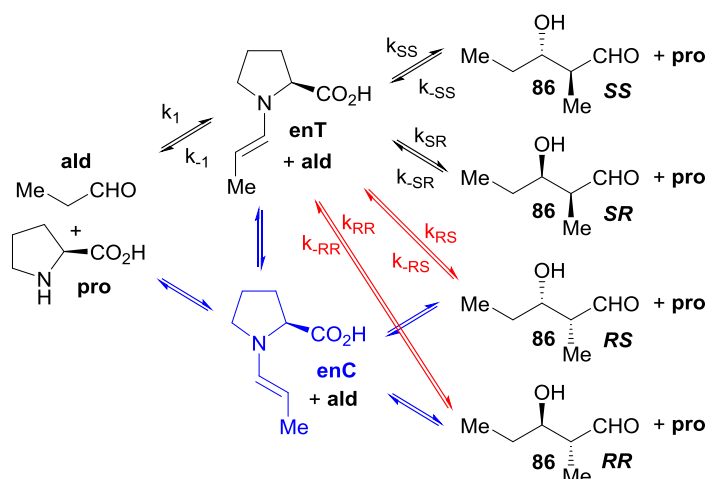
thermal stability of reagents and products. This multiple transition state approach can be employed for any reaction, at a comparable computational cost of the CHP TSs analysis.

More specifically, by calculating the rate constants associated to any reaction scheme and numerically integrating the resulting system of differential equations, a time-dependent picture of products concentration evolution is obtained. This modus operandi is commonly adopted in the field of chemical kinetics.⁶² However, at the best of our knowledge, this is the first time that it is applied to the field of computational organocatalysis as a tool for the simulation of reactions' outcomes, going beyond a static transition state picture. Indeed, our approach allows to quantitatively predict the time evolution of multi-channels chemical reaction products and provides useful insights about selectivity. The method here proposed includes reactants and products information, so it allows not only to obtain the stereochemical outcome of the simulated reaction at any times, but also the prediction of chemical yields.

As a starting benchmark reaction for this new methodology, we reproduce the experimentally observed epimerization of aldol **87**, previously reported by Gschwind et al..⁵⁹ Calculations are performed at the M06-2X/cc-PVTZ level of theory, on the basis of the recent report by Hubin,⁶³ who identified M06-2X as an optimum DFT functional for the treatment of the proline-catalyzed propionaldehyde self-condensation. The reaction scheme and the associated system of differential equations for this process are reported in Scheme 48. This picture considers the most important species in the reaction: the catalyst, reagents and products, to take the thermodynamic information about the system into account; the TSs to obtain the kinetic rate constants; and the enamine, which is the reactive species. In particular, this last compound can exist in two main conformations depending on the rotation of the C-N single bond; each conformer, *s-trans* (**enT**) or *s-cis* (**enC**), leads to the formation of two diastereoisomers.⁶⁴ The simulations of reactions considering in one case both enamines **enT** and **enC**, and in the other case only **enT** (the conformer experimentally observed to be the major species⁶⁵), provide the same reaction profiles. Hence, the free rotation of the C-N bond, becomes important only at the TS level. In other words, since the two enamine conformers are converting in a process faster than the stereodetermining step of the reaction, only the most stable conformer can be taken in consideration.

Finally, the complete reaction scheme, indicated by the black and blue arrows in Scheme 48, can be simplified to the black and red arrows one, reducing the number of variables in the differential equations system reported below.

Scheme 48

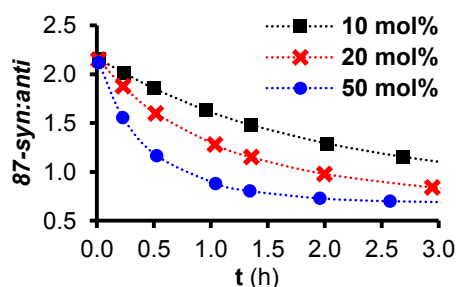


$$\left\{ \begin{array}{l} \frac{d[\text{ald}]}{dt} = -[\text{ald}][\text{pro}]k_1 - [\text{ald}][\text{enT}](k_{SS} + k_{SR} + k_{RS} + k_{RR}) + [\text{enT}]k_{-1} + [\text{pro}]([SS]k_{-SS} + [RR]k_{-RR} + [SR]k_{-SR} + [RS]k_{-RS}) \\ \frac{d[\text{pro}]}{dt} = -[\text{ald}][\text{pro}]k_1 - [\text{pro}]([SS]k_{SS} + [RR]k_{RR} + [SR]k_{SR} + [RS]k_{RS}) + [\text{enT}](k_{-1} + [\text{ald}](k_{SS} + k_{SR} + k_{RS} + k_{RR})) \\ \frac{d[\text{enT}]}{dt} = -[\text{enT}](k_{-1} + [\text{ald}](k_{SS} + k_{SR} + k_{RS} + k_{RR})) + [\text{ald}][\text{pro}]k_1 + [\text{pro}]([SS]k_{SS} + [RR]k_{RR} + [SR]k_{SR} + [RS]k_{RS}) \\ \frac{d[SS]}{dt} = -[SS][\text{pro}]k_{-SS} + [\text{enT}][\text{ald}]k_{SS} \\ \frac{d[RR]}{dt} = -[RR][\text{pro}]k_{-RR} + [\text{enT}][\text{ald}]k_{RR} \\ \frac{d[SR]}{dt} = -[SR][\text{pro}]k_{-SR} + [\text{enT}][\text{ald}]k_{SR} \\ \frac{d[RS]}{dt} = -[RS][\text{pro}]k_{-RS} + [\text{enT}][\text{ald}]k_{RS} \end{array} \right.$$

The rate constants of Scheme 48 are calculated according to the Transition State Theory (TST).⁶⁶ The numerical integration of the equations, under adequate boundary conditions, was performed by means of the ODE15s algorithm provided by the MatLab suite of codes.⁶⁷ The resulting matrix contains the values of the concentration of each species during time. The change in the *syn:anti* ratio faithfully reproduces the experimental profile of Gschwind et al..⁵⁹ Since the **87-SS** isomer presents the lower activation barrier, the *dr* is in favor of the *anti* isomer for short times. However, during the evolution of the simulated reaction, the *dr* enriches in favour of the *syn* isomer, by virtue of the higher stability of *syn-87* with respect to *anti-87*, as reported in Table 6.

Table 6

(S)-pro 10 mol%		(S)-pro 20 mol%		(S)-pro 50 mol%	
t (h)	<i>87-syn:anti</i>	t (h)	<i>87-syn:anti</i>	t (h)	<i>87-syn:anti</i>
0.02	2.15	0.02	2.15	0.02	2.12
0.24	2.01	0.23	1.88	0.23	1.56
0.50	1.85	0.52	1.60	0.53	1.17
0.96	1.63	1.04	1.28	1.04	0.88
1.36	1.48	1.36	1.15	1.34	0.80
2.03	1.29	2.00	0.98	1.96	0.73
2.69	1.15	2.95	0.84	2.58	0.70



After proving the ability of our method to predict the kinetic features of the proline-catalyzed self-aldol reaction of propionaldehyde, we moved toward a more challenging reaction. Our aim was to correctly predict the chemical and stereochemical outcome of proline-catalyzed addition of cyclohexanone to aldehydes **85a-**

c. For sake of comparison, we experimentally performed the reactions (**85** (0.4 M), cyclohexanone (5 equiv.), (S)-proline (30 mol%) in DMSO). We also calculated the stereoselectivity using the CHP with several computational set-ups (Table 7).

As previously reported,⁵⁷ sixteen TSs exist, because of two main conformational degrees for each products' isomer. On the basis of those reported calculations, the TSs involving a twisted conformation of the cyclic enamine moiety are neglected. Hence, DFT saddle point calculations identify seven transition states, two for each isomer, except for the *RS* isomer, for which only one structure was located with the M06-2X functional.

Table 7 reports the predicted stereoselectivities for the reaction between cyclohexanone and aldehyde **85b** using the CHP approach. Seventeen different computational set-up have been used. This table shows that independently on the chosen computational method, the calculated *ee* is always >99%. Furthermore, the wrong *anti*-diastereoisomer is always predicted as the major one, thus missing an appropriate qualitative prediction of the *dr*.

Table 7

Method	<i>dr</i> ^a	<i>ee</i> _{anti} (%)
B3LYP/6-31G(d,p)	<1:99	>99
B3LYP/6-311+G(3df,3pd) ^b	<1:99	>99
M06-2X/6-31G(d,p)	8:92	>99
M06-2X/6-311+G(d,p)	3:97	>99
M06-2X/6-311G(2d,2p)	8:92	>99
M06-2X/TZVP	1:99	>99
M06-2X/cc-PVTZ	2:98	>99
M06-2X/6-311+G(3df,3pd) ^c	4:96	>99
M06-2X/6-311+G(3df,3pd) ^{c,d}	2:98	>99
M06-HF/6-31G(d,p)	9:91	>99
M06-HF/6-311+G(d,p)	20:80	>99
M06-HF/TZVP	1:99	>99
M05-2X/6-31G(d,p)	3:97	>99
M05-2X/6-311+G(d,p)	1:99	>99
M05-2X/TZVP	<1:99	>99
MPW1PW91/6-31G(d,p)	1:99	>99
MPW1PW91/6-311+G(3df,3pd) ^e	1:99	>99

a) The *dr* is expressed as *syn:anti* ratio. b) Single Point Energy calculation on the B3LYP/6-31G(d,p) geometries and Gibbs free energy corrections. c) Single Point Energy calculation on the M06-2X/6-31G(d,p) geometries and Gibbs free energy corrections. d) IEFPCM-DMSO solvent reaction field used. e) Single Point Energy calculation on the MPW1PW91/6-31G(d,p) geometries and Gibbs free energy corrections.

These results are the same as previous calculations reported in the literature. Indeed, the lack of good computational prediction of proline catalyzed aldol reactions (in particular for the addition of cyclohexanone to benzaldehyde **85b**) is a well known unsolved issue, as recently recognized by Rzepa et al..⁵⁷

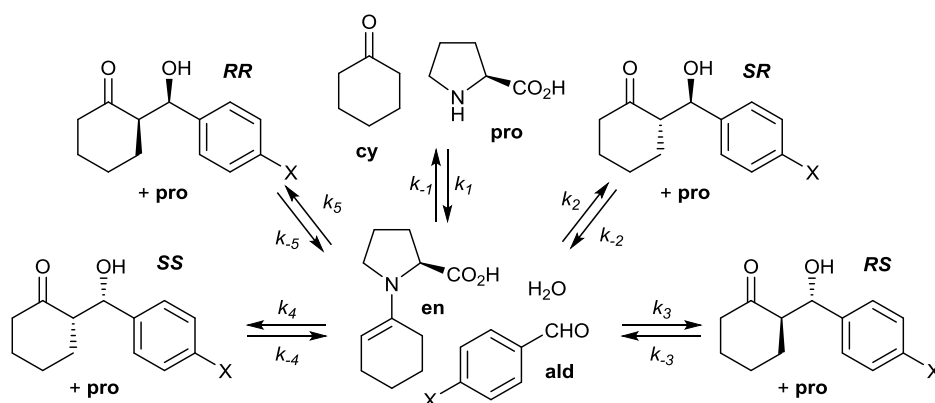
Hence, the simple analysis of the transition states through a CHP approach is affected by a main drawback: the description is limited to the TSs energy and it does not take into account any thermodynamic information arising from the comparison between the reagents and the products of different reaction channels. This

limitation leads to the wrong prediction of the diastereoselectivity toward the *anti* isomer and to the scarce prediction of the enantioselectivity. Since any calculation in Table 7 provides a large $\Delta\Delta G^\ddagger$, the poor description of this catalytic system may be ascribed also to the importance of the relative thermodynamic stability of the products and should not only be attributed to the level of DFT theory adopted. The physical reasons at the origin of the failure of the prediction are the catalyst-substrate interactions, and the bond formation and cleavage events, which are concomitants and different for different reaction path profiles. In this case, the straightforward application of the CHP, based on the pictorial late TSs assumptions, is quite misleading and, as we showed above, not supported by experimental evidences.

Then we turned our attention to the application of our model to those challenging reactions where the simple TSs analysis gives scarce results. The reaction's scheme has been simplified by considering only the *s-trans* enamine, because, as above, the simulations considering both the enamine conformers or only the *s-trans* enamine have led to superimposable reaction profiles. The system of differential equations for the reactions of Scheme 49 are reported below.

The reactions in Scheme 49 are more challenging than the one in Scheme 48. In Scheme 48, the nucleophilic and the electrophilic species are obtained from the same aldehyde (the propionaldehyde). Instead, in Scheme 49, the two reacting species are different (i.e. cyclohexanone and benzaldehyde), and the kinetic equations more challenging because of the presence of additional variables.

Scheme 49



$$\left\{ \begin{array}{l} \frac{d[\mathbf{cy}]}{dt} = [\mathbf{en}]k_{-1} - [\mathbf{cy}][\mathbf{pro}]k_1 \\ \frac{d[\mathbf{pro}]}{dt} = [\mathbf{ald}][\mathbf{en}](k_2 + k_3 + k_4 + k_5) + [\mathbf{en}]k_{-1} - [\mathbf{cy}][\mathbf{pro}]k_1 - [\mathbf{pro}]([\mathbf{SR}]k_2 + [\mathbf{RS}]k_3 + [\mathbf{SS}]k_4 + [\mathbf{RR}]k_5) \\ \frac{d[\mathbf{en}]}{dt} = -[\mathbf{ald}][\mathbf{en}](k_2 + k_3 + k_4 + k_5) - [\mathbf{en}]k_{-1} + [\mathbf{cy}][\mathbf{pro}]k_1 + [\mathbf{pro}]([\mathbf{SR}]k_2 + [\mathbf{RS}]k_3 + [\mathbf{SS}]k_4 + [\mathbf{RR}]k_5) \\ \frac{d[\mathbf{ald}]}{dt} = [\mathbf{pro}]([\mathbf{SR}]k_2 + [\mathbf{RS}]k_3 + [\mathbf{SS}]k_4 + [\mathbf{RR}]k_5) - [\mathbf{ald}][\mathbf{en}](k_2 + k_3 + k_4 + k_5) \\ \frac{d[\mathbf{SR}]}{dt} = -[\mathbf{SR}][\mathbf{pro}]k_2 + [\mathbf{en}][\mathbf{ald}]k_2 \\ \frac{d[\mathbf{RS}]}{dt} = -[\mathbf{RS}][\mathbf{pro}]k_3 + [\mathbf{en}][\mathbf{ald}]k_3 \\ \frac{d[\mathbf{SS}]}{dt} = -[\mathbf{SS}][\mathbf{pro}]k_4 + [\mathbf{en}][\mathbf{ald}]k_4 \\ \frac{d[\mathbf{RR}]}{dt} = -[\mathbf{RR}][\mathbf{pro}]k_5 + [\mathbf{en}][\mathbf{ald}]k_5 \end{array} \right.$$

We chose the M06-2X/6-311G(2d,2p) level of theory and apply our multiple transition states approach to the reactions involving aldehydes **85a-c**. The results are reported in Table 8. For sake of comparison, in the

same table the experimental results and the stereoselection predicted by the CHP approach are reported for the same reactions. We span by purpose different intrinsic electronic properties of the reactants. Going from **85a** to **85b** and to **85c**, the aldehyde become more electron-poor, and the relative aldol become thermodynamically more stable.

Table 8

Ald	t (h)	y (%)	Experimental			Multiple Transition State Approach				CHP	
			<i>dr</i> ^a	<i>ee</i> _{syn} (%)	<i>ee</i> _{anti} (%)	conv (%)	<i>dr</i> ^a	<i>ee</i> _{syn} (%)	<i>ee</i> _{anti} (%)	<i>dr</i> ^a	<i>ee</i> _{anti} (%)
85a	22	19	59:41	63	70	67	65:35	74	86	3:97	>99
85b	22	94	55:45	81	83	98	79:21	82	80	8:92	>99
85c	22	>99	54:46	87	84	>99	81:19	97	91	15:85	>99

a) *dr* is expressed as *syn:anti* ratio.

Experimental results show *syn:anti* ratios slightly in favor of the *syn* isomer and enantioselectivities between 63 and 87% *ee* (Table 8). Interestingly, for ketols **86a-b** a partial erosion of the *ee* is observed for long reaction times (in agreement with experimental data in Table 5). This may be due to the effect of the slow equilibration affecting the reaction.

When our approach was applied, a good agreement between computations and experiments was obtained.⁶⁸ Chemical yields can be predicted in quite good agreement with experiments, especially considering the relative trend between the yields of the three products (**86c** > **86b** > **86a**). We stress how our model provides the correct evaluation of the *dr*. Depending on the substrate, the *syn:anti* ratio is found to range between 65:35 and 8:2, in quite good agreement with experimentally obtained values of 55:45. Moreover, also the predicted *ee* is found to be in line with the experimental ones, since *ee* values between 74 and 97% are found. These results are valuable especially when compared with the state of the art provided by the simple TSs analysis. Calculations about quantitative evaluation of low stereoselectivities, yields and rate constants, are extremely sensitive, due to the exponential dependence of the *ee* on the Gibbs free energy. A small bias in Gibbs free energy is exponentially propagated into an *ee* bias. The current limitation of our model is given by the time-scale. Indeed, despite all the functionals give analogous qualitative results, deviations from the experimental time scale can be observed for other computational set-up. In Table 9 the data obtained in the simulation of the reaction relative to benzaldehyde **85b** with increasingly expensive basis sets are reported.

Table 9

basis set	n° functions ^a	$\Delta_{att}G^b$	$\Delta_R G^b$	t (h)	conv (%)	<i>syn:anti</i>	<i>ee</i> _{syn} (%)	<i>ee</i> _{anti} (%)
				22	96	79:21	80	83
6-311G(2d,2p)	713	18.7	-0.6	43	97	79:21	74	71
				140	97	79:21	41	36
				1.6	93	65:35	60	83
6-311+G(d,p)	622	16.8	-0.6	2.6	94	65:35	45	75
				2.9	81	65:35	72	84
TZVP	556	17.5	0.1	5.4	82	65:35	56	73
				81	>99	73:27	95	84
6-31G(d,p)	455	19.2	-1.1	132	>99	73:27	92	77

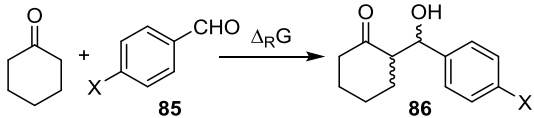
a) n° of functions relative to the structure of the TSs. b) kcal/mol

Next, we want to understand the relative importance of the thermodynamic aspects with respect to the kinetic ones. The works by Gschwind et al.,^{59a,65} the studies performed by List, Blackmond and Houk,^{55,56b} as

well as the observations hereby reported, show that the character of the proline-catalyzed aldol reaction strongly depends on the starting aldehyde and on the thermodynamic stability of the resulting aldol. We find that the more electron-poor is the aldehyde, the more stable is the resulting product (Scheme 46). Hence, the reaction Gibbs free energy ($\Delta_R G$) became important in the description of these kind of reactions. For these reasons, we calculated the *dr* and yields using the thermodynamics information of products and reactants. Clearly, the *ee* cannot be calculated by a thermodynamic approach, since enantiomers possess the same Gibbs free energy.

We report in Table 10 the calculated $\Delta_R G$ for the studied reactions at the M06-2X/6-311G(2d,2p) level of theory. The reported values shows how the relative stability of reagents and products is mainly responsible for the yields and diastereoselectivity. In particular, all the calculations predict the *syn* isomer to be more stable with respect to the *anti* one. We used the M06/2X functional, since Houk et al.⁶⁹ and Hubin and coworkers⁶³ reported it to be the functional which gives the best thermodynamic description of this class of reactions. Indeed, we find $\Delta_R G$ to provide results in good agreement with the experimental one, as reported in Table 8.

Table 10



product	$\Delta_R G$ (kcal/mol)	y (%) ^a	<i>dr</i> ^b
<i>syn</i> -86a	0.24	52	62:38
<i>anti</i> -86a	0.52		
<i>syn</i> -86b	-1.42	93	79:21
<i>anti</i> -86b	-0.62		
<i>syn</i> -86c	-2.45	99	84:16
<i>anti</i> -86c	-1.47		

a) Calculated according to the formula: $y(\%) = 100(\exp(-\Delta_R G_{anti}/RT) + \exp(-\Delta_R G_{syn}/RT)) / (1 + \exp(-\Delta_R G_{anti}/RT) + \exp(-\Delta_R G_{syn}/RT))$.
b) The *syn:anti* ratio was calculated according to the formula $\exp(-(\Delta_R G_{syn} - \Delta_R G_{anti})/RT)$.

These data support our observations that an approach that is uniquely based on TSs evaluation cannot provide a complete description of the process. Instead, our approach, which includes both kinetic and thermodynamic information, is able to describe the system providing the correct desired features, including chemical and stereochemical activity.

It must be noted that experiments performed in previous studies usually involve electron-poor substrates, such as Cl- and NO₂-substituted benzaldehydes.^{55b,55d,55g-h,55m} At the best of our knowledge, this is the first report in which the different nature of the electrophilic species in this paradigmatic reaction is experimentally and computationally studied. The results herein obtained have led to the formulation of our new approach for the treatment of the computational outcomes of equilibrating reactions. Indeed, while the CHP represents a very useful approximation for the treatment of a great number of irreversible reactions,⁷⁰ numerical integration of the kinetic equations is formally correct and applicable to any reaction. The CHP is actually the time-zero approximation of our approach, while the thermodynamic distribution of reagents and products is the infinite-time limit of the kinetic equations. The flexibility of our method allows us to show that the current limitations in reproducing the stereoselectivity of this family of reactions are not only due to the level of DFT

calculations, but rather to the theoretical model adopted. The present limitation of our model and the discrepancies from experimental values must be attributed to a non-correct description of the reaction scheme or to a bad evaluation of the involved rate constants due to computational issues.

4.4. Conclusions

In conclusions, the proposed computational method represents a rigorous and effective multiple transition state approach, that can be employed for any reaction, at a comparable computational cost of TSs analysis. It allows to predict the time evolution of multi-channels chemical reaction products and provides useful insights about selectivity, when the CHP cannot be applied. The method includes reactants and products information and provide a time-dependent picture of the evolution of products concentration and chemical yields. We have tested its efficiency in the evaluation of the time dependent proline-catalyzed epimerization of aldol **3** and found good agreements with previous experimental reports by Gschwind et al..⁵⁹ Then, we applied our approach to the proline-catalyze addition of cyclohexanone to benzaldehydes **85a-c** and obtained a realistic prediction of yields, *dr* and *ee* of this valuable and paradigmatic reaction.

5. HSiCl₃-mediated Reduction of Nitrogroups

5.1. Introduction

Reduction of nitro-groups represents one of the most straightforward entries to aliphatic and aromatic amines.⁷¹ Among the numerous available methodologies, reduction *via* hydrogenation, with classical and revisited protocols (Pd/C, PtO₂, Raney-Nickel or homogeneous transition metal catalysts),⁷² or under transfer hydrogenation conditions⁷³ is largely employed. However, these protocols sometimes lack functional group compatibility, often requiring high pressure equipment, and may suffer from the use of hazardous reagents (e.g. hydrazine) or the presence of potentially toxic transition metals. Similar considerations can be made for the reductions with SnCl₂⁷⁴ or for metal dissolving reductions involving Zn, Fe, In or Sm,⁷⁵ which were reported to be poorly compatible with the presence of halogen atoms.⁷⁶ Efforts have been made to discover new greener methodologies that would avoid the use of metal catalysts, but only few new protocols have been reported so far.

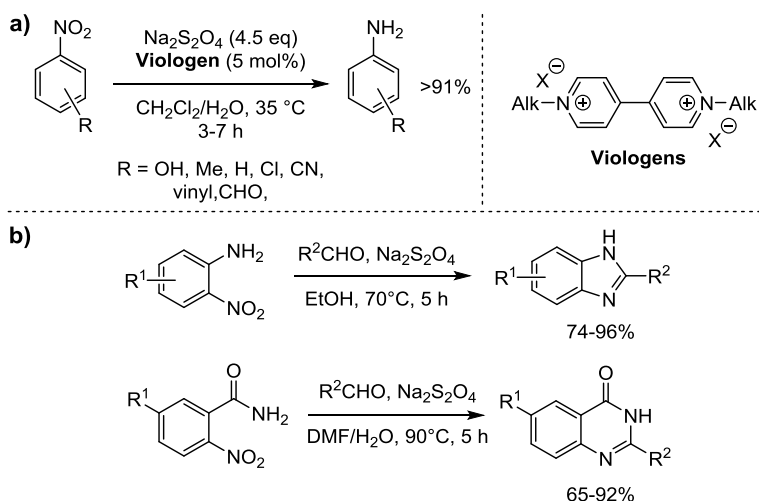
In the next paragraph a survey on the metal free reduction of nitro-groups is given. Then, a new methodology developed in our laboratories is presented in the following paragraphs. Even if the content of this chapter may seem disconnected from the main argument of this thesis (Brønsted acids), the reader will find out that, under certain conditions, HSiCl₃ counterintuitively behaves as a Brønsted acid. This peculiar feature of the reaction justifies the inclusion of the hereby presented work within this thesis' context.

5.2. Metal-free Reduction of Nitrogroups: Literature Background

Since the development of the concept of green chemistry, several research groups became involved in the research of metal-free methodologies for the reduction of nitro groups. In particular, several efforts have been made to develop methodologies that avoid the use of hydrogen gas, but only few papers have been reported so far.

First attempts arose from the observation by Bruce and Perez-Medina who, in the 1947,⁷⁷ showed that refluxing hydroiodic acid (57%) is a good nitro reducing agent. Toyokuni et al. have recently revisited this methodology.⁷⁸ Despite moderate to good yields were obtained in the reduction of simple aromatic nitro compounds, the very harsh reaction conditions, and the delivery of I₂ from the reaction environment, make this methodology unsuitable for the synthesis of valuable, functionalized molecules. In 1993,⁷⁹ Park showed that sodium dithionite (Na₂S₂O₄) is a single electron transfer reductant suitable for the mild transformation of several nitroarenes into the corresponding anilines. In particular, the reaction has been observed to be accelerated by Viologen (1,1'-dialkyl-4,4'-bipyridinium ions) via Electron Transfer Catalysis (Scheme 50a). Despite the use of Na₂S₂O₄ on a large scale⁸⁰ has been reported to result in highly exothermic reactions,⁸¹ it has been recently used in the synthesis of benzimidazoles⁸² and quinazolinones⁸³ (Scheme 50b). However, this methodology is still limited to the reduction of aromatic nitrogroups.

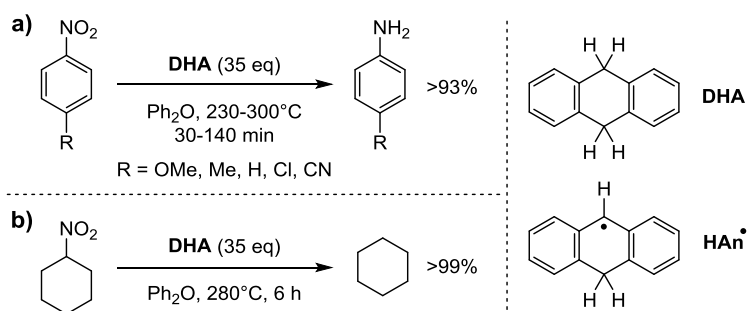
Scheme 50



Elemental sulfur (S_8) has been used as a nitro reducing agent in the presence of NaHCO_3 in DMF at 130°C . Seven different nitroarenes, also presenting CN, CO_2R and Cl substituents, have been selectively reduced in quite good yields.⁸⁴ Interestingly, also Na_2S^{85} or $(\text{NH}_4)_2\text{S}^{86}$ have been reported to be effective.

In 1995, Rüchardt discovered the ability of dihydroanthracene (**DHA**), xanthene and tetraline to act as reducing agents under harsh reaction conditions. When **DHA** is warmed up to $230\text{-}300^\circ\text{C}$ a radical splitting occurs delivering **HAn \cdot** and H^\cdot . These radical species are reductants able to react with unsaturated compounds (styrenes and fullerenes)⁸⁷ and with nitrogroups.⁸⁸ This method has been applied to the reduction of five different nitroarenes in almost quantitative yields (Scheme 51a). However, a large excess of **DHA** was required, and attempts in the reduction of nitrocyclohexane resulted in the generation of cyclohexane by denitration (Scheme 51b).

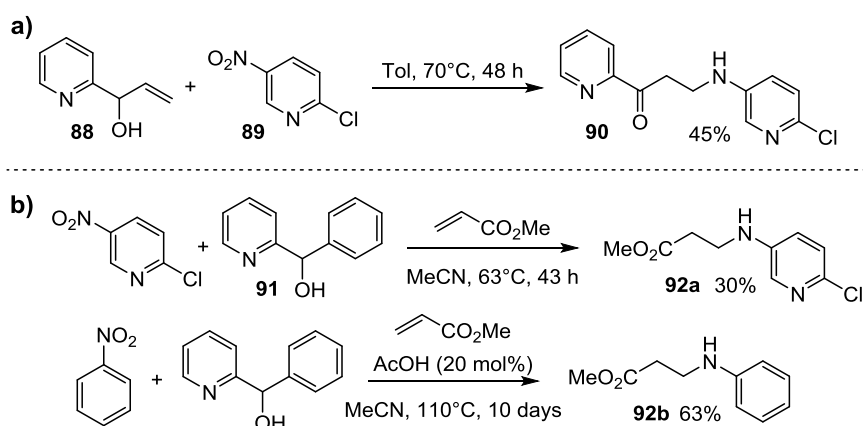
Scheme 51



Hence, due to the use of great amount of **DHA** (that lead to the formation of difficultly removable organic byproducts, e.g. anthracene) and to the really high reaction temperatures, this methodology is useless from a synthetic perspective. Other metal-free nitro reductions by transfer hydrogenation have been developed. In particular, it has been found that both mesoporous carbon⁸⁹ and reduced graphene oxide⁹⁰ catalyze the hydrogen transfer from hydrazine to nitrogroups. Since these two works serves as proofs of concept, only nitrobenzene or 4-nitrotoluene were reduced to the relative amines. Thus, no information about the effective synthetic scope of this methodologies can be deduced.

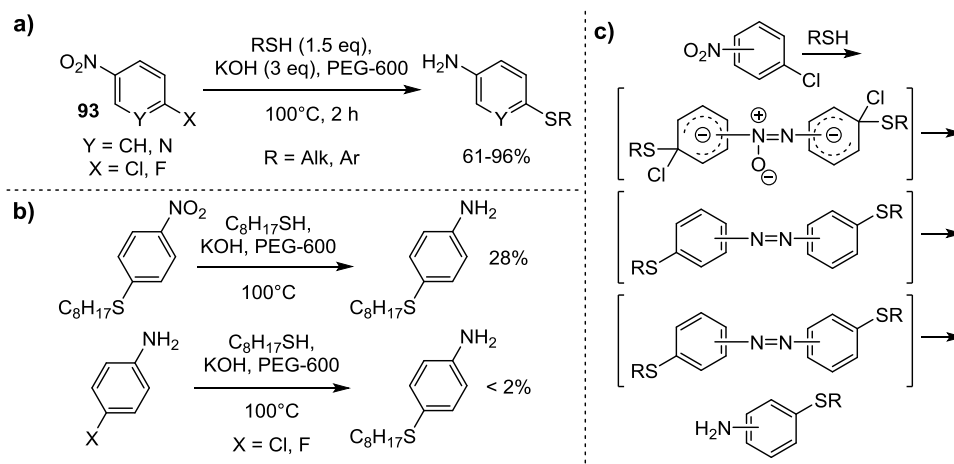
In 2008, Giomi et al. reported 1-(2-pyridyl)-2-propenol **88** to be an effective reagent in the reduction of nitropyridine **89**; the subsequent Michael addition of the resulting aminopyridine to the delivered ketone, led to the formation of product **90** (Scheme 52a). On the basis of these observations, the authors developed (2-pyridyl)phenyl methanol **91** as a new reagent able to give transfer hydrogenation without giving side reactions (Scheme 52b). Performing the reduction with this new compound in the presence of methyl acrylate, the author obtained as final products the secondary amines **92a-b**. The major drawbacks of this methodology are the moderate yields (<68%), very long reaction times (from 2 to 10 days), and the great amount of organic byproducts generated by the oxidation of the reductant (Scheme 52b).

Scheme 52



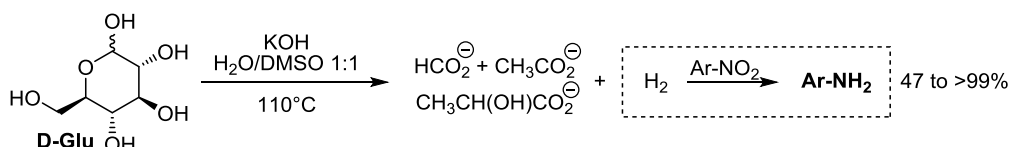
More recently, Liu reported that thiols can be used as reducing species in order to promote the reduction of nitrocompounds to amine under basic conditions.⁹¹ The reaction is reported in Scheme 53a. Despite the intrinsic value of the obtained products (aminoaryl sulfides) and the possibility to reuse the reaction media (polyethylene glycol, PEG-600), it can be noted that the synthetic suitability of this method is very limited in scope. Indeed, the substrate nitroarene **93** necessarily must be 2- or 4-substituted with a Cl or F atom, and no other functional groups have been reported to be compatible with the reaction conditions. Furthermore, the reduction of the nitrogroups in either the absence of the halogen atom on the aromatic ring or the sulfur substitution on the halogenated aniline, proceed sluggishly (Scheme 53b). Hence, the authors hypothesized that the reduction and the substitution may occur simultaneously as reported in Scheme 53c.

Scheme 53



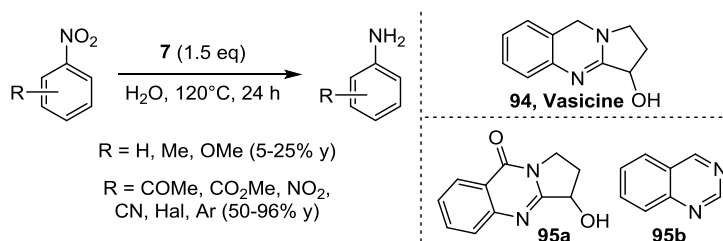
Glucose has been reported to reduce nitro group to azoxy compounds. Starting from this observation, Kumar et al. developed a new methodology for the reduction of nitroarenes under basic conditions by heating D-glucose at 110°C in a 1:1 mixture of H₂O/DMSO.⁹² This methodology is based on the delivery of H₂ by glucose degradation at high temperature (Scheme 54). However, even if the reaction occurs under harsh conditions, the authors were able to achieve the reduction of several nitro compounds in excellent yields and selectivity. In particular, CN, CHO, OMe, C=C, and halogen functionalities survived the reaction conditions providing the corresponding aniline without side reactions.

Scheme 54



The same authors reported also Vasicine **94** (Scheme 55), a natural alkaloid, to be able to perform transfer hydrogenation reactions in metal free conditions⁹³ leading to the reduction of several nitro groups in generally good yields and selectivity. In particular, despite several simple electronrich nitroarenes were reduced in very low yields (5-25%) due to the formation of considerable amount of undesired reduction intermediates (azo and azoxy compounds), nitroarenes bearing electronwithdrawing groups have been reduced with yields ranging between 60 and 96%. Notably, from a green perspective, the reaction is performed in water even if at 120°C. However, during the reaction the reducing agent is oxidized to organic byproducts **95a-b**, thus a chromatographic purification of the desired product is needed (Scheme 55). Furthermore, the extremely high cost of commercial vasicine force one to directly extract it from *Adhatoda vasica* leaves.

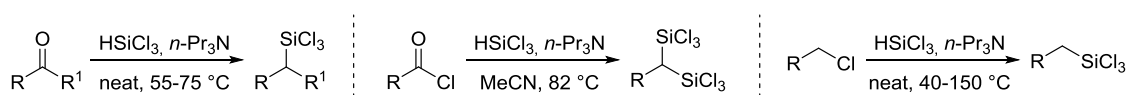
Scheme 55



5.3. HSiCl₃-mediated Reduction of Nitrogroups: Reaction Scope

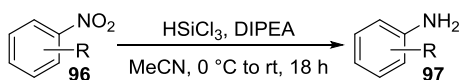
A very recent insight in the reduction of nitro groups has been provided by our research group.⁹⁴ We are active in the study of new reactions mediated by trichlorosilane (HSiCl₃), and we have found that mixtures of this reagent with tertiary amines (TEA or DIPEA) reduce nitro groups. HSiCl₃ is a green, cheap silicon-industry's waste byproduct, that may be activated as a reducing agent in combination with Lewis bases⁹⁵ and employed in enantioselective catalytic reductions of ketimines.⁹⁶ However, it is likewise known that when HSiCl₃ is used in combination with a tertiary amine, a formally nucleophilic silicon species is generated,⁹⁷ which was demonstrated to be reactive towards carbonyls,⁹⁸ alkyl halides⁹⁹ and acid chlorides, typically under harsh reaction conditions (Scheme 56).¹⁰⁰

Scheme 56



Here we report that the combination of HSiCl_3 and a tertiary amine allows to efficiently reduce both aliphatic and aromatic nitro-compounds under mild reaction conditions. The experimental protocol is simple and consists of mixing the nitro compounds with the tertiary amine (5 equiv.), and then of the addition of 3.5 equiv. of HSiCl_3 at 0°C to room temperature. The solvents of choice appear to be either dichloromethane or acetonitrile, providing the reduction of the benchmark substrate **96a** in excellent yields. Among the tertiary amines screened, the aliphatic ones provide optimum results (see the next paragraph for a discussion regarding the nature of the bases). The scope of the reaction was then explored (Table 11).

Table 11

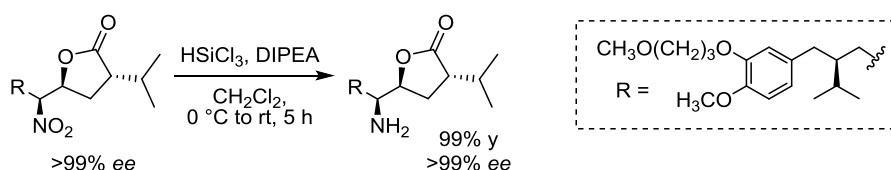


substrate	yield (%)	substrate	yield (%)	substrate	yield (%)
96a 4-Me	>98 (91)	96k 4-Bz	>98 (93)	96s	>98 (90)
96b 4-CH ₂ OH	>98 (95)	96l 3-CO ₂ H	60 (57)	96t	>98 (98)
96c 4-OAll	>98 (98)	96m 4-CO ₂ H	70 (65)	96u	>98 (90)
96d 2-OAll	>98 (91)	96n 3-CONBn ₂	>98 (95)	96v n-Hex-NO ₂	>98 (93)
96e 4-OBn	>98 (95)	96o 4-Cl	>98 (97)		
96f 2-OBn	98 (93)	96p 4-Br	>98 (97)		
96g 3-NHBn	nd (88)	96q 4-I	>98 (98)		
96h 4-CN	93 (89)	96r	96 (94)		
96i 4-NHAc	92 (90)				
96j 4-Ac	70 (70)				

Standard reaction conditions: to a solution of the nitro compound (0.7 mmol) and the base (5 equiv.), in acetonitrile (7 mL) HSiCl_3 (3.5 equiv.) is added at 0°C ; the reaction is then allowed to warm up to rt in 18 h; the reaction conversion based on the $^1\text{H-NMR}$ spectra of the crude mixture. Isolated yields are reported in parentheses.

In most cases, a complete conversion of the nitro derivative into the corresponding amine was observed. Isolated yields after a quick chromatographic purification were in good agreement with the $^1\text{H-NMR}$ -determined conversions. Allylic and benzylic protecting groups on both O and N atoms survived the reduction reaction conditions (**96c-g** and **96n**). Moreover, cyanides, amides, ketones, alcohols and carboxylic moieties were tolerated (**96h-n**). Nitropyridines can be efficiently reduced (**96r-s**), as well as nitroalkanes (**96t-v**); remarkably, halogenated nitro compounds can be converted to amines without any detectable traces of dehalogenated products (**96o-q** and **96s**). Furthermore, the metal-free reduction protocol was successfully employed in the total synthesis of Aliskiren (the step of interest is reported in Scheme 57).¹⁰¹

Scheme 57



The very mild procedure allowed the reduction of an enantiopure aliphatic nitrocompound with four stereocenters (one of which directly bearing the nitro group). The corresponding aliphatic amine was obtained in 99% isolated yield without altering the stereochemical integrity of the four stereogenic elements. Indeed, the new metal-free reduction methodology allowed the development of a novel and straightforward route for the synthesis of this important pharmaceutical product.

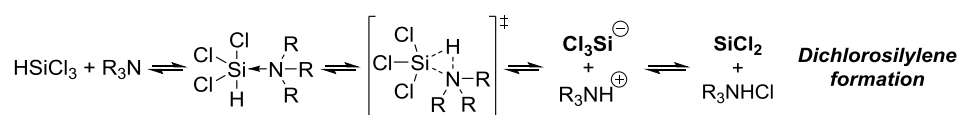
In summary, the hereby reported HSiCl₃-mediated reduction of both aromatic and aliphatic nitro-groups to amines has several positive features, being of general applicability, chemoselective, tolerant of many functional groups and respectful of the stereochemical integrity of the substrate. Moreover, the reduction protocol relies on the use of inexpensive and not hazardous chemicals, features a simple experimental procedure and is performed under mild conditions. Since the new method will offer the opportunity to redesign *ex novo* the synthetic plan of several important molecules, or key intermediates, it is expected that the metal-free protocol could possibly find useful applications also in industrially relevant processes.

5.4. HSiCl₃-mediated Reduction of Nitrogroups: Mechanistic Studies

5.4.1. HSiCl₃: Interaction with Lewis and Brønsted Bases

First studies reporting the use of HSiCl₃ in combination with a tertiary amine date back to 1969.⁹⁷⁻¹⁰⁰ Based on NMR experiments, it was hypothesized that the combination of HSiCl₃ with a base could lead to the formation of the R₃NH⁺/Cl₃Si⁻ ion pair according with the reaction mechanism reported in Scheme 58. Almost thirty years later, Karsch proposed that this equilibrium may further evolve toward the formation of a dichlorosilylene species (SiCl₂) (Scheme 58).¹⁰² More recently it was reported that reaction of HSiCl₃ with an organic base may generate SiCl₂ *in situ*.¹⁰³

Scheme 58

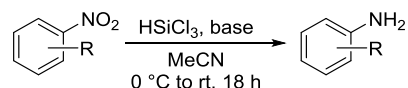


The reported behavior is surprising as trichlorosilane is believed to release an hydride ion. Indeed, HSiCl₃ is commonly known for its ability to be activated by Lewis bases such as amides or phosphine oxides by interaction with the Lewis acidic silicon atom. This interaction leads to an enhancement of the nucleophilic character of the hydride improving its reducing ability due to a redistribution of the electron density of the newly formed Lewis adduct.¹⁰⁴ Thus, the question arises whether the reaction proceeds through the generation of a reducing hydride rather than a Si(II) reducing species.

On the basis of the observations reported in the literature, we have performed a screening of different organic bases with increasing Lewis character in order to access new information regarding the nature of the involved reducing agent. The obtained results are listed in Table 12. It can be easily observed that by passing from bulky tertiary amine to less hindered amine up to bases with an increased Lewis character, the reactivity of the system decreases. In particular, DIPEA (diisopropyl ethylamine) and TEA (triethylamine) are more hindered than DBU (1,8-diazabicycloundec-7-ene, a known non-coordinating base). Among DMAP (4-dimethylaminopyridine), DABCO (1,4-diazabicyclo[2.2.2]octane), pyridine and DMF (dimethylformamide), the

former seems to provide better results than the other three compounds in spite of its supposed higher Lewis basicity. However, one could explain this better activity by taking into account the 4-NMe₂ moiety of the molecule that might act as a weak Brønsted base.

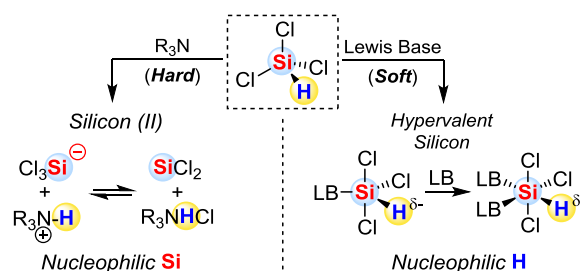
Table 12



Base	yield (%)
DIPEA	>99
TEA	89
DBU	54
DMAP	17
DABCO	0
Py	0
DMF	0

In order to explain the reason why HSiCl₃ reacts differently with Brønsted or Lewis bases we evoke the Hard and Soft Bases and Acids principle (HSAB). Indeed, while Lewis bases can be categorized as soft compounds, tertiary amines present a harder character. Thus, we hypothesize that Lewis bases preferentially interact with the soft silicon atom; on the other hand, tertiary amines prefer to interact with the harder acidic site in the molecule, that is with the proton (Scheme 59). This behavior can be emphasized by the steric hindrance of the tertiary amine, as the hydrogen is less shielded than the silicon atom. Hence, counterintuitively, the H atom in HSiCl₃ seems to be a proton rather than an hydride, unless activated by Lewis bases. Proof of this fact can be found in the ¹H-NMR chemical shift of HSiCl₃, which presents a singlet at 6.1 ppm, chemical shift far to be assigned to an hydride.

Scheme 59



A qualitative prediction of this reactivity picture can be provided by computations using the HSAB principle as reviewed by Geerlings.¹⁰⁵ In particular, the interaction's strength of both the acidic sites of HSiCl₃ with two different bases can be evaluated in terms of energy. To this purpose trimethylamine (TMA) and dimethylformamide (DMF) were chosen as benchmark bases due to their low number of atoms, which allow a more sophisticated calculation set-up. Energies of the three species with charges -1, 0 and +1 have been calculated with the aug-cc-PVTZ basis set in combination with MP2, B3LYP and wB97XD computational methods. Other functionals have been tested, but problems with the SCF convergence were met. In all these computations, atomic charges have been calculated according to the Merz-Singh-Kollman electrostatic method. For both the bases, the interaction energy with both the Si and H atoms are reported in kcal/mol and highlighted in grey when favored (Table 13).

Table 13

	method	H	Si
DMF	MP2	-0.02	-0.20
	B3LYP	-0.06	-1.55
	wB97XD	-0.08	-4.01
TMA	MP2	-0.14	+0.71
	B3LYP	-0.23	+0.62
	wB97XD	-0.27	+0.70

Energies reported in kcal/mol. Basis set: aug-cc-PVTZ

It is noteworthy that all the used computational methods predict the supposed correct trend: DMF interacts stronger with the silicon atom, while TMA give lower energies when interacting with the H atom. Thus, calculations within the HSAB principle seem to explain the peculiar behavior of trichlorosilane when reacting differently with Lewis or Brønsted bases.

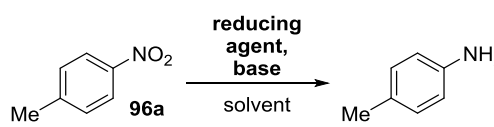
Hence, the experimental results reported in Table 12 as well as the HSAB principle seem to suggest that the reaction proceeds *via* deprotonation to give a Si(II) reducing agent (SiCl_3^- or SiCl_2) rather than through the basic activation of the formal hydride.

5.4.2. SiCl_3^- vs. SiCl_2 , Which is the Active Reducing Species?

It can be pointed out that, once formed, either SiCl_3^- or SiCl_2 may be the effective reducing agent, in fact both of them are Si(II) species. Moreover, SiCl_2 may be supposed to be a good nitro reducing agent by virtue of its similarity with SnCl_2 (a known nitro reducing agent), indeed Si and Sn both are elements of group 14 of the Mendeleev table.

In order to determine whether SiCl_3^- or SiCl_2 is the actual reducing species we have performed some experiments aiming to the generation of SiCl_2 from sources which do not allow the generation of SiCl_3^- . In this context, in 1998 Belzner et al. reported the generation of diaryl silylenes from the corresponding diaryl dichlorosilane in the presence of elemental magnesium in THF.¹⁰⁶ More recently, Lerner et al. reported the ability of tertiary amines to induce disproportionation of Si_2Cl_6 to give SiCl_2 and SiCl_4 .¹⁰⁷ Moreover, in both papers, the authors reported SiR_2 species to be stabilized by tertiary amines; indeed, it has been observed that dichlorosilylene is unstable, as such, at temperatures above -50°C .¹⁰⁸

In order to verify the validity of all the reported observations in our system, we have performed three different reactions: (i) we tried to generate naked dichlorosilylene from SiCl_4 and Mg according with the chemistry used by Belzner et al. in the presence of 4-nitrotoluene **96a** as a benchmark substrate (Table 14). (ii) This reaction has also been performed even in the presence of DIPEA, in order to verify whether higher yields might be obtainable by virtue of a stabilized dichlorosilylene (Table 14). (iii) We also tried to perform the reduction of **96a** by using a mixture of Si_2Cl_6 and either TEA or DIPEA according with Lerner's reaction (Table 14).

Table 14


entry	reducing agent	base	solvent	conv (%)
1	SiCl ₄ , Mg	-	THF	20
2	SiCl ₄ , Mg	DIPEA	THF	79 ^a
3	Si ₂ Cl ₆	DIPEA	MeCN	27
4	Si ₂ Cl ₆	TEA	MeCN	60
5	Si ₂ Cl ₆	TEA	DCM	9
6	Si ₂ Cl ₆	TEA	benzene	17

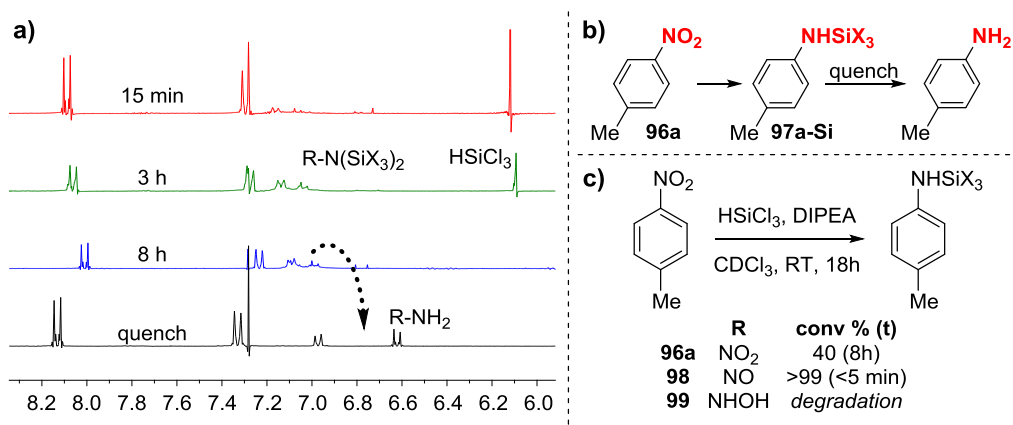
*a) a huge number of byproducts are present in the crude mixture; the value is obtained as **red96a**/(**red96a**+**96a**).*

The data reported in Table 14 suggest that SiCl₂ is involved in the reduction of nitrogroups. Moreover, the presence of a base notably improves the reactivity of the system (entries 1 and 2). A further proof of the involvement of an amine molecule in the reduction process can be found in the optimization of our reduction protocol, which requires more than 1 equiv of base for each equiv of HSiCl₃, that is one to deprotonate trichlorosilane and the excess in order to stabilize the resulting reducing species. Results obtained by using Si₂Cl₆ require some interpretation; the influence of the solvent seems to be important, and in particular acetonitrile proved to be the best (entries 4 to 5), as it did in the HSiCl₃ mediated reduction. It must be pointed out that Si₂Cl₆ and HSiCl₃ are different compounds, and their activation may occur by different modes. Furthermore, the former present more hindered silicon atoms which may result in a preference for less bulky amines; indeed, Lerner et al. used dimethyl ethylamine as the base of choice. This fact justifies the obtainment of higher yields when using the Si₂Cl₆/TEA combination rather than Si₂Cl₆/DIPEA one (entries 3 and 4).

In summary, even if the involvement of SiCl₃⁻ cannot be excluded, the reported experiments suggest that dichlorosilylene acts as the nitro reducing agent. Unfortunately, due to the instability and to the intrinsic coexistence of the two species in the involved equilibrium (Scheme 58), the unambiguous identification of the effective reducing species remains difficult. Hence, we moved towards computational chemistry in order to get new insights. In this context, computing a series of plausible TSs requires the identification of the rate determining step of the reaction.

By monitoring by NMR the reduction of **96a** in CDCl₃ (solvent in which the reaction is slow enough to be followed), we observe that the only detectable species are the starting materials and a broadened AB system whose signals shift to the product's expected chemical shift after the quench of the reaction (Scheme 60a). On the basis of ²⁹Si-NMR experiments (signals between -46 and -47 ppm, consistent with a silicon connected both to Cl and O or N atoms,¹⁰⁹ were detected) we attribute the observed signals to the silylated product **97a-Si** (Scheme 60b). Interestingly, no other reduction intermediates (nitroso- or hydroxylamine-compounds) were detected. This fact suggests that the first step (from nitro to nitroso) is rate determining. In order to verify our observation, we performed the reduction of nitrosotoluene **98**, which indeed was found to be reduced in less than 5 minutes (that is much faster than nitrotoluene **96a**)(Scheme 60c). Analogous experiments on hydroxylamine **99** furnished degradation byproducts due to the intrinsic poor stability of the starting material (Scheme 60c).

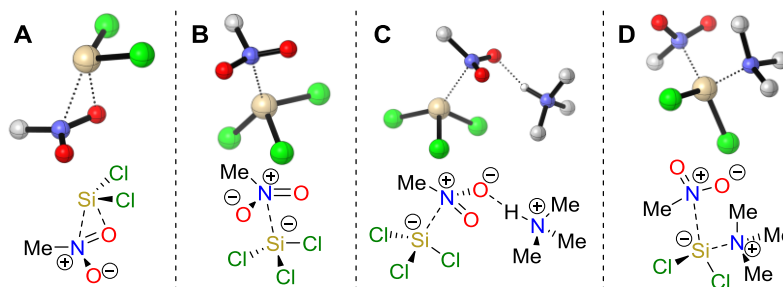
Scheme 60



After experimentally demonstrating that the first reduction step is the rate determining, we moved towards the computation of a series of TSs in which different reducing species attack nitromethane (which was chosen as a benchmark substrate due to its small number of atoms) (Scheme 61). In particular we computed the reduction promoted by species that present different electronic features: SiCl_2 is an electrophilic species, while SiCl_3^- and $\text{Me}_3\text{N-SiCl}_2$ are nucleophiles.

TSs have been calculated with B3LYP, M06-2X and wB97XD functionals with the 6-311++G(3df,3pd) basis set and PCM model for the inclusion of the solvent (chloroform, the same solvent used in the NMR experiments). Also post-Hartree-Fock electronic energies at the MP2/6-311+G(2d,2p) level of theory were calculated on all the B3LYP, M06-2X and wB97XD geometries in order to validate the obtained results within the DFT theory. The M06-2X geometries are also depicted in Scheme 61. All the structures show a single imaginary frequency, confirming that the found stationary point is a first order saddle. By IRC (Intrinsic Reaction Coordinate) analysis, it can be shown that all the obtained TSs directly lead to the generation of nitrosomethane coordinated with a new silicon species bearing a new strong Si-O bond.

Scheme 61



The reported structures take into account four different mechanisms. Structure **A** is relative to the SiCl_2 insertion in a $\text{N}=\text{O}$ bond of the nitro group. Indeed, SiCl_2 is a carbene analogue and in the presented structure is simultaneously: (i) donating electron density from the HOMO (mainly characterized by the sp^2 AO of Si) to nitromethane's π^* LUMO and (ii) accepting electrons from the nitromethane's π HOMO into the empty LUMO (mainly characterized by the p AO of Si). In structure **B** the simple addition of SiCl_3^- to nitrogen is depicted, and in TS **C** this same addition is considered while the nitro group is activated by the coordination of Me_3NH^+ through H-bond. TS **D** takes into account the addition of a TMA stabilized SiCl_2 that behaves as a nucleophile by virtue of the formal negative charge deriving from the coordination of the amine.

The Gibbs free energies of activation computed for the four mechanisms are reported in Table 15. Notably, while B3LYP predicts mechanism **A** to be the favorite one, all the other DFT computational set-up predict mechanism **D** to be preferred (by 8.7 and 3.2 kcal/mol for M06-2X and wB97XD respectively). Reliable MP2 calculations assign to the two processes even much higher activation energy differences of at least 10.0 kcal/mol). Hence, the addition of SiCl_3^- resulted to be an unfavorable pathway for this reaction, and interestingly, the addition of TMAH^+ as an H-bond activating species gives even higher energy barriers, probably due to steric effects.

Table 15

Theory Level	A	B	C	D
B3LYP ^a	27.0	33.5	44.6	33.5
M06-2X ^a	22.5	30.6	38.3	15.8
wB97XD ^a	26.2	32.7	43.1	23.0
MP2 ^b	28.0	28.1	-	18.0
MP2 ^c	26.6	26.8	-	15.6
MP2 ^d	26.6	27.1	-	16.8

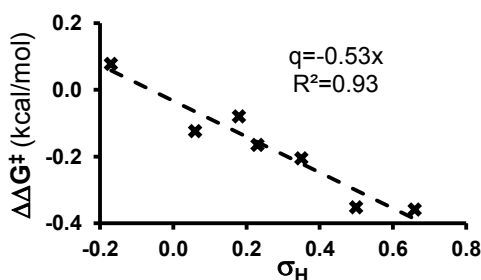
a) basis set: 6-311++G(3df,3pd); PCM-chloroform. b) calculated on the B3LYP/6-311++G(3df,3pd)[PCM] geometries. c) calculated on the M06-2X/6-311++G(3df,3pd)[PCM] geometries. d) calculated on the wB97XD/6-311++G(3df,3pd)[PCM] geometries.

In order to obtain further information about the operating mechanisms, we hypothesize that SiCl_2 and SiCl_3^- or TMA- SiCl_2 have opposite behaviors. Indeed, as stated before, while the former is an electrophilic species, the others two are nucleophiles. Thus, in principle, while mechanism **A** should be at work with electron-richer nitro groups, **B** and **D** should be favored by electron-poorer ones.

On the basis of this statement, we set up several competition experiments. Different nitroarenes were mixed with 1 equiv. of nitrobenzene, and the obtained mixtures have been submitted to the reduction protocol in the presence of the required HSiCl_3 amount for the reduction of only 1 equiv. of nitrocompound. The obtained crude mixtures were analyzed by $^1\text{H-NMR}$ revealing different selectivities of the reductant towards the two nitroarenes depending on the electronic nature of the arene's substituents. Since the obtained selectivities are in linear relationship with the ratio between the rate constants (k_X/k_H where k_X is the rate constant for the reduction of the nitroarene with substituent X), we are able to obtain, from the NMR spectra and by using the Curtin-Hammett principle, the activation energy difference between the two processes ($\Delta\Delta G^\ddagger$). The correlation between $\Delta\Delta G^\ddagger$ and the Hammett constants¹¹⁰ σ_H of the different nitrobenzenes is reported in Table 16 and in the relative graph.

Table 16

X	σ_H	k_X/k_H	$\Delta\Delta G^\ddagger$ (kcal/mol)
4-OMe	-0.27	<0.01	>2.0
4-Me	-0.17	0.74	0.08
4-F	0.06	1.62	-0.12
4-I	0.18	1.36	-0.08
4-Cl	0.23	1.90	-0.17
3-I	0.35	2.22	-0.21
4-Ac	0.50	3.94	-0.35
4-CN	0.66	4.05	-0.36



From Table 16 it is clear that electron-poorer nitro groups lead to higher reaction rates, indeed the obtained line present a negative angular coefficient of -0.53. Moreover, the high coefficient of determination obtained ($R^2=0.93$) highlights a good correlation between reactivity and the electronic character of the substrate.

On the basis of our hypothesis, these experiments strengthen the computational observation that a nucleophilic species (TMA-SiCl₂) is involved in the reaction. However, as further proof, we have calculated the energy barriers relatives to the reduction of the 4-substituted nitroarenes in Table 16 within mechanisms **A**, **B** and **D** (4-OMe-nitrobenzene is not considered because of the total selectivity obtained which does not allow a defined quantification of $\Delta\Delta G^\ddagger$ that may have every value > 2 kcal/mol; iodine substituted arenes are excluded as the iodine atom cannot be treated computationally at the used level of theory). The energy difference between the calculated activation energies ($\Delta\Delta G^\ddagger$) can then be correlated with the σ_H . (Tables 17-19). Due to the increased number of atoms, the computational optimizations have been performed with the 6-311+G(2d,2p) basis set and finer electronic energies have been calculated at the 6-311++G(3df,3pd) level with the PCM model for acetonitrile (the solvent used in the reduction protocol). The reported $\Delta\Delta G^\ddagger$ values in kcal/mol are relative to the computed reduction of PhNO₂.

Table 17

X	σ_H	B3LYP		
		A ($\Delta\Delta G^\ddagger$)	B ($\Delta\Delta G^\ddagger$)	D ($\Delta\Delta G^\ddagger$)
4-Me	-0.17	-0.56	1.36	1.08
4-F	0.06	0.15	-0.09	-0.41
4-Cl	0.23	0.11	-0.88	-0.63
4-Ac	0.50	0.50	-2.51	-1.48
4-CN	0.66	1.27	-3.72	-2.64

In the graph, values relative to mechanism **A** are reported in red triangles, values relative to mechanism **B** in black dots and values relative to mechanism **D** in blue squares.

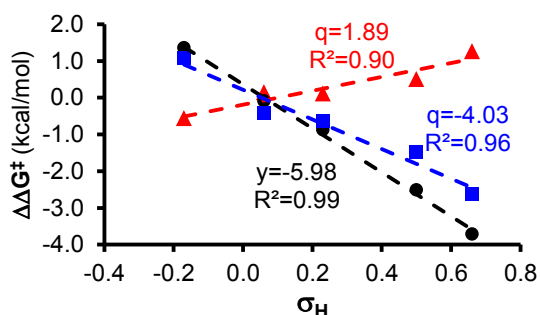


Table 18

X	σ_H	M06-2X		
		A ($\Delta\Delta G^\ddagger$)	B ($\Delta\Delta G^\ddagger$)	D ($\Delta\Delta G^\ddagger$)
4-Me	-0.17	-0.17	1.03	1.56
4-F	0.06	0.27	-0.07	-0.15
4-Cl	0.23	-0.19	-1.36	-0.99
4-Ac	0.50	-0.21	-3.00	-2.01
4-CN	0.66	0.56	-4.18	-2.65

In the graph, values relative to mechanism **A** are reported in red triangles, values relative to mechanism **B** in black dots and values relative to mechanism **D** in blue squares.

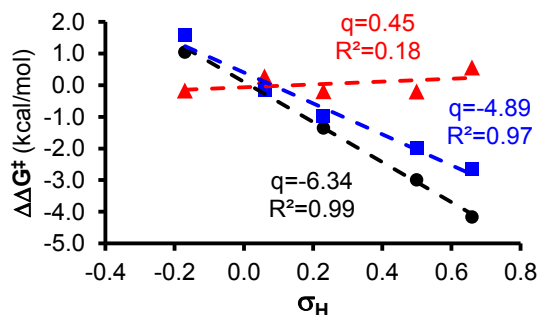
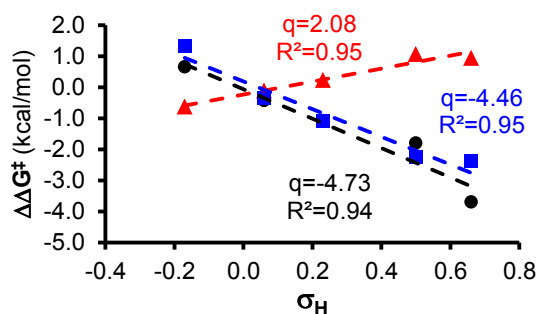


Table 19

X	σ_H	wB97XD		
		A ($\Delta\Delta G^\ddagger$)	B ($\Delta\Delta G^\ddagger$)	D ($\Delta\Delta G^\ddagger$)
4-Me	-0.17	-0.63	0.65	1.32
4-F	0.06	-0.11	-0.43	-0.37
4-Cl	0.23	0.23	-1.08	-1.09
4-Ac	0.50	1.07	-1.80	-2.25
4-CN	0.66	0.94	-3.70	-2.39

In the graph, values relative to mechanism **A** are reported in red triangles, values relative to mechanism **B** in black dots and values relative to mechanism **D** in blue squares.



Noteworthy, as can be seen from the data in Tables 17-19, there is a good agreement in the different computational methods. In particular, all of them predict SiCl_2 to react faster with nitrobenzenes that bear electron-donating group, and the opposite for SiCl_3^- and TMA- SiCl_2 .

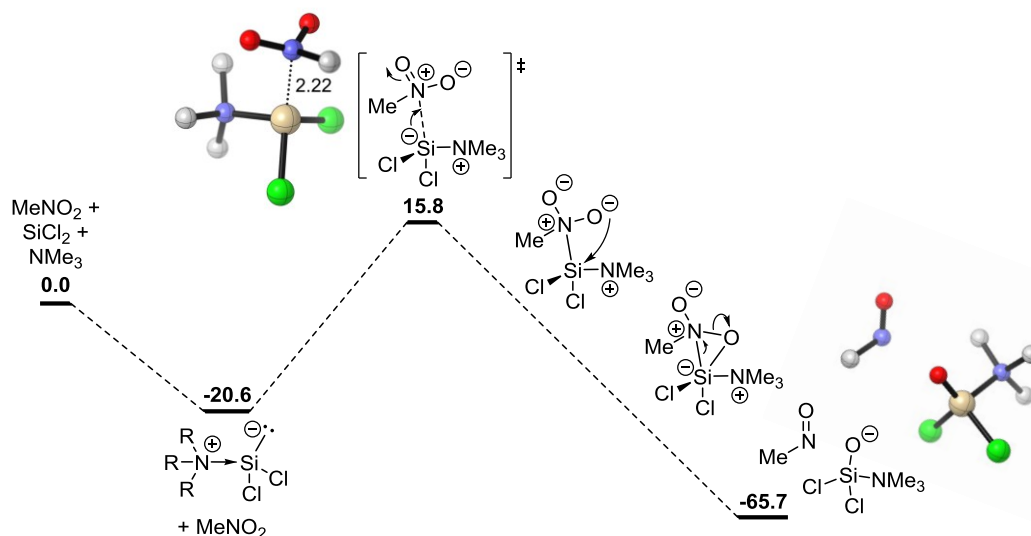
Thus, despite definitive proofs have not been provided, based on experimental and computational tools, the present study provides strong evidence about the operating mechanism. Specifically, it seems that an amine-stabilized SiCl_2 species is the main responsible of the reducing activity of the $\text{HSiCl}_3/\text{R}_3\text{N}$ system towards nitro groups.

5.5. Definitive Mechanism Hypothesis

On the basis of the presented mechanistic studies, we have calculated the whole reaction mechanism, involving three reduction steps by the TMA- SiCl_2 reducing species. In our preliminary studies, M06-2X has proved to be an excellent DFT functional for the description of the first reduction step, providing results very similar to the reliable and expensive post-Hartree-Fock method MP2 (Table 15). Hence, we have employed this functional also to compute the remaining two reduction steps. Thus, the results here presented have been obtained with the M06-2X/6-311++G(3df,3pd)[PCM=chloroform] computational set-up and are reported as Gibbs free energies.

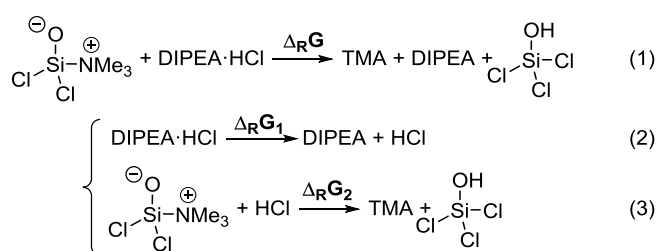
Firstly, we calculated that the generation of the TMA- SiCl_2 species is highly favored (20.6 kcal/mol) in agreement with the experimental observations by Lerner.¹⁰⁷ As previously stated, the addition of such a reducing species to nitromethane occurs with an energy barrier of 15.8 kcal/mol, where the zero energy is set for the separated reagents (Scheme 62). The transition state involves the addition of the negatively charged Si atom to the nitro group's nitrogen. Once the Si-N bond is formed, the Intrinsic Reaction Coordinate (IRC) directly leads to the formation of a transient three-membered cycle involving the Si, N and O atoms, which through electron rearrangement forms TMA- $\text{Si}(\text{O})\text{Cl}_2$ and nitrosomethane (Scheme 62). The reaction Gibbs free energy associated to this first step is of -65.7 kcal/mol.

Scheme 62



TMA-Si(O)Cl₂ is a TMA stabilized silicon analogue of phosgene. We have calculated that the addition of HCl from the hydrochloride salt of a tertiary amine (DIPEA for instance) is highly favored. According to equation (1) of Scheme 63, such a reaction would lead to the formation of trichlorosilanol (Cl₃SiOH) at the cost of the dissociation energy for the DIPEA·HCl salt. While the reaction Gibbs free energy $\Delta_R G_2$ associated to the addition of HCl to TMA-Si(O)Cl₂ (equation (3) in Scheme 63) is hardly obtainable from experiments, it can be easily calculated. On the other hand, the evaluation of the dissociation energy of DIPEA·HCl $\Delta_R G_1$ via calculations is a difficult issue due to the involvement of a charge separation, but it is easily accessible by experimentally tabulated pK_a values.

Scheme 63



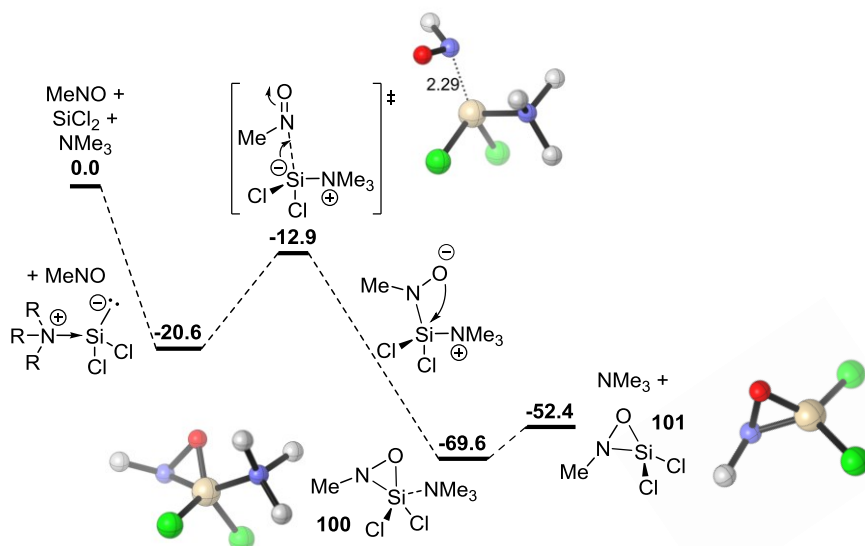
Since the pK_a difference between HCl and DIPEA·HCl is of ca. 8 units in acetonitrile¹¹¹ we obtained that:

$$\Delta_R G_1 = -RT \cdot \ln(10^{-\Delta pK_a}) = -0.592 \cdot \ln(10^{-8}) = 10.9 \text{ kcal/mol}$$

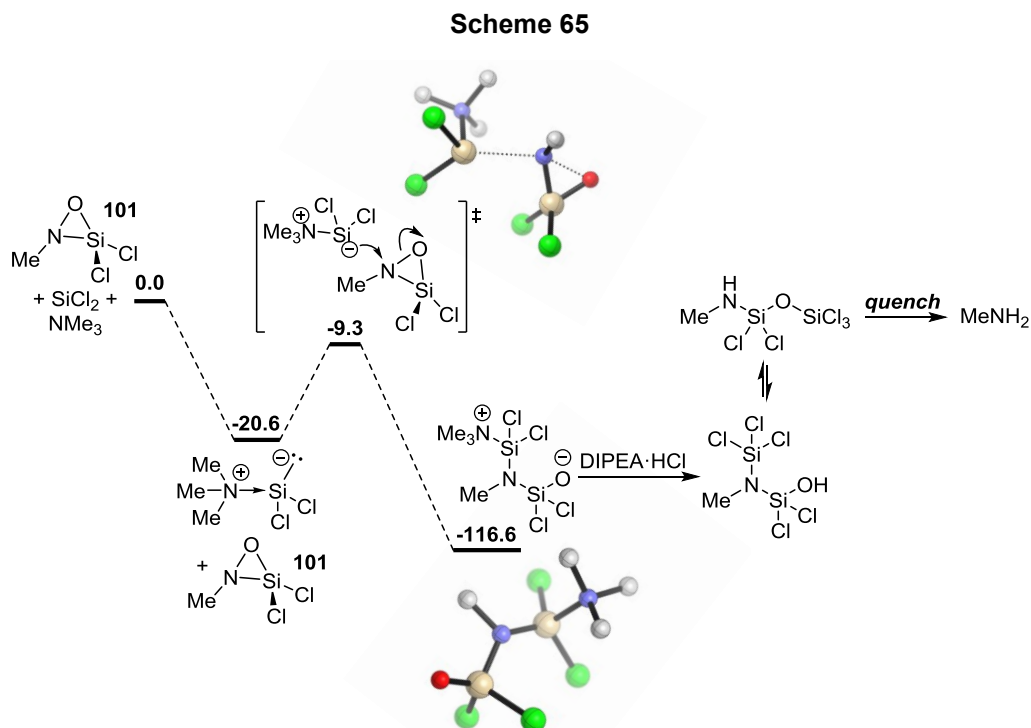
By calculating $\Delta_R G_2$ at different levels of theory,¹¹² we obtained values between -13.5 and -17.5 kcal/mol. Since $\Delta_R G = \Delta_R G_1 + \Delta_R G_2$, the Gibbs free energy associated to the overall process, is between -2.6 and -6.6 kcal/mol.

The second step of the reduction mechanism has a TS analogous to the first step, where TMA-SiCl₂ acts as a nucleophile towards the nitroso's N atom; the energy barrier associated to this process is -12.9 kcal/mol (when considering the dissociated reagents as a zero energy point), hence this reaction step is calculated to be spontaneous. In this case, the IRC leads to a stationary point where a Si-N-O three-membered cycle **100** (which presents an analogue oxidation state than that of a hydroxylamine) is formed with a reaction Gibbs free energy of -69.6 kcal/mol (Scheme 64).

Scheme 64



As third and last step of the reduction, we calculated that TMA-SiCl₂ can attack **101** by nucleophilic ring opening breaking the N-O bond. The process has an energy barrier of -9.3 kcal/mol (with respect to the separated reagents) and leads to the formation of the silylated amine, which upon the reaction quench leads to the final product (Scheme 65).



It is worth noticing that, by monitoring the reaction via ²⁹Si-NMR, some peaks at ca. -45, -55 and -65 ppm have been detected. These signals are consistent with species which present Si atoms directly bound to one, two or three O and/or N and Cl atoms.¹⁰⁹ These experimental observation confirms the formation of species compatible with the structure of the silylated product as well as of different possible side products deriving from the polymerization of trichlorosilanol (Cl₃SiOH).

5.6. Conclusions

In summary, a new convenient metal-free protocol for the reduction of nitrocompounds to amine, that was previously reported by our research group,⁹⁴ has been studied by computation, spectroscopy and experiments in order to clarify the reaction mechanism. On the basis of a screening of some bases, and of previous reports in the literature regarding the HSiCl₃ activation modes, the reaction is supposed to occur through the generation of a reducing Si(II) species. SiCl₂, SiCl₃⁻ and the R₃N-stabilized SiCl₂ are plausible candidates. However, the known instability of SiCl₂ at temperatures above -50°C and several experiments aiming to a different generation of such a species, suggest that SiCl₂'s ability to reduce the NO₂ group is considerably increased in the presence of tertiary amines. Even if these observations are not sufficient to exclude *a priori* the involvement of SiCl₃⁻, further computational studies and competition experiments hereby presented strongly suggest the amine-stabilized dichlorosilylene to be the most probable reducing agent.

Further computational studies voted to the full characterization of the reaction path involving TMA-SiCl₂ have been performed. Such computations predict the first reduction step (from NO₂ to NO) to be rate determining,

in agreement with the experimental observations, and present a low energy barrier, accordingly with the fast reaction rates observed.

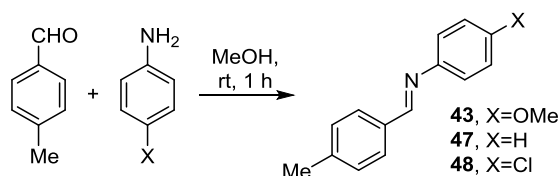
6. Experimental Section

6.1. General Information

Dry solvents were purchased and stored under nitrogen over molecular sieves (bottles with crown caps). Reactions were monitored by analytical thin-layer chromatography (TLC) using silica gel 60 F254 pre-coated glass plates (0.25 mm thickness) and visualized using UV light. Flash chromatography was carried out on silica gel (230-400 mesh). $^1\text{H-NMR}$ spectra were recorded on spectrometers operating at 300 MHz (Bruker Fourier 300 or AMX 300). $^{29}\text{Si-NMR}$ spectra were recorded on a spectrometer operating at 99.4 MHz (AMX 500). Proton and Silicon chemical shifts are reported in ppm (δ) with the solvent reference relative to tetramethylsilane (TMS) employed as the internal standard (CDCl_3 $\delta(1\text{H})= 7.26$ ppm, $\delta(29\text{Si})= 0$ ppm). $^{13}\text{C-NMR}$ spectra were recorded on 300 MHz spectrometers (Bruker Fourier 300 or AMX 300) operating at 75 MHz, with complete proton decoupling. Carbon chemical shifts are reported in ppm (δ) relative to TMS with the respective solvent resonance as the internal standard (CDCl_3 , $\delta = 77.0$ ppm). $^{19}\text{F-NMR}$ spectra were recorded on a 300 MHz spectrometer (AMX 300) operating at 282 MHz, with complete proton decoupling. Fluorine chemical shifts are reported in ppm (δ) relative to CFCl_3 as internal standard. $^{31}\text{P-NMR}$ spectra were recorded on a 300 MHz spectrometer (AMX 300) operating at 121.2 MHz, with complete proton decoupling. Phosphorous chemical shifts are reported in ppm (δ) relative to H_3PO_4 as internal standard. Enantiomeric excess determinations were performed with Chiral Stationary Phase HPLC analysis on an Agilent 1200 series HPLC instrument.

6.2. Information on Chapter 2

6.2.1. Synthesis of Imines 43, 47 and 48



Reagent	eq	mmol	MW (g/mol)	mg	d (g/mL)	V (μL)
4-tolualdehyde	1	8.3	120.15	1000	1.019	978
4-methoxyaniline	1	8.3	123.15	1022	-	-
aniline	1	8.3	93.13	773	1.022	756
4-Chloroaniline	1	8.3	127.57	1059	-	-

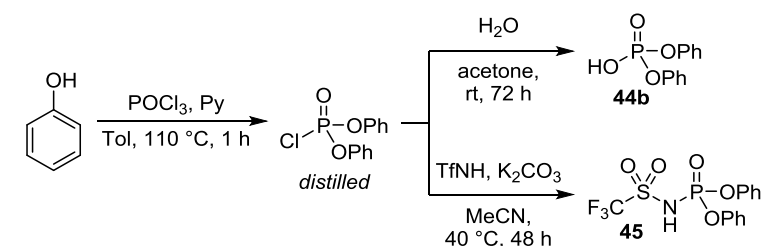
A round bottom flask of 50 mL equipped with magnetic stirrer was charged with the aniline and methanol (10 mL). The aldehyde was then added drop-wise. After 1 h the solvent was evaporated under reduced pressure, and the product was crystallized, and dried in high vacuum to give the pure imine.

(E)-N-(4-Methylbenzylidene)-4-methoxyaniline (43): the product precipitates from the reaction media and was filtered and washed with cold methanol resulting in a light grey solid (80% yield). $^1\text{H-NMR}$ (300 MHz, CDCl_3): 8.47 (s, 1H), 7.83 (d, 2H), 7.29 (d, 2H), 7.23 (d, 2H), 6.96 (d, 2H), 3.85 (s, 3H), 2.44 (s, 3H).

(E)-N-(4-Methylbenzylidene)-aniline (47): the product was dissolved in 5 mL of Hexane and then precipitated at 0°C, and the precipitate was filtered resulting in a light-brown crystal solid (90% yield). ¹H-NMR (300 MHz, CDCl₃): 8.45 (s, 1H), 7.86 (d, 2H), 7.38 (d, 2H), 7.20-7.34 (m, 5H), 2.47 (s, 3H).

(E)-N-(4-Methylbenzylidene)-4-chloroaniline (48): the product was crystallized in 5 mL of EtOH and the precipitate was filtered, resulting in a white crystal solid (quantitative yield). ¹H-NMR (300 MHz, CDCl₃): 8.42 (s, 1H), 7.80 (d, 2H), 7.38 (d, 2H), 7.30 (d, 2H), 7.16 (d, 2H), 2.47 (s, 3H).

6.2.2. Synthesis of Brønsted Acids 44b, 45



Reagent	eq	mmol	MW (g/mol)	g	d (g/mL)	V (mL)
Phenol	2.0	47.2	94.1	4.4	-	-
Pyridine	3.5	82.6	79	6.4	0.89	7.2
POCl ₃	1.0	23.6	153.3	3.6	1.645	2.2
(PhO) ₂ POCl	-	10.1	268.63	2.73	1.296	2.1
H ₂ O	-	-	-	-	-	5
(PhO) ₂ POCl	1	1.6	268.63	0.44	1.296	0.34
CF ₃ SO ₂ NH ₂	1.2	1.92	149.09	0.29	-	-
K ₂ CO ₃	2.4	3.84	138.2	0.53	-	-

A round bottom flask of 250 mL, equipped with magnetic stirrer and condenser under N₂ atmosphere, was charged with Phenol and POCl₃ in 60 mL of Toluene. The solution was warmed to refluxing temperature and then a solution of Pyridine in 20 mL of Toluene was added dropwise, resulting in the precipitation of pyridinium chloride. The solution was refluxed for 1 h, then cooled to room temperature, filtered over celite, the volatiles were evaporated and the resulting oil was distilled under vacuum (120-140 °C/0.04 mmHg). The resulting colorless oil (3.17 g, 11.8 mmol, 50% yield) was suddenly used in the second step.

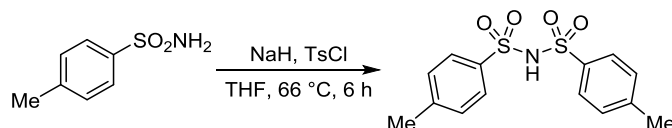
In order to obtain the phosphoric acid **44b**, a round bottom flask of 50 mL equipped with magnetic stirrer was charged with diphenyl phosphoryl chloride, and then acetone (10 mL) and water (5 mL) were added at room temperature. After three days at room temperature the solvent was removed under vacuum, and the product precipitated from a mixture of CH₂Cl₂ and Hexane (1:5), resulting in a white crystal solid (2.85 g, 91% yield).

In order to obtain the *N*-triflyl phosphoramidate **45**, a round bottom flask of 10 mL equipped with magnetic stirrer was charged with trifluoromethane sulfonamide and K₂CO₃, under nitrogen atmosphere, in dry acetonitrile (3 mL). The reaction mixture was allowed to stir until dissolution of the solids. diphenyl phosphoryl chloride (0.34 mL) was added dropwise, and the resulting mixture was allowed to react for 48 h at 40°C. After 48 h, the solvent was removed under vacuum, the crude mixture was dissolved in Et₂O, and the solution was extracted in a 6M HCl solution. The organic layer was dried over Na₂SO₄, filtered, and dried in vacuum to obtain a pale pink solid (473 mg, 67% yield).

Diphenyl hydrogen phosphate (44b): $^1\text{H-NMR}$ (300 MHz, CDCl_3): 7.61 (bs, 1H), 7.30 (t, 4H), 7.18 (t, 2H), 7.15 (d, 4H). $^{31}\text{P-NMR}$ (121.2 MHz, CDCl_3 , $\{^1\text{H}\}$): -8.09.

Diphenyl ((trifluoromethyl)sulfonyl)phosphoramidate (45): $^1\text{H-NMR}$ (300 MHz, CDCl_3): 7.30 (t, 4H), 7.18 (t, 2H), 7.15 (d, 4H). $^{19}\text{F-NMR}$ (282 MHz, CDCl_3 , $\{^1\text{H}\}$): -77.23. $^{31}\text{P-NMR}$ (121.2 MHz, CDCl_3 , $\{^1\text{H}\}$): -15.39.

6.2.3. Synthesis of Brønsted Acid 46

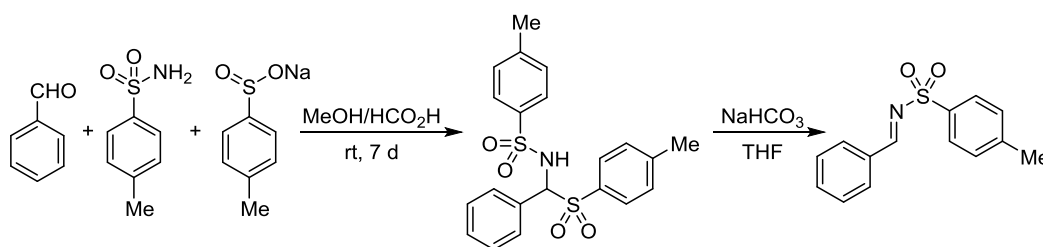


Reagent	eq	mmol	MW (g/mol)	g	d (g/mL)	V (μL)
4-Toluenesulfonyl chloride	1,5	5,2	190	1	-	-
4-Toluenesulfonamide	1	3,5	171	0,6	-	-
NaH (60%)	2	7	24	0,28	-	-

A round bottom flask of 100 mL, equipped with magnetic stirrer and condenser under N_2 atmosphere, was charged with sodium hydride and in 10 mL of dry THF. A solution of 4-toluenesulfonamide in 5 mL of dry THF was then added dropwise and the resulting solution was left to stir for 15 min. A solution of tosyl chloride in 5 mL of dry THF was then added dropwise, resulting in a white precipitate. The solution was left refluxing for 6 h, then cooled to room temperature, quenched with saturated solution of NH_4Cl and extracted with AcOEt (3x15 mL). The organic layer was dried over Na_2SO_4 , filtered and volatiles were evaporated to give the crude product. Purification via flash chromatography on silica gel (CH_2Cl_2 : MeOH 95:5 as eluent, $R_f=0.15$) furnished the desired product as a white solid which was washed twice with CH_2Cl_2 /6M HCl to give the desired compound in 88% yield.

bis-(4-toluene)-sulfonylimide (46): $^1\text{H-NMR}$ (300 MHz, CDCl_3): 7.90 (d, 4H), 7.35 (d, 2H), 2.48 (s, 6H).

6.2.4. Synthesis of Imine 51



Reagent	eq	mmol	MW (g/mol)	g	d (g/mL)	V (μL)
Benzaldehyde	1	10	106	1.05	1.04	1.04
Sodium 4-toluenesulfinate	1.1	11	180	1.96	-	-
4-Toluenesulfonamide	1	10	171	1.71	-	-

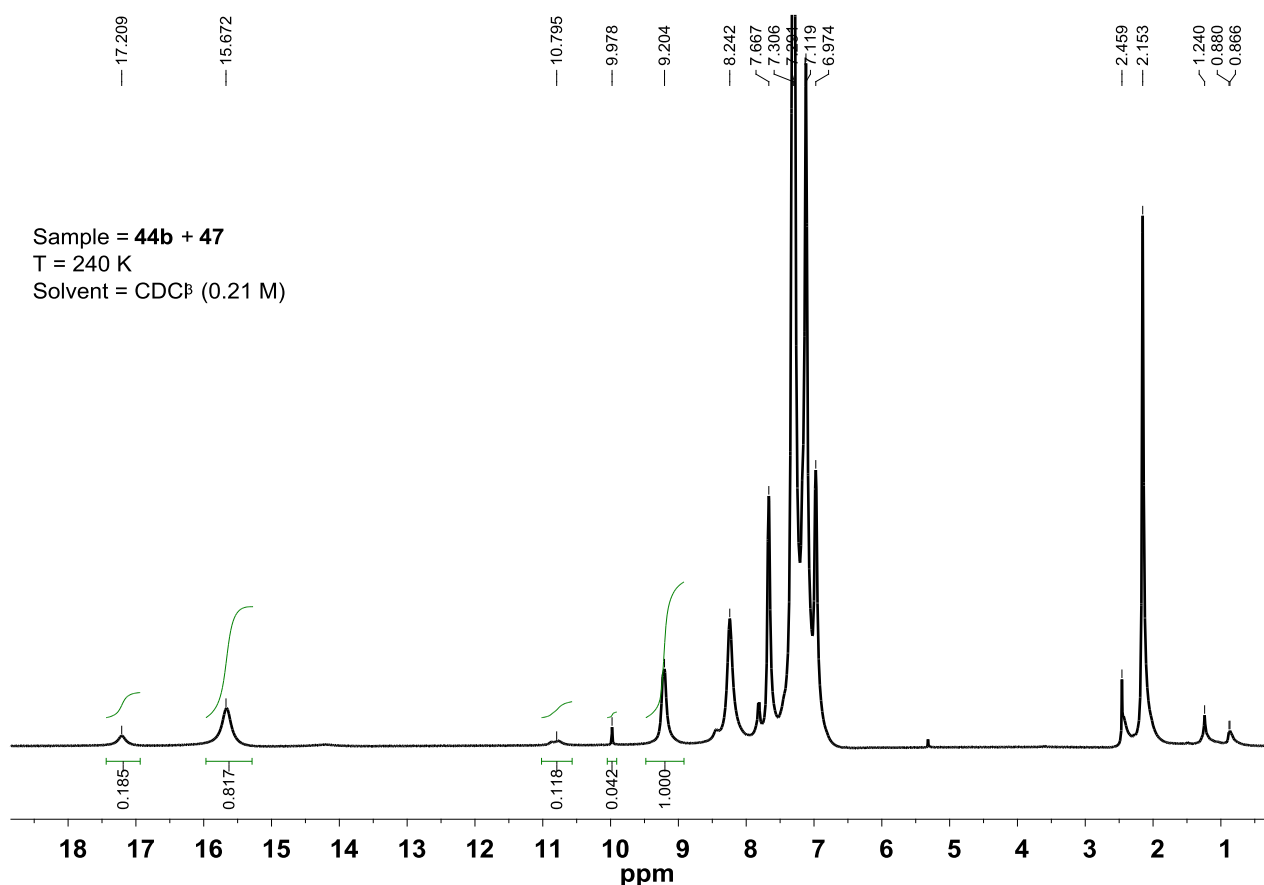
The solid reagents were mixed in a round bottom flask of 50 mL with a 1:1 mixture of methanol and formic acid (18 mL). The aldehyde was then dropped to the solution, and the resulting mixture was capped and allowed to stir for 7 days at room temperature. The precipitated was filtered and washed abundantly with hexane. The obtained solid product was dried in high vacuum resulting in a crystalline white solid (88% yield). $^1\text{H NMR}$ (300 MHz, CDCl_3): 4.91(d, 1H), 4.95 (d, 1H), 5.98 (d, 1H), 6.22 (d, 1H), 7.23-7.25 (m, 2H), 7.32-7.45 (m, 10H), 7.20-7.34 (m, 5H), 7.60 (t, 1H). A solution of the obtained solid intermediate was added

to a suspension of anhydrous potassium carbonate (8 g) in THF (12 mL). The suspension was refluxed for 15 hours and then cooled to room temperature. The solids were removed via filtration through a pad of celite, and the filtrate was concentrated under reduced pressure to give the pure imine in quantitative yield.

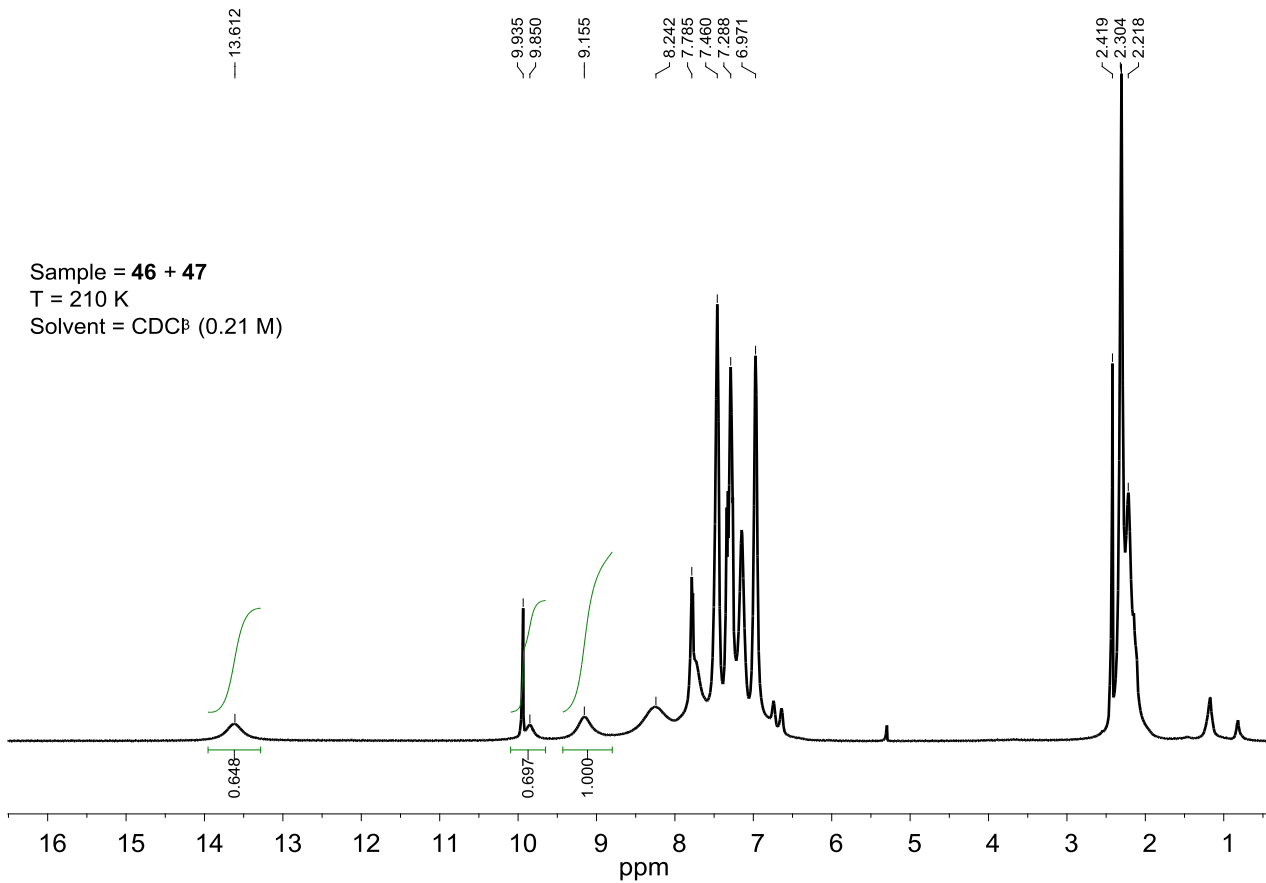
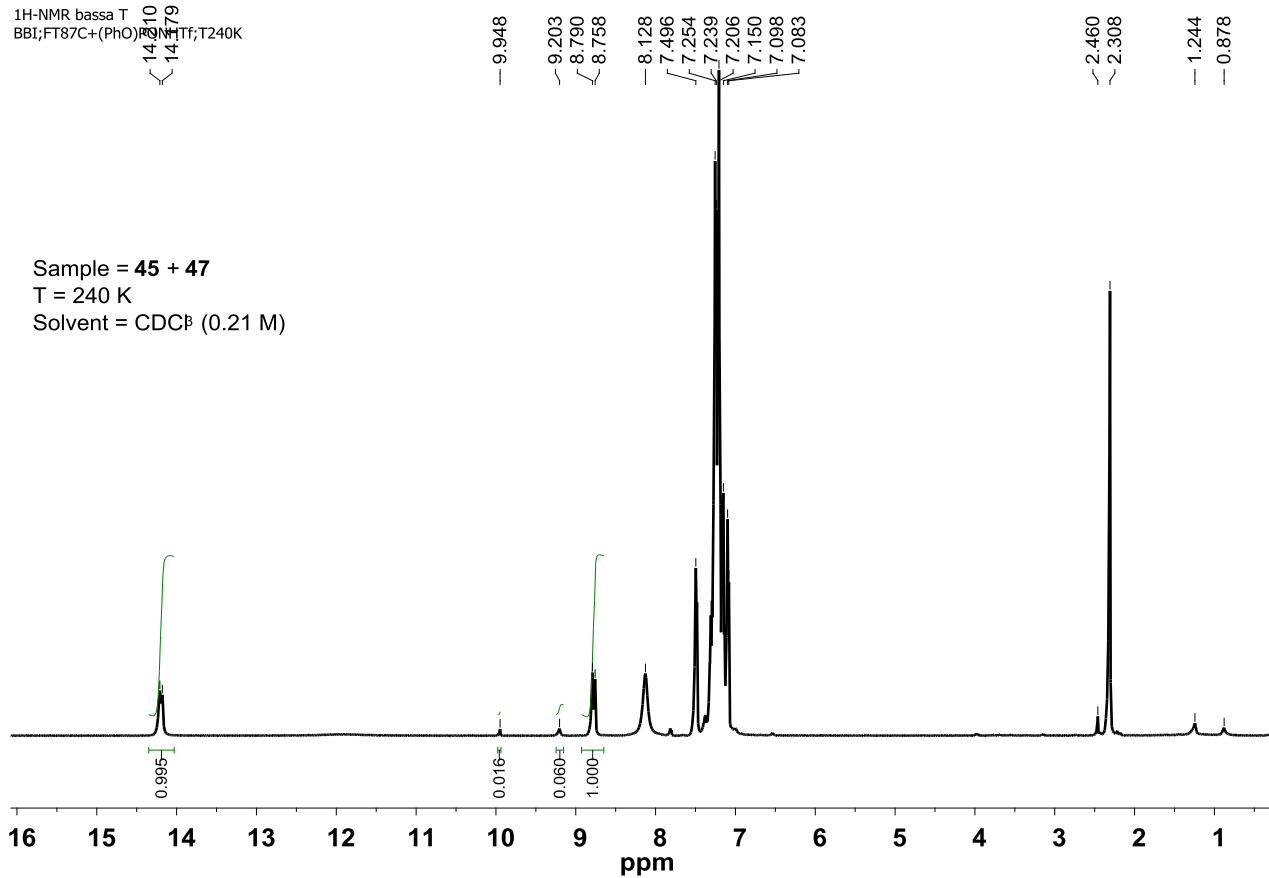
***N*-[(*E*)-Phenylmethylidene]-4-methylbenzenesulfonamide (**51**):** $^1\text{H-NMR}$ (300 MHz, CDCl_3): 8.99 (s, 1H), 7.88–7.82 (m, 4H), 7.53 (t, 1H), 7.40 (t, 2H), 7.28 (d, 2H), 2.35 (s, 3H). $^{13}\text{C-NMR}$ (75 MHz, CDCl_3): 169.9, 144.4, 134.7, 131.9, 130.9, 129.5, 128.8, 127.7, 21.3.

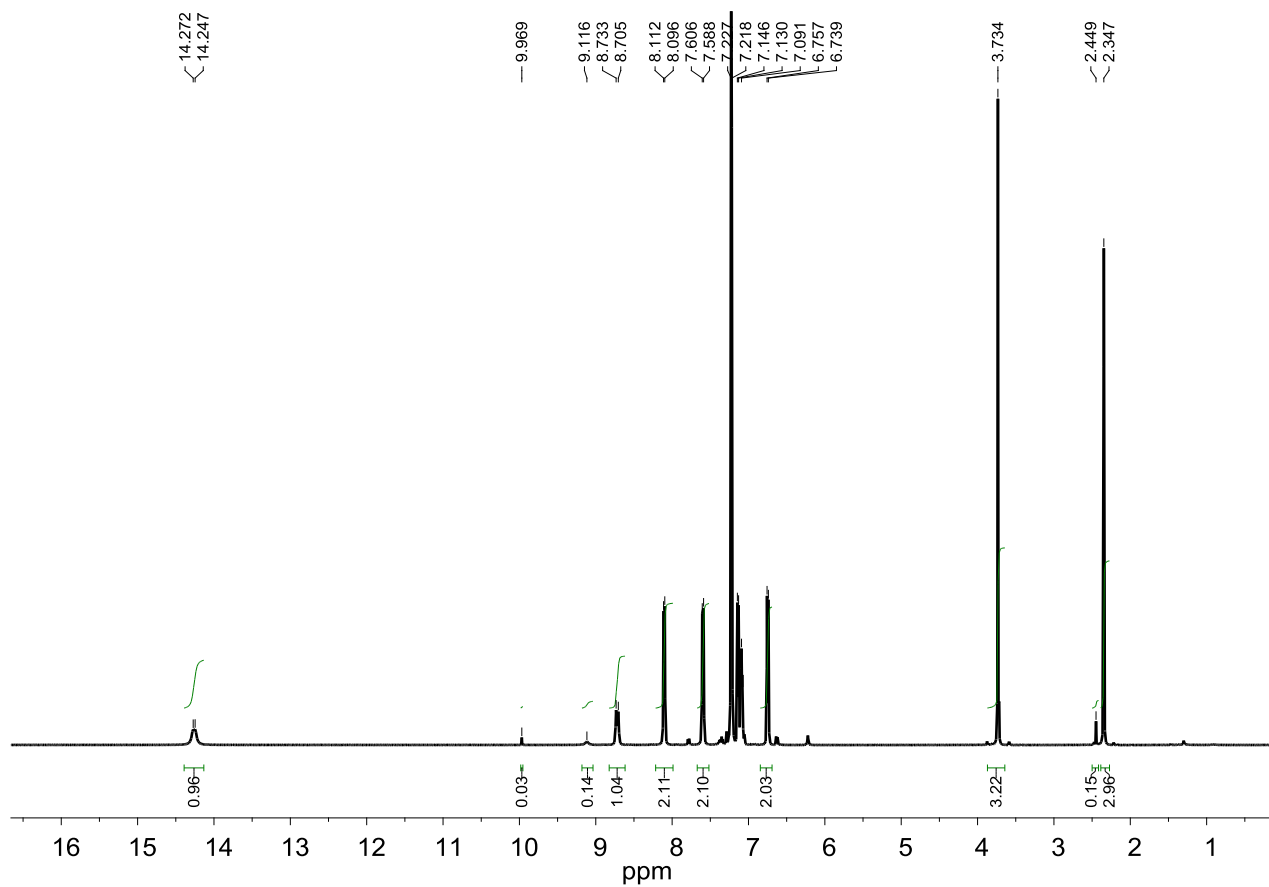
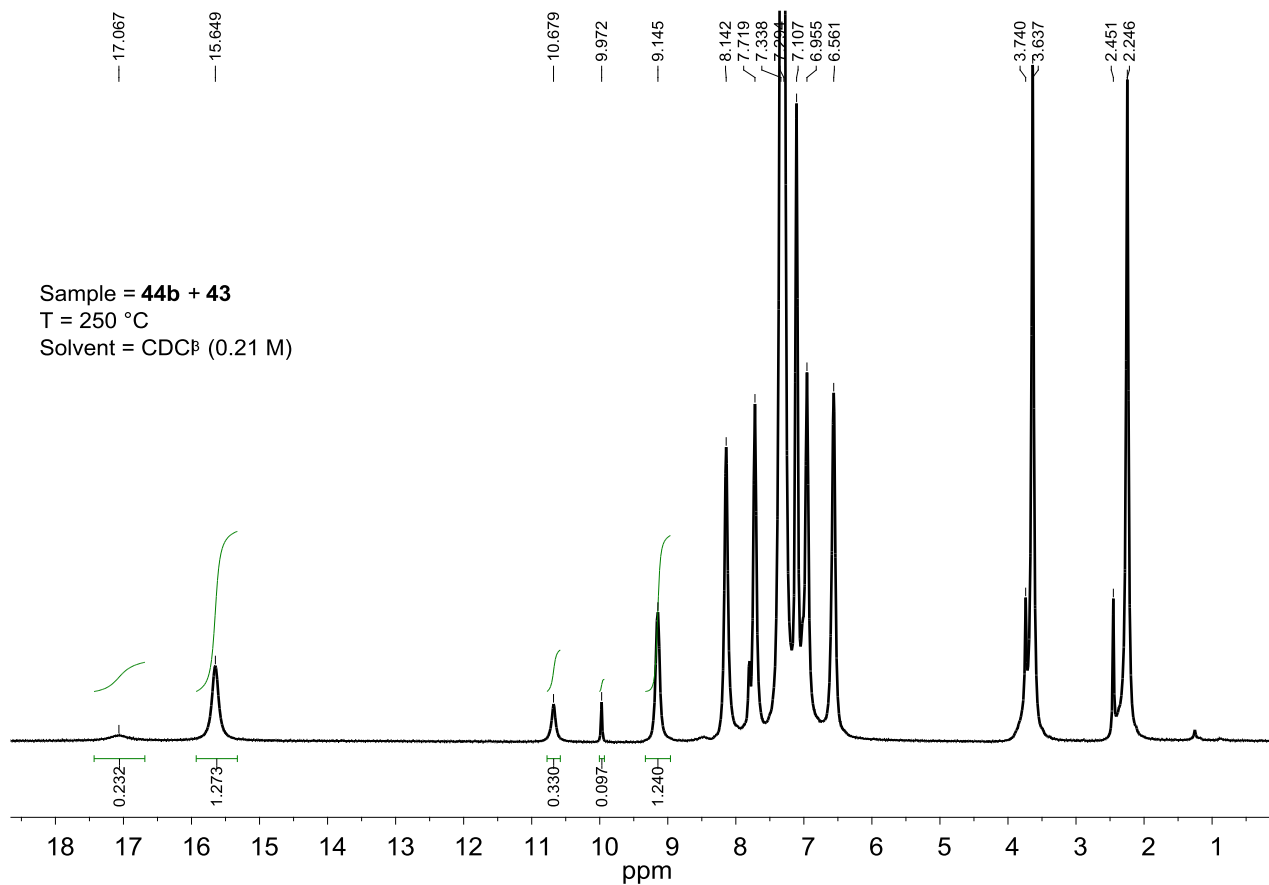
6.2.5. Acidity Scales: Determination of the Salts' Chemical Shifts

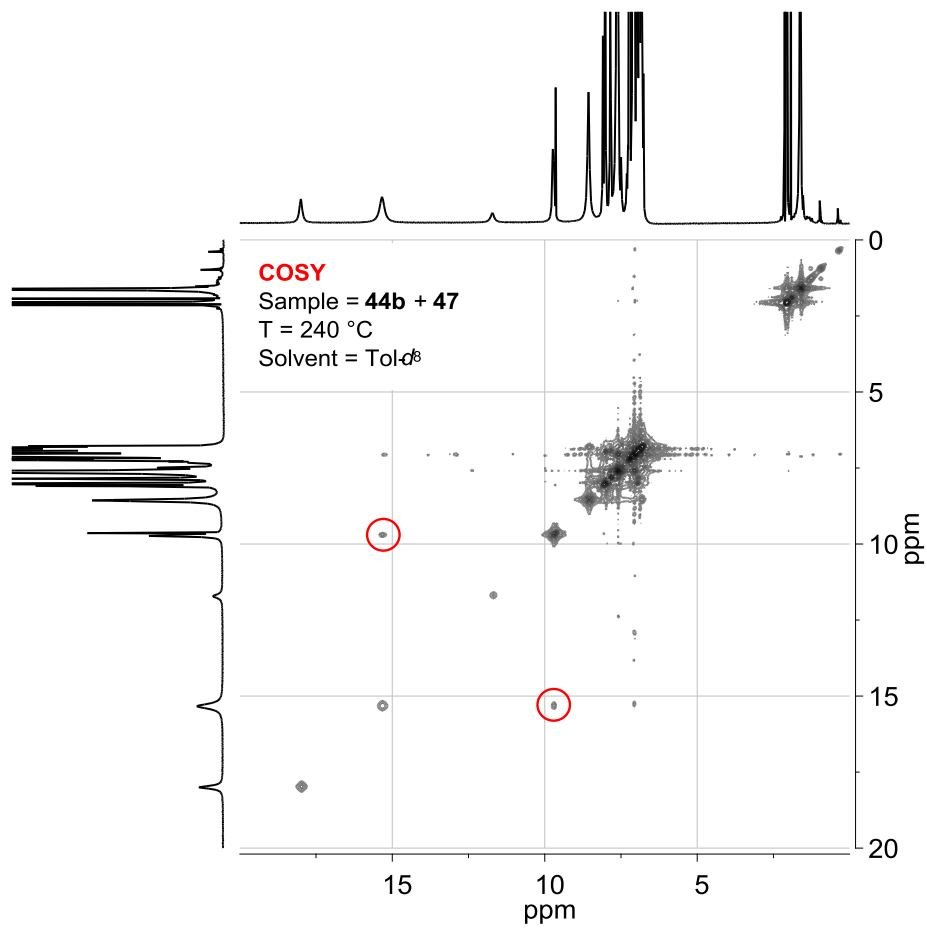
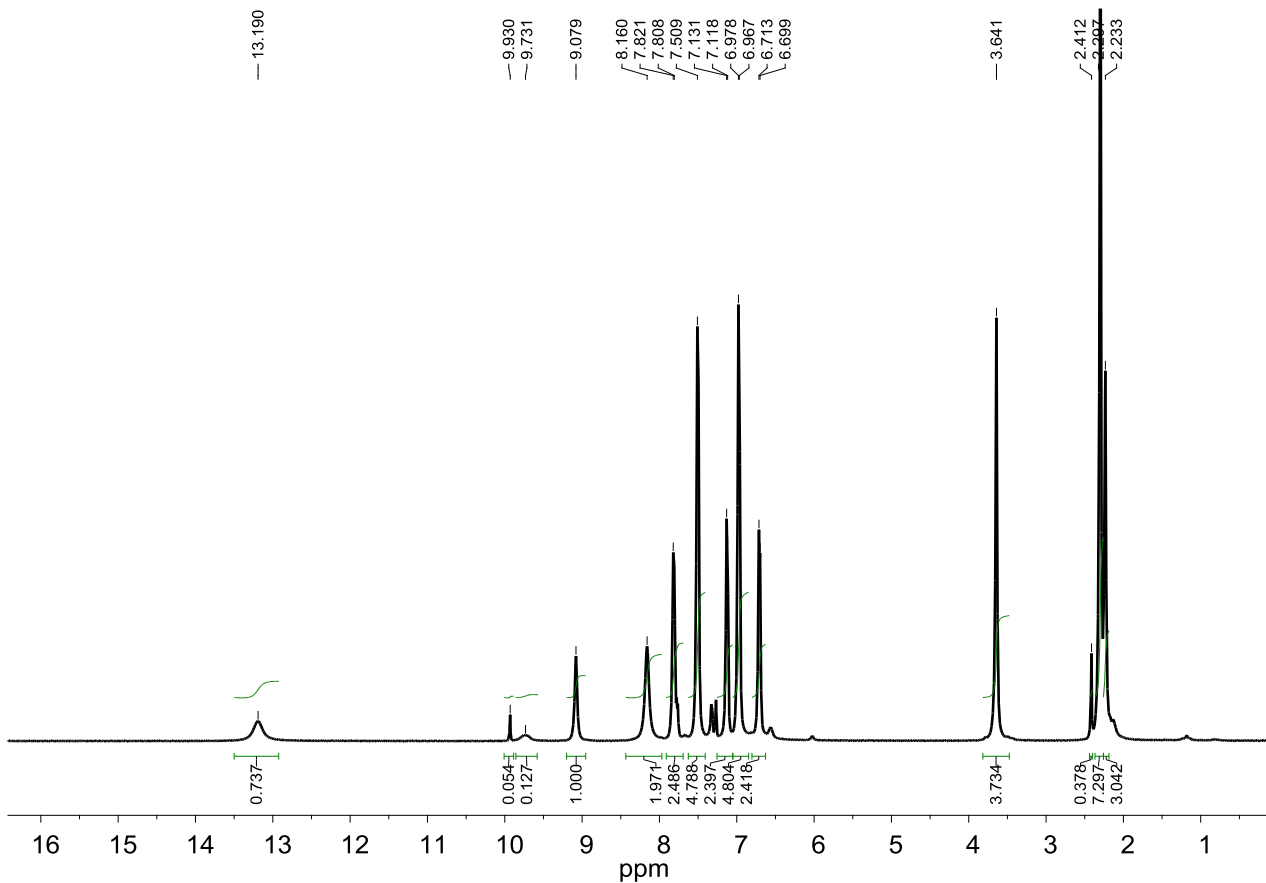
A vial was charged with the base (0.21 mmol – imines **43**, **47** and **48** or pyridine have been used in our studies), molecular sieves and 0.5 mL of deuterated solvent (CDCl_3 or CD_3CN). To the resulting mixture, a solution of the proper acid (0.21 mmol) in 0.5 mL of the chosen solvent, was added. The resulting mixture was charged in the NMR tube and the $^1\text{H-NMR}$ spectrum was recorded. The obtained results are reported in Chapter 2. Exemplificative low temperature $^1\text{H-NMR}$ and COSY spectra are reported below.



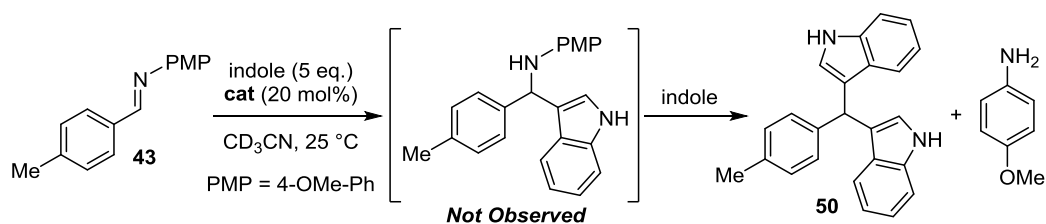
1H-NMR bassa T
BBI;FT87C+(PhO)2NHTf;T240K







6.2.6. Kinetic Experiments: Friedel-Craft Alkylation of Indole with *N*-4-Methoxyphenyl Imine **43**



To a vial charged with the acid (0.03 mmol, 20 mol%), anisole (as an internal standard) and indole (0.75 mmol, 5 eq.), the deuterated solvent (1.5 mL of acetonitrile- d_3) was added. The resulting solution was then transferred in a second vial containing the imine (0.15 mmol), while starting the chronometer. The resulting mixture, was charged in the NMR tube, and the kinetic experiment was performed recording a ^1H -NMR spectrum every 5 min.

Benzene- d_6 and CDCl_3 are unsuitable solvents for the present study. Indeed, salts generated from **46** exhibit poor solubility in benzene (consistent amounts of solid precipitate during the reaction in this solvent), and product **50** was found to undergo degradation in chloroform.

Reaction catalyzed by acid 44b:

In the following table the obtained absolute integral values for the signals relative to the starting imine **43** and to the final product **50** are reported. In the same table are reported also the normalized amount of these species. The reaction intermediate due to the attack of only one indole molecule to the imine was not detected.

t (min)	[43]	[50]	43 (mol%)	50 (mol%)
0	100	0	100.0	0.0
5	784.21	85.19	90.2	9.8
10	740.1	147.61	83.4	16.6
15	663.42	213.68	75.6	24.4
20	626.63	256.59	70.9	29.1
25	606.44	287.33	67.9	32.1
30	562.9	329.93	63.0	37.0
35	557.02	350.83	61.4	38.6
40	529.85	383.12	58.0	42.0
45	504.41	411.16	55.1	44.9
50	494.07	430.43	53.4	46.6
55	468.8	455.23	50.7	49.3
60	456.58	474.17	49.1	50.9
65	443.67	486.40	47.7	52.3
70	437.17	490.88	47.1	52.9
75	419.96	506.61	45.3	54.7
80	412.99	508.35	44.8	55.2
85	395.26	522.01	43.1	56.9
90	384.98	557.95	40.8	59.2

Reaction catalyzed by acid 45:

Brønsted acid **45** has demonstrated to be an extraordinary activating compound for this reaction, indeed, at the acquisition of the first spectrum, after 5 min from the reagents' mixing, the starting material **43** was already totally transformed into product **50**.

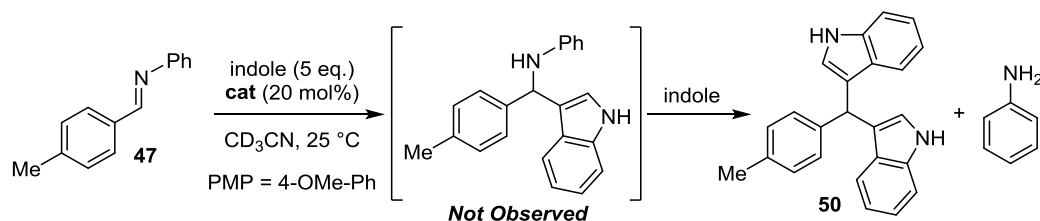
Reaction catalyzed by acid **46**:

In the following table the obtained absolute integral values for the signals relative to the starting imine **43** and to the final product **50** are reported. In the same table are reported also the normalized amount of these species. The reaction intermediate due to the attack of only one indole molecule to the imine was not detected.

t (min)	[43]	[50]	43 (mol%)	50 (mol%)
0	100	0	100.0	0.0
5	890	100.95	89.8	10.2
10	773	218.00	78.0	22.0
15	712	275.00	72.1	27.9
20	659	342.00	65.8	34.2
25	614	356.00	63.3	36.7
30	564	367.00	60.6	39.4
35	545	418.00	56.6	43.4
40	514	447.00	53.5	46.5
45	486	475.00	50.6	49.4
50	461	498.00	48.1	51.9
55	438	520.00	45.7	54.3
60	417	541.00	43.5	56.5
65	400	545.00	42.3	57.7
70	381	578.00	39.7	60.3
75	372	596.00	38.4	61.6
80	352	612.00	36.5	63.5
85	340	627.00	35.2	64.8
90	326	641.00	33.7	66.3
95	315	655.00	32.5	67.5
100	301	667.00	31.1	68.9
105	307	683.00	31.0	69.0

6.2.7. Kinetic Experiments: Friedel-Craft Alkylation of Indole with *N*-4-Methoxyphenyl Imine

47



To a vial charged with the acid (0.03 mmol, 20 mol%), anisole (as an internal standard) and indole (0.75 mmol, 5 eq.), the deuterated solvent (1.5 mL of acetonitrile-*d*₃) was added. The resulting solution was then transferred in a second vial containing the imine (0.15 mmol), while starting the chronometer. The resulting

mixture, was charged in the NMR tube, and the kinetic experiment was performed recording a $^1\text{H-NMR}$ spectrum every 5 min.

Benzene- d_6 and CDCl_3 are unsuitable solvents for the present study. Indeed, salts generated from **46** exhibit poor solubility in benzene (consistent amounts of solid precipitate during the reaction in this solvent), and product **50** was found to undergo degradation in chloroform.

Reaction catalyzed by acid 44b:

In the following table the obtained absolute integral values for the signals relative to the starting imine **47** and to the final product **50** are reported. In the same table are reported also the normalized amount of these species. The reaction intermediate due to the attack of only one indole molecule to the imine was not detected.

t (min)	$\int 47$	$\int 50$	47 (mol%)	50 (mol%)
0	-	-	100.0	0.0
5	271.14	672.46	28.7	71.3
10	130.13	825.73	13.6	86.4
15	74.49	874.26	7.9	92.1
20	42.56	900.45	4.5	95.5
25	22.53	909.45	2.4	97.6
30	16.44	923.99	1.7	98.3
35	11.6	921.98	1.2	98.8
40	7.8	934.65	0.8	99.2
45	4.93	926.18	0.5	99.5
50	3.85	920.19	0.4	99.6
55	2.02	932.04	0.2	99.8
60	0	100.00	0.0	100.0

Reaction catalyzed by acid 45:

Brønsted acid **45** has demonstrated to be an extraordinary activating compound for this reaction, indeed, at the acquisition of the first spectrum, after 5 min from the reagents' mixing, the starting material **47** was already totally transformed into product **50**.

Reaction catalyzed by acid 46:

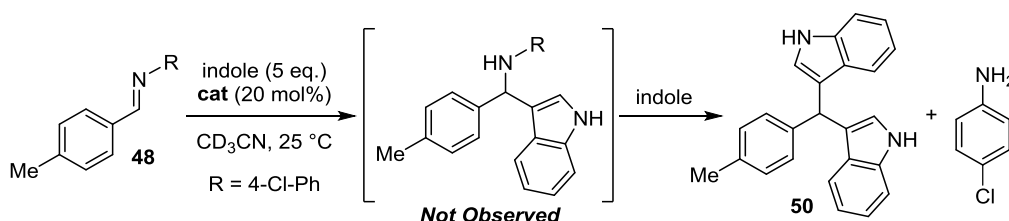
In the following table the obtained absolute integral values for the signals relative to the starting imine **47** and to the final product **50** are reported. In the same table are reported also the normalized amount of these species. The reaction intermediate due to the attack of only one indole molecule to the imine was not detected.

t (min)	$\int 47$	$\int 50$	47 (mol%)	50 (mol%)
0	100	0	100.0	0.0
5	136.16	2199.09	5.8	94.2
10	36.05	2006.18	1.8	98.2

15	21.54	1936.60	1.1	98.9
20	1.25	1945.32	0.1	99.9
25	0	100.00	0.0	100.0

6.2.8. Kinetic Experiments: Friedel-Craft Alkylation of Indole with *N*-4-Methoxyphenyl Imine

48

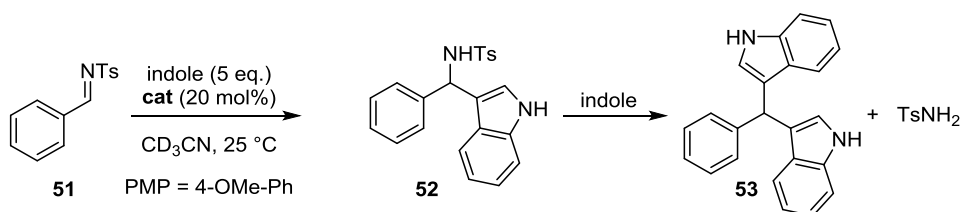


To a vial charged with the acid (0.03 mmol, 20 mol%), anisole (as an internal standard) and indole (0.75 mmol, 5 eq.), the deuterated solvent (1.5 mL of acetonitrile- d_3) was added. The resulting solution was then transferred in a second vial containing the imine (0.15 mmol), while starting the chronometer. The resulting mixture, was charged in the NMR tube, and the kinetic experiment was performed recording a $^1\text{H-NMR}$ spectrum every 5 min.

Benzene- d_6 and CDCl_3 are unsuitable solvents for the present study. Indeed, salts generated from **46** exhibit poor solubility in benzene (consistent amounts of solid precipitate during the reaction in this solvent), and product **50** was found to undergo degradation in chloroform.

When imine **48** is used as the substrate, the reaction results to be too fast to be monitored using time intervals of 5 min. Indeed, while catalyst **44b** was found to catalyze the reaction within 10 min, catalysts **45** and **46** are able to totally promote the process in less than 5 min.

6.2.9. Kinetic Experiments: Friedel-Craft Alkylation of Indole with *N*-Tosyl Imine 51



To a vial charged with the acid (0.03 mmol, 20 mol%), anisole (as an internal standard) and indole (0.75 mmol, 5 eq.), the deuterated solvent (1.5 mL of acetonitrile- d_3) was added. The resulting solution was then transferred in a second vial containing the imine (0.15 mmol), while starting the chronometer. The resulting mixture, was charged in the NMR tube, and the kinetic experiment was performed recording a $^1\text{H-NMR}$ spectrum every 5 min.

Benzene- d_6 and CDCl_3 are unsuitable solvents for the present study. Indeed, salts generated from **46** exhibit poor solubility in benzene (consistent amounts of solid precipitate during the reaction in this solvent), and product **50** was found to undergo degradation in chloroform.

Reaction catalyzed by acid 44b:

In the following table the obtained absolute integral values for the signals relative to the starting imine **51**, intermediate **52** and to the final product **50** are reported. In the same table are reported also the normalized amount of these species.

t (min)	∫51	∫52	∫53	51 (%)	52 (%)	53 (%)
0	-	-	-	100.0	0.0	0.0
5	557.23	13.57	117.09	81.0	17.0	2.0
10	489.33	21.66	205.92	68.3	28.7	3.0
15	424.29	32.25	284.92	57.2	38.4	4.3
20	364.33	44.4	353.11	47.8	46.3	5.8
25	313.85	54.2	410.29	40.3	52.7	7.0
30	274.15	69.49	471.33	33.6	57.8	8.5
35	231.17	77.8	510.12	28.2	62.3	9.5
40	201.55	88.63	550.46	24.0	65.5	10.5
45	171.36	97.92	583.64	20.1	68.4	11.5
50	145.61	109.23	617.08	16.7	70.8	12.5
55	121.76	117.71	642.71	13.8	72.9	13.3
60	101.77	130.57	670.06	11.3	74.3	14.5
65	85.57	138.33	686.77	9.4	75.4	15.2
70	68.97	145.9	704.27	7.5	76.6	15.9
75	57.71	157.96	723.81	6.1	77.0	16.8
80	45.19	165.64	733.75	4.8	77.7	17.5
85	35.79	174.21	746.64	3.7	78.0	18.2
90	26.99	183.06	753.96	2.8	78.2	19.0
95	20.76	191.47	763.46	2.1	78.2	19.6
100	13.11	200.53	771.34	1.3	78.3	20.4
105	9.51	208.04	775.97	1.0	78.1	20.9
110	6.11	214.5	778.27	0.6	77.9	21.5
115	2.65	222.86	779.85	0.3	77.6	22.2
120	0	233.83	788.59	0.0	77.1	22.9

Reaction catalyzed by acid 45:

In the following table the obtained absolute integral values for the signals relative to the starting imine **51**, intermediate **52** and to the final product **50** are reported. In the same table are reported also the normalized amount of these species.

t (min)	∫51	∫52	∫53	51 (%)	52 (%)	53 (%)
0	-	-	-	100.0	0.0	0.0
5	374.95	559.25	15.31	39.5	1.6	58.9
10	198.6	724.29	61.34	20.2	6.2	73.6
15	121.11	776.33	109.8	12.0	10.9	77.1
20	79.98	777.9	156.08	7.9	15.4	76.7
25	50.02	755.65	201.73	5.0	20.0	75.0
30	27.81	725.08	249.26	2.8	24.9	72.4
35	15.65	691.98	295.84	1.6	29.5	69.0
40	4.67	654.69	339.69	0.5	34.0	65.5
45	0	616.96	383.51	0.0	38.3	61.7
50	0	579.5	424.92	0.0	42.3	57.7
55	0	542.94	462.25	0.0	46.0	54.0
60	0	511.29	503.39	0.0	49.6	50.4
65	0	474.16	538.49	0.0	53.2	46.8
70	0	442.03	571.54	0.0	56.4	43.6

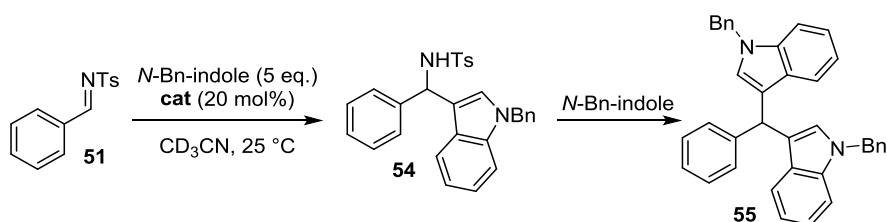
75	0	410.82	605.5	0.0	59.6	40.4
80	0	379.05	638.32	0.0	62.7	37.3
85	0	353.58	666.67	0.0	65.3	34.7
90	0	326.4	696.07	0.0	68.1	31.9
95	0	304.97	721.68	0.0	70.3	29.7
100	0	277.38	746.73	0.0	72.9	27.1
105	0	258.39	770.96	0.0	74.9	25.1
110	0	236	792.78	0.0	77.1	22.9
115	0	214.42	811.93	0.0	79.1	20.9
120	0	198.45	829.38	0.0	80.7	19.3

Reaction catalyzed by acid 46:

In the following table the obtained absolute integral values for the signals relative to the starting imine **51**, intermediate **52** and to the final product **50** are reported. In the same table are reported also the normalized amount of these species.

t (min)	[51]	[52]	[53]	51 (%)	52 (%)	53 (%)
0	-	-	-	100.0	0.0	0.0
5	799.05	103.42	5	88.1	11.4	0.6
10	743.31	170	7	80.8	18.5	0.8
15	700.42	225.25	8.96	74.9	24.1	1.0
20	658.54	278.62	9.98	69.5	29.4	1.1
25	620.51	330.01	11.53	64.5	34.3	1.2
30	586.97	373.19	12.51	60.3	38.4	1.3
35	555.94	414.02	14.53	56.5	42.1	1.5
40	528.77	448.36	15.21	53.3	45.2	1.5
45	504.81	480.33	16.61	50.4	47.9	1.7
50	482.42	506.9	17.52	47.9	50.3	1.7
55	461.15	534.8	20.7	45.4	52.6	2.0
60	442.74	560.07	21.29	43.2	54.7	2.1
65	425.97	580.98	23.26	41.3	56.4	2.3
70	409.96	602.95	25.08	39.5	58.1	2.4
75	393.61	622.11	27.58	37.7	59.6	2.6
80	379.6	642.92	31.69	36.0	61.0	3.0
85	368	656.88	32.39	34.8	62.1	3.1
90	355.03	673.44	36.1	33.3	63.3	3.4
95	344.21	686.67	36.89	32.2	64.3	3.5
100	333.67	699.07	38.92	31.1	65.2	3.6
105	324.53	711.2	41.62	30.1	66.0	3.9
110	315.9	721.97	43.81	29.2	66.7	4.1
115	307.46	732.82	45.78	28.3	67.5	4.2
120	298.72	739.18	47.66	27.5	68.1	4.4

6.2.10. Kinetic Experiments: Friedel-Craft Alkylation of *N*-Benzyl Indole with *N*-Tosyl Imine **51**



To a vial charged with the acid (0.03 mmol, 20 mol%), anisole (as an internal standard) and N-benzyl indole (0.75 mmol, 5 eq.) the deuterated solvent (1.5 mL of acetonitrile- d_3) was added. The resulting solution was then transferred in a second vial containing the imine (0.15 mmol), while starting the chronometer. The resulting mixture, was charged in the NMR tube, and the kinetic experiment was performed recording a ^1H -NMR spectrum every 5 min (for catalyst **44b**) or every 5 h (for catalyst **46**).

Benzene- d_6 and CDCl_3 are unsuitable solvents for the present study. Indeed, salts generated from **46** exhibit poor solubility in benzene (consistent amounts of solid precipitate during the reaction in this solvent), and product **50** was found to undergo degradation in chloroform.

Reaction catalyzed by acid 44b:

In the following table the obtained absolute integral values for the signals relative to the starting imine **51**, intermediate **54** and to the final product **55** are reported. In the same table are reported also the normalized amount of these species.

t (min)	∫ 51	∫ 54	∫ 55	51 (%)	54 (%)	55 (%)
0	1	0	0	100	0.0	0.0
5	720.89	42.54	47.95	88.8	5.2	5.9
10	667.48	116.78	69.99	78.1	13.7	8.2
15	625.74	209.32	88.23	67.8	22.7	9.6
20	587.87	298.50	111.96	58.9	29.9	11.2
25	559.44	380.33	126.82	52.5	35.7	11.9
30	524.14	520.33	157.42	43.6	43.3	13.1
35	499.01	590.94	164.85	39.8	47.1	13.1
40	466.78	720.13	182.13	34.1	52.6	13.3
45	440.3	840.72	197.71	29.8	56.9	13.4
50	413.06	979.64	209.58	25.8	61.1	13.1
55	386.55	1080.39	212.64	23.0	64.3	12.7
60	360.96	1192.21	227.45	20.3	67.0	12.8
65	340.16	1296.87	228.22	18.2	69.5	12.2
70	315.54	1427.20	237.09	15.9	72.1	12.0
75	295.51	1526.85	240.41	14.3	74.0	11.7
80	273.26	1641.89	250.46	12.6	75.8	11.6
85	249.39	1742.96	250.33	11.1	77.7	11.2
90	233	1839.91	255.05	10.0	79.0	11.0
95	219.63	1943.78	244.41	9.1	80.7	10.2
100	199.09	2041.16	259.61	8.0	81.7	10.4
105	187.68	2133.09	254.97	7.3	82.8	9.9
110	169.07	2180.19	263.67	6.5	83.4	10.1

Reaction catalyzed by acid 46:

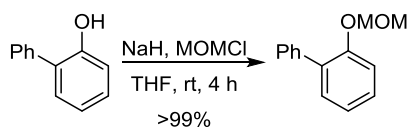
In the following table the obtained absolute integral values for the signals relative to the starting imine **51**, intermediate **54** and to the final product **55** are reported. In the same table are reported also the normalized amount of these species.

t (min)	∫ 51	∫ 54	∫ 55	51 (%)	54 (%)	55 (%)	t (min)
0	-	-	-	0	100.0	0.0	0.0

5	1402.52	701.26	166.31	27.52	87.9	10.4	1.7
10	1300	650	257.3	91.77	78.8	15.6	5.6
15	1215.2	607.6	344.36	138.57	71.6	20.3	8.2
20	1121.96	560.98	426.54	200.88	64.1	24.4	11.5
25	1038.36	519.18	491.86	276.31	57.5	27.2	15.3
30	961.28	480.64	535.40	348.69	52.1	29.0	18.9
35	888.02	444.01	585.33	442.19	46.4	30.6	23.1
40	819.98	409.99	628.12	530.20	41.4	31.8	26.8
45	772.36	386.18	648.37	616.98	37.9	31.8	30.3
50	716.04	358.02	675.76	715.74	34.0	32.1	34.0
55	664.22	332.11	686.49	807.57	30.8	31.8	37.4

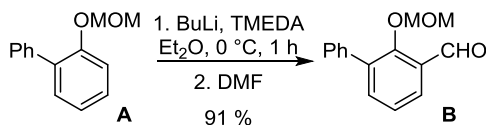
6.3. Information on Chapter 3

6.3.1. Synthesis of Aldehyde 58a



Reagent	eq	mmol	MW (g/mol)	g	d (g/mL)	V (mL)
2-Phenyl phenol	1	16.3	184	3	-	-
Sodium hydride (60% w/w)	3	48.9	24	1.95	-	-
Methoxymethyl chloride	2.5	40.7	80.5	3.3	1.06	3

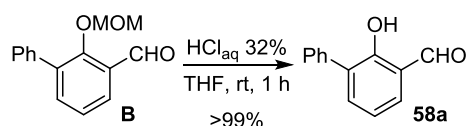
To a stirred suspension of NaH (60% w/w on mineral oil) in THF (70 mL) at 0°C under nitrogen atmosphere, a solution of 2-phenyl phenol in 20 mL of THF was added dropwise. After 30 min, a solution of MOMCl in 10 mL of THF was added, and the resulting mixture was allowed to stir at room temperature for 6 h. 100 mL of a saturated solution of NH₄Cl was then slowly added, and the resulting biphasic solution was separated. The aqueous phase was extracted twice with dichloromethane, and the reunited organic phases were dried over Na₂SO₄ and evaporated. The resulting crude oil was found to be pure, and was used in the following synthetic step without further purification (quantitative yield). ¹H-NMR (300 MHz, CDCl₃): 7.59 (d, 2H), 7.46 (t, 2H), 7.38 (m, 3H), 7.28 (d, 1H), 7.14 (t, 1H), 5.16 (s, 2H), 3.44 (s, 3H). ¹³C-NMR (75 MHz, CDCl₃): 154.2, 138.6, 131.9, 131.0, 129.6, 128.6, 128.0, 126.9, 122.3, 115.7, 95.1, 56.12.



Reagent	eq	mmol	MW (g/mol)	g	d (g/mL)	V (mL)
MOM-ether A	1	16.3	214.3	3.52	-	-
TMEDA	1.5	24.4	116	2.84	0.775	3.66
<i>n</i> -BuLi (1M)	1.2	20	-	-	-	20
DMF						5

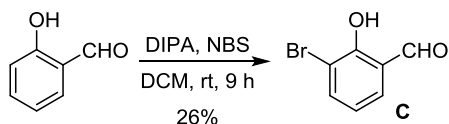
N,N,N',N'-Tetramethylethylenediamine (TMEDA) and freshly titrated 1.0 M *n*-BuLi in hexane were added to the MOM-ether **A** in dry Et₂O (17 mL) at 0 °C under nitrogen, and the mixture was stirred for 1 h to afford an orange/red suspension. This suspension was then cooled to -78 °C and 5 mL of DMF was added. After 5 min, the mixture was removed from the dry ice bath and stirred for 1 h at room temperature. The reaction

was quenched with saturated aqueous NH_4Cl . The crude product was extracted with Et_2O and dried over Mg_2SO_4 . The corresponding *o*-formylated MOM-ether **B** was purified by flash column chromatography (Hex/EtOAc from 97:3 to 9:1 mixtures as eluent; $R_f=0.42$ in 9:1 Hex/EtOAc) to give a transparent light yellow oil (91% yield). $^1\text{H-NMR}$ (300 MHz, CDCl_3): 10.52 (s, 1H), 7.90 (d, 1H), 7.65-7.30 (m, 7H), 4.73 (s, 2H), 3.28 (s, 3H). $^{13}\text{C-NMR}$ (75 MHz, CDCl_3): 190.62, 157.64, 137.44, 137.17, 136.35, 130.36, 129.28, 128.60, 127.77, 124.87, 100.5, 100.00, 57.76.



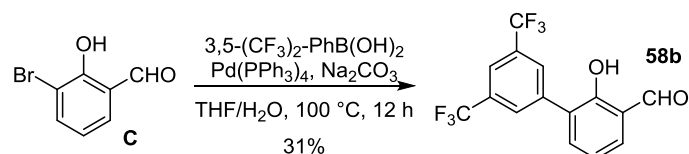
o-formylated MOM-ether **B** was dissolved in 21 mL of THF. To the stirred solution at 0°C , 6 mL of aqueous 32% HCl were added dropwise. The resulting mixture was allowed to stir at room temperature for 1 h (since the product **58a** presents the same retention factor R_f than the starting material **B**, the advancement of the reaction was monitored by $^1\text{H-NMR}$), and then the reaction was quenched by the addition of 20 mL of water. The biphasic mixture was extracted with Et_2O , the collected organic phase was dried over Na_2SO_4 and the volatiles removed under vacuum to give the pure salicylaldehyde **58a**. $^1\text{H-NMR}$ (300 MHz, CDCl_3): 11.63 (s, 1H), 9.96 (s, 1H), 7.68-7.64 (m, 3H), 7.60 (d, 1H), 7.50 (t, 2H), 7.72 (m, 1H), 7.15 (t, 1H). $^{13}\text{C-NMR}$ (75 MHz, CDCl_3): 196.89, 158.92, 137.84, 136.33, 133.23, 130.49, 129.30, 128.33, 127.71, 120.90, 119.96.

6.3.2. Synthesis of Aldehyde 58b



Reagent	eq	mmol	MW (g/mol)	g	d (g/mL)	V (mL)
Salicylaldehyde	1	12	122.12	1.46	1.15	1.27
Di-isopropyl-amine	0.1	1.2	101.2	0.12	0.722	0.17
<i>N</i> -Bromo succinimide	1	12	177.98	2.13	-	-

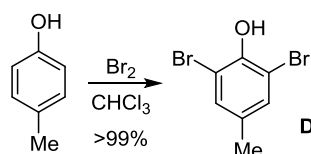
A solution of NBS in 90 mL of CH_2Cl_2 was added dropwise over 9 h to a mixture of salicylaldehyde and DIPA in 15 mL of CH_2Cl_2 . The resulting reaction mixture was stirred for 3 h, and then a 5% HCl solution was added. The phases were separated, the organic phase was dried over Na_2SO_4 and concentrated under vacuum to give an oil. Purification via flash column chromatography (Hex/AcOEt 95:5) furnished the desired product **C** as a clear solid (24% yield). $^1\text{H-NMR}$ (300 MHz, CDCl_3): 11.50 (s, 1H), 9.83 (s, 1H), 7.78 (d, 1H), 7.55 (d, 1H), 6.95 (t, 1H). $^{13}\text{C-NMR}$ (75 MHz, CDCl_3): 111.2, 120.8, 121.4, 132.9, 140.0, 158.1, 196.0.



Reagent	eq	mmol	MW (g/mol)	mg	d (g/mL)	V (mL)
3-Bromo-salicylaldehyde	1	201.2	0.75	150	-	-
3,5-bis-(trifluoromethyl)phenylboronic acid	2	257.93	1.5	387	-	-
Sodium carbonate	2	106	1.5	159	-	-
tetrakis-(triphenylphosphine)palladium (0)	0.2	1156	0.15	173.4	-	-

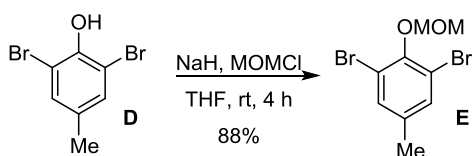
All the reagents were charged in a two neck round bottomed flask equipped with condenser, magnetic stirrer and under nitrogen atmosphere. 6 mL of THF/H₂O 1:1 were added and the resulting mixture was degassed by bubbling N₂ for 30 min. The obtained solution was then refluxed overnight, and upon cooling to room temperature, the reaction was extracted with CH₂Cl₂/H₂O. The organic phase was dried and the obtained crude mixture was purified through flash column chromatography (Hex/AcOEt 93:7; R_f=0.22 in Hex/AcOEt 9:1) to give the desired compound **58b** in 31% yield. ¹H-NMR (300 MHz, CDCl₃): 11.68 (s, 1H), 10.01 (s, 1H), 8.10 (s, 2H), 7.90 (s, 1H), 7.68 (t, 2H), 7.20 (t, 1H). ¹³C-NMR (75 MHz, CDCl₃): 196.70, 158.72, 138.30, 137.41, 134.56, 131.62 (q, ²J_{C-F} = 33 Hz), 129.47 (q, ³J_{C-F} = 3 Hz), 127.28, 123.36 (q, ¹J_{C-F} = 270 Hz), 121.34 (quint, ³J_{C-F} = 4 Hz), 121.07, 120.25. ¹⁹F-NMR (282 MHz, CDCl₃): -63.30.

6.3.3. Synthesis of Aldehyde 58c-f



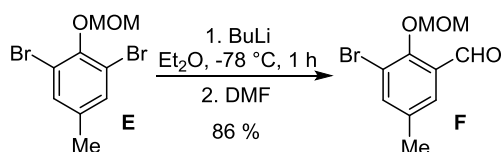
Reagent	eq	mmol	MW (g/mol)	g	d (g/mL)	V (mL)
<i>p</i> -cresol	1	92	108	10	-	-
Bromine	2.1	195	159.8	30.8	3.1	10

Bromine was added dropwise through a dropping funnel to a solution of *p*-cresol in 40 mL of CHCl₃ keeping the reaction temperature between 15 and 25°C (ATTENTION: the reaction generates a great amount of gaseous HBr! The use of an alkaline trap is recommendable). Once the addition was completed, the reaction was allowed to stir overnight and then quenched by the addition of a saturated solution of Na₂SO₃. The organic phase was separated, washed with water, dried over Na₂SO₄ and evaporated under vacuum to give the pure intermediate **D** in quantitative yield. ¹H-NMR (300 MHz, CDCl₃): 7.27 (s, 2H), 5.72 (s, 1H), 2.27 (s, 3H). ¹³C-NMR (75 MHz, CDCl₃): 147.13, 132.39 (2C), 109.43, 19.97.



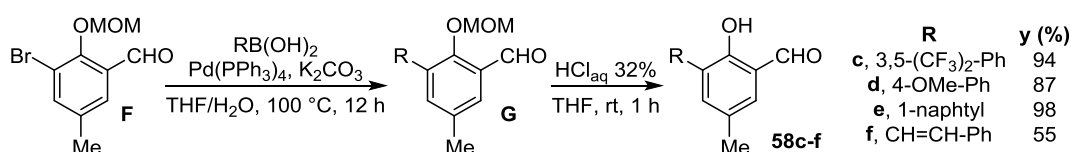
Reagent	eq	mmol	MW (g/mol)	g	d (g/mL)	V (mL)
2,6-Dibromo-4-methylphenol	1	92	265.8	24.4	-	-
Sodium hydride (80% w/w)	3	276	24	8.3	-	-
Methoxymethyl chloride	3	276	80.5	22.2	1.06	21

To a stirred suspension of NaH (80% w/w on mineral oil) in THF (300 mL) at 0°C under nitrogen atmosphere, a solution of 2,6-Dibromo-4-methylphenol **D** in 100 mL of THF was added dropwise. After 30 min, a solution of MOMCl in 100 mL of THF was added, and the resulting mixture was allowed to stir at room temperature for 6 h. 400 mL of a saturated solution of NH₄Cl was then slowly added, and the resulting biphasic solution was separated. The aqueous phase was extracted twice with dichloromethane, and the reunited organic phases were dried over Na₂SO₄ and evaporated. The resulting crude compound was purified through column chromatography (Hex/AcOEt 95:5; R_f=0.6 in Hex/AcOEt 9:1) to give the desired compound **E** in 88% yield. ¹H-NMR (300 MHz, CDCl₃): 7.33 (s, 2H), 5.14 (s, 2H), 3.72 (s, 3H), 2.27 (s, 3H). ¹³C-NMR (75 MHz, CDCl₃): 149.15, 137.78, 133.27, 117.91, 99.53, 58.41, 20.18.



Reagent	eq	mmol	MW (g/mol)	g	d (g/mL)	V (mL)
Intermediate E	1	32.7	309.8	10.15	-	-
<i>n</i> -BuLi (1 M)	1.1	36	-	-	-	36
DMF	-	-	-	-	-	10

The freshly titrated 1 M *n*-BuLi in Hexane was dropwise added to a solution of intermediate **E** in 100 mL of dry Et₂O at -78°C under nitrogen atmosphere. The resulting mixture was stirred at -78°C for 1.5 h, then the dry DMF was added and the reaction was allowed to warm to room temperature. After 1 h, 80 mL of water were slowly added, and the resulting phases were separated. The aqueous phase was extracted twice with Et₂O, and the collected organic phases were then dried over Na₂SO₄ and evaporated under vacuum to give the crude product. Purification through flash column chromatography (Hex/AcOEt 95:5; R_f=0.43 in Hex/AcOEt 9:1) furnished the pure *o*-formylated compound **F** in 86% yield. ¹H-NMR (300 MHz, CDCl₃): 10.23 (s, 1H), 7.57 (s, 1H), 7.52 (s, 1H), 5.10 (s, 2H), 3.55 (s, 3H), 2.28 (s, 3H). ¹³C-NMR (75 MHz, CDCl₃): 189.67, 154.99, 139.53, 136.05, 131.02, 127.70, 117.65, 100.85, 58.12, 20.33.



Reagent	eq	mmol	MW (g/mol)	g	d (g/mL)	V (mL)
Intermediate F	1	-	260	-	-	-
Boronic acid	1.5	-	-	-	-	-
Sodium carbonate	2	-	106	-	-	-
tetrakis-(triphenylphosphine)palladium (0)	0.1	-	1156	-	-	-

General procedure for the obtainment of salicylaldehydes 58c-f from intermediate F: All the reagents were charged in a two neck round bottomed flask equipped with condenser, magnetic stirrer and under nitrogen atmosphere. THF/H₂O 1:1 (substrate concentration: 0.15 M) were added and the resulting mixture was degassed by bubbling N₂ for 30 min. The obtained solution was then refluxed overnight, and upon cooling to room temperature, the reaction was extracted with CH₂Cl₂/H₂O. The obtained crude intermediate **G** was dissolved in X mL of THF (to give a 1 M solution) at 0°C, and then X/2 mL of 32% HCl_{aq} was dropped to the

solution. The resulting mixture was allowed to warm to room temperature and after 1 h the reaction was extracted with Et₂O/H₂O mixtures. The organic phase was dried over Na₂SO₄ and the obtained crude product was purified through flash column chromatography (Hex/AcOEt mixtures) to give the desired compounds **58c-f** in good yields.

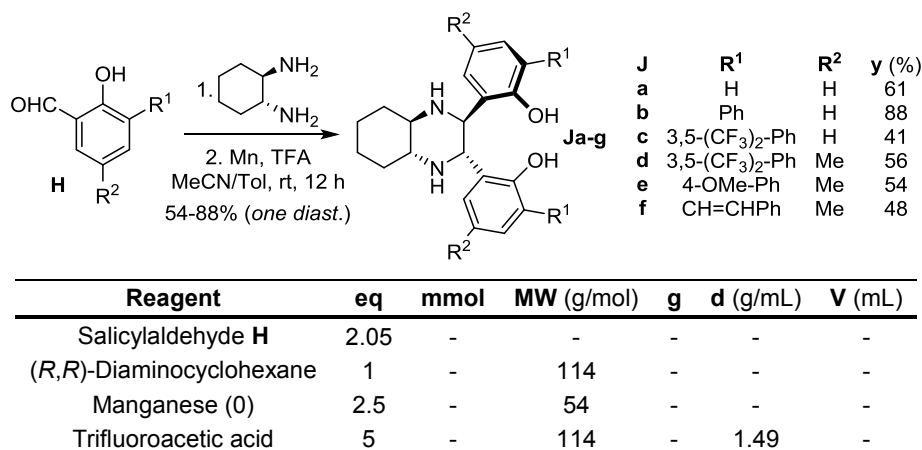
Salicylaldehyde 58c: 94% yield on a 2.3 mmol scale. Flash column chromatography eluent: Hex/AcOEt 95:5 ($R_f=0.34$ in Hex/AcOEt 9:1). ¹H-NMR (300 MHz, CDCl₃): 11.47 (s, 1H), 9.94 (s, 1H), 8.10 (s, 2H), 7.89 (s, 1H), 7.48 (s, 2H), 2.45 (s, 3H). ¹³C-NMR (75 MHz, CDCl₃): 196.70, 156.58, 138.47, 138.28, 134.42, 131.54 (q, q, ²J_{C-F} = 33 Hz), 129.76, 129.40 (q, ³J_{C-F} = 3 Hz), 126.94, 123.40 (q, ¹J_{C-F} = 270 Hz), 121.18 (quint, ³J_{C-F} = 4 Hz), 120.80, 20.17. ¹⁹F-NMR (282 MHz, CDCl₃): -63.25.

Salicylaldehyde 58d: 87% yield on a 2.5 mmol scale. Flash column chromatography eluent: Hex/AcOEt 9:1 ($R_f=0.31$ in Hex/AcOEt 9:1). ¹H-NMR (300 MHz, CDCl₃): 11.36 (s, 1H), 9.89 (s, 1H), 7.56 (d, 2H), 7.42 (s, 1H), 7.31 (s, 1H), 6.99 (d, 2H), 3.86 (s, 3H), 2.39 (s, 3H). ¹³C-NMR (75 MHz, CDCl₃): 196.82, 159.14, 156.79, 138.57, 132.44, 130.36, 129.85, 129.07, 128.77, 120.61, 113.74, 55.27, 20.28.

Salicylaldehyde 58e: 98% yield on a 1.9 mmol scale. Flash column chromatography eluent: Hex/AcOEt 95:5 ($R_f=0.37$ in Hex/AcOEt 9:1). ¹H-NMR (300 MHz, CDCl₃): 11.31 (s, 1H), 9.97 (s, 1H), 8.03 (d, 2H), 7.80 (d, 1H), 7.67-7.51 (m, 5H), 7.45 (s, 1H), 2.47 (s, 3H). ¹³C-NMR (75 MHz, CDCl₃): 196.89, 157.34, 140.21, 134.88, 133.75, 133.48, 131.99, 129.46, 129.11, 128.50, 127.73, 126.20, 126.01, 125.53, 120.56, 20.37.

Salicylaldehyde 58f: 55% yield on a 2.7 mmol scale. Flash column chromatography eluent: Hex/AcOEt 9:1 ($R_f=0.24$ in Hex/AcOEt 9:1). ¹H-NMR (300 MHz, CDCl₃): 11.45 (s, 1H), 9.82 (s, 1H), 7.62-7.56 (m, 3H), 7.47-7.38 (m, 3H), 7.33-7.26 (m, 2H), 7.20 (m, 1H), 2.38 (s, 3H). ¹³C-NMR (75 MHz, CDCl₃): 196.77, 127.16, 137.52, 134.48, 132.88, 130.33, 128.92, 128.71, 127.80, 126.71, 126.13, 121.55, 120.56, 20.40.

6.3.4. Synthesis of the (*R,R*)-DACH-based Diamines



General procedure for the obtainment of diamines Ja-f from salicylaldehydes H: To a solution of salicylaldehyde in MeOH (to give a 1 M solution) was added the (*R,R*)-DACH. The mixture was refluxed for 2 h and then cooled to room temperature. The solvent was removed by vacuum evaporation, and the yellow residue was dissolved in a dry 9:1 MeCN/Tol mixture (to give a 0.15 M solution) under nitrogen atmosphere. To the solution was added manganese powder, and the resulting mixture was cooled to 0°C before trifluoroacetic acid was added dropwise. The reaction mixture was stirred vigorously at room temperature for

24 h, and water was added to quench the reaction. The aqueous solution was extracted twice with dichloromethane. The combined organic layer was dried over Na₂SO₄ and concentrated to give the crude product that was purified through flash column chromatography (Hex/AcOEt mixtures).

Diamine Ja: 61% yield on a 20 mmol scale. The product was filtered through a short pad of silica gel with AcOEt. ¹H-NMR (300 MHz, CDCl₃): 1.41-1.46 (m, 4H), 1.76-1.82 (m, 4H), 2.41 (broad s, 2H), 2.67-2.70 (m, 2H), 4.15 (s, 2H), 6.12 (dd, 2H, J = 1.8, 7.5 Hz), 6.42 (dt, 2H, J = 1.2, 7.5 Hz), 6.84 (dd, 2H, J = 1.2, 8.1 Hz), 7.07 (dt, 2H, J = 1.8, 7.8 Hz), 10.86 (broad s, 2H). ¹³C-NMR (75 MHz, CDCl₃): 156.7, 130.0, 128.8, 123.1, 118.4, 116.4, 63.2, 59.5, 31.4, 24.2.

Diamine Jb: White solid obtained in 88% yield on a 2.4 mmol scale. Flash column chromatography eluent: Hex/AcOEt 95:5 to 8:2 (R_f=0.55 in Hex/AcOEt 8:2). ¹H-NMR (300 MHz, CDCl₃): 11.35 (bs, 2H), 7.65 (d, 4H, J = 9 Hz), 7.47 (t, 4H, J = 9 Hz), 7.35 (t, 2H, J = 9 Hz), 7.20 (d, 2H, J = 9 Hz), 6.65 (t, 2H, J = 9 Hz), 6.25 (d, 2H, J = 8 Hz), 4.38 (s, 2H), 2.73 (m, 2H), 2.57 (bs, 2H), 1.79 (m, 4H), 1.40 (m, 4H). ¹³C-NMR (75 MHz, CDCl₃): 153.96, 138.59, 130.17, 129.55, 129.45, 128.06, 126.82, 123.54, 118.78, 63.57, 59.66, 31.50, 24.35.

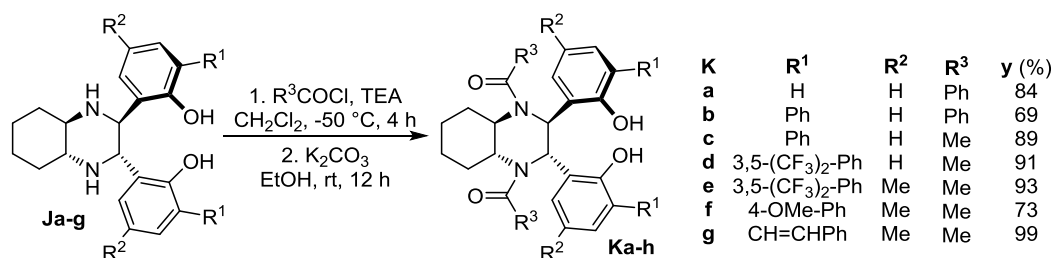
Diamine Jc: White solid obtained in 41% yield on a 0.36 mmol scale. Flash column chromatography eluent: Hex/AcOEt 9:1 (R_f=0.55 in Hex/AcOEt 8:2). ¹H-NMR (300 MHz, CDCl₃): 11.60 (bs, 2H), 8.14 (s, 4H), 7.85 (s, 2H), 7.22 (d, 2H, J = 7 Hz), 6.61 (t, 2H, J = 7 Hz), 6.27 (d, 2H, J = 7 Hz), 4.34 (s, 2H), 2.75 (m, 2H), 2.54 (bs, 2H), 1.86-1.72 (m, 4H), 1.44 (m, 4H). ¹⁹F-NMR (282 MHz, CDCl₃): -63.24.

Diamine Jd: White solid obtained in 56% yield on a 1.4 mmol scale. The product was filtered through a short pad of silica gel with Hex/AcOEt 85:15 (R_f=0.65 in Hex/AcOEt 8:2). ¹H-NMR (300 MHz, CDCl₃): 11.58 (bs, 2H), 8.20 (s, 4H), 7.90 (s, 2H), 7.06 (s, 2H), 5.93 (s, 2H), 4.10 (s, 2H), 2.90-2.42 (m, 4H), 2.05 (s, 6H), 1.84-1.76 (m, 4H), 1.42 (m, 4H). ¹³C-NMR (75 MHz, CDCl₃): 151.95, 140.64, 131.89, 131.23 (q, ²J_{C-F} = 33 Hz), 129.96, 129.61, 127.92, 125.60, 123.65 (q, ¹J_{C-F} = 270 Hz), 123.52, 120.28, 63.47, 59.45, 31.43, 24.22, 19.90. ¹⁹F-NMR (282 MHz, CDCl₃): -63.24.

Diamine Je: White solid obtained in 54% yield on a 1.0 mmol scale. Flash column chromatography eluent: Hex/AcOEt 8:2 (R_f=0.18 in Hex/AcOEt 8:2). ¹H-NMR (300 MHz, CDCl₃): 11.28 (bs, 2H), 7.63 (d, 4H, J = 9 Hz), 7.03 (d, 4H, J = 9 Hz), 7.00 (s, 2H), 5.85 (s, 2H), 4.13 (s, 2H), 3.89 (s, 6H), 2.54 (m, 2H), 2.46 (bs, 2H), 1.99 (s, 6H), 1.82-1.64 (m, 4H), 1.35 (m, 4H). ¹³C-NMR (75 MHz, CDCl₃): 158.54, 151.64, 131.29, 130.55, 130.06, 128.35, 127.27, 123.30, 113.57, 63.61, 59.56, 55.36, 31.55, 24.37, 20.05.

Diamine Jf: White solid obtained in 48% yield on a 0.7 mmol scale. Flash column chromatography eluent: Hex/AcOEt 9:1 (R_f=0.08 in Hex/AcOEt 9:1). ¹H-NMR (300 MHz, CDCl₃): 11.45 (bs, 2H), 7.64-7.53 (m, 6H), 7.45-7.40 (m, 4H), 7.32-7.19 (m, 6H), 5.72 (s, 2H), 3.93 (s, 2H), 2.52 (m, 2H), 2.36 (bs, 2H), 2.00 (s, 6H), 1.73 (m, 4H), 1.37-1.28 (m, 4H). ¹³C-NMR (75 MHz, CDCl₃): 152.61, 138.26, 131.00, 128.67, 128.19, 127.20, 126.49, 126.06, 124.41, 123.85, 123.14, 63.26, 59.28, 31.55, 24.28, 20.18.

6.3.5. Synthesis of the (*R,R*)-DACH-based Diols



Reagent	eq	mmol	MW (g/mol)	g	d (g/mL)	V (mL)
Diamine J	1	-	-	-	-	-
Benzoyl chloride	7	-	140.6	-	1.21	-
Acetyl chloride	7	-	78	-	1.1	-
Triethylamine	7	-	101	-	0.725	-

General procedure for the obtainment of diols Ka-h from diamines J: To a 0.1 M solution of the desired diamine J in dry CH₂Cl₂ was added the TEA and the mixture was cooled up to -50°C. The acetylating agent (benzoyl chloride or acetyl chloride) was added dropwise to the mixture, and after 2 h the reaction was allowed to warm to room temperature. a saturated solution of NaHCO₃ was added to quench the reaction, and the biphasic mixture was separated. The aqueous layer was extracted twice with CH₂Cl₂, and the collected organic layers were dried over Na₂SO₄ and concentrated under vacuum. The resulting crude compound was dissolved in X mL of EtOH to give a 0.06 M solution; then X mL of a saturated aqueous solution of K₂CO₃ was added. The resulting mixture was stirred overnight and then extracted three times with CH₂Cl₂. The organic layer was dried and concentrated to give the crude compound K, which was then purified through column chromatography (Hex/AcOEt 1:1) to give the pure desired compound in good yields.

Diol Ka: White solid obtained in 84% yield on a 3.7 mmol scale. Flash column chromatography eluent: Hex/AcOEt 1:1 (R_f=0.2 in Hex/AcOEt 1:1); the product can be further purified by trituration in ca. 4:1 CHCl₃/Hex mixtures. ¹H-NMR (300 MHz, CDCl₃): 8.12 (bs, 2H), 7.85 (dd, 2H, J = 9, 3 Hz), 7.27 (m, 4H), 7.18-7.03 (m, 8H), 6.85 (dd, 2H, J = 9, 3 Hz), 6.07 (s, 2H), 4.13 (m, 2H), 2.89 (m, 2H), 1.85-1.56 (m, 6H). ¹³C-NMR (75 MHz, CDCl₃): 173.53, 153.80, 137.17, 129.65, 128.65, 128.49, 127.64, 126.85, 126.72, 119.51, 115.37, 60.93, 55.84, 31.72, 25.19. ESI-MS: m/z = 555.4 (MNa⁺), 1087.3 (M₂Na⁺).

Diol Kb: White solid obtained in 69% yield on a 2.1 mmol scale. Flash column chromatography eluent: Hex/AcOEt 65:35 (R_f=0.5 in Hex/AcOEt 1:1). ¹H-NMR (300 MHz, CDCl₃): 7.83 (d, 2H, J = 9 Hz), 7.50-7.34 (m, 12 H), 7.28-7.23 (m, 4H), 7.07-7.01 (m, 8H), 5.94 (s, 2H), 5.17 (s, 2H), 4.24 (m, 2H), 2.97 (m, 2H), 1.93 (m, 2H), 1.73 (m, 4H). ¹³C-NMR (75 MHz, CDCl₃): 174.45, 148.27, 136.38, 136.08, 130.38, 130.02, 129.21, 129.18, 128.56, 128.08, 128.02, 127.87, 126.94, 126.35, 121.32, 61.14, 56.39, 32.27, 25.33.

Diol Kc: White solid obtained in 89% yield on a 0.58 mmol scale. Flash column chromatography eluent: Hex/AcOEt 65:35 (R_f=0.5 in Hex/AcOEt 1:1). ¹H-NMR (300 MHz, CDCl₃): 7.49-7.40 (m, 6H), 7.28 (d, 2H, J = 9 Hz), 7.07 (t, 2H, J = 9 Hz), 6.17 (s, 2H), 3.81 (m, 2H), 2.97 (m, 2H), 1.93 (s, 6H), 1.77 (m, 2H), 1.53-1.31 (m, 4H). ¹³C-NMR (75 MHz, CDCl₃): 173.78, 136.78, 130.35, 129.37, 129.23, 129.14, 128.05, 126.70, 125.86, 120.77, 57.57, 32.51, 29.70, 25.14, 22.28. [α]_D²⁰ = -12 (c = 0.1, CHCl₃).

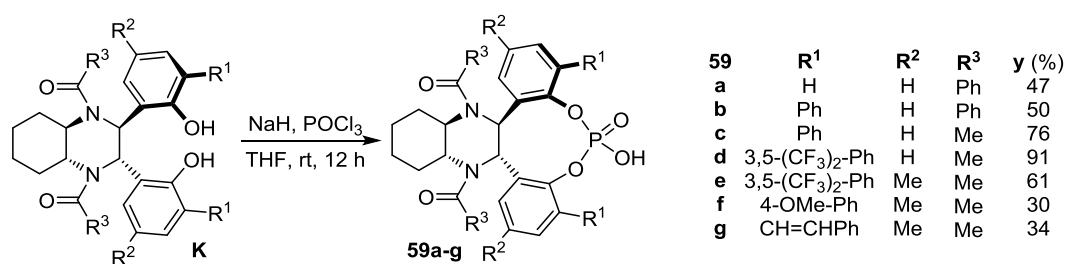
Diol Kd: White solid obtained in 91% yield on a 0.08 mmol scale. Flash column chromatography eluent: Hex/AcOEt 7:3 ($R_f=0.6$ in Hex/AcOEt 1:1). $^1\text{H-NMR}$ (300 MHz, CDCl_3): 7.94 (s, 4H), 7.84 (s, 2H), 7.33 (d, 2H, $J = 9$ Hz), 7.24 (d, 2H, $J = 9$ Hz), 7.05 (t, 2H, $J = 9$ Hz), 6.01 (s, 2H), 3.73 (m, 2H), 2.75 (m, 2H), 1.91 (s, 6H), 1.75 (m, 2H), 1.48-1.29 (m, 6H). $^{19}\text{F-NMR}$ (282 MHz, CDCl_3): -63.25.

Diol Ke: White solid obtained in 93% yield on a 0.8 mmol scale. Flash column chromatography eluent: Hex/AcOEt 7:3 ($R_f=0.55$ in Hex/AcOEt 1:1). $^1\text{H-NMR}$ (300 MHz, CDCl_3): 7.97 (s, 4H), 7.96 (bs, 2H), 7.82 (s, 2H), 7.14 (s, 2H), 7.05 (s, 2H), 6.09 (s, 2H), 3.68 (m, 2H), 2.70 (m, 2H), 2.35 (s, 6H), 1.84 (s, 6H), 1.74 (m, 2H), 1.45-1.32 (m, 4H). $^{13}\text{C-NMR}$ (75 MHz, CDCl_3): 174.44, 148.53, 140.33, 131.74 (q, $^2J_{\text{C-F}} = 33$ Hz), 130.82, 130.04, 129.55, 127.54, 126.86, 123.38 (q, $^1J_{\text{C-F}} = 271$ Hz), 120.79, 117.96, 58.29, 57.13, 33.35, 24.89, 21.44, 20.40, 20.36. $^{19}\text{F-NMR}$ (282 MHz, CDCl_3): -63.26. $[\alpha]_D^{20} = +21$ ($c = 0.1$, CHCl_3).

Diol Kf: White solid obtained in 73% yield on a 0.53 mmol scale. Flash column chromatography eluent: Hex/AcOEt 1:1 ($R_f=0.38$ in Hex/AcOEt 1:1). $^1\text{H-NMR}$ (300 MHz, CDCl_3): 7.36 (d, 4H, $J = 9$ Hz), 7.21 (s, 2H), 7.02 (s, 2H), 7.99 (d, 4H, $J = 9$ Hz), 6.24 (bs, 2H), 6.13 (s, 2H), 3.84 (s, 6H), 3.77 (m, 2H), 3.02 (m, 2H), 2.35 (s, 6H), 1.92 (s, 6H), 1.79 (m, 2H), 1.57-1.42 (m, 4H). $^{13}\text{C-NMR}$ (75 MHz, CDCl_3): 173.33, 159.37, 147.30, 130.73, 130.48, 129.69, 129.00, 128.57, 127.15, 125.53, 114.62, 58.11, 57.35, 55.33, 32.42, 25.25, 22.37, 20.90. $[\alpha]_D^{20} = -52$ ($c = 0.1$, CHCl_3).

Diol Kd: White solid obtained in quantitative yield on a 0.28 mmol scale. Flash column chromatography eluent: Hex/AcOEt 7:3 ($R_f=0.55$ in Hex/AcOEt 1:1). $^1\text{H-NMR}$ (300 MHz, CDCl_3): 7.98 (bs, 2H), 7.46 (d, 4H, $J = 9$ Hz), 7.38-7.24 (m, 10H), 7.02 (m, 4H), 5.99 (s, 2H), 3.73 (m, 2H), 2.81 (m, 2H), 2.32 (s, 6H), 1.88 (s, 6H), 1.69 (m, 2H), 1.42-1.27 (m, 4H). $^{13}\text{C-NMR}$ (75 MHz, CDCl_3): 174.60, 149.07, 137.64, 130.07, 129.39, 128.59, 127.52, 127.06, 126.59, 126.38, 125.96, 125.51, 123.03, 58.16, 57.23, 33.08, 25.00, 22.03, 21.04. $[\alpha]_D^{20} = -25$ ($c = 0.1$, CHCl_3).

6.3.6. Synthesis of the (*R,R*)-DACH-based Catalysts 59a-g



Reagent	eq	mmol	MW (g/mol)	mg	d (g/mL)	V (μL)
Diol K	1	-	-	-	-	-
Sodium hydride (60% w/w)	6	-	24	-	-	-
Phosphorous oxychloride (V)	2	-	153.33	-	1.645	-

To a suspension of NaH in THF under nitrogen atmosphere at 0°C was added a solution of the proper Diol K to give a 0.5 M solution of the corresponding dianion (which usually appears to be colored). After 15 min the POCl₃ was dropped to the solution, resulting in the discoloration of the reaction mixture, which was stirred at room temperature for further 12 h. 2 mL of water was slowly added, and after 1 h the reaction was extracted with CH₂Cl₂. The organic layer was dried over Na₂SO₄ and then concentrated under vacuum to provide the

crude product that was purified through flash column chromatography (Hex/AcOEt 7:3 to recover the unreacted starting diol, and then pure AcOEt to elute the acidic compound).

Catalyst 59a: White solid obtained in 47% yield. $^1\text{H-NMR}$ (300 MHz, CDCl_3): 7.51 (broad, 2H), 7.05-6.98 (broad, 14H), 6.70 (broad, 2H), 5.42 (broad, 2H), 4.15 (broad, 2H), 1.26 (broad, 2H), 1.63 (broad, 2H), 1.37 (m, 4H). $^{31}\text{P-NMR}$ (121.2 MHz, CDCl_3): -10.11. ESI-MS: $m/z = 617.4$ ($[\text{MH}]\text{Na}^+$), 639.6 ($[\text{MH}]_2\text{Na}^+$), 593.9 ($[\text{M}]$).

Catalyst 59c: White solid obtained in 76% yield. $^1\text{H-NMR}$ (300 MHz, CDCl_3): 7.44–7.15 (m, 8H), 6.16 (s, 1H), 3.89 (m, 1H), 3.11 (d, 1H), 1.84 (m, 1H), 1.61 (s, 3H), 1.48 (m, 2H). $^{31}\text{P-NMR}$ (121.2 MHz, CDCl_3): -14.8.

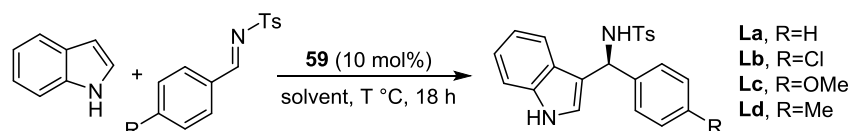
Catalyst 59d: White solid obtained in 91% yield. $^1\text{H-NMR}$ (300 MHz, CD_3OD): 8.15 (s, 4H), 8.01 (s, 2H), 7.65 (m, 2H), 7.51 (m, 4H), 6.35 (s, 2H), 4.00 (bs, 2H), 3.09 (bs, 2H), 1.90 (bs, 2H), 1.81 (s, 6H), 1.65 (bs, 4H). $^{13}\text{C-NMR}$ (75 MHz, CD_3OD): 175.16, 146.24, 146.13, 139.55, 133.10, 132.75, 132.68, 131.40 (q, $^2J_{\text{C-F}} = 33$ Hz), 130.85, 129.87, 126.84, 125.93, 124.70, 123.41 (q, $^1J_{\text{C-F}} = 272$ Hz), 121.18, 58.61, 57.43, 31.81, 24.82, 21.90. $^{19}\text{F-NMR}$ (282 MHz, CD_3OD): -62.1. $^{31}\text{P-NMR}$ (121 MHz, CD_3OD): -12.6. $[\alpha]_{\text{D}}^{20} = -108$ (c = 0.2, CHCl_3). $[\alpha]_{\text{D}}^{20} = -105$ (c = 0.17, CHCl_3).

Catalyst 59e: White solid obtained in 61% yield. $^1\text{H-NMR}$ (300 MHz, CDCl_3): 10.49 (bs, 1H), 8.02 (s, 4H), 7.69 (s, 2H), 7.24 (s, 2H), 7.22 (s, 2H), 6.14 (s, 2H), 3.86 (bs, 2H), 3.03 (bs, 2H), 2.46 (s, 6H), 1.82 (bs, 2H), 1.61 (s, 6H), 1.42 (bs, 2H). $^{13}\text{C-NMR}$ (75 MHz, CDCl_3): 176.05, 143.83, 143.73, 139.25, 136.31, 132.26, 132.19, 132.09, 132.02, 131.59, 131.14, 130.70, 129.84, 127.18, 123.22 (q, $1J_{\text{C-F}} = 272$ Hz), 58.64, 57.84, 31.88, 29.64, 22.07, 20.81. $^{19}\text{F-NMR}$ (282 MHz, CDCl_3): -63.7. $^{31}\text{P-NMR}$ (121 MHz, CDCl_3): -14.6.

Catalyst 59f: White solid obtained in 30% yield. $^1\text{H-NMR}$ (300 MHz, CDCl_3): 8.36 (bs, 1H), 7.34 (d, $J = 8.2$ Hz, 4H), 7.12 (s, 4H), 6.78 (d, $J = 8.1$ Hz, 4H), 6.10 (s, 2H), 3.90 (bs, 2H), 3.68 (s, 6H), 3.13 (m, 2H), 2.39 (s, 6H), 1.85 (bs, 2H), 1.65 (s, 6H), 1.48 (bs, 4H). $^{13}\text{C-NMR}$ (75 MHz, CDCl_3): 175.72, 158.98, 143.97, 143.86, 135.32, 134.88, 134.80, 131.93, 131.76, 130.69, 129.43, 125.34, 113.52, 58.79, 57.63, 55.08, 29.68, 25.15, 22.59, 21.05. $^{31}\text{P-NMR}$ (121 MHz, CDCl_3): -13.9. $[\alpha]_{\text{D}}^{20} = +171$ (c = 0.1, CHCl_3).

Catalyst 59g: White solid obtained in 34% yield. $^1\text{H-NMR}$ (300 MHz, CDCl_3): 7.35 (s, 4H), 7.24 (m, 2H), 7.15 (s, 6H), 7.03 (m, 4H), 6.83 (d, $J = 16.2$ Hz, 2H), 5.96 (s, 2H), 3.86 (bs, 2H), 3.09 (m, 2H), 2.29 (s, 6H), 1.74 (s, 6H), 1.52 (m, 4H), 1.38 (m, 2H). $^{13}\text{C-NMR}$ (75 MHz, CDCl_3): 175.03, 143.89, 143.78, 136.94, 135.53, 131.77, 130.30, 130.23, 128.50, 127.89, 126.72, 125.74, 120.79, 57.56, 53.42, 32.10, 29.69, 22.89, 21.26. $^{31}\text{P-NMR}$ (121 MHz, CDCl_3): -11.2. $[\alpha]_{\text{D}}^{20} = -275$ (c = 0.2, CHCl_3).

6.3.7. Stereoselective Friedel-Craft Alkylation



The indole (0.5 mmol) and the phosphoric acid catalyst (0.01 mmol) were dissolved in toluene (1 mL) under nitrogen at the desired temperature (generally -50°C). The imine (0.1 mmol) was then added in one portion and the mixture was stirred overnight. NaHCO_3 (1 mL) was added to quench the reaction, and the mixture

was extracted with CH₂Cl₂ (5 mL). The organic layer was separated and dried over anhydrous Na₂SO₄, the solvents were removed under reduced pressure and the residue was purified by flash chromatography (Hex/AcOEt 8:2) to afford the product. The conversion was evaluated by ¹H-NMR on the crude product, and the stereoselectivity by CSP-HPLC analysis on the purified product.

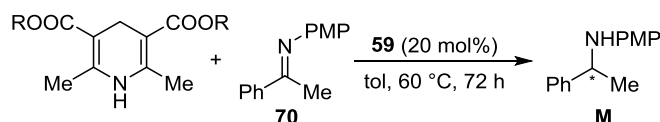
Sulfonamide La: R_f = 0.40 (Hex/AcOEt 2:1). 85% yield, 79% ee [Daicel Chiralcel OD-H, Hex/IPA 7:3, 0.6 ml/min, λ = 254 nm, t (major) = 16.92 min, t (minor) = 32.54 min]. ¹H-NMR (300 MHz, CDCl₃): 2.34 (s, 3H), 5.24 (d, J = 7.2 Hz, 1H), 5.82 (d, J = 6.9 Hz, 1H), 6.61 (d, J = 2.4 Hz, 1H), 6.97 (t, J = 7.8 Hz, 1H), 7.06 (d, J = 7.8 Hz, 2H), 7.11-7.27 (m, 8H), 7.53 (d, J = 8.4 Hz, 2H), 8.02 (br, 1H).

Sulfonamide Lb: R_f = 0.40 (Hex/AcOEt 2:1). 95% yield, 48% ee [Daicel Chiralcel OD-H, Hex/IPA 8:2, 1.0 ml/min, λ = 254 nm, t (major) = 15.13 min, t (minor) = 28.47 min]. ¹H-NMR (300 MHz, CDCl₃): 2.39 (s, 3H), 5.07 (d, J = 5.7 Hz, 1H), 5.82 (d, J = 6.6 Hz, 1H), 6.64 (s, 1H), 7.01 (t, J = 7.2 Hz, 1H), 7.12-7.21 (m, 8H), 7.31 (d, J = 8.4 Hz, 1H), 7.56 (d, J = 8.1 Hz, 2H), 8.02 (br, 1H).

Sulfonamide Lc: R_f = 0.40 (Hex/AcOEt 2:1). 96% yield, 63% ee [Daicel Chiralcel OD, Hex/IPA 6:4, 0.75 mL/min, λ 254 nm, t (major) = 12.09 min, t (minor) = 20.99 min]. ¹H NMR (300 MHz, CDCl₃): 8.01 (br, 1H), 7.57 (d, J = 8.3 Hz, 2H), 7.30 (d, J = 8.2 Hz, 1H), 7.167.21 (m, 1H), 7.147.12 (m, 5H), 6.99 (td, J1 = 0.9 Hz, J2 = 8.0 Hz, 1H), 6.756.71 (m, 3H), 5.79 (d, J = 6.7 Hz, 1H), 5.01 (d, J = 6.7 Hz, 1H), 3.77 (s, 3H), 2.38 (s, 3H).

Sulfonamide Ld: R_f = 0.50 (Hex/AcOEt 2:1). 37% yield, 56% ee [Daicel Chiralcel OD-H, Hex/IPA 7:3, 0.8 ml/min, λ = 254 nm, t (major) = 9.33 min, t (minor) = 16.71 min]. ¹H-NMR (300 MHz, CDCl₃): 2.26 (s, 3H), 2.33 (s, 3H), 5.27 (m, 1H), 5.76 (d, J = 7.2 Hz, 1H), 6.61 (m, 1H), 6.92-6.96 (m, 3H), 7.02-7.10 (m, 4H), 7.12 (d, J = 7.2 Hz, 1H), 7.22 (d, J = 8.1 Hz, 2H), 7.50 (dd, J1 = 1.8 Hz, J2 = 8.1 Hz, 2H), 8.03 (br, 1H).

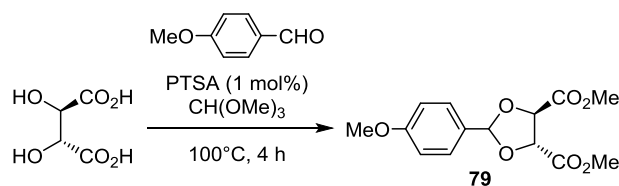
6.3.8. Stereoselective Transfer Hydrogenation with Hantzsch Esters



Imine **70** (0.1 mmol), the catalyst (20 mol%), the Hantzsch ester (0.2 mmol) and toluene (3.5 mL) were added to a screw-capped vial. The resulting yellow solution was allowed to stir at 60 °C for 3d in the sealed vial, and the solvent was then evaporated in vacuum. The resulting residue was purified by column chromatography on silica gel to afford the amine.

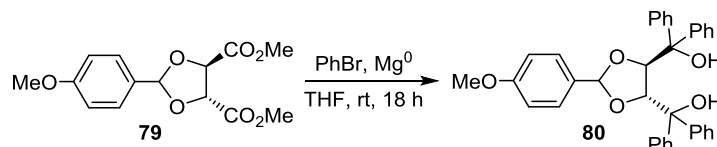
Amine M: R_f = 0.44 (CH₂Cl₂/Hex 8:2). up to 72% yield, up to 55% ee [Daicel Chiralcel OD, Hex/IPA 98:2, 0.6 mL/min, λ 254 nm, t (major) = 18.30 min, t (minor) = 20.42 min]. ¹H-NMR (300 MHz, CDCl₃): 1.41 (d, J = 6.8 Hz, 3H), 3.60 (s, 3H), 3.68 (bs, 1H), 4.32 (q, J = 6.8 Hz, 1H), 6.36–6.43 (m, 2H), 6.53–6.65 (m, 2H), 7.05–7.48 (m, 5H). The reported data was found to be in agreement with previously reported data.^{11b-c}

6.3.9. Synthesis of Phosphoric Acid 78



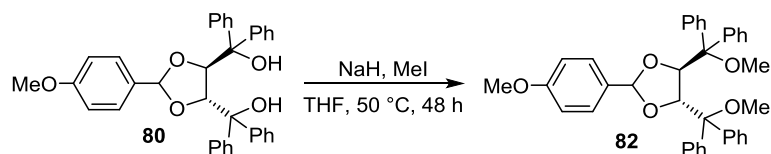
Reagent	eq	mmol	MW (g/mol)	g	d (g/mL)	V (mL)
(<i>R,R</i>)-Tartaric acid	1	66.6	150.1	10	-	-
<i>p</i> -Anisaldehyde	1.5	73.26	136.15	9.97	1.119	13.5
<i>p</i> -Toluenesulfonic acid	0.01	0.66	172.2	0.114	-	-
Methyl orthoformate	3.1	266.5	106.12	28.3	0.969	29.2
Methanol	5	333	32	10.6	0.741	14.3

A vigorously stirred mixture of all the reagents was refluxed (bath temp. 90°C) with Dean-Stark to remove the formed methyl formate and excess methanol until a volume of ca. 34 mL is collected. The oil residue is then dried in vacuum, diluted with CH₂Cl₂ and washed with NaHCO₃ s.s.. The organic layer was dried over Na₂SO₄, concentrated under vacuum and triturated in 300 mL of *i*-Pr₂O to give 9.7 g (50% yield) of the desired product **79** as a white solid. ¹H-NMR (300 MHz, CDCl₃): 7.50 (d, 2H, J = 8.6 Hz), 6.91 (d, 2H, J = 8.6 Hz), 6.09 (s, 1H), 4.95 (d, 1H, J = 4.0 Hz), 3.84 (s, 3H), 3.81 (s, 3H), 3.79 (s, 3H). ¹³C-NMR (75 MHz, CDCl₃): 170.11, 169.53, 160.96, 128.74, 127.44, 113.77, 106.71, 77.36, 77.04, 55.26, 52.76.



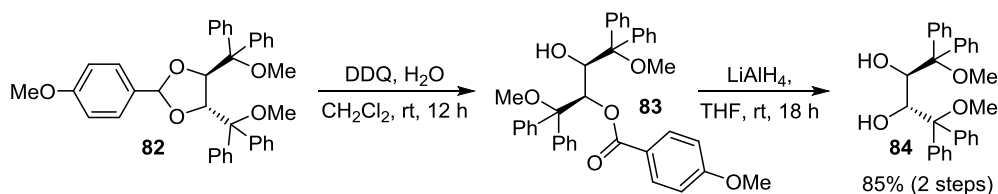
Reagent	eq	mmol	MW (g/mol)	g	d (g/mL)	V (mL)
Intermediate 79	1	5.8	296.3	1.72	-	-
Bromobenzene	10	58	157.01	6.1	1.495	4.1
Magnesium	10	58	24.3	1.41	-	-

Bromobenzene was slowly dropped to a suspension of Mg (0) in 16 mL of THF under nitrogen atmosphere, and the resulting mixture was refluxed for 1h. The reaction was cooled to 0°C and a solution of **79** in 10 mL of THF was dropped to the obtained PhMgBr solution. Once the addition was completed, the mixture was warmed to 60°C for 4 h and then cooled again to 0°C before the slow addition of 30 mL of NH₄Cl s.s.. 100 mL of Et₂O were added, and the two layers were separated. The aqueous phase was extracted twice with Et₂O, and the collected organic phases were dried with Na₂SO₄ and concentrated under vacuum to give diol **80** in quantitative yield. The obtained product was used in the following steps without further purification. ¹H-NMR (300 MHz, CDCl₃): 7.65-7.24 (m, 24H), 5.38 (d, 1H, J = 5.0 Hz), 5.24 (s, 1H), 5.20 (d, 1H, J = 5.0 Hz), 3.40 (s, 1H), 2.26 (s, 1H).



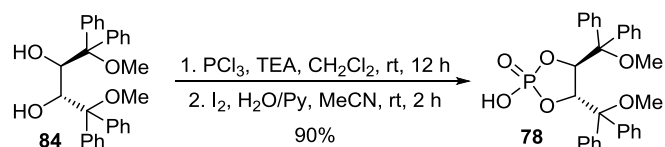
Reagent	eq	mmol	MW (g/mol)	g	d (g/mL)	V (mL)
Intermediate 80	1	6.5	544.6	3.54	-	-
Sodium hydride (50% w/w)	3	19.5	24	0.94	-	-
Methyl iodide	4	26	141.9	13.7	2.28	1.6

To a stirred suspension of NaH (50% w/w on mineral oil) in THF (6 mL) at 0°C under nitrogen atmosphere, a solution of **80** in THF (5 mL) was added dropwise. After 30 min, MeI was added, and the resulting mixture was allowed to stir at room temperature for 72 h. 10 mL of a saturated solution of NH₄Cl was then slowly added, and the resulting biphasic solution was separated. The aqueous phase was extracted twice with dichloromethane, and the reunited organic phases were dried over Na₂SO₄ and evaporated. The crude mixture was chromatographed (Hex/AcOEt 8:2; **82**'s R_f=0.48; monomethylated products' R_f=0.31). The recovered monomethylated byproducts were submitted again to this procedure in order to obtain additional amounts of product **82**. Overall yield: 89% from **79**. ¹H-NMR (300 MHz, CDCl₃): 6.61-7.34 (m, 20H), 7.02 (d, 2H, J = 8.5 Hz), 6.82 (d, 2H, J = 8.5 Hz), 5.52 (d, 1H, J = 5.0 Hz), 5.28 (d, 1H, J = 5.0 Hz), 5.07 (s, 1H), 3.82 (s, 3H), 3.19 (s, 3H), 3.15 (s, 3H). ¹³C-NMR (75 MHz, CDCl₃): 160.20, 143.11, 142.61, 142.28, 141.70, 130.00, 129.93, 129.80, 129.72, 129.36, 128.71, 127.84, 127.64, 127.52, 127.42, 127.17, 126.98, 113.16, 103.67, 84.27, 78.49, 77.61, 77.19, 76.77, 55.29, 52.62, 52.24.



Reagent	eq	mmol	MW (g/mol)	g	d (g/mL)	V (mL)
Intermediate 82	1	3.26	572.6	1.86	-	-
DDQ	1	3.26	227	0.74	-	-
Lithium aluminium hydride	3	9.78	38	0.37	-	-

Intermediate **82**, 2,3-dichloro-5,6-dicyano benzoquinone and 3 mL of water were dissolved in 30 mL of CH₂Cl₂. The mixture was stirred at room temperature for 12 h and then NaHCO₃ s.s. was added to quench the reaction. The layers were separated and the organic phase was dried over Na₂SO₄ and evaporated in vacuum to give the crude benzoate **83**. This crude product was dissolved in 5 mL of THF, and the resulting solution was dropwise added to a suspension of LiAlH₄ in 10 mL of THF at 0°C under nitrogen atmosphere. The reaction was stirred at room temperature overnight before it was quenched by the careful, dropwise addition of 3 mL of water and 10 mL of AcOEt. The obtained suspension was filtered through a pad of celite and the volatiles were removed by rotary evaporation. The resulting crude product was chromatographed (Hex/AcOEt 9:1; **84**'s R_f=0.44) to give the pure diol **84** in 85% yield from **82**. ¹H-NMR (300 MHz, CDCl₃): 7.45-7.24 (m, 20H), 4.72 (d, 2H, J = 3.6 Hz), 3.16 (s, 3H), 2.72 (d, 2H, J = 3.6 Hz). ¹³C-NMR (75 MHz, CDCl₃): 142.61, 141.29, 128.76, 128.08, 127.84, 127.74, 127.27, 127.16, 85.22, 71.15, 53.46.

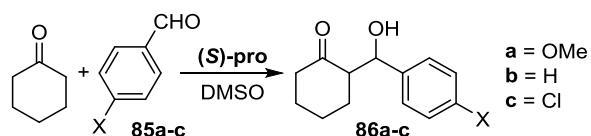


Reagent	eq	mmol	MW (g/mol)	mg	d (g/mL)	V (μL)
Diol 84	1	0.88	454.5	400	-	-
Phosphorous trichloride	1.5	1.32	137.33	181	1.57	120
Triethylamine	4	3.5	101	355	0.725	490
Iodine	3	2.6	253.8	670	-	-
Pyridine	3.5	3.08	79.1	243	0.982	250

PCl₃ was added dropwise to a solution of TEA and **84** in 5 mL of dry CH₂Cl₂ at -78°C under N₂ atmosphere. The mixture was stirred overnight at room temperature, and then 1 mL of H₂O was slowly added. After 24 h, the crude phosphite was extracted with CH₂Cl₂/HCl_{aq} 5%, separated, dried over Na₂SO₄ and concentrated by rotary evaporation. The obtained crude product was dissolved in 5 mL of acetonitrile, then pyridine, 500 μL of water and I₂ were added, and the resulting mixture were stirred for 2 h. The reaction was quenched with Na₂SO₃ s.s. and extracted with CH₂Cl₂ to furnish the crude acid **78**, which was purified through flash column chromatography (CH₂Cl₂/MeOH/AcOH 90.5:7.5:2; **78**'s R_f=0.6 in CH₂Cl₂/MeOH/AcOH 90:10:5). The obtained compound was washed with CH₂Cl₂/H₂O to remove the remaining AcOH affording the pure phosphoric acid **78**. NOTE: the product was found to degrade within 48 h. ¹H-NMR (300 MHz, CDCl₃): 10.36 (bs, 1H), 7.45-7.29 (m, 20H), 5.45 (d, 2H, ³J_{P-H} = 12.4 Hz), 2.85 (s, 6H). ³¹P-NMR (121.2 MHz, CDCl₃): 19.83.

6.4. Information on Chapter 4

6.4.1. General Procedure for the Proline-Catalyzed Aldol Reaction



To a stirred solution of L-proline (0.6 mmol) in DMSO (5 mL) the cyclohexanone (10 mmol) was added. After 10 minutes benzaldehyde (2 mmol) was added and the reaction was stirred at 25 °C. After the desired period of time the reaction was poured into 15 mL of a saturated solution of NH₄Cl and extracted with AcOEt (3x10). The collected organic phases were washed with brine, dried with Na₂SO₄ and then concentrated in vacuum to afford the crude product that was analyzed by ¹H-NMR for the determination of the conversion and of the *syn:anti* ratio. It was then purified by flash column chromatography (Hex/AcOEt 9:1 or 8:2 mixtures) to afford the pure ketol as mixture of diastereoisomers.

Ketol *syn*-86a: ¹H-NMR (300 MHz, CDCl₃): 7.21 (d, 2H, J = 8.7 Hz), 6.85 (d, 2H, J = 8.7 Hz), 5.28 (bs, 1H), 3.76 (s, 3H), 3.04 (bs, 1H), 2.53 (m, 1H), 2.43-2.26 (m, 2H), 2.04 (m, 1H), 1.85-1.45 (m, 5H). The enantiomeric excesses were evaluated by CSP-HPLC on a Chiralpak AD column (Hex/IPA 95:5; 0.5 mL/min; λ=230 nm): t (minor) = 35.9 min, t (major) = 41.9 min.

Ketol *anti*-86a: ¹H-NMR (300 MHz, CDCl₃): 7.17 (d, 2H, J = 8.6 Hz), 6.80 (d, 2H, J = 8.6 Hz), 4.68 (d, 1H, J = 8.8 Hz), 3.96 (bs, 1H), 3.71 (s, 3H), 2.53 (m, 1H), 2.37 (m, 1H), 2.28 (m, 1H), 1.97 (m, 1H), 1.71-1.39 (m,

5H). The enantiomeric excesses were evaluated by CSP-HPLC on a Chiralpak AD column (Hex/IPA 95:5; 0.5 mL/min; $\lambda=230$ nm): t (minor) = 63.3 min, t (major) = 68.5 min.

Ketol *syn*-86b: $^1\text{H-NMR}$ (300 MHz, CDCl_3): 7.32-7.23 (m, 5H), 5.37 (bs, 1H), 3.07 (bs, 1H), 2.59 (m, 1H), 2.42-2.34 (m, 2H), 2.09-2.03 (m, 1H), 1.85-1.42 (m, 5H). The enantiomeric excesses were evaluated by CSP-HPLC on a Chiralpak AD column (Hex/IPA 95:5; 0.5 mL/min; $\lambda=230$ nm): t (minor) = 35.9 min, t (major) = 41.9 min.

Ketol *anti*-86b: $^1\text{H-NMR}$ (300 MHz, CDCl_3): 7.28-7.22 (m, 5H), 4.75 (d, 1H, J = 8.6 Hz), 4.00 (s, 1H), 2.56 (m, 1H), 2.38 (m, 1H), 2.29 (m, 1H), 1.98 (m, 1H), 1.72-1.39 (m, 4H), 1.25 (m, 1H). The enantiomeric excesses were evaluated by CSP-HPLC on a Chiralpak AD column (Hex/IPA 95:5; 0.5 mL/min; $\lambda=230$ nm): t (minor)= 63.3 min, t (major)= 68.5 min.

Ketol *syn*-86c: $^1\text{H-NMR}$ (300 MHz, CDCl_3): 7.27 (d, 2H, J = 8.4 Hz), 7.21 (d, 2H, J = 8.4 Hz), 5.30 (bs, 1H), 3.20 (bs, 1H), 2.52 (m, 1H), 2.42-2.25 (m, 2H), 2.01 (m, 1H), 1.82 (m, 1H), 1.72-1.43 (m, 4H). The enantiomeric excesses were evaluated by CSP-HPLC on a Chiralpak AD column (Hex/IPA 9:1; 0.5 mL/min; $\lambda=230$ nm): t (min) = 16.6 min, t (major) = 19.5 min.

Ketol *anti*-86c: $^1\text{H-NMR}$ (300 MHz, CDCl_3): 7.28 (d, 2H, J = 8.5 Hz), 7.21 (d, 2H, J = 8.5 Hz), 4.72 (d, 1H, J = 8.6 Hz), 4.00 (bs, 1H), 2.52 (m, 1H), 2.41 (m, 1H), 2.34-2.24 (m, 1H), 1.73 (m, 1H), 1.67-1.42 (m, 3H), 1.23 (m, 1H). The enantiomeric excesses were evaluated by CSP-HPLC on a Chiralpak AD column (Hex/IPA 9:1; 0.5 mL/min; $\lambda=230$ nm): t (minor) = 25.3 min, t (major) = 29.6 min.

6.4.2. Proline-Catalyzed Retro-Aldol Reaction

The racemic *anti*-ketol **86** (0.2 mmol) synthesized according to a previously reported procedure, 1,3-dinitrobenzene (0.1 mmol, *internal standard*) and *rac*-proline (0.1 mmol; 50 mol%) was dissolved in 2 mL of $\text{DMSO-}d_6$. An NMR tube was filled with the resulting mixture and periodic $^1\text{H-NMR}$ analyses were performed providing the profiles reported in the text.

In order to prove the involvement of proline in the retro-aldol reaction, we repeated the reaction with *rac-anti*-**86a** and with different loadings of (*S*)-proline in $\text{DMSO-}d_6$ (0.075M) at 35°C, and we found a linear dependency of the reaction rate with respect to the catalyst's concentration. Moreover, a further proof of the involvement of proline in the retro-aldol reaction has been found when *rac-anti*-**86a** was mixed with (*S*)-proline (30 mol%) and cyclohexanone (4 eq.). The appearance of *syn*-**86a** was detected. After 72 h the crude mixture was extracted with $\text{AcOEt}/\text{NH}_4\text{Cl}$ s.s. and directly injected in a Chiral Stationary Phase HPLC revealing a 1:3 *syn:anti* ratio and 53% ee toward the *RS* enantiomer for *anti*-**86a**. *SR* is the favored product of the (*S*)-proline catalyzed reaction leading to compounds **86**, hence, a kinetic resolution of the racemic mixture occurred, where the (*S*)-proline preferentially reacted with **SR-86a**.

6.4.3. Geometries of Reaction the Involving Propionaldehyde

Geometries and energies obtained at the M06-2X/cc-PVTZ level of theory of the involved species are reported below.

Propionaldehyde:

	X	Y	Z
C	1.7616080	-0.2109800	0.0000730
H	1.8426200	-0.8491050	-0.8804370
H	1.8425200	-0.8489400	0.8807100
H	2.6123580	0.4672180	0.0000570
C	0.4468400	0.5535050	-0.0000770
H	0.3602580	1.2045770	0.8722400
H	0.3603780	1.2044010	-0.8725390
C	-0.7618500	-0.3527060	-0.0000800
H	-0.5473680	-1.4419780	-0.0002880
O	-1.8937950	0.0406130	0.0000950

Zero-point correction= 0.084439 (Hartree/Particle)
Thermal correction to Energy= 0.088802
Thermal correction to Enthalpy= 0.089746
Thermal correction to Gibbs Free Energy= 0.057904
Sum of electronic and zero-point Energies= -193.038811
Sum of electronic and thermal Energies= -193.034447
Sum of electronic and thermal Enthalpies= -193.033503
Sum of electronic and thermal Free Energies= -193.065346

Proline:

	X	Y	Z
N	-0.8775920	-0.9576630	-0.7857800
C	-2.0334110	-0.5754350	0.0460370
C	0.0870920	0.1353120	-0.7789730
H	-2.3529790	-1.4134590	0.6628590
H	-2.8724430	-0.2988830	-0.5974700
C	-1.5777820	0.6340120	0.8600360
C	-0.6426170	1.3282410	-0.1269730
H	0.4259630	0.3939300	-1.7845950
C	1.3251570	-0.2184510	0.0196960
H	-1.0195840	0.3072890	1.7395000
H	-2.3998590	1.2674040	1.1878260
H	0.0457460	2.0403540	0.3219660
H	-1.2209980	1.8468810	-0.8917720
O	1.4651590	-1.2050480	0.6894270
O	2.2833420	0.7170170	-0.0998080
H	3.0339660	0.4284470	0.4366830
H	-0.4353130	-1.7861430	-0.4104260

Zero-point correction= 0.146148 (Hartree/Particle)
Thermal correction to Energy= 0.153584
Thermal correction to Enthalpy= 0.154528
Thermal correction to Gibbs Free Energy= 0.113562
Sum of electronic and zero-point Energies= -401.001538
Sum of electronic and thermal Energies= -400.994102
Sum of electronic and thermal Enthalpies= -400.993158
Sum of electronic and thermal Free Energies= -401.034125

TS1 (addition of proline to propionaldehyde):

	X	Y	Z
N	0.1902540	0.5100590	0.0716880
C	-1.1532170	-0.0310300	0.4886100
C	-1.4432490	-1.2980640	-0.3507670
O	-0.5450810	-2.2209530	-0.2237280
C	0.1049840	1.9732010	0.3062480
C	-2.1393590	1.1287550	0.3173680
H	-2.9129930	0.8449110	-0.3910480
C	-1.2961120	2.3179370	-0.1733930
H	-2.6127950	1.3574070	1.2698640
H	-1.6387320	3.2753840	0.2111770
H	-1.3069080	2.3730680	-1.2629440
H	0.9169080	2.4839730	-0.2052700
H	0.2095680	2.1233330	1.3814430
H	-1.0310150	-0.3322040	1.5272580
H	0.2296310	-1.9350040	0.5644140
C	1.4634740	-0.2847320	0.7855310
H	1.8299240	0.5004750	1.4661120
O	1.0123640	-1.3522540	1.3906340
O	-2.4162070	-1.3373530	-1.0665360
C	2.4550020	-0.5346300	-0.3456540
H	2.0013420	-1.2486620	-1.0387250

H	3.2884420	-1.0551460	0.1265070
C	2.9588960	0.7086610	-1.0682090
H	3.3216650	1.4556010	-0.3593360
H	3.7828570	0.4589620	-1.7340240
H	2.1909800	1.1794070	-1.6868120
H	0.2882220	0.3519810	-0.9317970

Zero-point correction= 0.233258 (Hartree/Particle)
Thermal correction to Energy= 0.244549
Thermal correction to Enthalpy= 0.245494
Thermal correction to Gibbs Free Energy= 0.195597
Sum of electronic and zero-point Energies= -594.039455
Sum of electronic and thermal Energies= -594.028164
Sum of electronic and thermal Enthalpies= -594.027220
Sum of electronic and thermal Free Energies= -594.077116

Enamine:

	X	Y	Z
N	-0.2929610	0.5533280	-0.4701310
C	0.9472990	-0.0830210	-0.8343850
C	1.3669060	-1.2389900	0.0641710
O	0.9119240	-1.1074550	1.3236600
C	-0.0908930	1.6299060	0.4856950
C	1.9524620	1.0701370	-0.7092760
H	2.9769510	0.7229830	-0.5926940
C	1.4291000	1.8596490	0.4971380
H	1.8912410	1.6676530	-1.6176080
H	1.6892480	2.9138900	0.4383120
H	1.8541740	1.4628960	1.4172390
H	-0.4545550	1.3370460	1.4764200
H	-0.6528860	2.5130910	0.1716280
H	0.9090490	-0.4873590	-1.8459360
C	-1.4881520	-0.1345270	-0.5174100
H	-1.4683480	-1.0004480	-1.1733020
O	2.0548690	-2.1557060	-0.2875930
C	-2.6159890	0.1889790	0.1176870
H	-2.6336680	1.0559960	0.7671250
H	1.2367600	-1.8685080	1.8241100
C	-3.8908800	-0.5807520	-0.0400860
H	-3.7515310	-1.4330810	-0.7054290
H	-4.2517580	-0.9600950	0.9180200
H	-4.6874080	0.0396470	-0.4567060

Zero-point correction= 0.207307 (Hartree/Particle)
Thermal correction to Energy= 0.218493
Thermal correction to Enthalpy= 0.219437
Thermal correction to Gibbs Free Energy= 0.169558
Sum of electronic and zero-point Energies= -517.639582
Sum of electronic and thermal Energies= -517.628396
Sum of electronic and thermal Enthalpies= -517.627451
Sum of electronic and thermal Free Energies= -517.677331

87-SS:

	X	Y	Z
N	0.8466430	0.9656630	0.1821830
C	2.1609920	0.4839820	-0.2653830
C	2.1247500	-0.8445600	-1.0614470
O	1.0046410	-1.4885050	-1.1676750
C	0.7165030	0.9304460	1.6480300
C	2.9457820	0.3348720	1.0409180
H	3.7141130	-0.4265260	0.9434070
C	1.8535860	0.0046110	2.0591850
H	3.4251230	1.2806170	1.2966430
H	2.1631580	0.1630610	3.0890580
H	1.5252910	-1.0291960	1.9440430
H	-0.2603850	0.5541300	1.9293550
H	0.8571950	1.9428440	2.0375360
H	2.6159910	1.2117720	-0.9353840
C	-0.0977630	1.3065220	-0.6540300
H	0.1923080	1.2726400	-1.7015790
O	3.1702140	-1.1839680	-1.5600890
C	-1.4483300	1.4659130	-0.3390600
H	-1.6768040	1.7444500	0.6832610
C	-2.3473890	2.0536720	-1.3984530

H	-3.3636890	1.6694380	-1.3158230
H	-2.4043710	3.1404810	-1.3304660
H	-1.9838650	1.7993270	-2.3950850
H	0.1749630	-1.2829010	-0.4805860
C	-1.8403710	-0.4501310	-0.2130150
H	-2.0120050	-0.5869350	-1.2921180
C	-3.1206550	-0.4224760	0.6025850
H	-3.8207110	0.3212570	0.2238160
H	-2.8571150	-0.1534110	1.6272080
C	-3.7619310	-1.8084260	0.5775270
H	-4.6718850	-1.8265700	-1.1760930
H	-4.0228070	-2.0968060	-0.4416570
H	-3.0670350	-2.5478190	0.9710350
O	-0.8704820	-1.1070330	0.3171160

Zero-point correction= 0.294065 (Hartree/Particle)
 Thermal correction to Energy= 0.309161
 Thermal correction to Enthalpy= 0.310105
 Thermal correction to Gibbs Free Energy= 0.251660
 Sum of electronic and zero-point Energies= -710.675973
 Sum of electronic and thermal Energies= -710.660876
 Sum of electronic and thermal Enthalpies= -710.659932
 Sum of electronic and thermal Free Energies= -710.718378

87-RS:

	X	Y	Z
N	-0.8224090	0.8122940	0.5176790
C	-1.8814170	-0.2099190	0.3310240
C	-1.6102680	-1.5656430	-0.3599570
O	-2.3657340	-2.4531130	-0.0305590
C	-1.2596970	2.1306540	0.0272630
C	-2.9449890	0.5453760	-0.4761610
H	-2.7228910	0.4390450	-1.5398210
C	-2.7726200	2.0000880	-0.0488620
H	-3.9331580	0.1358170	-0.2895520
H	-3.2150550	2.1630370	0.9348350
H	-3.2114380	2.7074850	-0.7480850
H	-0.8215630	2.2855740	-0.9601880
H	-0.9053100	2.9100100	0.6998430
H	-2.2582550	-0.4595160	1.3231190
C	0.2948910	0.6566930	1.1759390
O	-0.7079010	-1.6489900	-1.2736500
C	0.9904310	-0.5458970	1.3150580
H	0.4193910	-1.4446450	1.1093150
H	0.0841400	-0.8299030	-1.3421160
C	2.0236050	-0.6975870	2.4004190
H	1.5802430	-1.0952470	3.3133260
H	2.8071690	-1.3902920	2.0885510
H	2.4925590	0.2564690	2.6421250
H	0.8056950	1.5797950	1.4403440
C	1.8710900	-0.3676880	-0.3871660
O	1.0287770	-0.0140740	-1.3073190
C	3.0530940	0.5638820	-0.2151500
H	2.6821620	1.5812880	-0.0759120
H	3.6467560	0.2909360	0.6561950
C	3.9197360	0.5047090	-1.4716790
H	4.7708670	1.1794850	-1.3903900
H	4.3027620	-0.5046400	-1.6284740
H	3.3313410	0.7809960	-2.3442880
H	2.1571720	-1.4303470	-0.3647210

Zero-point correction= 0.293363 (Hartree/Particle)
 Thermal correction to Energy= 0.308486
 Thermal correction to Enthalpy= 0.309430
 Thermal correction to Gibbs Free Energy= 0.251111
 Sum of electronic and zero-point Energies= -710.667415
 Sum of electronic and thermal Energies= -710.652292
 Sum of electronic and thermal Enthalpies= -710.651348
 Sum of electronic and thermal Free Energies= -710.709667

87-SR:

	X	Y	Z
N	-0.8156580	-0.9575390	-0.2945830
C	-1.8626670	-0.0625130	-0.8019070

C	-1.5831960	1.4456780	-0.5774460
O	-0.5437690	1.8011340	0.1078780
C	-1.2353340	-1.6436710	0.9440790
C	-3.1024790	-0.5033940	-0.0238680
H	-3.8323200	0.2990800	0.0267260
C	-2.5116820	-0.9041540	1.3283200
H	-3.5605370	-1.3666080	-0.5088030
H	-3.1771200	-1.5208740	1.9268250
H	-2.2519380	-0.0137170	1.9023800
H	-0.4606400	-1.5685030	1.6978060
H	-1.4307640	-2.6924120	0.7039850
H	-1.9743020	-0.1912370	-1.8773520
C	0.3429240	-1.1037540	-0.8822340
H	0.4433230	-0.5900640	-1.8352380
O	-2.3774870	2.2039290	-1.0806970
C	1.4800760	-1.6495400	-0.2818980
H	1.2919740	-2.2980340	0.5659420
C	2.6553590	-2.0495030	-1.1359130
H	2.7198730	-1.4331690	-2.0327820
H	3.5897130	-1.9333960	-0.5835150
H	2.5876900	-3.0915980	-1.4495880
H	0.0731850	1.0777840	0.6860840
C	1.9165380	-0.0626630	0.7256590
O	0.8808610	0.3241390	1.3909110
C	2.5500950	0.9276320	-0.2388770
H	1.8023940	1.2893000	-0.9462810
H	3.3529790	0.4484820	-0.7986150
C	3.0982170	2.1123530	0.5546770
H	3.8273370	1.7809170	1.2960560
H	3.5868870	2.8271360	-0.1057760
H	2.2886450	2.6191010	1.0767980
H	2.6692700	-0.6118490	1.3091450

Zero-point correction=	0.294292 (Hartree/Particle)
Thermal correction to Energy=	0.309046
Thermal correction to Enthalpy=	0.309990
Thermal correction to Gibbs Free Energy=	0.252767
Sum of electronic and zero-point Energies=	-710.676127
Sum of electronic and thermal Energies=	-710.661373
Sum of electronic and thermal Enthalpies=	-710.660429
Sum of electronic and thermal Free Energies=	-710.717652

87-RR:

	X	Y	Z
N	1.0365010	0.9833420	0.1478670
C	1.5949620	-0.0102460	-0.7780960
C	1.1483660	-1.4896480	-0.6262770
O	1.6526590	-2.2523490	-1.4192020
C	1.9379650	1.2303990	1.2905420
C	3.0926310	0.0945260	-0.4721790
H	3.6214510	-0.7861010	-0.8224350
C	3.0990230	0.2677810	1.0470020
H	3.5076350	0.9792280	-0.9575780
H	4.0378870	0.6554110	1.4338620
H	2.8954590	-0.6887070	1.5285050
H	1.3991870	1.0377640	2.2157550
H	2.2624430	2.2723790	1.2673370
H	1.3556970	0.2813830	-1.7989720
C	-0.0575440	1.6711110	-0.0383490
O	0.3327950	-1.8257810	0.3137530
C	-1.1344020	1.2944320	-0.8408680
H	-0.9347330	0.5228180	-1.5779820
H	-0.2941030	-1.0567970	0.8500510
C	-2.1495820	2.3358980	-1.2356100
H	-1.8860870	2.8320080	-2.1699190
H	-3.1349300	1.8884170	-1.3687280
H	-2.2375460	3.1014490	-0.4630810
H	-0.2022230	2.4916300	0.6613960
C	-1.9568520	0.2352930	0.5726040
H	-2.5833590	1.0519380	0.9570560
C	-2.7340260	-0.7727570	-0.2579210
H	-3.2878360	-0.2754950	-1.0548790
H	-2.0263490	-1.4674020	-0.7123500
C	-3.6933510	-1.5358780	0.6541450
H	-4.2530090	-2.2797200	0.0887780
H	-3.1379900	-2.0430500	1.4409150

H	-4.4086880	-0.8585630	1.1234840
O	-1.0893980	-0.2303010	1.4096680

Zero-point correction=	0.293167 (Hartree/Particle)
Thermal correction to Energy=	0.308353
Thermal correction to Enthalpy=	0.309297
Thermal correction to Gibbs Free Energy=	0.250438
Sum of electronic and zero-point Energies=	-710.670110
Sum of electronic and thermal Energies=	-710.654924
Sum of electronic and thermal Enthalpies=	-710.653980
Sum of electronic and thermal Free Energies=	-710.712838

6.4.4. Geometries of the Proline-Catalyzed Addition of Cyclohexanone to Aldehydes 85a-c

Geometries and energies obtained at the M06-2X/6-311G(2d,2p) level of theory of the involved species are reported below. TSs' conformational analysis was performed for benzaldehyde **85b**. These conformations were assumed to be the most stable also for the OMe or Cl 4-substituted benzaldehydes (**85a**, **85c**).

Cyclohexanone:

	X	Y	Z
C	-0.3885010	-1.2792760	0.3704150
C	-0.3885010	1.2792760	0.3704150
C	0.9972610	1.2579610	-0.2905980
C	1.7727200	0.0000000	0.0953280
C	0.9972610	-1.2579610	-0.2905980
H	-0.9936370	2.1210400	0.0409620
H	-0.2617560	-1.3487280	1.4557700
H	-0.9936370	-2.1210400	0.0409620
H	0.8745810	1.2850300	-1.3765210
H	1.5517340	2.1540880	-0.0119220
H	2.7508450	0.0000000	-0.3867580
H	1.9496070	0.0000000	1.1753140
H	0.8745810	-1.2850300	-1.3765210
H	1.5517340	-2.1540880	-0.0119220
H	-0.2617560	1.3487280	1.4557700
C	-1.1469000	0.0000000	0.0769780
O	-2.2627920	0.0000000	-0.3745960

Zero-point correction=	0.152152 (Hartree/Particle)
Thermal correction to Energy=	0.158571
Thermal correction to Enthalpy=	0.159516
Thermal correction to Gibbs Free Energy=	0.121837
Sum of electronic and zero-point Energies=	-309.690371
Sum of electronic and thermal Energies=	-309.683951
Sum of electronic and thermal Enthalpies=	-309.683007
Sum of electronic and thermal Free Energies=	-309.720686

Proline:

	X	Y	Z
N	0.5191730	1.2701750	-0.0207730
C	1.5796290	0.6776720	0.8044310
C	-0.1030030	0.1264680	-0.7211490
H	1.1245470	0.2737220	1.7106680
H	2.3015020	1.4387440	1.0935080
C	2.1612310	-0.4568740	-0.0402990
C	0.9056690	-1.0480120	-0.6999580
H	-0.3998570	0.4262800	-1.7233800
C	-1.3599220	-0.1877380	0.0696270
H	2.7136440	-1.1915790	0.5422680
H	2.8347850	-0.0440480	-0.7935090
H	0.5036610	-1.8558710	-0.0920190
H	1.0959690	-1.4323640	-1.6992230
O	-1.4143400	-0.9164930	1.0210940
O	-2.4230890	0.4976600	-0.3804980
H	-3.1531670	0.3008540	0.2198260
H	0.9425200	1.8746110	-0.7134170

Zero-point correction=	0.146473 (Hartree/Particle)
Thermal correction to Energy=	0.153866
Thermal correction to Enthalpy=	0.154811

Thermal correction to Gibbs Free Energy= 0.113870
 Sum of electronic and zero-point Energies= -400.969230
 Sum of electronic and thermal Energies= -400.961837
 Sum of electronic and thermal Enthalpies= -400.960893
 Sum of electronic and thermal Free Energies= -401.001834

TS1: TS for the addition of L-proline to the cyclohexanone.

	X	Y	Z
N	0.1724410	0.6654670	-0.1649620
C	1.2843590	-0.0313030	-0.8736360
C	2.1130940	-1.0735050	-0.0787230
O	3.0908960	-1.4917120	-0.6468560
H	-0.3886700	1.1008130	-0.8895460
C	0.8083490	1.7398110	0.6485210
C	2.2039800	1.1350020	-1.2433860
H	3.1800270	0.7785550	-1.5556030
C	2.2215080	1.9415560	0.0616730
H	1.7572180	1.7141030	-2.0540150
H	2.4542520	2.9917530	-0.0938710
H	2.9671450	1.5275560	0.7390330
H	0.8214630	1.3891430	1.6792820
H	0.1930990	2.6348080	0.5894380
H	0.8838810	-0.5542400	-1.7401770
H	0.8362330	-1.0886580	1.5043690
C	-1.0111500	-0.3082330	0.8846120
O	-0.3599540	-0.5745860	1.9449430
O	1.7608180	-1.4418110	1.1167200
C	-1.3525970	-1.4591290	-0.0578390
H	-2.0041210	-2.1059220	0.5370460
H	-0.4558490	-2.0437800	-0.2641320
C	-2.0885310	-1.0414400	-1.3315600
H	-1.4193840	-0.4914140	-2.0023430
H	-2.3953900	-1.9309920	-1.8818500
C	-2.1473880	0.6955080	1.0584340
H	-2.8330960	0.1960700	1.7487450
H	-1.7644040	1.5660320	1.5910900
C	-2.9033480	1.0717420	-0.2151570
H	-2.2980840	1.7279800	-0.8511850
H	-3.7867760	1.6551600	0.0456380
C	-3.3044000	-0.1722080	-1.0079250
H	-4.0091310	-0.7591190	-0.4117770
H	-3.8228490	0.1119570	-1.9239470

Zero-point correction= 0.300471 (Hartree/Particle)
 Thermal correction to Energy= 0.313496
 Thermal correction to Enthalpy= 0.314440
 Thermal correction to Gibbs Free Energy= 0.261008
 Sum of electronic and zero-point Energies= -710.658922
 Sum of electronic and thermal Energies= -710.645897
 Sum of electronic and thermal Enthalpies= -710.644953
 Sum of electronic and thermal Free Energies= -710.698385

Water:

	X	Y	Z
O	0.0000000	0.0000000	0.1176480
H	0.0000000	0.7564990	-0.4705920
H	0.0000000	-0.7564990	-0.4705920

Zero-point correction= 0.021693 (Hartree/Particle)
 Thermal correction to Energy= 0.024528
 Thermal correction to Enthalpy= 0.025472
 Thermal correction to Gibbs Free Energy= 0.004059
 Sum of electronic and zero-point Energies= -76.394755
 Sum of electronic and thermal Energies= -76.391920
 Sum of electronic and thermal Enthalpies= -76.390976
 Sum of electronic and thermal Free Energies= -76.412390

Enamine:

	X	Y	Z
H	-1.2528330	1.7691610	2.2147660
N	-0.6070970	-0.7290280	-0.4495460
C	-1.5038780	0.4025400	-0.6728190
C	-1.3272110	1.4996060	0.3653890
O	-1.1321600	2.6577740	0.1256230

C	-1.3120790	-1.7624670	0.2880960
C	-2.9265920	-0.2085620	-0.5808190
H	-3.4656940	0.2312450	0.2561770
C	-2.6987050	-1.7098800	-0.3413960
H	-3.4969620	-0.0101160	-1.4841520
H	-2.6827090	-2.2447160	-1.2896940
H	-3.4669440	-2.1500600	0.2899610
H	-1.3518400	-1.5482520	1.3635410
H	-0.8130720	-2.7201640	0.1435990
H	-1.3133450	0.8721680	-1.6361620
C	0.7524930	-0.4845220	-0.2105800
C	1.4645480	-1.1517870	0.7037690
C	1.3743370	0.5418160	-1.1322470
C	2.9410450	-0.9501100	0.9181670
H	0.9751450	-1.8871800	1.3280970
C	2.8973400	0.4441240	-1.1533660
H	0.9712930	0.3870980	-2.1353580
H	1.0712980	1.5484050	-0.8297180
C	3.4436700	0.3344330	0.2659890
H	3.4970640	-1.8049180	0.5167200
H	3.1513020	-0.9337420	1.9894940
H	3.1941540	-0.4433820	-1.7186890
H	3.3158810	1.3095310	-1.6673880
H	3.0995380	1.1943620	0.8472860
H	4.5337030	0.3584100	0.2650280
O	-1.4111030	1.0227510	1.6234030

Zero-point correction= 0.274075 (Hartree/Particle)
 Thermal correction to Energy= 0.286999
 Thermal correction to Enthalpy= 0.287943
 Thermal correction to Gibbs Free Energy= 0.233764
 Sum of electronic and zero-point Energies= -634.261937
 Sum of electronic and thermal Energies= -634.249013
 Sum of electronic and thermal Enthalpies= -634.248069
 Sum of electronic and thermal Free Energies= -634.302248

4-Methoxybenzaldehyde (85a):

	X	Y	Z
C	-0.5762280	1.4635290	-0.0000120
C	0.8011930	1.4137040	0.0000040
C	1.4667010	0.1883690	-0.0000090
C	0.7284750	-0.9896540	-0.0000430
C	-0.6549710	-0.9581420	-0.0000600
C	-1.3110090	0.2753190	-0.0000430
H	-1.1159350	2.3992930	0.0000030
H	1.3753010	2.3325500	0.0000310
H	1.2622820	-1.9305040	-0.0000580
H	-1.2117660	-1.8820300	-0.0000940
C	2.9412910	0.1442150	0.0000160
O	3.5914880	-0.8682950	-0.0000090
H	3.4371960	1.1347170	0.0000380
O	-2.6538700	0.4181780	-0.0000690
C	-3.4410510	-0.7563190	0.0001580
H	-4.4746180	-0.4258180	0.0002980
H	-3.2500560	-1.3567770	-0.8914060
H	-3.2497580	-1.3566270	0.8917580

Zero-point correction= 0.144102 (Hartree/Particle)
 Thermal correction to Energy= 0.152813
 Thermal correction to Enthalpy= 0.153757
 Thermal correction to Gibbs Free Energy= 0.110237
 Sum of electronic and zero-point Energies= -459.897968
 Sum of electronic and thermal Energies= -459.889257
 Sum of electronic and thermal Enthalpies= -459.888313
 Sum of electronic and thermal Free Energies= -459.931833

Benzaldehyde (85b):

	X	Y	Z
C	-1.7266960	1.0545020	-0.0000430
C	-0.3582770	1.2849200	0.0000040
C	0.5269930	0.2137140	0.0000210
C	0.0471670	-1.0941420	-0.0000070
C	-1.3168900	-1.3237430	-0.0000520

C	-2.2026190	-0.2493140	-0.0000700
H	-2.4183270	1.8850220	-0.0000580
H	0.0282650	2.2970230	0.0000290
H	0.7617290	-1.9059850	0.0000050
H	-1.6968380	-2.3357790	-0.0000720
H	-3.2685150	-0.4319720	-0.0001060
C	1.9873670	0.4679810	0.0000650
O	2.8219100	-0.3960520	0.0000740
H	2.2761300	1.5366020	0.0001010

Zero-point correction=	0.110832 (Hartree/Particle)
Thermal correction to Energy=	0.117085
Thermal correction to Enthalpy=	0.118030
Thermal correction to Gibbs Free Energy=	0.080340
Sum of electronic and zero-point Energies=	-345.413990
Sum of electronic and thermal Energies=	-345.407736
Sum of electronic and thermal Enthalpies=	-345.406792
Sum of electronic and thermal Free Energies=	-345.444482

4-Chlorobenzaldehyde (85c):

	X	Y	Z
C	0.7461930	1.2522650	-0.0000120
C	-0.6358630	1.3567850	-0.0000120
C	-1.4275080	0.2147390	-0.0000080
C	-0.8339240	-1.0454850	-0.0000050
C	0.5423760	-1.1638650	-0.0000070
C	1.3171050	-0.0097880	-0.0000100
H	1.3766450	2.1288420	-0.0000140
H	-1.1026950	2.3340470	-0.0000160
H	-1.4717340	-1.9187380	-0.0000050
H	1.0229430	-2.1307810	-0.0000040
C	-2.9042990	0.3379640	-0.0000130
O	-3.6548350	-0.5996730	0.0000710
H	-3.2888350	1.3756090	0.0000500
Cl	3.0516400	-0.1557230	-0.0000110

Zero-point correction=	0.101371 (Hartree/Particle)
Thermal correction to Energy=	0.108775
Thermal correction to Enthalpy=	0.109719
Thermal correction to Gibbs Free Energy=	0.068672
Sum of electronic and zero-point Energies=	-805.025222
Sum of electronic and thermal Energies=	-805.017818
Sum of electronic and thermal Enthalpies=	-805.016874
Sum of electronic and thermal Free Energies=	-805.057920

TS-H-SR-F: favored TS for the addition of the enamine to benzaldehyde 85b leading to SR-86b.

	X	Y	Z
H	-1.0326010	-0.6841570	1.5369930
N	-1.6877770	-0.3125890	-0.8228740
C	-2.9825810	-0.4640460	-0.1370710
C	-2.9880310	-0.0441270	1.3436250
O	-4.0026050	0.4373790	1.7830300
C	-1.3228570	-1.5339850	-1.5737570
C	-3.2683960	-1.9633810	-0.2740810
H	-2.7611920	-2.4939360	0.5335000
C	-2.6297340	-2.3183540	-1.6137200
H	-4.3330180	-2.1702250	-0.2155010
H	-3.2567190	-1.9703040	-2.4356100
H	-2.4589480	-3.3845420	-1.7391570
H	-0.5479550	-2.0706180	-1.0318550
H	-0.9534530	-1.2517910	-2.5584410
H	-3.7507860	0.1244370	-0.6390170
C	0.9050770	-0.0997990	0.7397540
O	0.1198960	-1.0912390	1.0000670
C	-0.9172560	0.7508640	-0.7286760
C	0.4681680	0.6534210	-0.9954990
C	-1.4693130	2.0042600	-0.1043200
C	1.2475750	1.9218160	-1.2870270
H	0.7698360	-0.1938120	-1.5992380
C	-0.7639750	3.2568100	-0.6258890
H	-2.5448280	2.0614050	-0.2670440
H	-1.3290770	1.9270890	0.9796310
C	0.7479310	3.1215600	-0.4860340
H	1.1621220	2.1507920	-2.3536340

H	2.3063800	1.7453530	-1.0999670
H	-1.0180320	3.4097560	-1.6779670
H	-1.1315620	4.1237440	-0.0780650
H	1.0018700	3.0034950	0.5706640
H	1.2448780	4.0282620	-0.8308830
H	0.7756830	0.8121080	1.3404080
C	2.3518790	-0.4256550	0.5174070
C	3.3460880	0.4889180	0.8460930
C	2.7106630	-1.6713900	0.0107470
C	4.6849000	0.1730070	0.6519000
H	3.0708110	1.4476870	1.2695370
C	4.0447430	-1.9865620	-0.1871520
H	1.9290950	-2.3900330	-0.1973750
C	5.0354130	-1.0629390	0.1291880
H	5.4520470	0.8879480	0.9157220
H	4.3180630	-2.9569870	-0.5785370
H	6.0767780	-1.3114840	-0.0218740
O	-1.9143820	-0.2784590	2.0400170

Zero-point correction=	0.385866 (Hartree/Particle)
Thermal correction to Energy=	0.404347
Thermal correction to Enthalpy=	0.405291
Thermal correction to Gibbs Free Energy=	0.339424
Sum of electronic and zero-point Energies=	-979.678291
Sum of electronic and thermal Energies=	-979.659810
Sum of electronic and thermal Enthalpies=	-979.658866
Sum of electronic and thermal Free Energies=	-979.724733

TS-H-SR-D: disfavored TS for the addition of the enamine to benzaldehyde 85b leading to SR-86b.

	X	Y	Z
H	-1.0886500	-0.7803950	1.3973900
N	-1.6847230	-0.1940930	-0.8847560
C	-3.0350680	-0.2811310	-0.3051780
C	-3.0727840	-0.2033700	1.2386540
O	-4.1326470	0.0867370	1.7346930
C	-1.3134450	-1.4565780	-1.5607050
C	-3.5593850	-1.6378660	-0.7946210
H	-4.2752580	-2.0536900	-0.0910600
C	-2.2854850	-2.4630990	-0.9635520
H	-4.0560860	-1.5123790	-1.7573220
H	-2.4186540	-3.3338430	-1.6006350
H	-1.9060030	-2.7861520	0.0061270
H	-0.2828130	-1.7132570	-1.3599180
H	-1.4697730	-1.3314790	-2.6359370
H	-3.6656390	0.5308750	-0.6569970
C	0.9047970	-0.1480660	0.7162760
O	0.1024400	-1.1404260	0.8838390
C	-0.8897820	0.8481970	-0.7353610
C	0.4976440	0.7526200	-0.9838460
C	-1.4348390	2.0720680	-0.0443280
C	1.3048770	2.0255640	-1.1528230
H	0.8032550	-0.0386160	-1.6552470
C	-0.6761390	3.3473500	-0.4112250
H	-2.4948950	2.1878080	-0.2594060
H	-1.3630510	1.8884950	1.0341500
C	0.8259860	3.1560280	-0.2477770
H	1.2337720	2.3552520	-2.1939950
H	2.3578780	1.8077930	-0.9771920
H	-0.8941480	3.6123880	-1.4490670
H	-1.0389130	4.1648800	0.2108040
H	1.0494560	2.9268380	0.7974300
H	1.3566530	4.0763890	-0.4911160
H	0.7720930	0.7243610	1.3717250
C	2.3497120	-0.4730570	0.4882620
C	3.3491180	0.4140280	0.8727920
C	2.7024270	-1.6943510	-0.0790070
C	4.6865520	0.0974470	0.6714640
H	3.0789810	1.3506530	1.3459440
C	4.0354100	-2.0096550	-0.2844040
H	1.9172260	-2.3965480	-0.3257900
C	5.0310410	-1.1119140	0.0858700
H	5.4573180	0.7905440	0.9793620
H	4.3033460	-2.9607310	-0.7239840
O	-1.9920820	-0.4707020	1.9109920
H	6.0714720	-1.3606830	-0.0711050

Zero-point correction=	0.386158 (Hartree/Particle)
Thermal correction to Energy=	0.404626
Thermal correction to Enthalpy=	0.405571
Thermal correction to Gibbs Free Energy=	0.339488
Sum of electronic and zero-point Energies=	-979.677759
Sum of electronic and thermal Energies=	-979.659290
Sum of electronic and thermal Enthalpies=	-979.658346
Sum of electronic and thermal Free Energies=	-979.724429

TS-H-RS: unique TS for the addition of the enamine to the benzaldehyde 85b leading to RS-86b.

	X	Y	Z
H	-0.4953020	-1.2890460	-1.1715220
N	-2.0358490	0.3118590	0.0561100
C	-2.1523560	-0.8945590	0.8928930
C	-1.3412730	-2.1465240	0.4910090
O	-1.2874210	-3.0258360	1.3163630
C	-3.1561940	0.4146320	-0.8988510
C	-3.6417550	-1.2384330	0.7454400
H	-3.8311120	-2.2739560	1.0112580
C	-3.9018820	-0.9058690	-0.7237730
H	-4.2358720	-0.5915100	1.3927830
H	-4.9571660	-0.8099940	-0.9656420
H	-3.4608550	-1.6708620	-1.3613040
H	-2.7578140	0.5663720	-1.9001030
H	-3.7973920	1.2558280	-0.6306910
H	-1.8779410	-0.6531620	1.9163240
C	0.9109220	0.4087540	-1.0025620
O	0.0267190	-0.2208880	-1.6968360
H	1.1211730	1.4294040	-1.3427650
C	2.1711090	-0.2690070	-0.5508770
C	3.3340340	0.4907280	-0.4406930
C	2.2230560	-1.6351350	-0.2768680
C	4.5291140	-0.0930250	-0.0446770
H	3.3055430	1.5460390	-0.6863570
C	3.4172100	-2.2157350	0.1219530
H	1.3356540	-2.2431400	-0.3830900
C	4.5703330	-1.4494330	0.2431620
H	5.4258100	0.5070700	0.0281290
H	3.4477690	-3.2753120	0.3352390
C	-1.1036310	1.2346340	0.1910780
C	0.1562210	0.9368280	0.7456330
C	-1.2890600	2.5579980	-0.4955280
C	0.9873210	2.0579650	1.3394430
H	0.2290870	-0.0058670	1.2784380
C	-0.5962150	3.6912090	0.2681060
H	-0.8719190	2.4553060	-1.5043230
H	-2.3466400	2.7800450	-0.6160930
C	0.8649070	3.3667460	0.5598170
H	2.0286760	1.7405080	1.3944650
H	0.6670460	2.2277130	2.3717130
H	-0.6803010	4.6140110	-0.3056070
H	-1.1241110	3.8536970	1.2113740
H	1.3216380	4.1771150	1.1281360
H	1.4133380	3.3003900	-0.3821340
H	5.4986050	-1.9103270	0.5518360
O	-0.8640660	-2.2262730	-0.7134100

Zero-point correction=	0.385335 (Hartree/Particle)
Thermal correction to Energy=	0.403870
Thermal correction to Enthalpy=	0.404815
Thermal correction to Gibbs Free Energy=	0.338301
Sum of electronic and zero-point Energies=	-979.669884
Sum of electronic and thermal Energies=	-979.651349
Sum of electronic and thermal Enthalpies=	-979.650405
Sum of electronic and thermal Free Energies=	-979.716918

TS-H-SS-D: disfavored TS for the addition of the enamine to benzaldehyde 85b leading to SS-86a.

	X	Y	Z
H	0.8033570	1.2451810	-0.9702680
N	1.9284980	-0.6977500	0.0243220
C	2.7856480	0.3975050	0.5086230
C	2.0761280	1.7573620	0.6252390
O	2.4473710	2.5068620	1.4947730
C	2.5612250	-1.4255360	-1.0975450

C	3.8977430	0.4617280	-0.5449380
H	3.5681260	1.0969660	-1.3685710
C	4.0174590	-0.9840990	-1.0183800
H	4.8120640	0.8747920	-0.1291700
H	4.5553190	-1.5810750	-0.2807820
H	4.5226030	-1.0813730	-1.9759490
H	2.0923080	-1.1136700	-2.0283930
H	2.4259380	-2.4957950	-0.9540780
H	3.1918200	0.1569740	1.4907660
C	-0.6889400	-0.3593350	-1.5470570
O	0.3292180	0.3941450	-1.8331660
C	0.7306290	-0.9632810	0.4927780
C	-0.1853440	-1.7200920	-0.2871330
C	0.2649120	-0.3041530	1.7589830
C	-1.3446540	-2.4030090	0.4215960
H	0.2933060	-2.3688930	-1.0101260
C	-0.6866470	-1.2191860	2.5340710
H	1.1161950	-0.0111500	2.3715280
H	-0.2563700	0.6190790	1.4845040
C	-1.8520980	-1.6517630	1.6527240
H	-1.0123460	-3.3985170	0.7319280
H	-2.1607700	-2.5648150	-0.2826420
H	-0.1385400	-2.0979640	2.8847610
H	-1.0436970	-0.6903480	3.4169140
H	-2.4223700	-0.7712340	1.3530080
H	-2.5292750	-2.2962840	2.2137160
H	-0.9338600	-1.0985210	-2.3197580
C	-1.9536240	0.2560100	-1.0181050
C	-3.1690450	-0.3834270	-1.2567950
C	-1.9538680	1.4650920	-0.3238020
C	-4.3545640	0.1296400	-0.7520060
H	-3.1863610	-1.2862240	-1.8548940
C	-3.1408040	1.9804250	0.1790370
H	-1.0301180	2.0094440	-0.1872730
C	-4.3402470	1.3079130	-0.0172050
H	-5.2888000	-0.3810200	-0.9414000
H	-3.1280740	2.9162750	0.7207990
H	-5.2617870	1.7120440	0.3788920
O	1.1644600	2.0289460	-0.2583910

Zero-point correction=	0.386141 (Hartree/Particle)
Thermal correction to Energy=	0.404245
Thermal correction to Enthalpy=	0.405190
Thermal correction to Gibbs Free Energy=	0.341236
Sum of electronic and zero-point Energies=	-979.676647
Sum of electronic and thermal Energies=	-979.658542
Sum of electronic and thermal Enthalpies=	-979.657598
Sum of electronic and thermal Free Energies=	-979.721552

TS-H-SS-F: favored TS for the addition of the enamine to benzaldehyde 85b leading to the SS-86b.

	X	Y	Z
H	0.9049790	1.2511480	-0.8061450
N	1.8799520	-0.8097940	-0.0141110
C	2.7896870	0.1168440	0.6783350
C	2.2556190	1.5643620	0.7685350
O	2.7651090	2.2741070	1.5998120
C	2.4735110	-1.2837780	-1.2851370
C	4.0762580	0.0654520	-0.1551450
H	4.6212940	1.0023300	-0.0820470
C	3.5661790	-0.2613390	-1.5563540
H	4.7189210	-0.7364860	0.2098130
H	4.3368530	-0.6499580	-2.2170870
H	3.1146710	0.6186490	-2.0149200
H	1.7321020	-1.3017080	-2.0711210
H	2.8839650	-2.2837370	-1.1201240
H	2.9702430	-0.2014980	1.7010160
C	-0.6982260	-0.2022700	-1.5749470
O	0.3552230	0.5252510	-1.7694210
C	0.6704550	-1.1033020	0.4104570
C	-0.2690420	-1.7234220	-0.4566380
C	0.2159030	-0.5839220	1.7464260
C	-1.4775100	-2.4133980	0.1569550
H	0.1878100	-2.3266970	-1.2309290
C	-0.8103090	-1.5121940	2.3979170
H	1.0641090	-0.4245800	2.4078590

H	-0.2342160	0.4002090	1.5742610
C	-1.9757800	-1.7751670	1.4532010
H	-1.2075040	-3.4539360	0.3622350
H	-2.2843400	-2.4515880	-0.5752690
H	-0.3262070	-2.4554710	2.6650280
H	-1.1583320	-1.0577280	3.3249170
H	-2.4887910	-0.8352850	1.2445690
H	-2.7017050	-2.4385610	1.9239990
H	-0.9755820	-0.8444150	-2.4208640
C	-1.9283820	0.4156250	-0.9753630
C	-3.1797550	-0.1162720	-1.2794830
C	-1.8544670	1.5353010	-0.1476510
C	-4.3318040	0.4072830	-0.7111780
H	-3.2523650	-0.9418410	-1.9766720
C	-3.0068850	2.0599390	0.4204910
H	-0.8989660	2.0056880	0.0381740
C	-4.2451540	1.4883530	0.1557610
H	-5.2956070	-0.0199520	-0.9520170
H	-2.9386710	2.9257900	1.0649130
H	-5.1403360	1.8997050	0.6014110
O	1.3279450	1.9406310	-0.0590570

Zero-point correction=	0.386335 (Hartree/Particle)
Thermal correction to Energy=	0.404410
Thermal correction to Enthalpy=	0.405354
Thermal correction to Gibbs Free Energy=	0.341183
Sum of electronic and zero-point Energies=	-979.676779
Sum of electronic and thermal Energies=	-979.658704
Sum of electronic and thermal Enthalpies=	-979.657760
Sum of electronic and thermal Free Energies=	-979.721932

TS-H-RR-F: favored TS for the addition of the enamine to benzaldehyde 85b leading to the RR-86b.

	X	Y	Z
H	-1.2095730	-1.5431890	-0.8834720
N	-1.8529760	0.7727060	-0.1220720
C	-2.8251540	-0.0139160	0.6622960
C	-2.7732250	-1.5586470	0.5402540
O	-3.4174050	-2.1587000	1.3703660
C	-2.4633680	1.2885490	-1.3656050
C	-4.1625500	0.4595820	0.0790880
H	-4.9518440	-0.2551730	0.2909260
C	-3.8283970	0.6081560	-1.4045730
H	-4.4343030	1.4263730	0.5062690
H	-4.5564430	1.1948440	-1.9588440
H	-3.7397570	-0.3755730	-1.8636890
H	-1.8252290	1.0433850	-2.2114360
H	-2.5757360	2.3722190	-1.2977960
H	-2.7204920	0.2301900	1.7157990
C	0.6064390	-1.1602270	-0.1051320
O	-0.1180650	-1.0857780	-1.1784030
H	0.3444120	-1.9529330	0.6025000
C	2.0724030	-0.9830930	-0.2749950
C	2.9556830	-1.3847920	0.7236260
C	2.5780720	-0.4491780	-1.4589330
C	4.3201650	-1.1871620	0.5753320
H	2.5695240	-1.8608640	1.6162390
C	3.9421580	-0.2507050	-1.6077220
H	1.8861960	-0.2198790	-2.2573390
C	4.8142320	-0.6026120	-0.5842480
H	4.9989310	-1.4982470	1.3573380
H	4.3296060	0.1672780	-2.5268990
C	-0.6250830	1.0442840	0.2614730
C	0.0512910	0.2556960	1.2207550
C	0.1657230	2.0609850	-0.5031390
C	1.1788530	0.8986650	2.0132320
H	-0.5917280	-0.3705310	1.8298740
C	1.1074480	2.8429340	0.4175940
H	0.7395830	1.5081870	-1.2562290
H	-0.4916400	2.7419180	-1.0375310
C	2.0066400	1.9063680	1.2161920
H	1.8302260	0.1283080	2.4243990
H	0.7342610	1.4058650	2.8756360
H	1.7049030	3.5286460	-0.1828450
H	0.5091630	3.4536040	1.0991270
H	2.6298810	2.4821250	1.9009850

H	2.6803840	1.3861750	0.5350610
H	5.8778700	-0.4469620	-0.7009360
O	-2.1514480	-2.0810250	-0.4614130

Zero-point correction=	0.384429 (Hartree/Particle)
Thermal correction to Energy=	0.403039
Thermal correction to Enthalpy=	0.403983
Thermal correction to Gibbs Free Energy=	0.337335
Sum of electronic and zero-point Energies=	-979.670962
Sum of electronic and thermal Energies=	-979.652351
Sum of electronic and thermal Enthalpies=	-979.651407
Sum of electronic and thermal Free Energies=	-979.718055

TS-H-RR-D: disfavored TS for the addition of the enamine to benzaldehyde 85b leading to RR-86b.

	X	Y	Z
H	-1.1879860	-1.6542490	-0.9604900
N	-1.8089910	0.7306510	-0.2092550
C	-2.8493110	-0.1103740	0.4418600
C	-2.6708350	-1.6423830	0.5173690
O	-3.2014840	-2.1812100	1.4635410
C	-2.3601800	1.3747150	-1.4111150
C	-4.1177240	0.1652550	-0.3876020
H	-4.2334600	-0.6273840	-1.1276920
C	-3.8428770	1.4896370	-1.0945720
H	-4.9999850	0.1714050	0.2453470
H	-4.0121960	2.3320190	-0.4224870
H	-4.4467960	1.6299330	-1.9877070
H	-2.1844080	0.7027450	-2.2538120
H	-1.8784280	2.3220050	-1.6189740
H	-2.9568290	0.2438880	1.4653970
C	0.6133660	-1.2212350	-0.2162970
O	-0.1452520	-1.1335610	-1.2675690
H	0.4405790	-2.0833080	0.4358650
C	2.0574710	-0.9206610	-0.4127610
C	3.0104860	-1.4018190	0.4813800
C	2.4745410	-0.1927770	-1.5256720
C	4.3521690	-1.0936230	0.3112650
H	2.6990990	-2.0282380	1.3074750
C	3.8148900	0.1178440	-1.6953930
H	1.7341880	0.0978590	-2.2581250
C	4.7545870	-0.3164820	-0.7676000
H	5.0848990	-1.4679900	1.0128820
H	4.1308890	0.6878780	-2.5585400
C	-0.6214070	0.9584120	0.3136650
C	-0.0352930	0.0203770	1.1971070
C	0.2154020	2.1108450	-0.1645870
C	1.0430540	0.4817740	2.1614730
H	-0.7370620	-0.6686850	1.6540530
C	1.0711010	2.6853630	0.9693290
H	0.8585760	1.7511060	-0.9739650
H	-0.4112280	2.8969580	-0.5756120
C	1.9244410	1.6070570	1.6216990
H	1.6581270	-0.3681470	2.4581690
H	0.5511590	0.8256780	3.0766210
H	1.6960510	3.4837220	0.5697220
H	0.4110510	3.1376670	1.7145700
H	2.5064850	2.0338700	2.4389490
H	2.6366350	1.2216080	0.8910050
O	-2.0907230	-2.2291790	-0.4714970
H	5.7999670	-0.0748360	-0.9009460

Zero-point correction=	0.384407 (Hartree/Particle)
Thermal correction to Energy=	0.403100
Thermal correction to Enthalpy=	0.404044
Thermal correction to Gibbs Free Energy=	0.337508
Sum of electronic and zero-point Energies=	-979.666276
Sum of electronic and thermal Energies=	-979.647583
Sum of electronic and thermal Enthalpies=	-979.646639
Sum of electronic and thermal Free Energies=	-979.713175

TS-OMe-SR: TS for the addition of the enamine to 4-anisaldehyde 85a leading to SR-86a.

	X	Y	Z
H	-1.5386130	-0.7225950	1.5350610

N	-2.2359790	-0.4776840	-0.8216090
C	-3.5060740	-0.8051530	-0.1511390
C	-3.5814810	-0.3907540	1.3298190
O	-4.6622910	-0.0727540	1.7617290
C	-1.6881190	-1.6411440	-1.5510190
C	-3.5859600	-2.3291490	-0.2936650
H	-3.0308430	-2.7906120	0.5247980
C	-2.8755120	-2.5941460	-1.6189900
H	-4.6144960	-2.6760020	-0.2579550
H	-3.5244890	-2.3308370	-2.4551450
H	-2.5609890	-3.6277650	-1.7383000
H	-0.8627420	-2.0654040	-0.9844340
H	-1.3326050	-1.3169310	-2.5277700
H	-4.3410350	-0.3241860	-0.6606170
C	0.2870570	0.1453820	0.7642180
O	-0.3451190	-0.9520980	1.0283040
C	-1.6305650	0.6885380	-0.7375440
C	-0.2417360	0.7922600	-0.9855310
C	-2.3714720	1.8574100	-0.1459670
C	0.3422950	2.1558300	-1.3015420
H	0.1909860	-0.0138890	-1.5652000
C	-1.8524840	3.1901130	-0.6873380
H	-3.4409970	1.7521440	-0.3224950
H	-2.2368630	1.8219230	0.9404020
C	-0.3390100	3.2831400	-0.5300100
H	0.2314370	2.3469350	-2.3733100
H	1.4141500	2.1446750	-1.1063140
H	-2.1125330	3.2814640	-1.7451970
H	-2.3520680	4.0040490	-0.1631760
H	-0.0837080	3.2234250	0.5313160
H	0.0229830	4.2467640	-0.8885590
H	0.0091140	1.0332820	1.3495000
C	1.7672210	0.0387840	0.5730500
C	2.6147290	1.1062320	0.8668890
C	2.3271530	-1.1522480	0.1345540
C	3.9819350	0.9926770	0.7054440
H	2.1979410	2.0332660	1.2429970
C	3.6983630	-1.2844560	-0.0355510
H	1.6724280	-1.9934510	-0.0508220
C	4.5319020	-0.2038310	0.2468760
H	4.6504590	1.8092080	0.9381530
H	4.1034060	-2.2256030	-0.3742990
O	-2.4879570	-0.4517700	2.0285780
O	5.8822720	-0.2226500	0.1179080
C	6.4790810	-1.4286730	-0.3066070
H	6.1327190	-1.7132190	-1.3028070
H	7.5481540	-1.2430920	-0.3364200
H	6.2708840	-2.2404670	0.3940060

Zero-point correction=	0.418993 (Hartree/Particle)
Thermal correction to Energy=	0.439941
Thermal correction to Enthalpy=	0.440885
Thermal correction to Gibbs Free Energy=	0.369406
Sum of electronic and zero-point Energies=	-1094.160309
Sum of electronic and thermal Energies=	-1094.139361
Sum of electronic and thermal Enthalpies=	-1094.138416
Sum of electronic and thermal Free Energies=	-1094.209895

TS-OMe-RS: TS for the addition of the enamine to 4-anisaldehyde 85a leading to RS-86a.

	X	Y	Z
H	0.9222620	-1.2165030	1.2665330
N	2.6394840	0.0196020	-0.1272790
C	2.4671200	-1.1982450	-0.9357450
C	1.5032580	-2.2846990	-0.4065670
O	1.2432340	-3.1773400	-1.1776160
C	3.8395890	-0.0727590	0.7274360
C	3.8833590	-1.7875720	-0.9268020
H	3.8688440	-2.8407560	-1.1900000
C	4.3348800	-1.5006130	0.5051390
H	4.5115170	-1.2504670	-1.6392710
H	5.4095260	-1.5818710	0.6466070
H	3.8356860	-2.1802090	1.1944530
H	3.5658970	0.1431080	1.7585460
H	4.5881470	0.6476120	0.3934810
H	2.1327700	-0.9279160	-1.9335290

C	-0.2011410	0.6598790	1.0848520
O	0.6098460	-0.0796570	1.7639030
H	-0.2348950	1.7087930	1.4008760
C	-1.5622010	0.1725310	0.7022180
C	-2.6011390	1.0867810	0.5905390
C	-1.8389540	-1.1818510	0.4807490
C	-3.8901660	0.6917520	0.2467340
H	-2.4117380	2.1346860	0.7931870
C	-3.1096450	-1.5866880	0.1352970
H	-1.0571960	-1.9203890	0.5904490
C	-4.1431950	-0.6547250	0.0104750
H	-4.6735510	1.4302640	0.1769060
H	-3.3363660	-2.6287200	-0.0403480
C	1.8821510	1.0948850	-0.2247280
C	0.5608060	1.0284770	-0.7057790
C	2.3434160	2.3677370	0.4254810
C	-0.0839060	2.2773950	-1.2744890
H	0.2872490	0.1129270	-1.2190930
C	1.8308750	3.6019180	-0.3231940
H	1.9683040	2.3509030	1.4558620
H	3.4285970	2.3937370	0.4886450
C	0.3214030	3.5503950	-0.5319220
H	-1.1670860	2.1539690	-1.2619050
H	0.1975810	2.3745410	-2.3272410
H	2.1145580	4.4987510	0.2272880
H	2.3274660	3.6548880	-1.2956340
H	-0.0071310	4.4241710	-1.0951720
H	-0.1775290	3.5999960	0.4380160
O	1.1190330	-2.2300790	0.8303290
O	-5.3535670	-1.1596580	-0.3331060
C	-6.4296820	-0.2546950	-0.4429040
H	-7.2971530	-0.8466840	-0.7174980
H	-6.6200840	0.2490940	0.5076240
H	-6.2414070	0.4933160	-1.2166550

Zero-point correction=	0.418457 (Hartree/Particle)
Thermal correction to Energy=	0.439433
Thermal correction to Enthalpy=	0.440378
Thermal correction to Gibbs Free Energy=	0.368482
Sum of electronic and zero-point Energies=	-1094.152153
Sum of electronic and thermal Energies=	-1094.131176
Sum of electronic and thermal Enthalpies=	-1094.130232
Sum of electronic and thermal Free Energies=	-1094.202128

TS-OMe-SS: TS for the addition of the enamine to 4-anisaldehyde 85a leading to SS-86a.

	X	Y	Z
H	1.1392510	1.0719830	-1.1599270
N	2.5658330	-0.4329410	0.1633140
C	3.1573480	0.8697470	0.5110050
C	2.1866080	2.0592840	0.4025320
O	2.3446480	2.9773870	1.1708780
C	3.3960270	-1.1599320	-0.8204840
C	4.2982090	1.0157600	-0.5031060
H	3.8999860	1.4517880	-1.4207200
C	4.7298250	-0.4256380	-0.7581860
H	5.0850770	1.6602770	-0.1226600
H	5.3286790	-0.7956410	0.0750180
H	5.3010220	-0.5462850	-1.6751170
H	2.9340580	-1.0766130	-1.8022150
H	3.4645040	-2.2070680	-0.5314430
H	3.5411410	0.8537860	1.5307020
C	0.0215470	-0.8273150	-1.5292660
O	0.9025030	0.0570110	-1.8907760
C	1.4131920	-0.8675320	0.6225280
C	0.7108330	-1.8904370	-0.0652630
C	0.7513480	-0.1471200	1.7619110
C	-0.3441590	-2.6812010	0.6900170
H	1.3431570	-2.5221540	-0.6772660
C	-0.0483660	-1.1191150	2.6329050
H	1.4891510	0.3956990	2.3502590
H	0.0754190	0.6027050	1.3371070
C	-1.0557300	-1.8869320	1.7855510
H	0.1432750	-3.5479060	1.1473860
H	-1.0736030	-3.0837740	-0.0131970
H	0.6368950	-1.8167140	3.1221620

H	-0.5516600	-0.5584310	3.4197130
H	-1.7637370	-1.1828560	1.3459250
H	-1.6315580	-2.5710740	2.4092710
H	-0.0311210	-1.7016530	-2.1881350
C	-1.3586920	-0.3997660	-1.1353260
C	-2.4258860	-1.2860530	-1.3051040
C	-1.6327180	0.8681520	-0.6354090
C	-3.7084020	-0.9470840	-0.9265400
H	-2.2489510	-2.2543810	-1.7569480
C	-2.9201480	1.2268440	-0.2516650
H	-0.8402940	1.5987140	-0.5513760
C	-3.9618770	0.3124670	-0.3813550
H	-4.5371290	-1.6283750	-1.0564740
H	-3.0947800	2.2198820	0.1327470
O	1.3023420	2.0155560	-0.5442480
O	-5.2487380	0.5587280	-0.0337900
C	-5.5491270	1.8376880	0.4835030
H	-6.6132010	1.8346290	0.6979960
H	-4.9937900	2.0334360	1.4034530
H	-5.3276420	2.6202710	-0.2454440

Zero-point correction=	0.418651 (Hartree/Particle)
Thermal correction to Energy=	0.439387
Thermal correction to Enthalpy=	0.440332
Thermal correction to Gibbs Free Energy=	0.370453
Sum of electronic and zero-point Energies=	-1094.160050
Sum of electronic and thermal Energies=	-1094.139313
Sum of electronic and thermal Enthalpies=	-1094.138369
Sum of electronic and thermal Free Energies=	-1094.208248

TS-OMe-RR: TS for the addition of the enamine to 4-anisaldehyde 85a leading to RR-86a.

	X	Y	Z
H	-1.7039640	-1.5299700	-0.9092980
N	-2.5009590	0.7306750	-0.1262390
C	-3.4468540	-0.1022090	0.6410670
C	-3.2988510	-1.6418450	0.5258710
O	-3.8917930	-2.2771010	1.3702900
C	-3.1112570	1.2197030	-1.3794590
C	-4.7948150	0.2925160	0.0251540
H	-5.5454410	-0.4688920	0.2149090
C	-4.4357490	0.4658020	-1.4503700
H	-5.1368110	1.2392870	0.4470990
H	-5.1830990	1.0137270	-2.0186000
H	-4.2825030	-0.5101110	-1.9084990
H	-2.4441480	1.0138700	-2.2135190
H	-3.2828930	2.2958090	-1.3108910
H	-3.3795090	0.1530830	1.6951600
C	0.0540920	-1.1015370	-0.0958870
O	-0.6610300	-1.0461240	-1.1791350
H	-0.1952930	-1.9010550	0.6064920
C	1.5068880	-0.8623870	-0.2449460
C	2.3979120	-1.2383170	0.7505440
C	2.0139470	-0.2906610	-1.4159080
C	3.7607190	-0.9960330	0.6310850
H	2.0274250	-1.7395490	1.6360770
C	3.3628130	-0.0415230	-1.5500930
H	1.3289920	-0.0719500	-2.2232190
C	4.2447020	-0.3784150	-0.5193590
H	4.4267570	-1.3025550	1.4223090
H	3.7723310	0.3967560	-2.4491780
C	-1.2896110	1.0504350	0.2774190
C	-0.5990570	0.2905870	1.2452490
C	-0.5309360	2.1035110	-0.4711840
C	0.4991660	0.9637860	2.0497880
H	-1.2203160	-0.3727700	1.8371500
C	0.3649180	2.9172840	0.4672220
H	0.0749850	1.5802870	-1.2201890
H	-1.2097720	2.7596470	-1.0100300
C	1.2923770	2.0119030	1.2696380
H	1.1779920	0.2116530	2.4513490
H	0.0352420	1.4416340	2.9188030
H	0.9408700	3.6327610	-0.1193680
H	-0.2672560	3.4959100	1.1459880
H	1.8850540	2.6071210	1.9649210
H	1.9930130	1.5249210	0.5914110

O	-2.6588050	-2.1192390	-0.4829740
O	5.5485820	-0.0897560	-0.7420990
C	6.4774700	-0.4495690	0.2588190
H	6.4827140	-1.5293480	0.4220480
H	7.4501930	-0.1339470	-0.1045740
H	6.2592880	0.0585210	1.2007710

Zero-point correction=	0.417616 (Hartree/Particle)
Thermal correction to Energy=	0.438670
Thermal correction to Enthalpy=	0.439614
Thermal correction to Gibbs Free Energy=	0.367833
Sum of electronic and zero-point Energies=	-1094.153578
Sum of electronic and thermal Energies=	-1094.132524
Sum of electronic and thermal Enthalpies=	-1094.131580
Sum of electronic and thermal Free Energies=	-1094.203361

TS-CI-SR: TS for the addition of the enamine to 4-chlorobenzaldehyde 85c leading to SR-86c.

	X	Y	Z
H	-1.5973560	-0.7270850	1.5462210
N	-2.2472810	-0.4204920	-0.8179560
C	-3.5311840	-0.7090390	-0.1555660
C	-3.5995040	-0.3136400	1.3292450
O	-4.6648980	0.0452020	1.7632640
C	-1.7511850	-1.5893880	-1.5760440
C	-3.6697220	-2.2262040	-0.3225350
H	-3.1296180	-2.7225460	0.4854250
C	-2.9755920	-2.4936200	-1.6558260
H	-4.7108600	-2.5336010	-0.2884690
H	-3.6176170	-2.1899660	-2.4835920
H	-2.7026640	-3.5362870	-1.7961640
H	-0.9402610	-2.0594380	-1.0253490
H	-1.3894910	-1.2588040	-2.5483180
H	-4.3453800	-0.1893820	-0.6606940
C	0.2966040	0.0707450	0.7644380
O	-0.3767570	-0.9989840	1.0153570
C	-1.5991730	0.7212020	-0.7195520
C	-0.2098720	0.7774040	-0.9788130
C	-2.2905360	1.9062020	-0.1002930
C	0.4226200	2.1242920	-1.2731880
H	0.1864600	-0.0332350	-1.5779350
C	-1.7257260	3.2285250	-0.6202840
H	-3.3646780	1.8449000	-0.2693230
H	-2.1483240	1.8459060	0.9841810
C	-0.2086140	3.2611520	-0.4738230
H	0.3097020	2.3396440	-2.3400160
H	1.4954970	2.0707010	-1.0906140
H	-1.9900880	3.3507700	-1.6738280
H	-2.1902210	4.0500470	-0.0762500
H	0.0526360	3.1708710	0.5839180
H	0.1865820	4.2171530	-0.8171730
H	0.0672960	0.9639500	1.3633680
C	1.7704120	-0.0994570	0.5483860
C	2.6641000	0.9238390	0.8419230
C	2.2615630	-1.3172350	0.0865970
C	4.0287020	0.7516570	0.6543860
H	2.2947760	1.8634710	1.2348260
C	3.6189920	-1.5032250	-0.1079130
H	1.5626880	-2.1229620	-0.0921040
C	4.4902200	-0.4609210	0.1735760
H	4.7284760	1.5413330	0.8844730
H	4.0085430	-2.4457070	-0.4641440
O	-2.5131880	-0.4326030	2.0385180
Cl	6.2029980	-0.6893500	-0.0693030

Zero-point correction=	0.376951 (Hartree/Particle)
Thermal correction to Energy=	0.396640
Thermal correction to Enthalpy=	0.397585
Thermal correction to Gibbs Free Energy=	0.328304
Sum of electronic and zero-point Energies=	-1439.289520
Sum of electronic and thermal Energies=	-1439.269830
Sum of electronic and thermal Enthalpies=	-1439.268886
Sum of electronic and thermal Free Energies=	-1439.338167

TS-CI-RS: TS for the addition of the enamine to 4-chlorobenzaldehyde 85c leading to RS-86c.

	X	Y	Z
H	0.8481480	-1.2522430	1.2477340
N	2.6118800	-0.0592110	-0.1124500
C	2.4015320	-1.2720910	-0.9208670
C	1.3913900	-2.3222950	-0.4086280
O	1.1178540	-3.2111100	-1.1766260
C	3.8007370	-0.1946340	0.7528220
C	3.7942120	-1.9155430	-0.8941340
H	3.7425210	-2.9677460	-1.1561170
C	4.2391080	-1.6424860	0.5424710
H	4.4501340	-1.4040700	-1.6002390
H	5.3072660	-1.7684750	0.6983650
H	3.7030060	-2.2981690	1.2274660
H	3.5263140	0.0390340	1.7797160
H	4.5803220	0.4925660	0.4207180
H	2.0902210	-0.9906090	-1.9230380
C	-0.1840090	0.7178550	1.0839370
O	0.5766700	-0.0667450	1.7617080
H	-0.1621210	1.7694980	1.3937580
C	-1.5746900	0.3044990	0.7011190
C	-2.5577870	1.2830950	0.5727070
C	-1.9225970	-1.0317140	0.5067290
C	-3.8603490	0.9509950	0.2323660
H	-2.3083140	2.3207900	0.7591000
C	-3.2198090	-1.3752490	0.1634830
H	-1.1823240	-1.8093720	0.6316490
C	-4.1752500	-0.3802850	0.0247910
H	-4.6243970	1.7082170	0.1364310
H	-3.4932600	-2.4084340	0.0081320
C	1.9058400	1.0484640	-0.2274170
C	0.5840010	1.0340940	-0.7136500
C	2.4199850	2.3075720	0.4101700
C	0.0003330	2.3034900	-1.3037390
H	0.2735730	0.1245020	-1.2172760
C	1.9612750	3.5553680	-0.3515260
H	2.0447800	2.3184200	1.4405700
H	3.5052510	2.2881740	0.4740850
C	0.4519250	3.5647670	-0.5683250
H	-1.0871540	2.2293930	-1.3080290
H	0.3012180	2.3765290	-2.3530310
H	2.2788190	4.4440970	0.1934270
H	2.4647240	3.5800890	-1.3214690
H	0.1624880	4.4464860	-1.1402070
H	-0.0497800	3.6421200	0.3984580
O	0.9769060	-2.2521580	0.8216480
Cl	-5.8094770	-0.8142130	-0.4041620

Zero-point correction= 0.376291 (Hartree/Particle)
 Thermal correction to Energy= 0.395991
 Thermal correction to Enthalpy= 0.396935
 Thermal correction to Gibbs Free Energy= 0.327370
 Sum of electronic and zero-point Energies= -1439.281632
 Sum of electronic and thermal Energies= -1439.261932
 Sum of electronic and thermal Enthalpies= -1439.260988
 Sum of electronic and thermal Free Energies= -1439.330552

TS-CI-SS: TS for the addition of the enamine to 4-chlorobenzaldehyde 85c leading to SS-86c.

	X	Y	Z
H	-1.2880890	-1.1601800	-0.9591860
N	-2.5239100	0.5951910	0.1348360
C	-3.2348240	-0.5541150	0.7190300
C	-2.4671410	-1.8889630	0.5975860
O	-2.7979360	-2.7732960	1.3459660
C	-3.2555380	1.1315200	-1.0351120
C	-4.5534010	-0.6118280	-0.0621030
H	-4.9322080	-1.6289630	-0.1085300
C	-4.1801550	-0.0144810	-1.4167550
H	-5.2996550	0.0105420	0.4327200
H	-5.0396960	0.3234620	-1.9898450
H	-3.6163540	-0.7336930	-2.0111750
H	-2.5710650	1.3807790	-1.8332280
H	-3.8132780	2.0157350	-0.7150570
H	-3.4127850	-0.4054310	1.7802240
C	0.0197790	0.6499830	-1.5824660
O	-0.9069070	-0.2152170	-1.8394010

C	-1.3563870	1.0261190	0.5587710
C	-0.5775010	1.9073940	-0.2396320
C	-0.7509740	0.4121140	1.7896620
C	0.5386310	2.6968200	0.4279550
H	-1.1684670	2.5294670	-0.9001600
C	0.1419250	1.4038110	2.5371940
H	-1.5228810	0.0185750	2.4462760
H	-0.1531480	-0.4456870	1.4621970
C	1.1990850	1.9812430	1.6053000
H	0.1184390	3.6414180	0.7863890
H	1.2884350	2.9665340	-0.3164140
H	-0.4746950	2.2084830	2.9464690
H	0.6062620	0.8950680	3.3811090
H	1.8436030	1.1747610	1.2530050
H	1.8342230	2.6848140	2.1437120
H	0.1390090	1.4390700	-2.3365230
C	1.3683370	0.1705550	-1.1261670
C	2.5007570	0.9363120	-1.3923650
C	1.5241740	-1.0521160	-0.4747670
C	3.7553470	0.5384310	-0.9571950
H	2.4061510	1.8538040	-1.9591720
C	2.7731680	-1.4627830	-0.0341640
H	0.6701340	-1.6975720	-0.3240230
C	3.8746830	-0.6542990	-0.2636740
H	4.6330180	1.1335210	-1.1620820
H	2.8973150	-2.4081460	0.4733880
O	-1.5417420	-1.9975890	-0.3110100
Cl	5.4456470	-1.1628350	0.2997070

Zero-point correction=	0.376961 (Hartree/Particle)
Thermal correction to Energy=	0.396294
Thermal correction to Enthalpy=	0.397238
Thermal correction to Gibbs Free Energy=	0.329522
Sum of electronic and zero-point Energies=	-1439.288460
Sum of electronic and thermal Energies=	-1439.269127
Sum of electronic and thermal Enthalpies=	-1439.268183
Sum of electronic and thermal Free Energies=	-1439.335900

TS-CI-RR: TS for the addition of the enamine to 4-chlorobenzaldehyde 85c leading to RR-86c.

	X	Y	Z
H	-1.7429870	-1.5797710	-0.8510490
N	-2.4553060	0.7416960	-0.1769260
C	-3.4401450	-0.0559820	0.5806630
C	-3.3610240	-1.6006340	0.4749730
O	-4.0517400	-2.2032270	1.2626180
C	-3.0290130	1.2205640	-1.4535860
C	-4.7640230	0.3888490	-0.0534900
H	-5.5491130	-0.3344380	0.1437830
C	-4.3816270	0.5187130	-1.5272350
H	-5.0635020	1.3579980	0.3489230
H	-5.0984980	1.0858910	-2.1151600
H	-4.2643410	-0.4704480	-1.9679200
H	-2.3556310	0.9678720	-2.2693240
H	-3.1597370	2.3031530	-1.4124930
H	-3.3773390	0.1989070	1.6348520
C	0.0469270	-1.1186060	0.0030280
O	-0.6212180	-1.0865600	-1.1080960
H	-0.2246740	-1.9087790	0.7114680
C	1.5180890	-0.9179400	-0.1034310
C	2.3679710	-1.2711940	0.9409880
C	2.0657610	-0.4102780	-1.2795250
C	3.7331630	-1.0520510	0.8502840
H	1.9603160	-1.7293510	1.8330620
C	3.4286750	-0.1853580	-1.3845740
H	1.4065980	-0.2184460	-2.1143570
C	4.2474380	-0.4918340	-0.3084750
H	4.3967500	-1.3196590	1.6591360
H	3.8607010	0.2118000	-2.2913890
C	-1.2530140	1.0536260	0.2491540
C	-0.5942500	0.3002640	1.2528070
C	-0.4535980	2.0688660	-0.5076320
C	0.4758950	0.9977510	2.0788190
H	-1.2496370	-0.3220090	1.8528610
C	0.4269140	2.8995710	0.4311230
H	0.1656760	1.5059660	-1.2163060

H	-1.1002670	2.7172140	-1.0928780
C	1.3123300	2.0085690	1.2947210
H	1.1278370	0.2570810	2.5405520
H	-0.0215010	1.5140140	2.9060450
H	1.0336830	3.5832790	-0.1620470
H	-0.2153940	3.5136990	1.0679280
H	1.8878740	2.6177070	1.9919680
H	2.0314630	1.4917060	0.6589750
O	-2.6656220	-2.1293640	-0.4769590
Cl	5.9628640	-0.1999670	-0.4276660

Zero-point correction= 0.375522 (Hartree/Particle)
 Thermal correction to Energy= 0.395213
 Thermal correction to Enthalpy= 0.396157
 Thermal correction to Gibbs Free Energy= 0.326768
 Sum of electronic and zero-point Energies= -1439.281992
 Sum of electronic and thermal Energies= -1439.262301
 Sum of electronic and thermal Enthalpies= -1439.261357
 Sum of electronic and thermal Free Energies= -1439.330746

Ketol syn-86a:

	X	Y	Z
C	-1.5279500	1.0594320	-0.6357180
C	-1.6609040	-0.0824340	0.3879410
C	-3.0995250	-0.5699740	0.3976690
C	-4.1463360	0.4940160	0.6308290
C	-3.9788890	1.6125290	-0.4101560
C	-2.5547770	2.1629180	-0.3916220
C	-0.6865200	-1.2436530	0.1281570
O	-3.3953940	-1.7227790	0.1781130
O	-0.9330860	-1.8204050	-1.1365520
C	3.3779050	0.1684610	0.3316510
C	2.8511810	-0.2489530	-0.8838350
C	1.5410690	-0.7188580	-0.9435290
C	0.7481880	-0.7786350	0.1897430
C	1.2946990	-0.3630900	1.4051390
C	2.5893330	0.1064670	1.4817440
H	-1.6588390	0.6366420	-1.6346430
H	-0.5139070	1.4567510	-0.5878200
H	-1.4636520	0.3336660	1.3834310
H	-5.1285580	0.0289660	0.5843820
H	-4.0004370	0.9132240	1.6306170
H	-4.1983320	1.2084880	-1.4019150
H	-4.7055890	2.4020550	-0.2195820
H	-2.3620080	2.6316590	0.5782610
H	-2.4454160	2.9424380	-1.1462910
H	3.4416520	-0.2197110	-1.7867560
H	1.1317900	-1.0523990	-1.8860000
H	0.6989710	-0.4163250	2.3092590
H	3.0217260	0.4266620	2.4191930
H	-1.8045820	-2.2246150	-1.0735870
H	-0.8452530	-1.9919510	0.9128370
O	4.6395630	0.6430760	0.5051510
C	5.4640630	0.7175330	-0.6363920
H	6.4180740	1.1086900	-0.2964490
H	5.6144030	-0.2686060	-1.0818810
H	5.0420710	1.3906660	-1.3864830

Zero-point correction= 0.301536 (Hartree/Particle)
 Thermal correction to Energy= 0.316920
 Thermal correction to Enthalpy= 0.317865
 Thermal correction to Gibbs Free Energy= 0.258213
 Sum of electronic and zero-point Energies= -769.608820
 Sum of electronic and thermal Energies= -769.593436
 Sum of electronic and thermal Enthalpies= -769.592492
 Sum of electronic and thermal Free Energies= -769.652143

Ketol anti-86a:

	X	Y	Z
C	-1.5858130	-1.2911940	0.3634280
C	-1.6467390	0.1374730	-0.2057030
C	-3.0851170	0.6307670	-0.1444610
C	-4.1198560	-0.2790440	-0.7652100

C	-4.0145620	-1.6923860	-0.1774850
C	-2.5904000	-2.2244890	-0.3089650
C	-0.6921400	1.1222360	0.4893470
O	-3.3950860	1.6685880	0.3945170
O	-0.7792560	2.3949720	-0.1186670
H	-1.7918150	-1.2499500	1.4385300
H	-0.5726290	-1.6747200	0.2506170
H	-1.3699320	0.0981410	-1.2667850
H	-5.1013440	0.1644040	-0.6125850
H	-3.9209580	-0.3251680	-1.8404410
H	-4.2949170	-1.6615870	0.8786430
H	-4.7246650	-2.3518260	-0.6761200
H	-2.3368920	-2.3229790	-1.3686580
H	-2.5182530	-3.2207710	0.1282330
H	-1.6766170	2.7036340	0.0428220
C	0.7406870	0.6596320	0.4054400
C	1.3288290	-0.0715830	1.4358280
C	1.4953410	0.9282390	-0.7261700
C	2.6262930	-0.5345660	1.3317060
H	0.7625370	-0.2777490	2.3362930
C	2.8045180	0.4753650	-0.8466620
H	1.0586590	1.5230360	-1.5168720
C	3.3723200	-0.2645360	0.1855100
H	3.0929150	-1.0975940	2.1276120
H	3.3661620	0.7113430	-1.7373640
H	-0.9827570	1.1830040	1.5452900
O	4.6392240	-0.7556410	0.1744540
C	5.4262810	-0.4908370	-0.9653210
H	6.3886110	-0.9603600	-0.7858980
H	4.9768860	-0.9176410	-1.8651010
H	5.5680890	0.5829760	-1.1083350

Zero-point correction= 0.300917 (Hartree/Particle)
 Thermal correction to Energy= 0.316411
 Thermal correction to Enthalpy= 0.317355
 Thermal correction to Gibbs Free Energy= 0.257264
 Sum of electronic and zero-point Energies= -769.607955
 Sum of electronic and thermal Energies= -769.592461
 Sum of electronic and thermal Enthalpies= -769.591517
 Sum of electronic and thermal Free Energies= -769.651608

Ketol syn-86b:

	X	Y	Z
C	0.9487410	-1.0106910	-0.7213010
C	0.8881620	0.0606600	0.3826320
C	2.2526240	0.7174320	0.5006210
C	3.4090160	-0.2254660	0.7328880
C	3.4341580	-1.2845010	-0.3812910
C	2.0889940	-1.9993420	-0.4858790
C	-0.2082500	1.1133920	0.1498340
O	2.4130790	1.9085760	0.3600840
O	0.0059470	1.7929650	-1.0677910
C	-4.0722350	-0.7722730	0.1357620
C	-3.5480280	-0.2579020	-1.0409420
C	-2.3062620	0.3652620	-1.0444990
C	-1.5777480	0.4784640	0.1332360
C	-2.1123760	-0.0324150	1.3131670
C	-3.3505170	-0.6554420	1.3170980
H	1.0814430	-0.5041940	-1.6802060
H	-0.0090410	-1.5297790	-0.7640670
H	0.6970840	-0.4473920	1.3354180
H	4.3278340	0.3552350	0.7722330
H	3.2634390	-0.7231150	1.6959730
H	3.6566320	-0.7920060	-1.3313370
H	4.2390000	-1.9949040	-0.1937110
H	1.9020330	-2.5555630	0.4376700
H	2.1175100	-2.7299230	-1.2948550
H	-5.0395080	-1.2553010	0.1357170
H	-4.1082390	-0.3378590	-1.9627230
H	-1.8947350	0.7766850	-1.9546150
H	-1.5595310	0.0686490	2.2401200
H	-3.7558480	-1.0437070	2.2416340
H	0.8186840	2.2943570	-0.9469140
H	-0.1666330	1.8234350	0.9833500

Zero-point correction=	0.268216 (Hartree/Particle)
Thermal correction to Energy=	0.281101
Thermal correction to Enthalpy=	0.282045
Thermal correction to Gibbs Free Energy=	0.228306
Sum of electronic and zero-point Energies=	-655.127528
Sum of electronic and thermal Energies=	-655.114643
Sum of electronic and thermal Enthalpies=	-655.113699
Sum of electronic and thermal Free Energies=	-655.167438

Ketol anti-86b:

	X	Y	Z
C	0.9321490	-1.3042000	-0.2267550
C	0.9069540	0.1723980	0.2066300
C	2.2776980	0.7869870	-0.0404890
C	3.4549960	0.0304820	0.5305790
C	3.4286770	-1.4375050	0.0862690
C	2.0827610	-2.0750390	0.4162010
C	-0.1966970	1.0026570	-0.4700860
O	2.4268980	1.8059510	-0.6751790
O	-0.2005960	2.3185740	0.0423740
H	1.0290270	-1.3507100	-1.3170140
H	-0.0220520	-1.7650380	0.0241720
H	0.7335310	0.2109270	1.2894550
H	4.3666980	0.5418890	0.2299250
H	3.3762260	0.0731400	1.6215800
H	3.5993570	-1.4876530	-0.9921790
H	4.2447970	-1.9795340	0.5636120
H	1.9439530	-2.0897400	1.5011660
H	2.0650750	-3.1122020	0.0802680
H	0.6395430	2.7069520	-0.2210960
C	-1.5610670	0.4016340	-0.2364190
C	-2.1182940	-0.4788620	-1.1570450
C	-2.2602700	0.6936390	0.9307710
C	-3.3475070	-1.0751540	-0.9111780
H	-1.5862220	-0.6973830	-2.0751280
C	-3.4914330	0.1028610	1.1759910
H	-1.8385960	1.4029300	1.6297610
C	-4.0361320	-0.7865210	0.2585960
H	-3.7700900	-1.7579530	-1.6356770
H	-4.0302180	0.3407300	2.0831330
H	-4.9963660	-1.2454400	0.4501880
H	0.0039080	1.0126240	-1.5481230

Zero-point correction=	0.268081 (Hartree/Particle)
Thermal correction to Energy=	0.281036
Thermal correction to Enthalpy=	0.281980
Thermal correction to Gibbs Free Energy=	0.228030
Sum of electronic and zero-point Energies=	-655.126112
Sum of electronic and thermal Energies=	-655.113157
Sum of electronic and thermal Enthalpies=	-655.112213
Sum of electronic and thermal Free Energies=	-655.166163

Ketol syn-86c:

	X	Y	Z
C	-1.5503450	1.0045780	-0.7263370
C	-1.6250740	-0.0470700	0.3949930
C	-3.0605250	-0.5302360	0.5207310
C	-4.0941040	0.5512810	0.7257420
C	-3.9870520	1.5803030	-0.4110800
C	-2.5652490	2.1266540	-0.5183610
C	-0.6686840	-1.2317720	0.1786480
O	-3.3629880	-1.6960810	0.4061870
O	-0.9744600	-1.9017660	-1.0242010
C	3.3848510	0.1458250	0.0776270
C	2.8056410	-0.3357470	-1.0824200
C	1.4957240	-0.7948030	-1.0483580
C	0.7688320	-0.7723540	0.1352510
C	1.3767570	-0.2902340	1.2908910
C	2.6826520	0.1717570	1.2715340
H	-1.7349930	0.5003520	-1.6777790
H	-0.5370690	1.4047810	-0.7692350
H	-1.3740410	0.4482420	1.3405610
H	-5.0765550	0.0871480	0.7742780
H	-3.8918540	1.0498000	1.6781360
H	-4.2628720	1.0977570	-1.3521770

H	-4.7025560	2.3849810	-0.2439640
H	-2.3189750	2.6746330	0.3961210
H	-2.5002420	2.8398080	-1.3405190
H	3.3753240	-0.3521110	-2.0000340
H	1.0311390	-1.1834950	-1.9422940
H	0.8293030	-0.2843030	2.2258320
H	3.1570060	0.5422200	2.1682610
H	-1.8406380	-2.2998490	-0.8881970
H	-0.7880350	-1.9163200	1.0258350
Cl	5.0325940	0.7247080	0.0409480

Zero-point correction=	0.258290 (Hartree/Particle)
Thermal correction to Energy=	0.272512
Thermal correction to Enthalpy=	0.273457
Thermal correction to Gibbs Free Energy=	0.215566
Sum of electronic and zero-point Energies=	-1114.739793
Sum of electronic and thermal Energies=	-1114.725571
Sum of electronic and thermal Enthalpies=	-1114.724626
Sum of electronic and thermal Free Energies=	-1114.782517

Ketol *anti*-86c:

	X	Y	Z
C	-1.5378290	-1.3061760	0.3268040
C	-1.6436280	0.1362690	-0.1995110
C	-3.0854190	0.6053640	-0.0581760
C	-4.1324520	-0.3001630	-0.6623480
C	-3.9819650	-1.7286490	-0.1229930
C	-2.5572590	-2.2353800	-0.3289380
C	-0.6789740	1.1215000	0.4807380
O	-3.3834010	1.6194620	0.5301320
O	-0.8126310	2.4073480	-0.0861240
H	-1.6990060	-1.2978160	1.4102560
H	-0.5259160	-1.6733210	0.1603150
H	-1.4149310	0.1311000	-1.2724850
H	-5.1126620	0.1229600	-0.4546300
H	-3.9788510	-0.3105860	-1.7458390
H	-4.2188200	-1.7341400	0.9441060
H	-4.7024770	-2.3837960	-0.6119480
H	-2.3464100	-2.3024050	-1.4001890
H	-2.4530900	-3.2414780	0.0780020
H	-1.7029280	2.7017270	0.1318990
C	0.7576800	0.6909190	0.3188810
C	1.3907840	-0.0776530	1.2884080
C	1.4608270	1.0382070	-0.8306290
C	2.6972740	-0.5114800	1.1157570
H	0.8607080	-0.3389290	2.1958820
C	2.7679260	0.6160960	-1.0158250
H	0.9817210	1.6640260	-1.5704160
C	3.3714430	-0.1602860	-0.0404960
H	3.1925550	-1.1052010	1.8696950
H	3.3204760	0.8881760	-1.9031940
H	-0.9215990	1.1466220	1.5497900
Cl	5.0187670	-0.6948730	-0.2684320

Zero-point correction=	0.258311 (Hartree/Particle)
Thermal correction to Energy=	0.272556
Thermal correction to Enthalpy=	0.273500
Thermal correction to Gibbs Free Energy=	0.215689
Sum of electronic and zero-point Energies=	-1114.738322
Sum of electronic and thermal Energies=	-1114.724077
Sum of electronic and thermal Enthalpies=	-1114.723133
Sum of electronic and thermal Free Energies=	-1114.780944

6.5. Information on Chapter 5

6.5.1. General Procedure for the HSiCl₃-Mediated Reduction of NO₂-groups

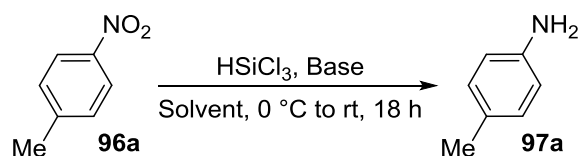
In a round bottomed flask the nitro-compound (0.7 mmol) and the tertiary amine (3.5 mmol) were dissolved into the dry solvent (5 mL) under magnetic stirring and nitrogen atmosphere. A solution of freshly distilled HSiCl₃ (2.5 mmol) in 2 mL of dry solvent was prepared apart, and it was added drop-wise to the first solution

over 10 minutes at 0 °C. After stirring the reaction mixture for 18 h, 5 mL of a saturated solution of NaHCO₃ was added drop-wise and the biphasic mixture was allowed to stir for 30 min. The crude mixture was extracted with ethyl acetate, dried over Na₂SO₄, filtered and then dried under reduced pressure to afford the crude product.

The starting material conversion was evaluated through ¹H-NMR analysis of the crude products. **In some cases, deviations from the expected products' chemical shifts were observed due to the presence of residual tertiary amine hydrochlorides.** However, further purification of such crude mixtures by means of flash column chromatography (Hex/AcOEt mixtures) or by washing with DCM/NaOH 1M restored the NMR signals to the expected chemical shifts.

In the following table the optimization of the reaction conditions is reported. By varying both the solvent and the base the optimum reaction conditions were found to be the use of either acetonitrile or dichloromethane as solvent in combination with both TEA or DIPEA as bases of choice.

Table S1. Reaction conditions optimization



entry	Solvent	Base	Conv. (%)
1	CH ₂ Cl ₂	DIPEA	>99
2	CH ₃ CN	DIPEA	>99
3	CHCl ₃	DIPEA	32
4	THF	DIPEA	n.r.
5	Toluene	DIPEA	n.r.
6	Hexane	DIPEA	n.r.
7	CH ₃ CN	TEA	90
8	CH ₃ CN	DMAP	17
9	CH ₃ CN	Pyridine	n.r.
10	CH ₃ CN	DABCO	n.r.
11	CH ₃ CN	DBU	54
12	CH ₃ CN	DMF	n.r.

6.5.2. Characterization of the Anilines 97a-v

Characterizations of the products were found to agree with authentic samples (if commercially available) or with previously reported data. Some products have been isolated in slightly lower yields with respect to the reported quantitative conversion. This is due to the combination of two factors: loss of material during the extraction process due to the hydrophilicity of the obtained amines, or during the chromatographic purification.

4-toluidine (97a)

Conv. >98%. In the following spectrum no signals of the starting material are detectable. Purification through flash column chromatography gave 69 mg (0.64 mmol) of the pure product as a white solid (91% yield). ¹H-NMR (300 MHz, CDCl₃) δ: 6.95 (d, *J*=8.2 Hz, 2H), 6.63 (d, *J*=8.2 Hz, 2H), 3.52 (bs, 2H, NH), 2.27 (s, 3H). ¹³C-NMR (75 MHz, CDCl₃) δ: 143.9, 129.5, 127.2, 115.1, 20.4.

4-aminobenzylalcohol (97b)

Conv. >98%. In the following spectrum no signals of the starting material are detectable. Purification through flash column chromatography gave 82 mg (0.67 mmol) of the pure product as a yellow solid (95% yield). ¹H-NMR (300 MHz, CDCl₃) δ: 7.13 (d, *J*=8.6 Hz, 2H), 6.64 (d, *J*=8.6 Hz, 2H), 4.53 (s, 2H). ¹³C-NMR (75 MHz, CDCl₃) δ: 146.0, 131.1, 128.8, 115.2, 65.2.

4-allyloxyaniline (97c)

Conv. >98%. In the following spectrum no signals of the starting material are detectable. Purification through flash column chromatography gave 103 mg (0.69 mmol) of the pure product as a solid (98% yield). ¹H-NMR (300 MHz, CDCl₃) δ: 6.62 (d, *J*=6.2 Hz, 2H), 6.51 (d, *J*=6.2 Hz, 2H), 5.89 (ddt, *J*=16.3 Hz, 11.9 Hz, 2.8 Hz, 1H), 5.16 (d, *J*=16.3 Hz, 1H), 4.97 (d, *J*=11.9 Hz, 1H), 4.21 (d, *J*=2.8 Hz, 2H). ¹³C-NMR (75 MHz, CDCl₃) δ: 152.0, 140.3, 134.1, 117.5, 116.7, 116.2, 69.9.

2-allyloxyaniline (97d)

Conv. >98%. In the following spectrum no signals of the starting material are detectable. Purification through flash column chromatography gave 95 mg (0.64 mmol) of the pure product as a solid (91% yield). ¹H-NMR (300 MHz, CDCl₃) δ: 7.02 (m, 1H), 6.45 (m, 3H), 5.93 (ddt, *J*=17.7 Hz, 12.1 Hz, 4.8 Hz, 1H), 5.33 (d, *J*=17.8 Hz, 1H), 5.20 (d, *J*=12.1 Hz, 1H), 4.43 (d, *J*=4.8 Hz, 2H). ¹³C-NMR (75 MHz, CDCl₃) δ: 69.2, 112.1, 115.2, 117.4, 118.4, 121.4, 133.6, 136.5, 146.3

4-benzyloxyaniline (97e)

Conv. >98%. In the following spectrum no signals of the starting material are detectable. Purification through flash column chromatography gave 133 mg (0.67 mmol) of the pure product as a solid (95% yield). ¹H-NMR (300 MHz, CDCl₃) δ: 7.40 (m, 5H), 6.85 (d, *J*=8.7 Hz, 2H), 6.66 (s, *J*=8.7 Hz, 2H), 5.02 (s, 2H), 3.37 (bs, 2H). ¹³C-NMR (75 MHz, CDCl₃) δ: 152.0, 140.3, 137.6, 128.4, 127.7, 127.4, 116.3, 116.2, 70.9.

2-benzyloxyaniline (97f)

Conv. 98%. Purification through flash column chromatography gave 129 mg (0.65 mmol) of the pure product as a solid (93% yield). ¹H-NMR (300 MHz, CDCl₃) δ: 7.40 (m, 5H), 6.77 (m, 4H), 5.07 (s, 2H), 3.80 (bs, 2H). ¹³C-NMR (75 MHz, CDCl₃) δ: 70.4, 112.1, 115.2, 118.4, 121.5, 127.5, 127.9, 128.5, 136.5, 137.2, 146.5.

N-Benzyl-3-phenylene diamine (97g)

The starting material conversion was not determinable from the NMR spectrum of the crude mixture. Hence, the product was isolated through flash column chromatography in 88% yield as a solid (122 mg, 0.62 mmol). ¹H-NMR (300 MHz, CDCl₃) δ: 7.30 (m, 5H), 6.99 (t, *J*=7.5 Hz, 1H), 6.13 (d, *J*=7.5 Hz, 2H), 6.04 (s, 1H), 4.32 (s, 2H). ¹³C-NMR (75 MHz, CDCl₃) δ: 149.3, 147.4, 139.5, 130.1, 128.6, 127.5, 127.2, 105.2, 104.2, 99.6, 48.3.

4-aminobenzonitrile (97h)

Conv. 93%. Purification through flash column chromatography gave 74 mg (0.63) of the pure product a solid (89% yield). ¹H-NMR (300 MHz, CDCl₃) δ: 7.43 (d, *J*=8.7 Hz, 2H), 6.67 (d, *J*=8.7 Hz, 2H), 4.16 (bs, 2H, NH). ¹³C-NMR (75 MHz, CDCl₃) δ: 150.8, 133.7, 120.4, 114.3, 99.3.

4'-aminoacetanilide (97i)

Conv. 92%. In the following spectrum 8% integrating signals of the starting material (SM) with respect to the product are detectable. Purification through flash column chromatography gave 95 mg (0.63 mmol) of the pure product a solid (90% yield). ¹H-NMR (300 MHz, CDCl₃) δ: 7.22 (d, *J*=8.5 Hz, 2H), 6.63 (d, *J*=8.5 Hz, 2H), 2.13 (s, 3H). ¹³C-NMR (75 MHz, CDCl₃) δ: 167.2, 144.3, 128.2, 120.7, 114.5, 23.8.

4-aminoacetophenone (97j)

Conv. 70%. In the following spectrum 30% integrating signals of the starting material (SM) with respect to the product are detectable. Purification through flash column chromatography gave 68 mg (0.5 mmol) of the pure product as a yellow solid (70% yield). ¹H-NMR (300 MHz, CDCl₃) δ: 7.72 (d, *J*=8.7 Hz, 2H), 6.63 (d, *J*=8.7 Hz, 2H), 4.03 (bs, 2H), 2.44 (s, 3H). ¹³C-NMR (75 MHz, CDCl₃) δ: 196.3, 151.0, 130.7, 128.0, 113.7, 25.9

4-aminobenzophenone (97k)

Conv. >98%. In the following spectrum no signals of the starting material are detectable. Purification through flash column chromatography gave 129 mg (0.65 mmol) of the pure product a solid (93% yield). ¹H-NMR (300 MHz, CDCl₃) δ: 7.72 (m, 4H), 7.54 (t, *J*=7.4 Hz, 1H), 7.46 (t, *J*=7.4 Hz, 2H), 6.68 (d, *J*=8.4 Hz, 2H), 4.10 (bs, 2H, NH). ¹³C-NMR (75 MHz, CDCl₃) δ: 195.4, 151.5, 138.9, 132.9, 131.4, 129.4, 128.1, 126.9, 113.6.

3-aminobenzoic acid (97l)

Conv. 60%. Purification through flash column chromatography gave 55 mg (0.4 mmol) of the pure product as a white solid (57% yield). ¹H-NMR (300 MHz, DMSO-*d*₆) δ: 12.47 (m, 1H), 7.08-7.18 (m, 3H), 6.76 (m, 1H), 5.29 (bs, 2H). ¹³C-NMR (75 MHz, DMSO-*d*₆) δ: 167.9, 148.8, 131.3, 128.9, 118.0, 116.6, 114.4.

4-aminobenzoic acid (97m)

Conv. 70%. Purification through flash column chromatography gave 62 mg (0.45 mmol) of the pure product as white solid (65% yield). ¹H-NMR (300 MHz, DMSO-*d*₆) δ: 11.93 (bs, 1H), 7.62 (d, *J*=8.6 Hz, 2H), 6.55 (d, *J*=8.6 Hz, 2H), 5.86 (bs, 2H). ¹³C-NMR (75 MHz, DMSO-*d*₆) δ: 167.9, 153.6, 131.7, 117.4, 113.1.

3-amino-*N,N*-dibenzylbenzamide (97n)

Conv. >98%. Purification through flash column chromatography gave 210 mg (0.66 mmol) of the pure product as a white solid (95% yield). By NMR analysis, two benzyl groups are detectable at rt. ¹H-NMR (300 MHz, CDCl₃) δ: 7.40-7.10 (m, 11H), 6.86 (m, 1H), 6.81 (m, 1H), 6.71 (ddd, *J*=8.0, 2.5, 1.0 Hz, 1H), 4.69 (s, 2H), 4.44 (s, 2H), 2.02 (bs, 2H, NH). ¹³C-NMR (75 MHz, CDCl₃) δ: 172.4, 146.8, 137.2, 136.6, 129.5, 128.7, 128.4, 127.6, 127.2, 116.4, 116.2, 113.2, 51.5, 46.7. HRMS (ESI) *m/z* Calc for C₂₁H₂₁N₂O⁺ [M+H]⁺ 317.16484, found 317.16454.

4-chloroaniline (97o)

Conv. >98%. Purification through flash column chromatography gave 87 mg (0.68 mmol) of the pure product as a solid (97% yield). ¹H-NMR (300 MHz, CDCl₃) δ: 7.12 (d, *J*=8.9 Hz, 2H), 6.63 (d, *J*=8.9 Hz, 2H), 3.67 (bs, 2H, NH). ¹³C-NMR (75 MHz, CDCl₃) δ: 144.8, 128.9, 123.0, 116.0.

4-bromoaniline (97p)

Conv. >98%. The crude product (117 mg, 0.68 mmol) was found to be pure (97% yield). ¹H-NMR (300 MHz, CDCl₃) δ: 7.25 (d, *J*=8.6 Hz, 2H), 6.57 (d, *J*=8.6 Hz, 2H), 3.68 (bs, 2H, NH). ¹³C-NMR (75 MHz, CDCl₃) δ: 110.4, 116.9, 132.2, 145.6.

4-iodoaniline (97q)

Conv. >98%. The crude product (150 mg, 0.68 mmol) was found to be pure (98% yield). $^1\text{H-NMR}$ (300 MHz, CDCl_3) δ : 7.44 (d, $J=8.6$ Hz, 2H), 6.48 (d, $J=8.6$ Hz, 2H), 3.69 (bs, 2H, NH). $^{13}\text{C-NMR}$ (75 MHz, CDCl_3) δ : 79.6, 117.5, 138.1, 146.3.

2-aminopyridine (97r)

Conv. 96%. Purification through flash column chromatography gave 61 mg (0.65 mmol) of the pure product as a white solid (94% yield). $^1\text{H-NMR}$ (300 MHz, CDCl_3) δ : 8.05 (m, 1H), 7.42 (m, 1H), 6.62 (m, 1H), 6.49 (d, 1H), 4.10 (bs, 2H). $^{13}\text{C-NMR}$ (75 MHz, CDCl_3) δ : 158.3, 148.1, 137.7, 114.0, 108.6.

2-chloro-3-aminopyridine (97s)

Conv. >98%. In the following spectrum no signals of the starting material are detectable. Purification through flash column chromatography gave 81 mg (0.63 mmol) of the pure product as a white solid (90% yield). $^1\text{H-NMR}$ (300 MHz, CDCl_3) δ : 7.80 (m, 1H), 7.05 (m, 2H), 4.20 (bs, 2H, NH). $^{13}\text{C-NMR}$ (75 MHz, CDCl_3) δ : 141.5, 135.1, 134.6, 123.7, 121.6.

2-phenethylamine (97t)

Conv. >98%. Purification through flash column chromatography gave 83 mg (0.68 mmol) of the pure product as a pale yellow liquid (98% yield). $^1\text{H-NMR}$ (300 MHz, CDCl_3) δ : 7.23 (m, 5H), 2.94 (t, $J=6.2$ Hz, 2H), 2.72 (t, $J=6.2$ Hz, 2H), 1.25 (bs, 2H, NH). $^{13}\text{C-NMR}$ (75 MHz, CDCl_3) δ : 40.0, 43.5, 126.0, 128.3, 128.7, 139.7.

2-aminopropanol (97u)

Conv. >98%. Purification through flash column chromatography gave 47 mg (0.62 mmol) of the pure product as a colourless liquid (90% yield). $^1\text{H-NMR}$ (300 MHz, CDCl_3) δ : 2.82-3.63 (m, 3H), 2.53 (bs, 3H), 1.03 (d, $J=6.2$ Hz, 3H). $^{13}\text{C-NMR}$ (75 MHz, CDCl_3) δ : 68.2, 48.4, 19.9.

Hexylamine (97v)

Conv. >98%. Purification through flash column chromatography gave 66 mg (0.65 mmol) of the pure product as a colourless liquid (93% yield). $^1\text{H-NMR}$ (300 MHz, CDCl_3) δ : 2.69 (t, $J=6.5$ Hz, 2H), 1.50-1.05 (m, 10H), 0.89 (t, $J=5.6$ Hz, 3H). $^{13}\text{C-NMR}$ (75 MHz, CDCl_3) δ : 42.3, 34.1, 31.7, 26.3, 22.8, 14.0.

6.5.3. Use of the HSAB Theory

HSiCl_3 , DMF (*N,N*-dimethylformamide) and TMA (trimethylamine) were optimized with MP2, B3LYP and wB97XD methods and aug-cc-PVTZ basis set. The electronic energies have been calculated on the optimized geometry of the three compounds with charges -1, 0 and +1 with the three methods. Atomic charges on the acidic sites of $\text{HSiCl}_3^{(-,0,+)}$ and basic sites of $\text{DMF}^{(-,0,+)}$ and $\text{TMA}^{(-,0,+)}$ were calculated according to the Merz-Singh-Kollman method. The obtained results are reported in the following tables, and the values were obtained accordingly with the formulae reported below.

MP2/aug-cc-PVTZ											
Species	Global Properties							Local Properties			
	E [au]	EA [au]	IP [au]	μ [au]	η [au]	S [au]	MK	f^+	$\eta(r)$	$s(r)$	
	-	-1668.906717									
	0	-1668.946157	-0.441	0.039	0.201	0.481	2.079	0.10	0.092	0.190	0.044
	+	-1668.504660									0.19
	-	-1668.906717									2.04
	0	-1668.946157	-0.441	0.039	0.201	0.481	2.079	0.13	-0.287	-0.596	-0.137
	+	-1668.504660									-0.15
	-	-248.038672									-0.73
	0	-248.055326	-0.373	0.017	0.178	0.390	2.565	-0.57	0.155	0.397	0.060
	+	-247.682086									-0.21
	-	-174.077308									-0.67
	0	-174.101021	-0.324	0.024	0.150	0.348	2.875	-0.02	0.651	1.871	0.226
	+	-173.776939									0.47

B3LYP/aug-cc-PVTZ											
Species	Global Properties							Local Properties			
	E [au]	EA [au]	IP [au]	μ [au]	η [au]	S [au]	MK	f^+	$\eta(r)$	$s(r)$	
	-	-1670.963738									-1.00
	0	-1670.983978	-0.418	0.020	0.199	0.438	2.282	0.08	0.125	0.284	0.054
	+	-1670.566078									0.20
	-	-1670.963738									2.23
	0	-1670.983978	-0.418	0.020	0.199	0.438	2.282	0.05	-0.234	-0.533	-0.102
	+	-1670.566078									-0.18
	-	-248.603708									-0.67
	0	-248.613414	-0.340	0.010	0.165	0.35	2.856	-0.51	0.167	0.475	0.058
	+	-248.272976									-0.25
	-	-174.528678									-0.83
	0	-174.544599	-0.306	0.016	0.145	0.322	3.104	-0.04	0.784	2.433	0.252
	+	-174.238382									0.42

wB97XD/aug-cc-PVTZ											
Species	Global Properties							Local Properties			
	E [au]	EA [au]	IP [au]	μ [au]	η [au]	S [au]	MK	f^+	$\eta(r)$	$s(r)$	
	-	-1670.885074									-1.33
	0	-1670.913774	-0.432	0.029	0.202	0.461	2.172	0.01	0.116	0.252	0.054
	+	-1670.481965									0.13
	-	-1670.885074									2.73
	0	-1670.913774	-0.432	0.029	0.202	0.461	2.172	0.27	-0.228	-0.495	-0.105
	+	-1670.481965									0.04
	-	-248.508746									-0.68
	0	-248.526613	-0.341	0.018	0.161	0.36	2.789	-0.51	0.167	0.466	0.060
	+	-248.185967									-0.24
	-	-174.457225									-1.17
	0	-174.483288	-0.306	0.026	0.140	0.332	3.009	-0.16	1.014	3.050	0.337
	+	-174.176985									0.46

E [au] is the electronic energy expressed in atomic units (Hartree), EA is the Electron Affinity (calculated as $E^0 - E^+$, where E^X refers to the electron energy of the molecule with charge X), I is the Ionization Potential ($E^- - E^0$), μ is the Chemical Potential $(EA+I)/2$, η is the Hardness $(EA-I)$, S is the Softness $(1/\eta)$, MK are the

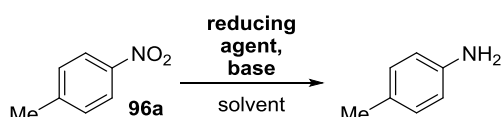
calculated charges on the highlighted atom, f^+ is the Fukui function ($MK^+ - MK^0$), $\eta(r)$ is the local hardness ($\eta \cdot f^+$) and $s(r)$ is the local softness ($S \cdot f^+$).

By inserting the obtained values in the following formula, the energy change associated to the interaction between the k atom of the acid A and the n atom of the base B can be evaluated.

$$\Delta E = -\frac{1}{2} (\mu_A - \mu_B)^2 \frac{S_{A_k} S_{B_n}}{S_{A_k} + S_{B_n}}$$

The obtained results are reported in Chapter 5, Table 13.

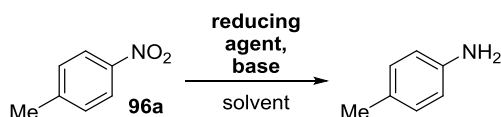
6.5.4. Generation of SiCl_2 from other sources



entry	reducing agent	base	solvent, T°C	conv (%)
1	SiCl_4 , Mg	-	THF	20
2	SiCl_4 , Mg	DIPEA	THF	79 ^a

a) a huge number of byproducts are present in the crude mixture; the value is obtained as $\text{red}96a/(\text{red}96a+96a)$.

4-Nitrotoluene (400 mg, 2.91 mmol), magnesium (638 mg, 26.25 mmol) and DIPEA (2.6 mL, 14.55 mmol), were added to 10 mL of THF under nitrogen atmosphere. The mixture was cooled to -78°C before the addition of SiCl_4 (1.06 mL, 8.75 mmol) was performed dropwise. The reaction was then allowed to warm to room temperature and stirred for 18 h, then the reaction was cautiously quenched with NaHCO_3 s.s. and extracted with CH_2Cl_2 . The organic layer was dried over Na_2SO_4 and concentrated to give the crude product that was analyzed by $^1\text{H-NMR}$ to evaluate the reaction conversion.



entry	reducing agent	base	solvent	conv (%)
1	Si_2Cl_6	DIPEA	MeCN	27
2	Si_2Cl_6	TEA	MeCN	60
3	Si_2Cl_6	TEA	DCM	9
4	Si_2Cl_6	TEA	benzene	17

In a round bottomed flask the nitro-compound (0.7 mmol) and the tertiary amine (3.5 mmol) were dissolved into the dry solvent (5 mL) under magnetic stirring and nitrogen atmosphere. Hexachlorodilane was added drop-wise to the first solution over 10 minutes at 0°C . After stirring the reaction mixture for 18 h, 5 mL of a saturated solution of NaHCO_3 was added drop-wise and the biphasic mixture was allowed to stir for 30 min. The crude mixture was extracted with ethyl acetate, dried over Na_2SO_4 , filtered and then dried under reduced pressure to afford the crude product. The crude product was analyzed by $^1\text{H-NMR}$ to evaluate the reaction conversion.

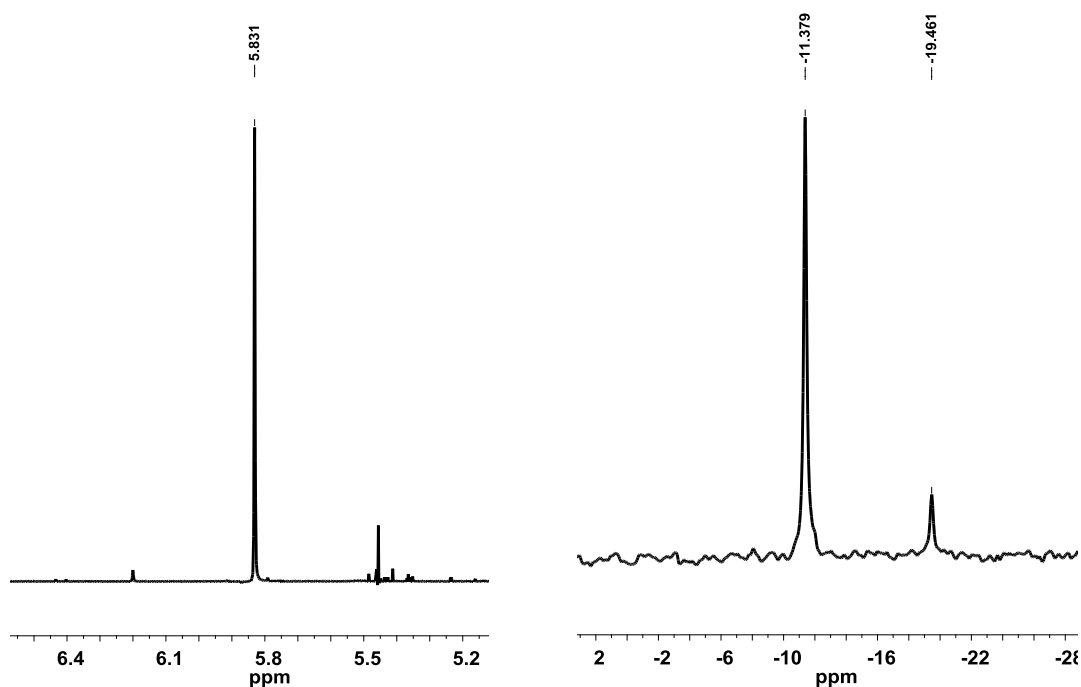
6.5.5. ^1H - and ^{29}Si -NMR experiments

Since HSiCl_3 can be easily hydrolyzed in presence of wet atmosphere, tubes for all the NMR experiments were prepared in a Schlenk line, equipped with a rubber septum, containing the NMR tube under nitrogen

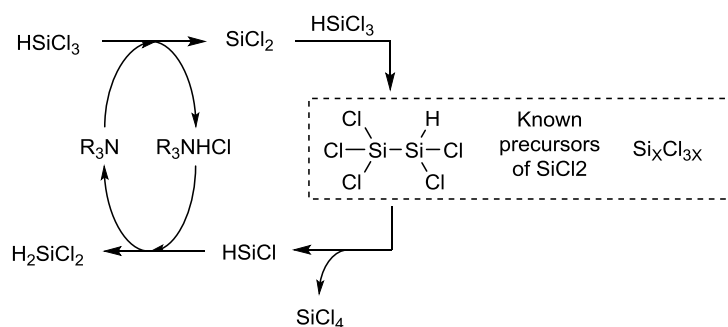
atmosphere. First experiments were voted to the characterization of the reagents. ^1H and ^{29}Si chemical shifts of HSiCl_3 were found in agreement with the literature (Thorshaug, K.; Swang, O.; Dahl, I. M.; Olafsen, A. *J. Phys. Chem. A* **2006**, *110*, 9801). ^1H -NMR (300 MHz, CDCl_3) δ : 6.09. ^{29}Si -NMR (99.3 MHz, CDCl_3) δ : -7.99.

Secondly, experiments regarding the observation of the reaction between HSiCl_3 and DIPEA or TEA were performed. ^1H -NMR experiments revealed the instauration of an equilibrium between HSiCl_3 and the hydrochloride salts of the base ($\text{R}_3\text{N}\cdot\text{HCl}$), accordingly with previous observations by Bernstein.⁹⁷ Despite we were not able to directly observe the evanescent SiCl_2 specie by ^{29}Si -NMR experiments, indirect observation of its formation can be hypothesized. Indeed, for longer times, an equilibration occurs between HSiCl_3 and SiCl_4 (^{29}Si -NMR (99.3 MHz, CDCl_3): δ : -19.46) + H_2SiCl_2 (^1H -NMR (300 MHz, CDCl_3) δ : 5.83. ^{29}Si -NMR (99.3 MHz, CDCl_3): δ : -11.38) (Figure ES1), accordingly with previous reports by Karsch.¹⁰² The reaction mechanism associated to this transformation can be hypothesized accordingly with the formation of SiCl_2 as in Scheme S1.

Figure S1. ^1H - and ^{29}Si -NMR spectra of the 1:1 HSiCl_3 /TEA mixture. In the first spectrum only H_2SiCl_2 is detectable (^1H -NMR). In the second spectrum both H_2SiCl_2 and SiCl_4 are observed (^{29}Si -NMR).



Scheme S1. $\text{HSiCl}_3 \rightarrow \text{SiCl}_4 + \text{H}_2\text{SiCl}_2$ through SiCl_2 formation.



First attempts to perform the reaction in a NMR tube were made using CD₃CN. However, in this solvent the reaction was found to be too fast to be followed by NMR techniques. Hence, we turned our attention on CDCl₃, since it demonstrated to be a less effective solvent for this reaction providing the desired product in only 32% of conversion (Table S1 of this chapter).

When performing the reaction in the NMR tube in CDCl₃ (**96a** 0.1 M, HSiCl₃ 3.5 eq., DIPEA 5 eq.), HSiCl₃ was observed to disappear within 8h, while a second broadened AB system (evidence of a newly formed 1,4 bi-substituted aromatic compound) appeared (7.0-7.2 ppm, see **Figure S2**). Similarly, the HSiCl₃ ²⁹Si-NMR peak was observed to disappear while new peaks were appearing between -46 and -47 ppm (see **Figure S3**). On the basis of these observations and by comparison with the literature, we attributed the new forming AB-system to the silylated product **97a-Si**. Indeed, once quenched the reaction, this AB system was found to shift, while sharpening, at the expected chemical shift of 4-toluidine **97a** (Figure S2).

Figure S2. ¹H-NMR spectra of the reduction reaction evolution in CDCl₃ in the 6.0 - 8.3 ppm region.

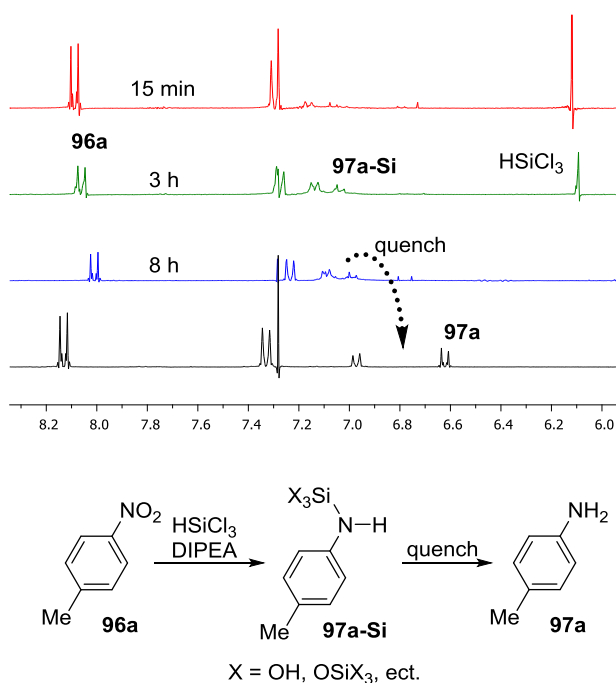
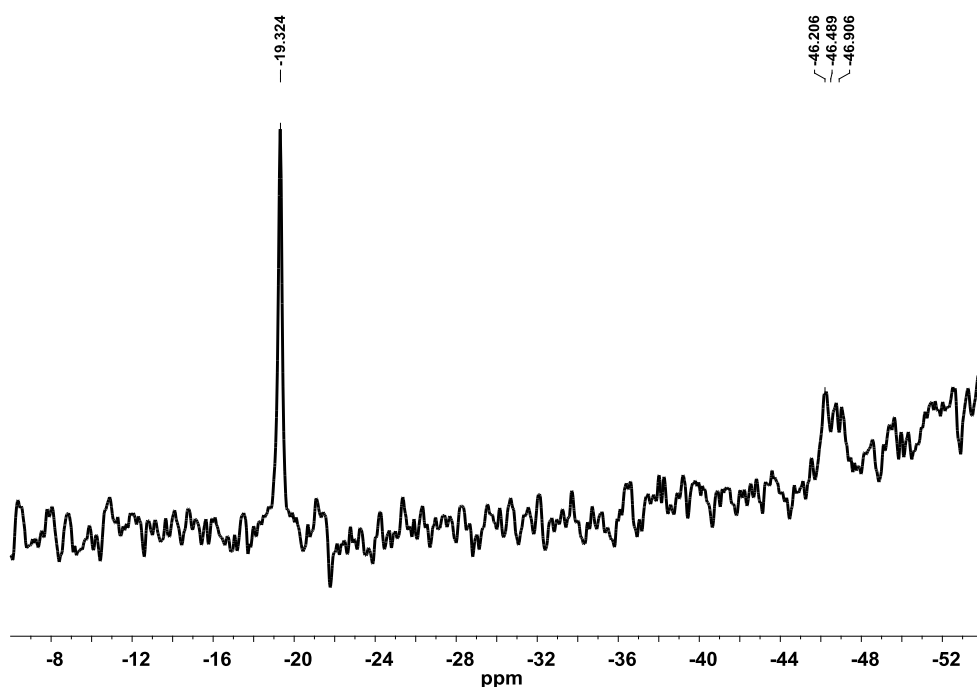


Figure S3. ^{29}Si -NMR spectrum of the reduction reaction in CDCl_3 in the -38 to -54 ppm region.



6.5.6. Determination of the Reaction Rate Determining Step

The nitro reduction mechanism can be considered composed of three reduction steps: i) from nitro to nitroso, ii) from nitroso to hydroxylamine, and iii) from hydroxylamine to amine. Since the only observed species in solution were **96a** and **97a-Si** (Figure S2), we hypothesized the reduction of the nitro- to the nitroso-group to be the reaction rate determining step. Indeed, neither 4-nitrosotoluene **98** nor hydroxylamine **99** were detected monitoring the reaction by NMR spectroscopy. To verify this hypothesis, the intermediates **98** and **99** were synthesized and reacted under our standard reduction conditions in a NMR tube. While nitro-compound **96a** was reduced in a few hours in 35% conversion (Figure S2), we found **98** to be reduced quantitatively in less than 5 minutes. However, when the same experiment was performed with **99**, only degradation products from hydroxylamine were detected, probably due to the poor stability of the starting material. Thus, the great difference in the reaction times changing the substrate from **96a** to **98** clearly shows that the reduction from nitro to nitroso is the reaction rate determining step.

Table S 2. Reduction of the reaction intermediates

Substrate	R	Conv. (%)
96a	NO_2	35 (8h)
98	$\text{N}=\text{O}$	>99 (<5 min)
99	NHOH	degradation

6.5.7. Geometries of TSs A, B, C and D

TS A: $\text{MeNO}_2 + \text{SiCl}_2$

	X	Y	Z
Si	0.4191370	-0.0701510	-0.5108260
Cl	1.3834230	1.7309990	-0.0516840
Cl	1.7584730	-1.5372870	0.1441970
N	-1.7672770	0.0815090	0.1198130
O	-0.6986430	-0.1082020	0.9169910
O	-2.3377860	1.1170350	0.1457870
C	-2.4586430	-1.1330210	-0.3864740
H	-2.8819890	-0.8820520	-1.3510080
H	-1.7434960	-1.9419420	-0.4391000
H	-3.2404520	-1.3300960	0.3468870

Zero-point correction= 0.054176 (Hartree/Particle)
 Thermal correction to Energy= 0.062402
 Thermal correction to Enthalpy= 0.063346
 Thermal correction to Gibbs Free Energy= 0.019306
 Sum of electronic and zero-point Energies= -1454.894398
 Sum of electronic and thermal Energies= -1454.886171
 Sum of electronic and thermal Enthalpies= -1454.885227
 Sum of electronic and thermal Free Energies= -1454.929267

TS B: MeNO₂ + SiCl₃⁻

	X	Y	Z
C	-2.2079670	-1.1131390	1.0801970
H	-1.8213780	-0.8878650	2.0668050
H	-1.7602130	-2.0048980	0.6566010
H	-3.2956940	-1.1905170	1.0908620
N	-1.8965660	0.0361560	0.1841060
O	-2.1174440	-0.2004130	-1.0452710
O	-2.1919970	1.1658730	0.6710170
Si	0.3777350	-0.0364290	0.1170570
Cl	1.0482590	-1.5631280	-1.1826540
Cl	1.9336060	0.0409870	1.5673770
Cl	0.6997980	1.7159840	-0.9864260

Zero-point correction= 0.054970 (Hartree/Particle)
 Thermal correction to Energy= 0.064879
 Thermal correction to Enthalpy= 0.065823
 Thermal correction to Gibbs Free Energy= 0.017163
 Sum of electronic and zero-point Energies= -1915.291125
 Sum of electronic and thermal Energies= -1915.281215
 Sum of electronic and thermal Enthalpies= -1915.280271
 Sum of electronic and thermal Free Energies= -1915.328931

TS C: MeNO₂ + SiCl₃⁻ + TMAH⁺

	X	Y	Z
C	-0.5658080	2.9559500	-0.3820460
H	-1.2424950	3.0751600	0.4541130
H	-1.0885820	2.8375800	-1.3221850
H	0.1536280	3.7740930	-0.4284470
N	0.2438990	1.7304620	-0.1446170
O	0.9075310	1.3280920	-1.1477890
O	0.7308570	1.6117350	1.0020000
Si	-1.4926450	0.0339700	-0.0522940
Cl	-0.4648890	-1.5071230	-1.1015080
Cl	-3.4978830	-0.3069150	-0.6231570
Cl	-1.4392590	-0.6899000	1.9295310
N	2.6876710	-0.4415470	-0.0415230
H	1.8816610	0.0965040	-0.4427470
C	2.2475790	-1.1399440	1.1907370
H	1.8324480	-0.4019530	1.8688850
H	1.4859690	-1.8670060	0.9269370
H	3.1103660	-1.6349890	1.6306200
C	3.1581040	-1.3937140	-1.0733360
H	2.3674850	-2.1104700	-1.2706280
H	3.3929460	-0.8396870	-1.9771580
H	4.0453410	-1.9008710	-0.7022110
C	3.7133170	0.5848730	0.2625360
H	3.9728630	1.0980440	-0.6584690
H	3.2848240	1.2869630	0.9704870
H	4.5878680	0.0939720	0.6821420

Zero-point correction= 0.193149 (Hartree/Particle)
 Thermal correction to Energy= 0.209864
 Thermal correction to Enthalpy= 0.210808

Thermal correction to Gibbs Free Energy=	0.147666
Sum of electronic and zero-point Energies=	-2090.091491
Sum of electronic and thermal Energies=	-2090.074777
Sum of electronic and thermal Enthalpies=	-2090.073833
Sum of electronic and thermal Free Energies=	-2090.136975

TS D: MeNO₂ + TMA...SiCl₂

	X	Y	Z
Si	0.0417500	-0.5122710	-0.0659830
Cl	0.4442590	-1.3257340	1.7978320
Cl	1.1649320	-1.6496930	-1.4193090
N	-2.0188580	0.3042530	-0.1229160
O	-2.2260660	0.4911260	1.1216250
O	-1.9734060	1.3192840	-0.9046520
C	-2.7915140	-0.8386070	-0.6906130
H	-2.4315130	-1.0275820	-1.6954540
H	-2.6629930	-1.6943940	-0.0367380
H	-3.8294300	-0.5080690	-0.7000500
N	1.1133060	1.0721160	0.0003090
C	0.5015050	2.0222630	0.9829280
H	-0.5125130	2.2480750	0.6677980
H	0.4928050	1.5565780	1.9642360
H	1.1130260	2.9225490	1.0019260
C	2.5281660	0.8230960	0.3911520
H	2.5588740	0.4256990	1.4002320
H	2.9758640	0.1185450	-0.3027580
H	3.0594520	1.7724360	0.3501040
C	1.0895920	1.7032330	-1.3562090
H	1.6033530	1.0534630	-2.0579310
H	0.0538050	1.8501240	-1.6506670
H	1.6066580	2.6588370	-1.2929120

Zero-point correction=	0.179608 (Hartree/Particle)
Thermal correction to Energy=	0.193335
Thermal correction to Enthalpy=	0.194279
Thermal correction to Gibbs Free Energy=	0.139617
Sum of electronic and zero-point Energies=	-1629.250438
Sum of electronic and thermal Energies=	-1629.236712
Sum of electronic and thermal Enthalpies=	-1629.235767
Sum of electronic and thermal Free Energies=	-1629.290429

7. References and Notes

- 1) Reviews: (a) Akiyama, T. *Chem. Rev.* **2007**, *107*, 5744. (b) Akiyama, T.; Mori, K. *Chem. Rev.* **2015**, *115*, 9277.
- 2) Yamamoto, H.; Ishihara, K. In *Acid Catalysis in Modern Organic Synthesis*; Yamamoto, H.; Ishihara, K.; Ed. Wiley-VCH: Weinheim, **2008**.
- 3) Reviews: (a) Zamfir, A.; Schenker, S.; Freund, M.; Tsogoeva, S. B. *Org. Biomol. Chem.* **2010**, *8*, 5262. (b) Mahlau, M.; List, B. *Angew. Chem. Int. Ed.* **2013**, *52*, 518. (c) Brak, K.; Jacobsen, E. N. *Angew. Chem. Int. Ed.* **2013**, *52*, 534. (d) Parmar, D.; Sugiono, E.; Raja, S.; Rueping, M. *Chem. Rev.* **2014**, *114*, 9047.
- 4) T. Akiyama, Y. Saitoh, H. Morita, K. Fuchibe, *Adv. Synth. Catal.* **2005**, *347*, 1523.
- 5) Stemper, J.; Isaac, K.; Pastor, J.; Frison, G.; Retailleau, P.; Voituriez, A.; Betzer, J.-F.; Marinetti, A. *Adv. Synth. Catal.* **2013**, *355*, 3613.
- 6) Uraguchi, D.; Terada, M. *J. Am. Chem. Soc.* **2004**, *126*, 5356.
- 7) (a) Akiyama, T.; Itoh, J.; Yokota, K.; Fuchibe, K. *Angew. Chem. Int. Ed.* **2004**, *43*, 1566. (b) Sickert, M.; Schneider, C. *Angew. Chem. Int. Ed.* **2008**, *47*, 3631. (c) Giera, D. S.; Sickert, M.; Schneider, C. *Org. Lett.* **2008**, *10*, 4259. (d) Kashikura, W.; Mori, K.; Akiyama, T. *Org. Lett.* **2011**, *13*, 1860.
- 8) (a) Uraguchi, D.; Sorimachi, K.; Terada, M. *J. Am. Chem. Soc.* **2004**, *126*, 11804. (b) Rowland, G. B.; Rowland, E. B.; Liang, Y.; Perman, J. A.; Antilla, J. C. *Org. Lett.* **2007**, *9*, 2609. (c) Terada, M.; Yokoyama, S.; Sorimachi, K.; Uraguchi, D. *Adv. Synth. Catal.* **2007**, *349*, 1863. (d) Li, G.; Rowland, G. B.; Rowland, E. B.; Antilla, J. C. *Org. Lett.* **2007**, *9*, 4065. (e) Enders, D.; Seppelt, M.; Beck, T. *Adv. Synth. Catal.* **2010**, *352*, 1413. (f) Kang, Q.; Zhao, Z.-A.; You, S.-L. *J. Am. Chem. Soc.* **2007**, *129*, 1484. (g) Wanner, M. J.; Hauwert, P.; Schoemaker, H. E.; de Gelder, R.; van Maarseveen, J. H.; Hiemstra, H. *Eur. J. Org. Chem.* **2008**, 180. (h) Kang, Q.; Zhao, Z.-A.; You, S.-L. *Tetrahedron* **2009**, *65*, 1603. (i) Qian, Y.; Jing, C.; Zhai, C.; Hu, W.-h. *Adv. Synth. Catal.* **2012**, *354*, 301. (j) Xu, F.; Huang, D.; Han, C.; Shen, W.; Lin, X.-F.; Wang, Y. *J. Org. Chem.* **2010**, *75*, 8677.
- 9) (a) Akiyama, T.; Suzuki, T.; Mori, K. *Org. Lett.* **2009**, *11*, 2445. (b) Zeng, X.; Zeng, X.; Xu, Z.; Lu, M.; Zhong, G. *Org. Lett.* **2009**, *11*, 3036. (c) Hashimoto, T.; Nakatsu, H.; Yamamoto, K.; Maruoka, K. *J. Am. Chem. Soc.* **2011**, *133*, 9730.
- 10) Rueping, M.; Sugiono, E.; Azap, C. *Angew. Chem., Int. Ed.* **2006**, *45*, 2617. (b) Rueping, M.; Sugiono, E.; Moreth, S. A. *Adv. Synth. Catal.* **2007**, *349*, 759. (c) Zamfir, A.; Tsogoeva, S. B. *Org. Lett.* **2010**, *12*, 188. (d) Zhang, G.-W.; Zheng, D.-H.; Nie, J.; Wang, T.; Ma, J.-A. *Org. Biomol. Chem.* **2010**, *8*, 1399.
- 11) (a) Rueping, M.; Sugiono, E.; Azap, C.; Theissmann, T.; Bolte, M. *Org. Lett.* **2005**, *7*, 3781. (b) Hoffmann, S.; Seayad, A. M.; List, B. *Angew. Chem. Int. Ed.* **2005**, *44*, 7424. (c) Storer, R. I.; Carrera, D. E.; Ni, Y.; MacMillan, D. W. C. *J. Am. Chem. Soc.* **2006**, *128*, 84. (d) Li, G.; Liang, Y.; Antilla, J. C. *J. Am. Chem. Soc.* **2007**, *129*, 5830. (e) Kang, Q.; Zhao, Z.-A.; You, S.-L. *Adv. Synth. Catal.* **2007**, *349*, 1657. (f) Kang, Q.; Zhao, Z.-A.; You, S.-L. *Org. Lett.* **2008**, *10*, 2031. (g) Nguyen, T. B.; Bousserouel, H.; Wang, Q.; Guéritte, F. *Org. Lett.* **2010**, *12*, 4705.
- 12) (a) Akiyama, T.; Morita, H.; Fuchibe, K. *J. Am. Chem. Soc.* **2006**, *128*, 13070. (b) Liu, H.; Dagousset, G.; Masson, G.; Retailleau, P.; Zhu, J. *J. Am. Chem. Soc.* **2009**, *131*, 4598. (c) Brioché, J.; Courant, T.; Alcaez, L.; Stocks, M.; Furber, M.; Zhu, J.; Masson, G. *Adv. Synth. Catal.* **2014**, *356*, 1719. (d) Dagousset, G.; Zhu, J.; Masson, G. *J. Am. Chem. Soc.* **2011**, *133*, 14804. (e) Dagousset, G.; Retailleau, P.; Masson, G.; Zhu, J. *Chem. Eur. J.* **2012**, *18*, 5869. (f) Lin, J.-H.; Zong, G.; Du, R.-B.; Xiao, J.-C.; Liu, S. *Chem. Commun.* **2012**, *48*, 7738. (g) Shi, F.; Xing, G.-J.; Tao, Z.-L.; Luo, S.-W.; Tu, S.-J.; Gong, L.-Z. *J. Org. Chem.* **2012**, *77*, 6970. (h) Huang, D.; Xu, F.; Chen, T.; Wang, Y.; Lin, X. *RSC Adv.* **2013**, *3*, 573. (i) Luo, C.; Huang, Y. *J. Am. Chem. Soc.* **2013**, *135*, 8193. (j) Bergonzini, G.; Gramigna, L.; Mazzanti, A.; Fochi, M.; Bernardi, L.; Ricci, A. *Chem. Commun.* **2010**, *46*, 327. (k) Caruana, L.; Fochi, M.; Ranieri, S.; Mazzanti, A.; Bernardi, L. *Chem. Commun.* **2013**, *49*, 880.
- 13) Chen, X.-H.; Zhang, W.-Q.; Gong, L.-Z. *J. Am. Chem. Soc.* **2008**, *130*, 5652.
- 14) Simon, L.; Goodman, J. M. *J. Am. Chem. Soc.* **2008**, *130*, 8741.
- 15) Marcelli, T.; Hammar, P.; Himo, F. *Chem. Eur. J.* **2008**, *14*, 8562.

- 16) (a) Nakashima, D.; Yamamoto, H. *J. Am. Chem. Soc.* **2006**, *128*, 9626. (b) Jiao, P.; Nakashima, D.; Yamamoto, H. *Angew. Chem., Int. Ed.* **2008**, *47*, 2411.
- 17) (a) Rueping, M.; leawsuwan, W.; Antonchick, A. P.; Nachtsheim, B. J. *Angew. Chem. Int. Ed.* **2007**, *46*, 2097. (b) Raja, S.; leawsuwan, W.; Korotkov, V.; Rueping, M. *Chem. Asian J.* **2012**, *7*, 2361.
- 18) Rueping, M.; Uria, U.; Lin, M.-Y.; Atodiresei, I. *J. Am. Chem. Soc.* **2011**, *133*, 3732.
- 19) (a) Wang, P.-S.; Zhou, X.-L.; Gong, L.-Z. *Org. Lett.* **2014**, *16*, 976. (b) Zhuang, M.; Du, H. *Org. Biomol. Chem.* **2014**, *12*, 4590.
- 20) Ackermann, L.; Althammer, A. *Synlett* **2008**, 995.
- 21) Shapiro, N. D.; Rauniyar, V.; Hamilton, G. L.; Wu, J.; Toste, F.D. *Nature* **2011**, *470*, 245.
- 22) Alix, A.; Lalli, C.; Retailleau, P.; Masson, G. *J. Am. Chem. Soc.* **2012**, *134*, 10389.
- 23) Drouet, F.; Lalli, C.; Liu, H.; Masson, G.; Zhu, J. *Org. Lett.* **2011**, *13*, 94.
- 24) Lu, M.; Zhu, D.; Lu, Y.; Zeng, X.; Tan, B.; Xu, Z.; Zhong, G. *J. Am. Chem. Soc.* **2009**, *131*, 4562.
- 25) Lu, M.; Lu, Y.; Zhu, D.; Zeng, X.; Li, X.; Zhong, G. *Angew. Chem. Int. Ed.* **2010**, *49*, 8588.
- 26) Mori, K.; Ichikawa, Y.; Kobayashi, M.; Shibata, Y.; Yamanaka, M.; Akiyama, T. *J. Am. Chem. Soc.* **2013**, *135*, 3964.
- 27) (a) Liu, Z.-M.; Zhao, H.; Li, M.-Q.; Lan, Y.-B.; Yao, Q.-B.; Tao, J.-C.; Wang, X.-W. *Adv. Synth. Catal.* **2012**, *354*, 1012. (b) Liao, S.; Čorić, I.; Wang, Q.; List, B. *J. Am. Chem. Soc.* **2012**, *134*, 10765.
- 28) Čorić, I.; List, B. *Nature* **2012**, *483*, 315.
- 29) (a) Monaco, M. R.; Poladura, B.; de Los Bernardos, M. D.; Leutzsch, M.; Goddard, R.; List, B. *Angew. Chem. Int. Ed.* **2014**, *53*, 7063. (b) Monaco, M. R.; Prévost, S.; List, B. *Angew. Chem. Int. Ed.* **2014**, *53*, 8142. (c) Monaco, M. R.; Prévost, S.; List, B. *J. Am. Chem. Soc.* **2014**, *136*, 16982.
- 30) Christ, P.; Lindsay, A. G.; Vormittag, S. S.; Neudoerfl, J.-M.; Berkessel, A.; O'Donoghue, A. C. *Chem. Eur. J.* **2011**, *17*, 8524.
- 31) Selected papers: (a) Kütt, A.; Leito, I.; Kaljurand, I.; Sooväli, L.; Vlasov, V. M.; Yagupolskii, L. M.; Koppel, I. A. *J. Org. Chem.* **2006**, *71*, 2829. (b) Eckert, F.; Leito, I.; Kaljurand, I.; Kütt, A.; Klamt, A.; Diedenhofen, M. *J. Comp. Chem.* **2009**, *30*, 799. (c) Kütt, A.; Rodima, T.; Saame, J.; Raamat, E.; Mäemets, V.; Kaljurand, I.; Koppel, I. A.; Garlyauskayte, R. Y.; Yagupolskii, Y. L.; Yagupolskii, L. M.; Bernhardt, E.; Willner, H.; Leito, I. *J. Org. Chem.* **2011**, *76*, 391.
- 32) Kaupmees, K.; Tolstoluzhsky, N.; Raja, S.; Rueping, M.; Leito, I. *Angew. Chem. Int. Ed.* **2013**, *52*, 11569.
- 33) James, T.; van Gemmeren, M.; List, B. *Chem. Rev.* **2015**, DOI: 10.1021/acs.chemrev.5b00128.
- 34) Anslyn, E. V.; Dougherty, D. A. *Modern Physical Organic Chemistry*; University Science Books: Sausalito, CA, **2006**; p 466.
- 35) For recent examples of calculating pK_a values in aqueous solution, see (a) Marenich, A. V.; Ding, W.-D.; Cramer, C.; Truhlar, D. G. *J. Phys. Chem. Lett.* **2012**, *3*, 1437. (b) Ho, J.; Coote, M. L. *J. Phys. Chem. A.* **2010**, *114*, 11992. (c) Zhang, S. M.; Baker, J.; Pulay, P. *J. Phys. Chem. A.* **2010**, *114*, 432. (d) Sharma, I.; Kaminski, G. A. *J. Comput. Chem.* **2012**, *33*, 2388. (e) Zhang, S. M. *J. Comput. Chem.* **2012**, *33*, 517. (f) Ho, J.; Coote, M. L. *J. Chem. Theory Comput.* **2009**, *5*, 295. For reviews on calculating aqueous pK_a constants, see (g) Ho, J. M.; Coote, M. L. *Theor. Chem. Acc.* **2010**, *125*, 3. (h) Ho, J. M.; Coote, M. L. *Wiley Interdiscip. Rev.: Comput. Mol. Sci.* **2011**, *1*, 649.
- 36) For recent examples of calculating pK_a values in MeCN, DCE, THF, and DMSO, see (a) Trummal, A.; Rummel, A.; Lippmaa, E.; Koppel, I.; Koppel, I. A. *J. Phys. Chem. A.* **2011**, *115*, 6641. (b) Radić, N.; Maksić, Z. B. *J. Phys. Org. Chem.* **2012**, *25*, 1168. (c) Raamat, E.; Kaupmees, K.; Ovsiannikov, G.; Trummal, A.; Kütt, A.; Saame, J.; Koppel, I.; Kaljurand, I.; Lipping, L.; Rodima, T.; Pihl, V.; Koppel, I. A.; Leito, I. *J. Phys. Org. Chem.* **2013**, *26*, 162. (d) Ding, F. Z.; Smith, J. M.; Wang, H. B. *J. Org. Chem.* **2009**, *74*, 2679.
- 37) Yang, C.; Xue, X.-S.; Jin, J.-L.; Li, X.; Cheng, J.-P. *J. Org. Chem.* **2013**, *78*, 7076.
- 38) Yang, C.; Xue, X.-S.; Li, X.; Cheng, J.-P. *J. Org. Chem.* **2014**, *79*, 4340.
- 39) Fleischmann, M.; Drettwan, D.; Sugiono, E.; Rueping, M.; Gschwind, R. M. *Angew. Chem. Int. Ed.* **2011**, *50*, 6364.

40) (a) Sharif, S.; Denisov, G. S.; Toney, M. D.; Limbach, H.-H. *J. Am. Chem. Soc.* **2007**, *129*, 6313. (b) Sharif, S.; Fogle, E.; Toney, M. D.; Denisov, G. S.; Shenderovich, I. G.; Buntkowsky, G.; Tolstoy, P. M.; Chan-Huot, M.; Limbach, H.-H. *J. Am. Chem. Soc.* **2007**, *129*, 9558. (c) Sharif, S.; Schagen, D.; Toney, M. D.; Limbach, H.-H. *J. Am. Chem. Soc.* **2007**, *129*, 4440. (d) Chan-Huot, M.; Sharif, S.; Tolstoy, P. M.; Toney, M. D.; Limbach, H.-H. *Biochemistry* **2010**, *49*, 10818.

41) (a) Akakura, M.; Kawasaki, M.; Yamamoto, H. *Eur. J. Org. Chem.* **2008**, 4245 (b) Marcelli, T.; Hammar, P.; Himo, F. *Chem. Eur. J.* **2008**, *14*, 8562 (c) Simon, L.; Goodman, J. M. *J. Am. Chem. Soc.* **2009**, *131*, 4070. (d) Yamanaka, M.; Hirata, T. *J. Org. Chem.* **2009**, *74*, 3266. (e) Jain, P.; Wang, H.; Houk, K. N.; Antilla, C. *Angew. Chem. Int. Ed.* **2012**, *51*, 1391. (f) Wang, H.; Jain, P.; Antilla, J. C.; Houk, K. N. *J. Org. Chem.* **2013**, *78*, 1208. (g) Shibata, Y.; Yamanaka, M. *J. Org. Chem.* **2013**, *78*, 3731. (h) Meng, S. S.; Liang, Y.; Cao, K.-S.; Zou, L.; Lin, X.-B.; Yang, H.; Houk, K. N.; Zheng, W. H. *J. Am. Chem. Soc.* **2014**, *136*, 12249. (i) Hong, X.; Küçük, H. B.; Maji, M. S.; Yang, Y. S.; Rueping, M.; Houk, K. N. *J. Am. Chem. Soc.* **2014**, *136*, 13769. (j) Fu, A.; Meng, W.; Li, H.; Nieb, J.; Ma, J.-A. *Org. Biomol. Chem.* **2014**, *12*, 1908. (k) Overvoorde, L. M.; Grayson, M. N.; Luo, Y.; Goodman, J. M. *J. Org. Chem.* **2015**, *80*, 2634.

42) Milo, A.; Neel, A. J.; Toste, F. D.; Sigman, M. S. *Science* **2015**, *347*, 737.

43) Neel, A. J.; Hehn, J. P.; Tripet, P. F.; Toste, F. D. *J. Am. Chem. Soc.* **2013**, *135*, 14044.

44) (a) Harper, K. C.; Sigman, M. S. *Science* **2011**, *333*, 1875. (b) Milo, A.; Bess, E. N.; Sigman, M. S. *Nature* **2014**, *507*, 210. (c) Bess, E. N.; DeLuca, R. J.; Tindall, D. J.; Oderinde, M. S.; Roizen, J. L.; Du Bois, J.; Sigman, M. S. *J. Am. Chem. Soc.* **2014**, *136*, 5783. (d) Bess, E. N.; Bischoff, A. J.; Sigman, M. S. *Proc. Natl. Acad. Sci. USA* **2014**, *111*, 14698. (e) Bess, E. N.; Guptill, D. M.; Davies, H. M. L.; Sigman, M. S. *Chem. Sci.* **2015**, *6*, 3057.

45) Gutmann, V. *Coord. Chem. Rev.* **1976**, *18*, 225.

46) (a) Kang, Q.; Zhao, Z.-A.; You, S.-L. *J. Am. Chem. Soc.* **2007**, *129*, 1484 (b) Terada, M.; Sorimachi, K. *J. Am. Chem. Soc.* **2007**, *129*, 292. (c) Wu, K.; Jiang, Y.-J.; Fan, Y.-S.; Sha, D.; Zhang, S. *Chem. Eur. J.* **2013**, *19*, 474. (d) Chen, L.-Y.; He, H.; Chan, W.-H.; Lee, A. W. M. *J. Org. Chem.* **2011**, *76*, 7141.

47) (a) Zhao, B.; Wang, Z.; Ding, K. *Adv. Synth. Catal.* **2006**, *348*, 1049. (b) Liu, Y.; Sandoval, C. A.; Yamaguchi, Y.; Zhang, X.; Wang, Z.; Kato, K.; Ding, K. *J. Am. Chem. Soc.* **2006**, *128*, 14212. (c) Liu, Y.; Ding, K. *J. Am. Chem. Soc.* **2005**, *127*, 10488.

48) Mercer, G. J.; Sigman, M. S. *Org. Lett.* **2003**, *5*, 1591.

49) Bishop, M.; Cmrecki, V.; Ophoven, V.; Pietruszka, J. *Synthesis* **2008**, *15*, 2488.

50) Westheimer, F. H. *Acc. Chem. Res.* **1968**, *1*, 70.

51) List, B.; Lerner, R. A.; Barbas III, C. F. *J. Am. Chem. Soc.* **2000**, *122*, 2395.

52) (a) Sigman, M. S.; Jacobsen, E. N. *J. Am. Chem. Soc.* **1998**, *120*, 4901; (b) Sigman, M. S.; Vachal, P.; Jacobsen, E. N. *Angew. Chem. Int. Ed.* **2000**, *39*, 1279.

53) Ahrendt, K. A.; Borths, C. J.; MacMillan, D. W. C. *J. Am. Chem. Soc.* **2000**, *122*, 4243.

54) (a) Allemann, C.; Gordillo, R.; Clemente, F. R.; Cheong, P. H.-Y.; Houk, K. N. *Acc. Chem. Res.* **2004**, *37*, 558. (b) Cheong, P. H.-Y.; Legault, C. Y.; Um, J. M.; Çelebi-Ölçüm, N.; Houk, K. N. *Chem. Rev.* **2011**, *111*, 5042. (c) Sunoj, R. B. *Comput. Mol. Sci.* **2011**, *1*, 920. (d) Fu, A.; Zhao, C.; Li, H.; Tian, F.; Yuan, F.; Duan, Y.; Wang, Z. *J. Phys. Chem. A* **2013**, *117*, 2862. (e) Rankin, K. N.; Gauld, J. W.; Boyd, R. J. *J. Phys. Chem. A* **2002**, *106*, 5155.

55) Selected examples: (a) Hayashi, Y.; Matsuzawa, M.; Yama-guchi, J.; Yonehara, S.; Matsumoto, Y.; Shoji, M.; Hashizume, D.; Koshino, H. *Angew. Chem. Int. Ed.* **2006**, *45*, 4593. (b) Zotova, N.; Franzke, A.; Armstrong, A.; Blackmond, D. G. *J. Am. Chem. Soc.* **2007**, *129*, 15100. (c) Zhu, H.; Clemente, F. R.; Houk, K. N.; Meyer, N. P. *J. Am. Chem. Soc.* **2009**, *131*, 1632. (d) Zotova, N.; Broadbelt, L. J.; Armstrong, A.; Blackmond, D. G. *Bioorg. Med. Chem. Lett.* **2009**, *19*, 3934. (e) Hein, J. E.; Burés, J.; Lam, Y.-Y.; Hughes, M.; Houk, K. N.; Armstrong, A.; Blackmond, D. G. *Org. Lett.* **2011**, *13*, 5644. (f) Sánchez, D.; Bastida, D.; Burés, J.; Isart, C.; Pineda, O.; Vilarrasa, O. *Org. Lett.* **2012**, *14*, 536. (g) Klussmann, M.; Iwamura, H.; Mathew, S. P.; Wells Jr., D. H.; Pandya, U.; Armstrong, A.; Blackmond, D. G. *Nature* **2006**, *441*, 621. (h) Klussmann, M.; Mathew, S. P.; Iwamura, H.; Wells Jr., D. H.; Armstrong, A.; Blackmond, D. G. *Angew. Chem. Int. Ed.* **2006**, *45*, 7989. (i) Hoang, L.; Bahmanyar, S.; Houk, K. N.; List, B. *J. Am. Chem. Soc.* **2003**, *125*,

16. (j) Sharma, A. K.; Sunoj, R. B. *Angew. Chem. Int. Ed.* **2010**, *49*, 6373. (k) Seebach, D.; Beck, A. K.; Badine, D. M.; Limbach, M.; Eschenmoser, A.; Treasurywala, A. M.; Hobi, R. *Helv. Chim. Acta* **2007**, *90*, 425. (l) List, B.; Hoang, L.; Martin, H. *J. Proc Natl Acad Sci USA* **2004**, *101*, 5839. (m) Sakthivel, K.; Notz, W.; Bui, T.; Barbas III, C. F. *J. Am. Chem. Soc.* **2001**, *123*, 5260. (n) Clemente, F. R.; Houk, K. N. *Angew. Chem. Int. Ed.* **2004**, *43*, 5766.
- 56) (a) Bahmanyar, S.; Houk, K. N. *J. Am. Chem. Soc.* **2001**, *123*, 12911. (b) Bahmanyar, S.; Houk, K. N.; Martin, H. J.; List, B. *J. Am. Chem. Soc.* **2003**, *125*, 2475.
- 57) Armstrong, A.; Boto, R. A.; Dingwall, P.; Contreras-Garcia, J.; Harvey, M. J.; Mason, N. J.; Rzepa, H. S. *Chem. Sci.* **2014**, *5*, 2057.
- 58) See supporting information of: Bahmanyar, S.; Houk, K. N.; Martin, H. J.; List, B. *J. Am. Chem. Soc.* **2003**, *125*, 2475.
- 59) (a) Schmid, M. B.; Zeitler, K.; Gschwind, R. M. *J. Org. Chem.* **2011**, *76*, 3005. The ability of aminocatalysts to promote the retro-aldol reaction has also been reported in: (b) Luo, S.; Zhou, P.; Li, J.; Cheng, P. *J. Chem. Eur. J.* **2010**, *16*, 4457. Phenomena of racemization in solution for an aminocatalyzed reaction have also been observed in: (c) Duangdee, N.; Harnying, W.; Rulli, G.; Neudörfel, J.-M.; Gröger, H.; Berkessel, A. *J. Am. Chem. Soc.* **2012**, *134*, 11196.
- 60) (a) Curtin, D. Y. *Rec. Chem. Prog.* **1954**, *15*, 111. (b) Pollak, P. I.; Curtin, D. Y. *J. Am. Chem. Soc.* **1950**, *72*, 961. (c) Seeman, J. I. *J. Chem. Edu.* **1986**, *63*, 42.
- 61) Seeman, J. I. *Chem. Rev.* **1983**, *83*, 83.
- 62) Steinfeld, J. I.; Francisco, J. S.; Hase, W. L. in *Chemical Kinetics and Dynamics*, 2nd Ed., Prentice Hall, Upper Saddle River (New Jersey), **1998**, pp. 55-65.
- 63) Hubin, P. O.; Jacquemin, D.; Leherte, L.; Vercauteren, D. P. *Chem. Phys.* **2014**, *434*, 30.
- 64) It is well known that the formation of enamines with *E* configuration is largely favored, as demonstrated also in previous NMR studies where the (*E*)-enamines were detected as preferential conformer (see ref. 59a and 65).
- 65) (a) Schmid, M. B.; Zeitler, K.; Gschwind, R. M. *Angew. Chem. Int. Ed.* **2010**, *49*, 4997. (b) Schmid, M. B.; Zeitler, K.; Gschwind, R. M. *Chem. Eur. J.* **2012**, *18*, 3362.
- 66) The used rate constants were calculated with the formula

$$k(T) = \frac{K_B T Q^\ddagger(T) e^{-\Delta E^\ddagger/RT}}{h Q_R(T)} \cong \frac{K_B T}{h} e^{-\Delta G^\ddagger/RT}$$

where K_B and h are respectively the Boltzmann's and Planck's constants, R the gas constant, $Q_R(T)$ is the partition function of the reactants and $Q^\ddagger(T)$ of the transition state. ΔE^\ddagger is the reaction activation energy. For monomolecular reactions the dimensions are s^{-1} , while for bimolecular reactions the units are $M^{-1}s^{-1}$.

- (a) Wigner, E. *Trans. Faraday Soc.* **1938**, *34*, 29. (b) Eyring, H. *Chem. Rev.* **1935**, *17*, 65. (c) Eyring, H. *J. Chem. Phys.* **1935**, *3*, 107. (d) Miller, W. H. *Acc. Chem. Res.* **1993**, *26*, 174. (e) Miller, W. H. *J. Chem. Phys.* **1974**, *61*, 1823. (f) Pollak, E. *J. Chem. Phys.* **1986**, *85*, 865. (g) Ceotto, M.; Yang, S.; Miller, W. H. *J. Chem. Phys.* **2005**, *122*, 44109. (h) Ceotto, M.; Miller, W. H. *J. Chem. Phys.* **2004**, *120*, 6356. (i) Miller, W. H.; Zhao, Y.; Ceotto, M.; Yang, S. *J. Chem. Phys.* **2003**, *119*, 1329. (j) Ceotto, M. *Mol. Phys.* **2012**, *110*, 547.
- 67) MATLAB 8.0 and Statistics Toolbox 8.1, The MathWorks, Inc., Natick, Massachusetts, United States.
- 68) The standard compounds concentration for the simulation is set to 0.4M for the aldehyde with 5 equiv. of cyclohexanone and the proline loading to 30 mol%, in analogy with experimental conditions.
- 69) Wheeler, S. E.; Moran, A.; Pieniazek, S. N.; Houk, K. N. *J. Phys. Chem. A* **2009**, *113*, 10376.
- 70) Harper, K. C.; Sigman, M. S. *J. Org. Chem.* **2013**, *78*, 2813.
- 71) (a) Downing, R. S.; Kunkeler, P. J.; van Bekkum, H. *Catal. Today* **1997**, *37*, 121. (b) *The Nitro Group in Organic Synthesis*; Ono, N., Ed.; Wiley-VCH: New York, **2001**.
- 72) (a) For a review on selective hydrogenation of nitroarenes, see: Blaser, H. U.; Steiner, H.; Studer, M. *ChemCatChem* **2009**, *1*, 210. (b) Chandrasekhar, S.; Prakash, S. J.; Rao, C. L. *J. Org. Chem.* **2006**, *71*, 2196. (c) Schabel, T.; Belger,

- C.; Plietker, B. *Org. Lett.* **2013**, *15*, 2858. (d) Vanier, G. S. *Synlett* **2007**, 131. (e) Spencer, J.; Anjum, N.; Patel, H.; Rathnam, R. P.; Verma, J. *Synlett* **2007**, 2557.
- 73) (a) Sharma, U.; Verma, P. K.; Kumar, N.; Kumar, V.; Bala, M.; Singh, B. *Chem. Eur. J.* **2011**, *17*, 5903; (b) Rahaim, R. J., Jr.; Maleczka, R. E., Jr. *Org. Lett.* **2005**, *7*, 5087. (c) Wienhöfer, G.; Sorribes, I.; Boddien, A.; Westerhaus, F.; Junge, K.; Junge, H.; Llusar, R.; Beller, M. *J. Am. Chem. Soc.* **2011**, *133*, 12875. (d) Kelly, S. M.; Lipshutz, B. H. *Org. Lett.* **2014**, *16*, 98. (e) Saha, A.; Ranu, B.-d. *J. Org. Chem.* **2008**, *73*, 6867. (f) Liu, L.; Qiao, B.; Chen, Z.; Zhangab, J.; Deng, J. *Chem. Commun.* **2009**, *45*, 653. (g) Junge, K.; Wendt, B.; Shaikh, N.; Beller, M. *Chem. Commun.* **2010**, *46*, 1769.
- 74) (a) Bellamy, F. D.; Ou, K. *Tetrahedron Letters* **1984**, *25*, 839. For two recent applications of SnCl₂ nitro reducing ability, see: (b) Sawant, D.; Kumar, R.; Maulik, P. R.; Kundu, B. *Org. Lett.* **2006**, *8*, 1525. (c) Yoo, C. L.; Fettinger, J. C.; Kurth, M. J. *J. Org. Chem.* **2005**, *70*, 6941.
- 75) (a) Liu, Y.; Lu, Y.; Prashad, M.; Repic, O.; Blacklock, T. J. *Adv. Synth. Catal.* **2005**, *347*, 217. (b) Chandrappa, S.; Vinaya, T.; Ramakrishnappa, T.; Rangappa, K. S. *Synlett*, **2010**, 3019. (c) Kommi, D. N.; Kumar, D.; Bansal, R.; Chebolu, R.; Chakraborti, A. K. *Green Chem.* **2012**, *14*, 3329. (d) Yu, C.; Liu, B.; Hu, L. *J. Org. Chem.* **2001**, *66*, 919.
- 76) (a) Kasparian, A. J.; Savarin, C.; Allgeier, A. M.; Walker, S. D. *J. Org. Chem.* **2011**, *76*, 9841. (b) Armitage, M.; Bret, G.; Choudary, B. M.; Kingswood, M.; Loft, M.; Moore, S.; Smith, S.; Urquhart, M. W. *J. Org. Process Res. Dev.* **2012**, *16*, 1626.
- 77) Bruce, W. F.; Perez-Medina, L. A. *J. Am. Chem. Soc.* **1947**, *69*, 2571.
- 78) Kumar, J. S. D.; Ho, M. M.; Toyokuni, T. *Tetrahedron Lett.* **2001**, *42*, 5601.
- 79) Park, K. K.; Oh, C. H.; Joung, W. K. *Tetrahedron Lett.* **1993**, *34*, 7445.
- 80) *Bretherick's Handbook of Reactive Chemical Hazards*; Urben, P., 7th ed.; Elsevier: Amsterdam, **2007**.
- 81) Oda, S.; Shimizu, H.; Aoyama, Y.; Ueki, T.; Shimizu, S.; Osato, H.; Takeuchi, Y. *Org. Process Res. Dev.* **2012**, *16*, 96.
- 82) Yang, D.; Fokas, D.; Li, J.; Yu, L.; Baldino, C. M. *Synthesis* **2015**, *47*, 47.
- 83) Romero, A. H.; Salazar, J.; López, S. E. *Synthesis* **2013**, *45*, 2043.
- 84) McLaughlin, M. A.; Barnes, D. M. *Tetrahedron Lett.* **2006**, *47*, 9095.
- 85) (a) Nickson, T. E. *J. Org. Chem.* **1986**, *51*, 3903. (b) Leleu, S.; Papamicael, C.; Marsais, F.; Dupas, G.; Levacher, V. *Tetrahedron: Asymmetry* **2004**, *15*, 3919–3928.
- 86) Gallagher, W. P.; Marlatt, M.; Livingston, R.; Kiau, S.; Muslehiddinglu, J. *Org. Process Res. Dev.* **2012**, *16*, 1665.
- 87) (a) Gerst, M.; Morgenthaler, J.; Rüdhardt, C. *Chem. Ber.* **1994**, *127*, 691. (b) Rüdhardt, C.; Gerst, M.; Nölke, M. *Angew. Chem. Int. Ed. Eng.* **1992**, *31*, 1523. (c) Gerst, M.; Beckhaus, H.-D.; Rüdhardt, C.; Campbell, E. E. B.; Tellgmann, R. *Tetrahedron Lett.* **1993**, *34*, 7729. (d) Gerst, M.; Rüdhardt, C. *Tetrahedron Lett.* **1993**, *34*, 7733. (e) Rüdhardt, C.; Gerst, M.; Ebenhoch, J.; Beckhaus, H.-D.; Campbell, E. E. B.; Tellgmann, R.; Schwarz, H.; Weiske, T.; Pitter, S. *Angew. Chem. Int. Ed. Eng.* **1993**, *32*, 584.
- 88) Coellen, M.; Rüdhardt, C. *Chem. Eur. J.* **1995**, *4*, 564.
- 89) Wang, H.-C.; Li, B.-L.; Zheng, Y.-J.; Wang, W.-Y. *Bull. Korean Chem. Soc.* **2012**, *33*, 2961.
- 90) Gao, Y.; Ma, D.; Wang, C.; Guan, J.; Bao, X. *Chem. Commun.* **2011**, *47*, 2432.
- 91) Duan, Z.; Ranjit, S.; Liu, X. *Org. Lett.* **2010**, *12*, 2430.
- 92) Kumar, M.; Sharma, U.; Sharma, S.; Kumar, V.; Singh, B.; Kumar, N. *RSC Adv.* **2013**, *3*, 4894.
- 93) Sharma, S.; Kumar, M.; Kumar, V.; Kumar, N. *J. Org. Chem.* **2014**, *79*, 9433.
- 94) (a) Orlandi, M.; Tosi, F.; Bonsignore, M.; Benaglia, M. *Org. Lett.* **2015**, *17*, 3941. (b) The methodology is also described in a patent: International Patent Application: M. Bonsignore, M. Benaglia, PCT/EP/2013/0683 (Università degli Studi di Milano, Milano, Italy), now owned by DexLeChem GmbH (Berlin, Germany).
- 95) Reviews: (a) Guizzetti, S.; Benaglia, M. *Eur. J. Org. Chem.* **2010**, 5529. (b) Jones, S.; Warner, C. J. A. *Org. Biomol. Chem.* **2012**, *10*, 2189.

- 96) For the most recent contributions of our group in the field see: (a) Genoni, A.; Benaglia, M.; Massolo, E.; Rossi, S. *Chem. Commun.* **2013**, 49, 8365. (b) Barrulas, P.; Genoni, A.; Benaglia, M.; Burke, A. *Eur. J. Org. Chem.* **2014**, 7339.
- 97) Bernstein, C. S. *J. Am. Chem. Soc.* **1969**, 91, 699.
- 98) Benkeser, R. A.; Smith, W. E. *J. Am. Chem. Soc.* **1969**, 91, 1556.
- 99) (a) Benkeser, R. A.; Smith, W. E. *J. Am. Chem. Soc.* **1968**, 90, 5307. (b) Benkeser, R. A.; Gaul, J. M.; Smith, W. E. *J. Am. Chem. Soc.* **1969**, 91, 3666.
- 100) Benkeser, R. A.; Foley, K. M.; Gaul, J. M.; Li, G. S.; Smith, W. E. *J. Am. Chem. Soc.* **1969**, 91, 4578.
- 101) Rossi, S.; Benaglia, M.; Porta, R.; Cotarca, L.; Maragni, P.; Verzini, M. *Eur. J. Org. Chem.* **2015**, 2531.
- 102) Karsch, H. H.; Schlüter, P. A.; Bienlein, F.; Herker, M.; Witt, E.; Sladek, A.; Heckel, M. *Z. anorg. allg. Chem.* **1998**, 295.
- 103) Roy, S.; Stollberg, P.; H.-Irmer, R.; Stalke, D.; Andrada, D. M.; Frenking, G.; Roesky, H. W. *J. Am. Chem. Soc.* **2015**, 137, 150.
- 104) Denmark, S. E.; Beutner, G. L. *Angew. Chem. Int. Ed. Engl.* **2008**, 47, 1560.
- 105) Geerlings, P.; De Proft, F.; Langenaeker, W. *Chem. Rev.* **2003**, 103, 1793.
- 106) Belzner, J.; Dehnert, U.; Ihmels, H.; Hübner, M.; Müller, P.; Usón, I. *Chem. Eur. J.* **1998**, 4, 852.
- 107) Meyer-Wegner, F.; Nadj, A.; Bolte, M.; Auner, N.; Wagner, M.; Holthausen, M. C.; Lerner, H.-W. *Chem. Eur. J.* **2011**, 17, 4715.
- 108) (a) Schmeisser, M.; Voss, P. *Z. Anorg. Allg. Chem.* **1964**, 334, 50. (b) Schenk, P. W.; Bloching, H. Z. *Anorg. Allg. Chem.* **1964**, 334, 57. (c) Swihart, M. T.; Carr, R. W. *J. Phys. Chem. A* **1998**, 102, 785. (d) Timms, P. L. *Inorg. Chem.* **1968**, 7, 387.
- 109) (a) Uhlig, F.; Marsmann, H. C. in *²⁹Si NMR, Some Practical Aspects, from: Gelest Catalog: Silicon Compounds, Silanes & Silicones*, ed. B. Arkles and G. Larson, Gelest Inc., Morrisville, PA, **2008**, 2nd edn, pp. 208–222 (www.pascal-man.com/periodic-table/29Si.pdf). (b) Frenzel, A.; Buffy, J. J.; Powell, D. R.; West, R.; Müller, T. *Chem. Ber.* **1997**, 130, 1579.
- 110) (a) Anslyn, E. V.; Dougherty, D. A. in *Modern Physical Organic Chemistry*, University Science Books, Herson, VA, **2006**. (b) Hansh, C.; Leo, A.; Taft, R. W. *Chem. Rev.* **1991**, 91, 165.
- 111) (a) Kütt, A.; Rodima, T.; Saame, J.; Raamat, E.; Mäemets, V.; Kaljurand, I.; Koppel, I. A.; Garlyauskayte, R. Y.; Yagupolskii, Y. L.; Yagupolskii, L. M.; Bernhardt, E.; Willner, H.; Leito, I. *J. Org. Chem.* **2011**, 76, 391. (b) Coetzeel, J. F.; Padmanabhan, G. R. *J. Am. Chem. Soc.* **1965**, 87, 5005.
- 112) The calculation of $\Delta_{\text{R}}G_2$ has been performed with different computational methods (M06-2X/6-311++G(3df,3pd) [PCM=acetonitrile], B3LYP/6-311++G(3df,3pd) [PCM=acetonitrile] and wB97XD/6-311++G(3df,3pd) [PCM=acetonitrile]), and all these computational set-ups give analogous results, thus confirming the validity of the obtained value.